

**SCHOOL OF CHEMISTRY**  
**CARDIFF UNIVERSITY**



---

**Microporous Polymers Containing Tertiary  
Amine Functionality for Gas Separation  
Membrane Fabrication**

---

Thesis submitted for the degree of Doctor of Philosophy by:

**Richard Malpass-Evans**

Supervisor: Neil B. McKeown

2014



## **Acknowledgements**

First and foremost, I would like to thank my supervisor, Professor Neil McKeown, for giving me the opportunity to join his research group and for his constant guidance and support throughout my MChem, PhD and PDRA position.

Special thanks should also go to Lino, Grazia and Kadhum for their guidance and support. I would also like to thank everyone who has made lab 1.107A a friendly and fun place to work over the past five years: Alaa, Alex, Ali, Ben, Heulyn, Ian, James, Jono, Luke, Matt, Mike, Mo, Rhodri, Rhys, Rupert, Sabeeha, Sadiq and Yulia.

A big thanks to all our collaborators, especially Johannes (John) Jansen and everyone at ITM CNR for measuring the transport parameters of our membranes.

I would like to thank Dr. Rob Jenkins, Robin Hicks, Dave Walker, Gaz Coleman, Simon James and all of the technical staff within the School of Chemistry, for their expertise and willingness to help at any given moment. I would also like to thank Dr. Benson Kariuki and Grazia for measuring and solving the crystal structures featured in this thesis.

I would like to thank my family and friends for their love and support, especially my wife Ellie for putting up with me working evenings and weekends and my son William for letting me get just enough sleep to complete this thesis on time.

Finally I would like to thank the European Commission for funding under the DoubleNanomem project (Nanocomposite and Nanostructured Polymeric Membranes for Gas and Vapour Separations), a collaborative research project under the EU's Seventh Framework Programme.



## **Abstract**

This research reported in this thesis is based on the synthesis of novel polymers of intrinsic microporosity (PIMs) with the aim of fabricating membranes for gas separation applications. PIMs are composed of rigid and awkwardly-shaped monomeric segments which lack the conformational and rotational freedom needed to pack space efficiently. As a result these polymers display high BET surface areas and display excellent gas permeabilities when solution-cast into films which can be used as gas separation membranes.

This thesis describes the synthesis of a range of aromatic diamine, tetraamine, dianhydride, and dicarboxylic acid monomers that conform to the PIM design concept, featuring rigid and contorted architectures. These monomers were then used to synthesise five classes of polymer featuring tertiary amine functionality. Structure-property relationships were established between these polymers and BET surface area measurements. Polymers that displayed adequate film forming properties were also evaluated by our collaborators at The Institute of Membrane Technology for their gas transport parameters.

Chapter 6 describes the synthesis of a new class of polymer, Tröger's Base PIMs, featuring a novel polymerisation reaction using chemistry first reported 127 years ago. One of these polymers, DMEA.TB, displays a BET surface area of 1028 m<sup>2</sup>/g which is the highest recorded for any soluble polymer to date. DMEA.TB places gas permeation data for technologically important gas pairs far over the present Robeson upper bound and has unrivalled potential to separate mixtures containing hydrogen. Chapter 7 deals with quaternisation and subsequent ion exchange of selected Tröger's Base polymers. Chapter 8 discusses the synthesis of three novel polyimides using highly rigid and contorted ethanoanthracene monomers containing methyl groups that restrict rotation around polymer segments. These polymers display only moderate gas permeation characteristics and possess BET surface areas of up to 694 m<sup>2</sup>/g. Chapter 9 describes the synthesis of a new class of zwitterionic polysquaraines however, these polymers were shown to be non-porous due to strong ionic/hydrogen bonding. Chapter 10 describes the synthesis of polybenzimidazoles using the PIM design concept but it was found that extensive hydrogen bonding reduces free volume, forming non porous solids. Chapter 11 describes the synthesis of novel polypyrrolones with surface areas of up to 284 m<sup>2</sup>/g however, film formation was not possible with these materials. Chapter 12 features a brief investigation onto the cross-linking of a Tröger's Base membrane using hydrolysed PIM-1 as polyanionic counterion.

## Abbreviations

<b>4MPDA</b>	Tetramethylphenyldiamine	<b>IUPAC</b>	International Union of Pure and Applied Chemistry
<b>6FDA</b>	Hexafluoroisopropylidene diphthalic anhydride	<b>Lit</b>	Literature
<b>AIBN</b>	Azobisisobutyronitrile	<b>MALDI</b>	Matrix Assisted Laser Desorption Ionisation
<b>Anth</b>	Anthracene	<b>min</b>	Minute(s)
<b>APCI</b>	Atmospheric pressure chemical ionisation	<b>M<sub>n</sub></b>	Number average molecular weight
<b>Asymm</b>	Asymmetric	<b>MOF</b>	Metal Organic Framework
<b>Benz</b>	Benzene	<b>MTR</b>	Membrane Technology and Research, Inc
<b>BET</b>	Brunauer, Emmett and Teller	<b>Mw</b>	Weight average molecular weight
<b>BTFSI</b>	Bistrifluoromethanesulfonimide	<b>NDSA</b>	Naphthalenedisulfonic acid
<b>COF</b>	Covalent Organic Framework	<b>NMDCEA</b>	N-methyldicarboximide ethanoanthracene
<b>DCE</b>	Dichloroethane	<b>NMP</b>	N-methyl pyrrolidone
<b>DCEA</b>	Dichloroethanoanthracene	<b>NMR</b>	Nuclear Magnetic Resonance
<b>DCM</b>	Dichloromethane	<b>OMIM</b>	Organic Molecule of Intrinsic Microporosity
<b>DEEEA</b>	Diethyl ester ethanoanthracene	<b>PAAA</b>	Polyamide amino acid
<b>DHEA</b>	Dihydroethanoanthracene	<b>PAN</b>	Polyacrylonitrile
<b>DIM</b>	Dendrimer of Intrinsic Microporosity	<b>PBI</b>	Polybenzimidazole
<b>DMAc</b>	N,N-Dimethylacetamide	<b>Pc</b>	Phthalocyanine
<b>DMAnth</b>	Dimethylantracene	<b>PDI</b>	Polydispersity index
<b>DMDPM</b>	Dimethylphenylmethane	<b>PDMS</b>	Polydimethylsiloxane
<b>DMEA</b>	Dimethylethanoanthracene	<b>PI</b>	Polyimide
<b>DMF</b>	N,N-Dimethylformamide	<b>PIM</b>	Polymer of Intrinsic Microporosity
<b>DMN</b>	Dimethylnaphthidine	<b>PPA</b>	Polyphosphoric acid
<b>DMSO</b>	Dimethylsulfoxide	<b>Ppy</b>	Polypyrrolone
<b>DPM</b>	Diphenylmethane	<b>PSQU</b>	Polysquaraine
<b>DSC</b>	Differential scanning calorimetry	<b>PTFE</b>	Polytetrafluoroethylene
<b>Fig</b>	Figure	<b>PTMSP</b>	Polytrimethylsilylpropyne
<b>IR</b>	Infrared spectroscopy	<b>SBI</b>	Tetramethylspirobisindane
<b>GPC</b>	Gel Permeation Chromatography	<b>Symm</b>	Symmetric
<b>h</b>	Hour(s)	<b>TB</b>	Tröger's base
<b>HCP</b>	Hyper-cross-linked polymer	<b>TFA</b>	Trifluoroacetic acid
<b>HFIP</b>	Hexafluoroisopropylidene dianiline	<b>TGA</b>	Thermal gravimetric Analysis
<b>HMEA</b>	Hexamethylethanoanthracene	<b>THF</b>	Tetrahydrofuran
<b>HPLC</b>	High performance liquid chromatography	<b>TLC</b>	Thin Layer Chromatography
<b>HRMS</b>	High Resolution Mass Spectrometry	<b>TMEA</b>	Tetramethylethanoanthracene
<b>IMFV</b>	Internal molecular free volume	<b>TMPI</b>	Trimethylphenylindane
<b>IPA</b>	Isopropyl alcohol	<b>TOF</b>	Time of flight
<b>ITM</b>	Institute of Membrane Technology	<b>ZTC</b>	Zeolite templated carbons

---

## Table of Contents

<b>Declaration</b> .....	<b>i</b>
<b>Acknowledgements</b> .....	<b>ii</b>
<b>Abbreviations</b> .....	<b>iv</b>
<b>Chapter 1: Introduction</b> .....	<b>1</b>
<b>1.1: Porous Materials</b> .....	<b>1</b>
<b>1.2: Microporous Materials</b> .....	<b>2</b>
<b>1.3: Zeolites</b> .....	<b>2</b>
<b>1.4: Metal-Organic Frameworks</b> .....	<b>4</b>
<b>1.5: Covalent Organic Frameworks</b> .....	<b>5</b>
<b>1.6: Activated Carbons</b> .....	<b>6</b>
<b>1.7: Hyper Cross-Linked Polymers</b> .....	<b>7</b>
<b>1.8: Polymers of Intrinsic Microporosity</b> .....	<b>8</b>
<b>1.8.1: Linear Polymers</b> .....	<b>12</b>
<b>1.8.1.1: Polyacetylenes</b> .....	<b>12</b>
<b>1.8.2: PIM Polyimides</b> .....	<b>13</b>
<b>1.8.3: Ladder Polymers</b> .....	<b>15</b>
<b>1.8.3.1: PIM-1</b> .....	<b>15</b>
<b>1.8.3.2: PIM-7</b> .....	<b>17</b>
<b>1.8.4: Network Polymers</b> .....	<b>18</b>
<b>1.8.4.1: Triptycene Network PIMs</b> .....	<b>18</b>
<b>1.8.4.2: Phthalocyanine Network PIMs</b> .....	<b>19</b>
<b>Chapter 2: Background Theory</b> .....	<b>21</b>
<b>2.1: Determination of Surface Area</b> .....	<b>21</b>
<b>2.2: Membrane Technology</b> .....	<b>26</b>
<b>2.3: Membrane Theory</b> .....	<b>28</b>
<b>2.3.1: Mass Transport Through Membranes</b> .....	<b>28</b>
<b>2.3.2: Transport Parameters</b> .....	<b>31</b>
<b>2.4: Measurement of Transport Parameters</b> .....	<b>35</b>
<b>Chapter 3: Research Aims</b> .....	<b>38</b>
<b>Chapter 4: Monomer Synthesis</b> .....	<b>39</b>
<b>4.1: 1,3,3-trimethyl-1-phenylindane</b> .....	<b>39</b>
<b>4.2: Spirobisindanes</b> .....	<b>40</b>
<b>4.3: Ethanoanthracenes</b> .....	<b>41</b>
<b>4.3.1: Ethanoanthracene Compounds Derived from Anthracene</b> .....	<b>41</b>
<b>4.3.2: Ethanoanthracene Compounds Derived from Diols</b> .....	<b>43</b>
<b>4.4: Carboxylic Acid Compounds</b> .....	<b>47</b>
<b>4.5: Dianhydride Compounds</b> .....	<b>48</b>
<b>4.6: Dinitro Compounds</b> .....	<b>48</b>
<b>4.7: Tetranitro Compounds</b> .....	<b>50</b>
<b>4.8: Diamino Compounds</b> .....	<b>51</b>

---

4.9: Tetraamine Hydrochloride Salts .....	54
4.10: Tetraamino Compounds.....	55
4.11: Diamine Hydrochloride Salts.....	55
4.12: 9,10-dimethyl-9,10-dihydro-2,6(7)-diamino-9,10-ethanoanthracene trifluoroacetate	56
<b>Chapter 5: Polymer Synthesis.....</b>	<b>56</b>
<b>Chapter 6: Tröger's Base Polymers .....</b>	<b>58</b>
6.1: Tröger's Base.....	58
6.2: Tröger's Base Polymerisation .....	60
6.3: Tröger's Base Polymers from Synthetic Monomers .....	62
6.3.1: DMEA.TB .....	62
6.3.2: DHEA.TB.....	71
6.3.3: DCEA.TB .....	74
6.3.4: TMEA.TB .....	75
6.3.5: Anth.TB.....	77
6.3.6: TMPL.TB .....	79
6.3.7: SBI.TB.....	81
6.4: Tröger's Base Polymers from Commercial Monomers.....	84
<b>Chapter 7: Quaternerised Tröger's Base Polymers .....</b>	<b>88</b>
7.1: Tröger's Base Polymer Methylation .....	88
7.2: Ion Exchange .....	89
7.2.1: Exchange with Fluoride .....	89
7.2.2: Exchange with Bistrifluoromethanesulfonimide (Bistriflimide).....	90
7.2.3: Exchange with 2,6-Naphthalene Disulfonic acid.....	93
<b>Chapter 8: Polyimides .....</b>	<b>96</b>
<b>Chapter 9: Polysquaraines .....</b>	<b>102</b>
<b>Chapter 10: Polybenzimidazoles .....</b>	<b>106</b>
<b>Chapter 11: Polypyrrrolones .....</b>	<b>110</b>
<b>Chapter 12: Preliminary Study of Cross-Linking DHEA.TB with PIM-1.....</b>	<b>118</b>
<b>Chapter 13: Conclusions .....</b>	<b>123</b>
<b>Chapter 14: Experimental.....</b>	<b>125</b>
14.1: General Methods and Equipment.....	125
14.2: Monomer Synthesis .....	128
14.3: Polymers Synthesis .....	161
14.4: Membrane Cross-linking .....	185
<b>Bibliography .....</b>	<b>189</b>
<b>Publications .....</b>	<b>196</b>

## Chapter 1: Introduction

### 1.1: Porous Materials

A porous material is defined as a solid material that contains a void, cavity or interstice<sup>1</sup> known as a pore. The structure of a pore can vary greatly depending upon the material or post treatment of that material. IUPAC (International Union of Pure and Applied Chemistry) defines pores by three parameters; size, shape and accessibility to an external fluid<sup>1</sup>. These factors influence the physical and chemical properties of that material and hence potential applications. Three classes of porous materials have been defined by IUPAC according to their pore size: Microporous (< 2 nm), Mesoporous (2-50 nm) and Macroporous (>50 nm)<sup>1</sup>. A sub-classification of pore size is accessibility (i.e. if the pore is open or closed). A closed pore (a in Fig 1.1a<sup>1</sup>) is inaccessible to external probes such as fluids and gas molecules. This type of pore influences only the macroscopic properties of a material such as bulk density and mechanical strength. Open pores (b, c, d, e and f in Fig 1.1a) possess an opening from the surface of the material. These type of pores are accessible to external probes, and therefore influence microscopic properties such as porosity and surface area.

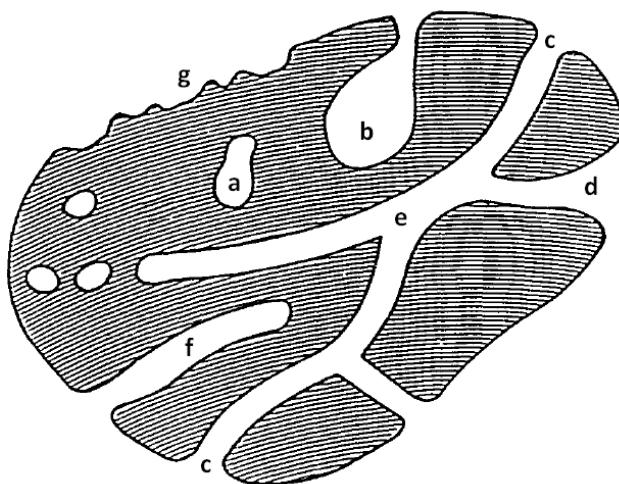


Fig 1.1a. Schematic Cross-Section of a Porous Solid.

Open pores are further classified by their shape (c and f are cylindrical and b is "ink-bottled shaped" in Fig 1.1a, if a pore has only one opening (b and f) or if a pore penetrates the entire material (e). Rough surfaces (g) are not considered porous as convention states that irregularities must be deeper than they are wide to be defined as pores.



## 1.2: Microporous Materials

The smaller pore size a material possesses, the greater is the surface area to volume ratio of that material. It is for this reason that microporous materials have among the highest surface areas of all three classes of porous materials. High surface area materials have become of interest for a number of applications such as adsorption<sup>2</sup>, hydrogen storage<sup>3-5</sup>, gas purification<sup>4, 6, 7</sup>, liquid purification<sup>8</sup>, heterogeneous catalysis<sup>9-11</sup>, sensors<sup>12</sup> and ion exchange<sup>13</sup>. Microporous materials can be sub-divided into two broad classes: ordered crystalline materials and disordered amorphous materials.

Ordered crystalline materials possess a long range order and have well defined pore structures which can be important factors for applications such as catalysis. Typical examples are zeolites, metal-organic frameworks (MOFs) and covalent organic frameworks (COFs).

Amorphous materials usually possess little or no long-range order and have poorly defined pore structures. Typical examples include activated carbons, hyper cross-linked polymers (HCPs) and high free-volume polymers such as polymers of intrinsic microporosity (PIMs). There are however examples of amorphous materials that can be modified to demonstrate long range order such as zeolite templated carbons (ZTCs)<sup>14</sup>.

Each of these materials possess their own unique properties and applications which will be discussed in the following sections.

## 1.3: Zeolites

Zeolites are members of a large family of natural and synthetic microporous crystalline aluminosilicates discovered by the Swedish mineralogist Axel Fredrick Cronstedt. He noted in 1756 the ability of the mineral stilbite to absorb water and release it as steam upon heating. This observation led to the name zeolite, derived from the Greek words 'zein' (boiling) and 'lithos' (stone)<sup>15</sup>.

Zeolites possess highly regular and well defined microporous cage-like framework structures. Zeolite frameworks can contain smaller sub-structures known as supercages and sodalite cages that form connected channels of roughly (1-20 Å) in diameter through the material.

Zeolites are most commonly composed of tetrahedral silicate  $[\text{SiO}_4]^{4-}$  and aluminate  $[\text{AlO}_4]^{5-}$  units connected through bridging oxygen atoms, although other compositions are known<sup>16</sup>.

The framework has a net negative charge due to the presence of  $[\text{AlO}_4]^{5-}$  units and this enables the sub cage structures to accommodate a wide variety of loosely bound cationic species such as  $\text{Na}^+$ ,  $\text{K}^+$ ,  $\text{Ca}^{2+}$  and  $\text{Mg}^{2+}$ . There are over 170 topologies known<sup>17</sup> and one example is the Faujasite framework  $(\text{X})_{3.5}[\text{Al}_7\text{Si}_{17}\text{O}_{48}] \cdot 32(\text{H}_2\text{O})$  where  $\text{X} = \text{Na}_2, \text{Ca}$  or  $\text{Mg}$  (Fig 1.3a<sup>9, 17</sup>).

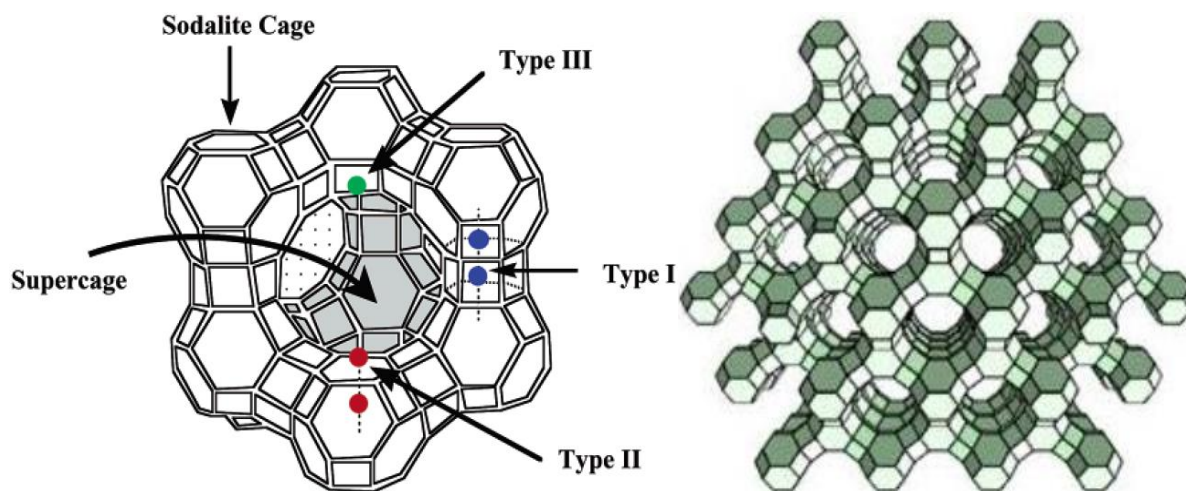


Fig 1.3a. Structure model of a Faujasite showing potential bonding positions of cations (types I, II and III). (left), Structure model of a Faujasite showing pore channels (right).

Since their discovery 250 years ago zeolites have benefited many industries with their numerous applications:

Zeolites have high thermal stability and upon removal of the adsorbed water by heating to 350-400 °C, zeolites remain highly stable frameworks<sup>10</sup> with BET surface areas up to and in excess of 900 m<sup>2</sup> g<sup>-1</sup><sup>18, 19</sup>. The high surface areas of zeolites combined with well-defined pore structures allows them to act as ‘*molecular sieves*’ in which external molecules are selectively adsorbed based on their size<sup>20</sup>. Guest cations can be readily exchanged for other species in solution. This has seen zeolites used in a number of ion exchange applications such as the treatment of liquid radioactive waste<sup>13</sup>. These guest cations may be utilised as evenly distributed catalytic sites that may be accessed selectively by reactants through the porous zeolite structure. For example, acidic zeolites ( $\text{H}^+$  counter ions) are commonly used in the petrochemical industry in the catalytic cracking of long chain hydrocarbons<sup>16, 21</sup>. The unique structure of a particular catalytic zeolite can be used to allow the shape and size of the pore system to exert a steric influence on reactants; a process known as “*shape selective catalysis*”<sup>11</sup>.

## 1.4: Metal-Organic Frameworks

Research in the area of coordination chemistry, especially by Yaghi and co-workers<sup>22</sup>, has provided a new class of microporous materials known as metal-organic frameworks (MOFs). MOF structures consist of a regular network of metal oxide or metal ion units linked together via organic molecules to give an ordered three-dimensional microporous structure. The organic linker molecules can act as both “spacers” for the metal units and also as “joints” to give the resulting MOF architecture flexibility. These structures give rise to an array of interconnected pores that can accommodate a number of guest species such as large organic molecules and hydrogen<sup>22</sup>. The wide range of potential metal centres and organic linkers gives rise to a large synthetic diversity within the field of MOFs (in contrast to zeolites).

The first MOF to exceed surface areas of the best activated carbons was MOF-177 [ $\text{Zn}_4\text{O}(\text{1,3,5-benzenetricarboxylate})_2$ ] reported in 2004 by Yaghi and co-workers<sup>22</sup> with an estimated BET surface area of over  $4500 \text{ m}^2 \text{ g}^{-1}$ . In 2012, a research group from Northwestern University reported a MOF structure with the formula [ $\text{Cu}_3(\text{1,3,5-tris(4-ethynylphenyl)butadiynyl-1,3-carboxylate-benzene})(\text{H}_2\text{O})_3$ ] named NU-110 (Fig 1.4a<sup>23</sup>) with a surface area over  $7000 \text{ m}^2 \text{ g}^{-1}$ .

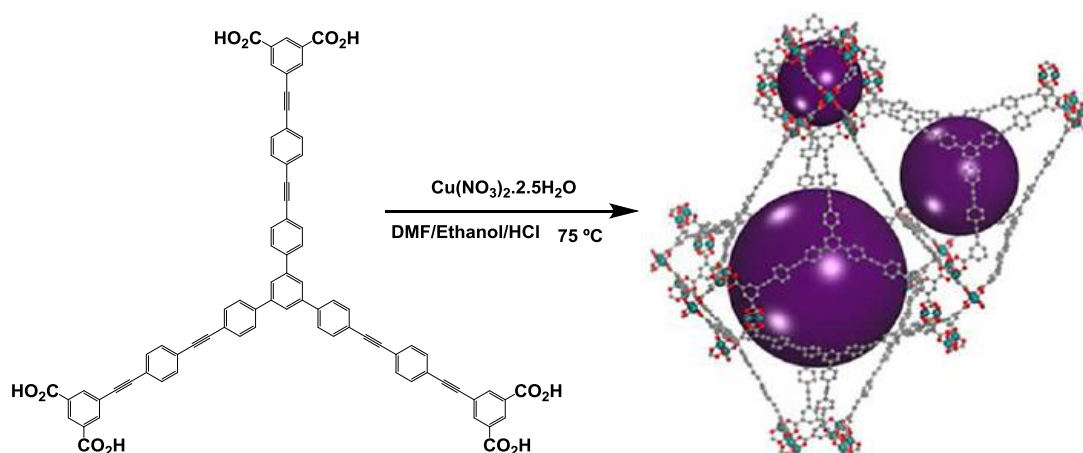


Fig 1.4a. Structure of MOF NU-110 showing pore volumes (purple), largest of which was measured to be  $35 \text{ \AA}$ . MOFs have a number of potential applications including gas purification<sup>24</sup>, hydrogen storage<sup>22</sup>, catalysis<sup>25</sup> and drug delivery<sup>26</sup>. There are however a number of disadvantages concerned with MOFs such as their low stability towards heat, moisture and chemical environment<sup>27, 28</sup>. Many, but not all, MOFs can collapse when heated resulting in an amorphous solid and the loss of porosity. The oxygen-metal coordination bonds in MOFs structures often undergo hydrolysis in presence of water and even with exposure to air, irreversibly destroying the framework<sup>3, 27</sup>.

## 1.5: Covalent Organic Frameworks

Covalent organic frameworks (COFs) are a family of porous crystalline macromolecules constructed solely from light elements (H, B, C, N and O) linked together through strong covalent bonds<sup>29</sup>. COFs are synthesised from organic linkers which are functionalised with groups that allow the formation of strong covalent bonds between each other (e.g. boronic acids (forming boroxines)<sup>2</sup>, boronic acids/catechols (forming dioxaborolanes)<sup>2</sup>, nitriles (forming triazines)<sup>30</sup> and anilines/benzaldehydes (forming imines)<sup>31</sup>. COFs offer low densities, high thermal stability (up to 600 °C), long range order, well defined pore structures and permanent porosity with surface areas comparable with MOF structures.

One of the first reported COFs by Yaghi and co-workers in 2005 was COF-5<sup>32</sup>, produced from the reaction between benzene-1,4-diboronic acid and hexahydroxytriphenylene. COF-5 has two dimensional layered structure with a surface area of 1590 m<sup>2</sup> g<sup>-1</sup>. Using so called ‘*reticular synthesis*’<sup>33</sup> COFs can be expanded into three dimensions through the use of tetrahedral shaped linkers. COF-105 (Fig 1.5a<sup>34</sup>) was reported in 2007, prepared from the dioxaborolane forming reaction of tetra(4-(dihydroxy)borylphenyl)silane with 2,3,6,7,10,11-hexahydroxytriphenylene and has a surface area of 6450 m<sup>2</sup>/g<sup>35</sup>.

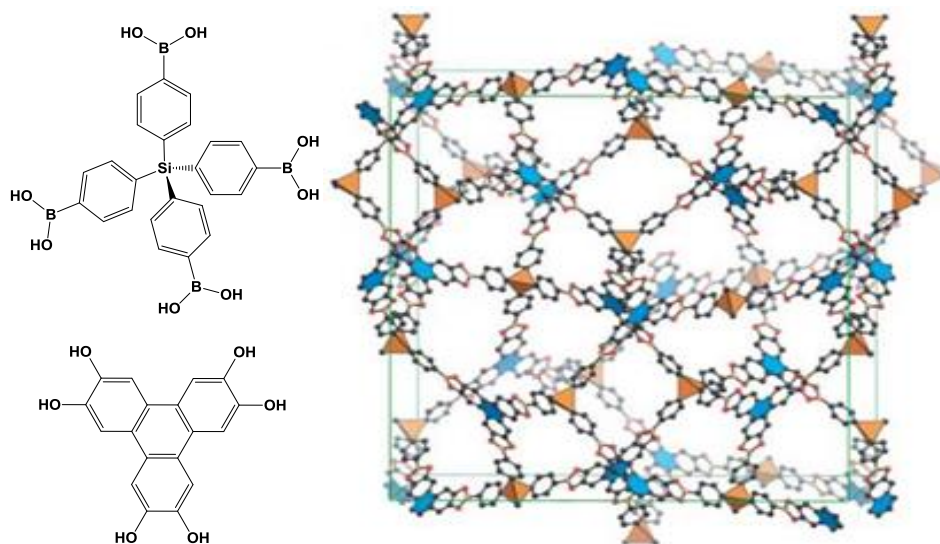


Fig 1.5a. Building blocks (left), Structure model of COF-105 (right).

Due to their analogous structures, application of COFs are similar to those of MOFs such as catalysis<sup>36</sup>, hydrogen storage<sup>37</sup> and filtration<sup>38</sup>. Two dimensional layered COFs generate ordered  $\pi$  systems which can possess additional electronic and optical<sup>39, 40</sup> properties.

## 1.6: Activated Carbons

Wood charcoal was used by the ancient Egyptians to purify water around 1500 BC and later by the Greeks and Romans to treat various diseases<sup>15</sup>. Activated carbons are used today in enormous quantities in industry for applications such as catalyst supports<sup>41</sup>, adsorbents<sup>42</sup> and filters<sup>15, 43</sup>. Activated carbons are generally believed to exist as an extended network polymer consisting of randomly interconnected graphene sheets, although their actual structure is not fully understood and is likely to contain random fragments of various known allotropes of carbon<sup>44</sup> (Fig 1.6a<sup>45</sup>).

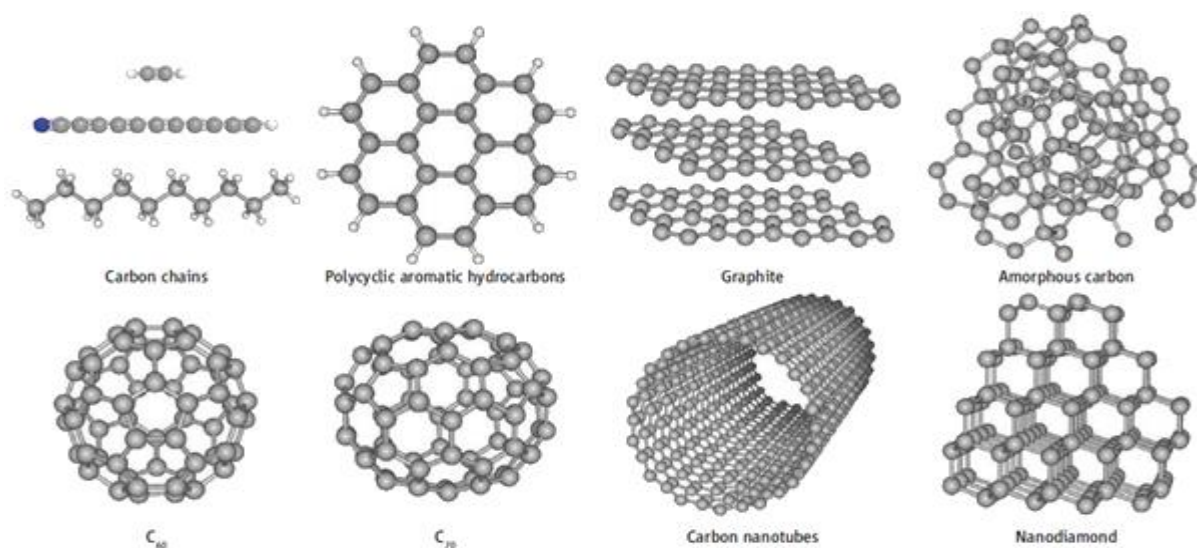


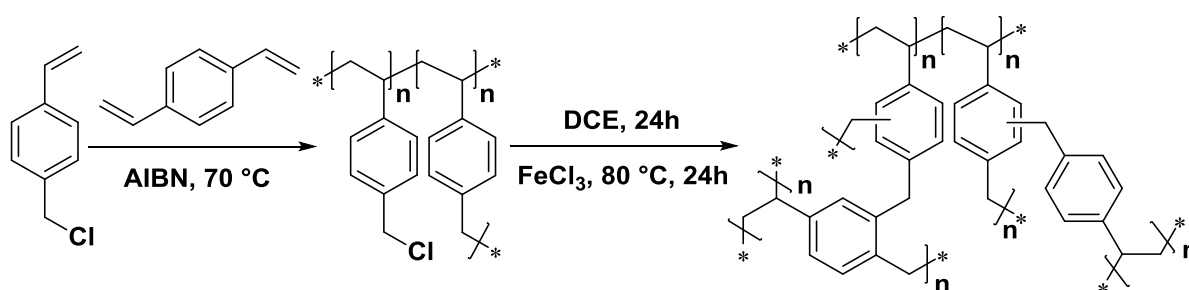
Fig 1.6a. Various known allotropes of carbon.

The surface chemistry of activated carbons are also ill-defined<sup>46</sup> and have the ability to absorb a wide range of organic compounds due to the presence of oxygen and nitrogen functional groups<sup>47</sup>. The surface area arises from the wide distribution of pore sizes ranging from microporous to macroporous<sup>44</sup>. These properties also unfortunately limit the potential of activated carbons for size and chemo-selective applications.

The manufacturing process of activated carbons involves the high temperature carbonisation of carbonaceous starting materials such as wood chips and cellulose<sup>48</sup>. Subsequent activation *via* either: gasification (heating in the presence of oxidising gases) or dehydration/oxidation of the carbonised material with impregnated chemicals, enlarges the size of the existing pores to produce *activated carbon*. In the 1970's, researchers at the oil company AMOCO developed a process for producing activated carbons with surface areas exceeding  $3000 \text{ m}^2 \text{ g}^{-1}$  by activating various precursors such as petroleum coke, with potassium hydroxide<sup>15</sup>.

## 1.7: Hyper Cross-Linked Polymers

The first hyper cross-linked polymers (HCPs) were based on cross-linked polystyrene, published in 1983 by Davankov<sup>49</sup>. These polymers, known as "*Davankov resins*", were prepared *via* the post-polymerisation cross-linking of a solvent swollen polystyrene gel. First, vinylbenzyl chloride is polymerised in the presence of a small quantity of divinylbenzene producing a partially cross-linked co-polymer. The co-polymer is then swollen in a suitable solvent such as 1,2-dichloroethane and cross-linked further *via* a Friedel-Crafts alkylation reaction using a Lewis acid, such as iron (III) chloride (Scheme 1.7a)<sup>50</sup>. This reaction introduces a number of CH<sub>2</sub> bridges between the polymer chains which fixes the polymer in its swollen state, forming pores that persist upon solvent removal.



Scheme 1.7a. Preparation of poly(vinylbenzyl) chloride partially cross-linked with divinylbenzene *via* radical initiation, and subsequent hyper-cross-linking *via* intra-molecular Friedel-Crafts alkylation.

By manipulating the reaction conditions of the cross-linking reaction, Ahn and co-workers were able to selectively tailor Davankov resins with surface areas ranging from 300-2000 m<sup>2</sup> g<sup>-1</sup><sup>51</sup>. It was also shown that these polymers exhibit bimodal pore size distributions from the original macropores present in the non-cross-linked polymer and micropores formed during cross-linking reaction. HCPs have also been prepared by a more direct approach using a Friedel-Crafts self-condensation reaction of bis(chloromethyl) aromatic monomers with iron (III) chloride to produce materials with surface areas up to 1900 m<sup>2</sup> g<sup>-1</sup><sup>52</sup>.

Since cross-linking does not occur at every possible site, these polymers contain residual chloromethyl groups. Functional groups, such as amines and carboxylic acids, can then be transferred into the polymer matrix, replacing residual chlorine atoms by post-synthetic modification<sup>53</sup>. A diverse range of HCPs with a wide variety of surface chemistries have found extensive use in industry as stationary phases in chromatography<sup>54</sup> and ion exchange resins<sup>55</sup>. The high surface areas of HCPs also show a potential application in hydrogen storage<sup>56</sup>.

## 1.8: Polymers of Intrinsic Microporosity

Generally, polymers are not thought to be microporous as they tend to have enough conformational and rotational freedom to twist and bend into the correct complementary shapes to pack efficiently as to maximise attractive intermolecular interactions between chains. As seen in the case of HCPs, the bulk structure of a generic linear polymer must be modified by post-polymerisation processing to give rise to microporosity. Polymers of Intrinsic Microporosity (PIMs) however, are highly rigid polymers typically composed wholly of fused ring systems that have highly contorted structures which prevent efficient packing of polymer chains. The inefficient packing of polymer chains leads to the polymers possessing microporosity and surface area that results solely from the molecular structure of the material and not from any post-polymerisation modification. The microporosity is then said to be an *intrinsic* property of these polymers and hence the name.

This concept has been mathematically illustrated for 2D<sup>57</sup> and 3D<sup>58</sup> shapes by S.Torquato, F.Stillinger and Y.Jiao in which they describe the random packing efficiency ( $\Phi$ ) of concave “superballs” as a function of their deformation parameter ( $P$ ) (Fig 1.8a<sup>58</sup>).

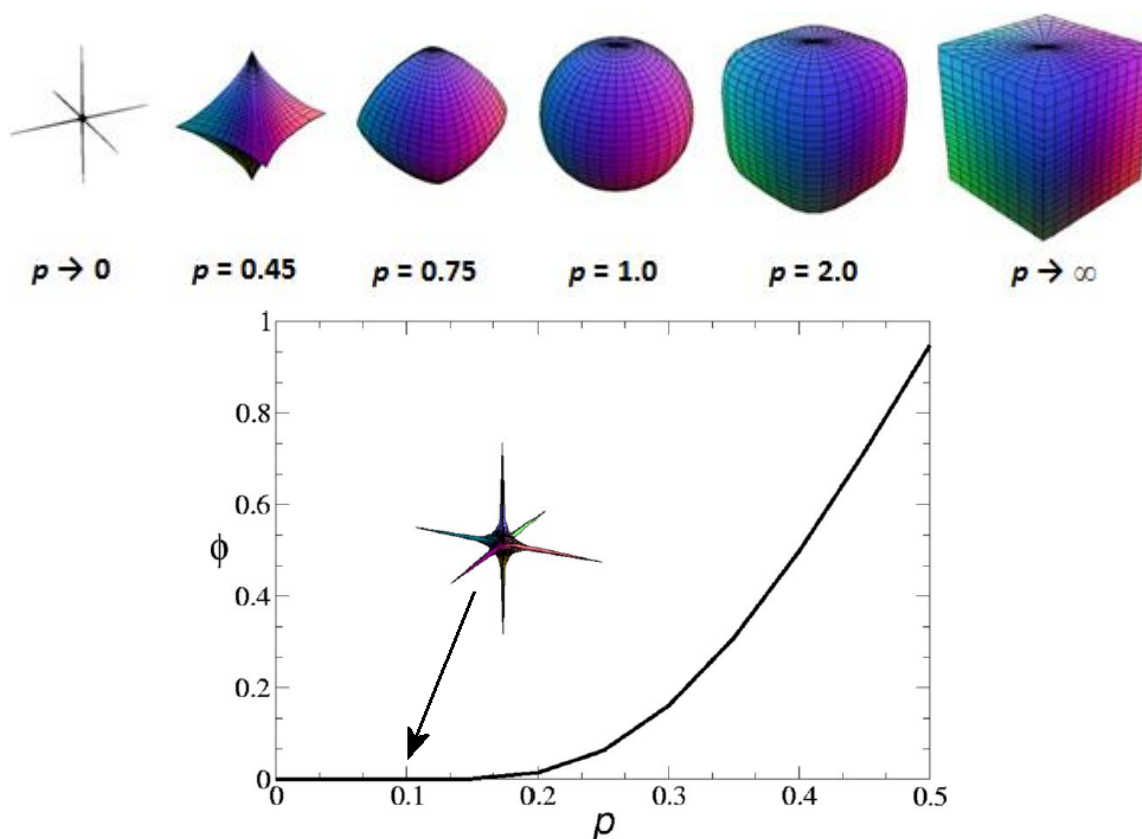


Fig 1.8a. Various three-dimensional shapes as defined by their deformation parameter ( $p$ ) (top), and packing efficiency ( $\Phi$ ) vs. deformation parameter ( $p$ ) for concave octahedral (bottom) with inset  $p = 0.1$  octahedra.

The authors studied various octahedra with varying degrees of concavity/convexity as measured by their deformation parameter where  $p = 0.5$  represents a regular octahedron,  $p < 0.5$  represents a concave octahedron, reaching the limit of three dimensional cross at  $p = 0$  and  $p > 0.5$  represents a convex octahedron, reaching a perfect cube at  $p = 1$  and a perfect sphere at  $p = \infty$ . They show that as the deformation parameter decreases and the sides of an octahedron become more concave, the packing efficiency also decreases with an increase in free volume and surface area. It was also shown that although convex octahedra reach a minimum packing efficiency ( $\Phi$ ) of around 0.75 for a sphere ( $p = 1$ ), concave octahedra are capable of exhibiting much lower packing efficiencies. It follows that concave molecular geometries will maximise the void space in a porous material. A classic example of such a molecule is triptycene (Fig 1.8b<sup>59</sup>).

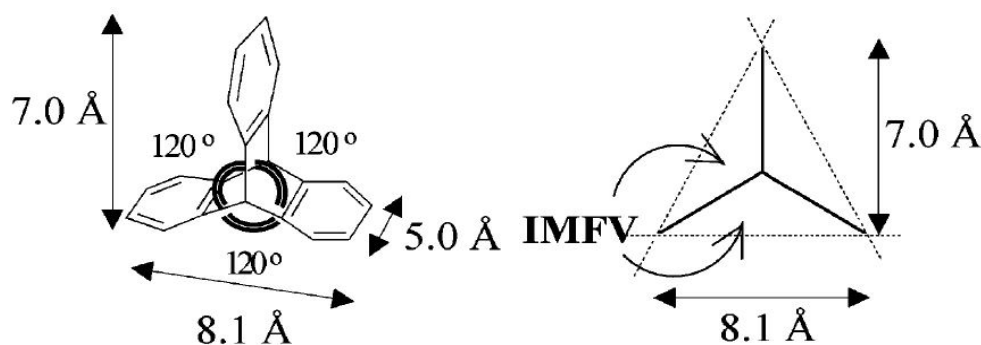


Fig 1.8b Triptycene molecule in perspective view (left) and schematic view (right) with dimensions calculated from the centroids of the hydrogen atoms at the extremities.

The triptycene molecule is a rigid, shape persistent, fused ring system that possesses concave surfaces. When constituent triptycene molecules come together to form a solid, they do so in an inefficient manner and form local cavities containing what has been coined as “internal molecular free volume” (IMFV)<sup>59, 60</sup>. Organic molecules which possess such properties are known as “*Organic Molecules of Intrinsic Microporosity*” (OMIMs)<sup>61</sup>.

The OMIM concept can be extended by using a multi-functionalised OMIM ( $f > 2$ ) as a core for dendrimer formation. A suitably functionalised OMIM core can be subjected to stepwise addition of subsequent OMIMs to give branched macromolecular structures with a higher internal molecular free volume than the sum of its parts (Fig 1.8c). These compounds are known as “*Dendrimers of Intrinsic Microporosity*” (DIMs)<sup>62</sup>.



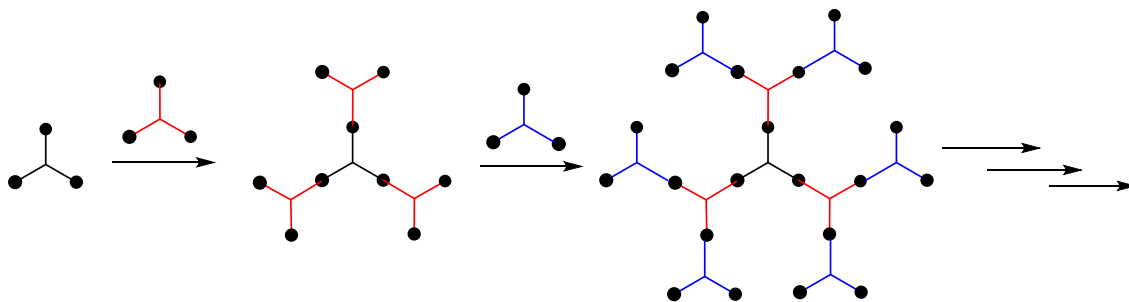


Fig 1.8c Schematic diagram of dendrimer formation.

Extending the OMIM concept even further, suitably functionalised OMIMs may be used as monomers that can be polymerised to form an amorphous solid composed of a large proportion of internal molecular free volume. This free volume arises from the concave molecular units of the polymer chain itself and also from the secondary structures that form from irregular folding and packing of the polymer chains (Fig 1.8d<sup>63</sup>). A polymeric material of this type belongs to the family known as *Polymers of Intrinsic Microporosity* (PIMs).

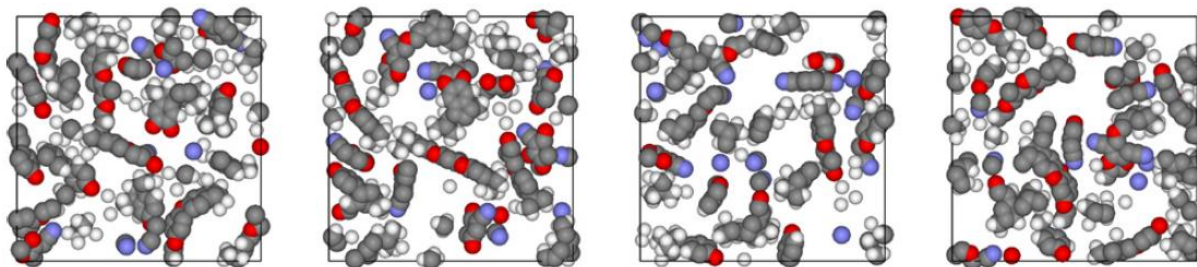


Fig 1.8d Packing model of PIM-1 represented as a sequence of 3.1Å slices through a 3D cube illustrating elements of free volume.

This family of polymers can trap large quantities of interconnected “free volume” at room temperature in the glassy state<sup>64</sup>. Unlike “rubbery” polymers (a polymer above its glass transition temperature), the thermal motion of the polymer chains in glassy polymers (a polymer below its glass transition temperature) is not energetic enough to homogenise the structure of the polymer which allows the presence of immobilised, interconnected and disconnected “microvoids” to be “frozen in” throughout the polymer. The free volume contained in these polymers is however only a transient property. PIMs are considered to be in a non-equilibrium state and free volume is lost over time by relaxation of the polymer chains into a dense solid. This is known as *physical ageing* and is observed markedly in thin membranes<sup>65, 66</sup>. This process is known to be reversed by soaking the material in a solvent such as methanol<sup>65</sup> which swells the polymer back to its non-equilibrium state. When PIMs are used to cast membranes, methanol is used to remove casting solvent and adsorbed species before permeation tests which has a profound effect on membrane properties.

Three main classes of PIMs have so far emerged based on molecular chain configurations: *Linear*, *Ladder* and *Network* PIMs (Fig 1.8e). In the case of most linear and ladder PIMs, there is also at least some degree of branching and cross-linking of the polymer chains.

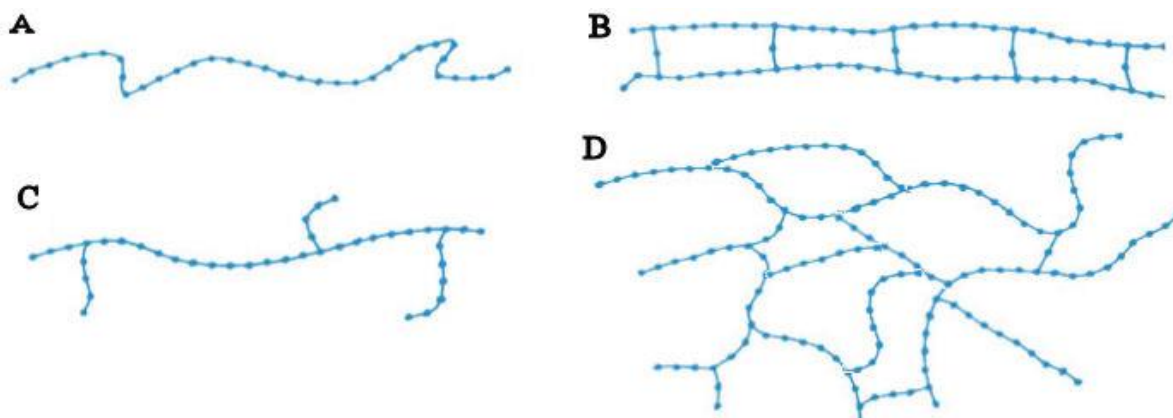


Fig 1.8e. Different PIM molecular chain configurations: A: Linear, B: Ladder, C : Branched, D: Network.

Linear polymers contain only a single bond between each monomer and are usually soluble. To create a linear high free volume polymer, the shape of the polymer chain must be contorted and rotation around the single bond must be hindered such that the chain remains rigid. Examples of high free volume polymers include polyacetylenes<sup>7, 67</sup>, perfluoropolymers<sup>68, 69</sup> and polynorbornenes<sup>70</sup>. To create a linear PIM such as a PIM polyimide<sup>71</sup>, monomers that also possess rigid and awkward molecular geometries must be incorporated.

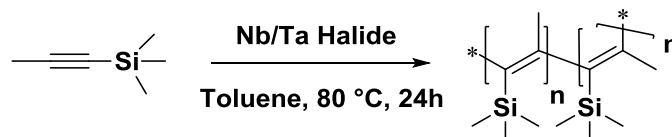
Ladder PIMs contain two bonds between each monomer and hence rotation is prevented. To create a microporous ladder PIM, both monomers and linking units must be rigid and at least one monomer must either possess an awkward molecular geometry such as triptycenes<sup>72</sup> or a site of contortion such as spirobisindanes<sup>73</sup>. A common method for producing soluble ladder PIMs is a double nucleophilic aromatic substitution reaction between an aromatic monomer functionalised with two sets of *ortho*-dihydroxy groups (catechols) and an aromatic monomer functionalised with two sets of *ortho*-difluoro groups (chlorine can also be used<sup>74</sup>). The polymerisation forms rigid dibenzodioxane linking units that inhibit twisting or bending between monomer segments. Some examples of ladder PIMs are PIM-1<sup>73</sup> and PIM-7<sup>75</sup>.

Network PIMs are formed from monomers and linkers that possess the same characteristics as ladder PIM monomers except at least one monomer is functionalised with a minimum of three sets of reactive groups. This causes the polymer to form an insoluble three dimensional porous structure. Some examples of network PIMs are Triptycene<sup>76</sup> PIMs and phthalocyanine<sup>77</sup> PIMs.

## 1.8.1: Linear Polymers

### 1.8.1.1: Polyacetylenes

The first glimpse of a polymer with a high free-volume was poly[(1-trimethylsilyl)-1-propyne] (PTMSP) reported by Masuda<sup>7</sup> in 1983. This glassy polymer was synthesised by the polymerisation of 1-(trimethylsilyl)-1-propyne with a range of niobium (V) and tantalum (V) halides (Scheme 1.8.1.1a). Studies by Izumikawa and co-workers found that NbCl<sub>5</sub> produced a more *cis*-rich polymer than TaCl<sub>5</sub> and hence different properties<sup>78</sup>.



Scheme 1.8.1.1a. Synthesis of poly[(1-trimethylsilyl)-1-propyne].

The polyacetylene backbone consists of a chain of trimethylsilyl substituted alkene units linked together via single carbon-carbon bonds. The alkene  $sp^2$  bond geometries force the polymer backbone into a staggered conformation while the bulky trimethylsilyl groups hinder polymer segment rotation around the single carbon-carbon bonds<sup>79</sup>. This rigid contorted structure causes the formation of microvoids when chains pack together leading to a BET surface area of  $550 \text{ m}^2 \text{ g}^{-1}$ <sup>80, 81</sup>.

PTMSP membranes exhibit extremely high gas permeabilities, particularly for oxygen, carbon dioxide and larger  $C_3+$  hydrocarbons<sup>82</sup>. PTMSP was considered the most permeable of all known polymers until 2008 when Masuda reported an indan based polyacetylene<sup>67</sup>. Membranes formed from PTMSP are more permeable to large hydrocarbon molecules than small gas molecules. This anomalous behaviour suggests solubility-controlled permeation; a property usually observed in rubbery polymers (see Background Theory, Chapter 2.3).

Due to its attractive properties, PTMSP was initially considered as a promising material for the fabrication of industrial membranes for the separation of hydrocarbon/hydrogen mixtures. The polymer however, has a poor chemical resistance to aliphatic and aromatic compounds found in the feed streams of interest and also suffers from rapid physical ageing where permeability decreases over time<sup>83</sup>. It has been found that cross-linking PTMSP using for example, bis aryl azides<sup>79</sup>, can improve the solvent resistance and reduce ageing of the polymer. Cross-linking however leads to a reduction in free volume and a compromise is made in permeability.

## 1.8.2: PIM Polyimides

Polyimides are classically synthesised by a cycloimidisation polycondensation reaction between bis-carboxylic anhydride and diamine monomers. Polyimides have received considerable attention in gas separation membrane applications as a result of high selectivities but with many, at the expense of lower permeabilities<sup>84</sup>. Some polyimides show higher permeabilities such as the widely available Matrimid®<sup>85</sup> polyimide (Fig 1.8.2a) although it suffers somewhat low permeability towards oxygen and carbon dioxide. Blending Matrimid with other polymers such as PIM-1 has been found to further improve both permeability and selectivity<sup>86</sup>.

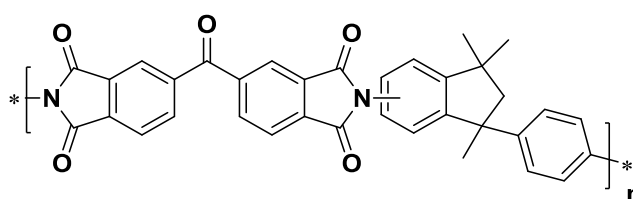


Fig 1.8.2a. Structure of the polyimide Matrimid®.

Highly permeable polyimides are known to be formed from diamines that place bulky functional groups adjacent to the imide linkage that restrict rotation. For example, polyimides formed from 4,4'-(hexafluoroisopropylidene)diphthalic anhydride (6FDA) with diamines such as 2,3,5,6-tetramethyl-1,4-phenyldiamine (4MPDA)<sup>87</sup> and 3,3'-dimethylnaphthidine (DMN)<sup>88</sup> (Fig 1.8.2b) are amongst the most permeable of conventional polyimides.

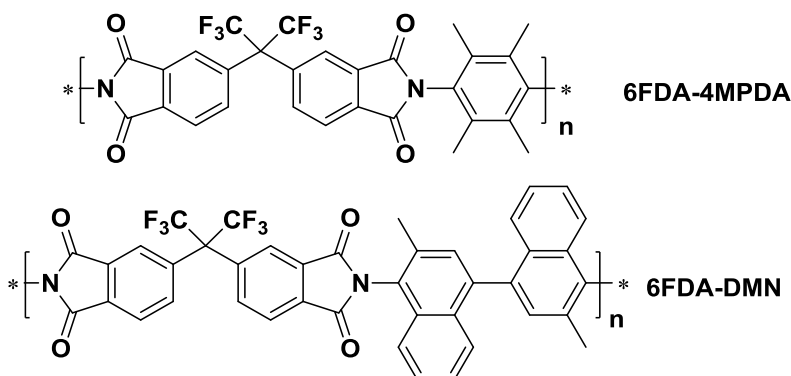
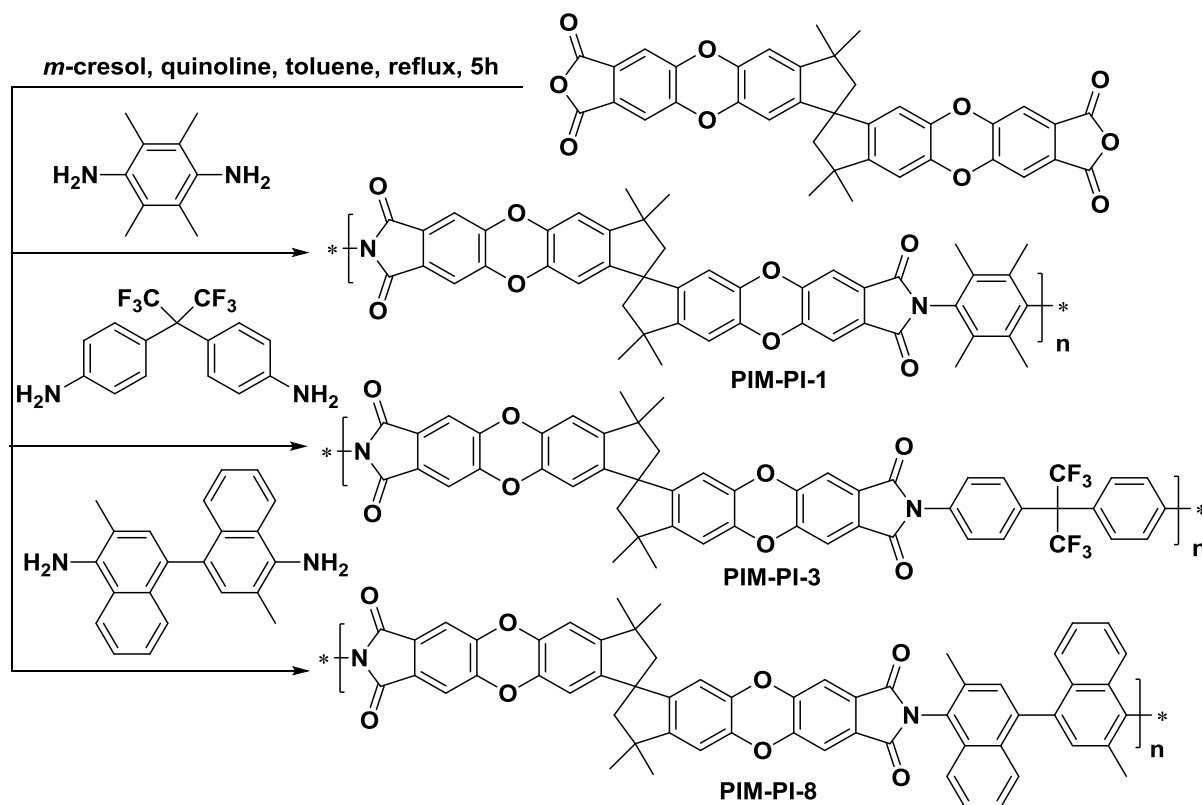


Fig 1.8.2b Structures of polyimides 6FDA-4MPDA and 6FDA-DMN.

PIM-polyimides are formed from rigid aromatic monomers, at least one of which possessing a site of contortion. The first examples of PIM polyimides were reported in 2008<sup>71</sup>. Three polyimides designated PIM-PI-1, PIM-PI-3 and PIM-PI-8 were prepared from the polymerisation of a bis-carboxylic anhydride functionalised spirobisindane monomer with three different diamines known for their success in conventional polyimides (Scheme 1.8.2a).



Scheme 1.8.2a. Synthesis of PIM-PI-1, PIM-PI-3 and PIM-PI-8.

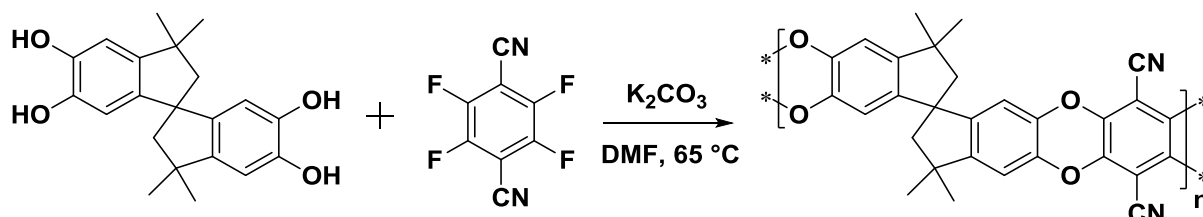
The spirobisindane unit is a very common structure used in PIM synthesis. The directions imposed by the spiro-centre (a single tetrahedral carbon centre shared by two rings) contained in these units force the geometry of the polymer segments into right angled orientations from each other. This site of contortion prevents efficient packing of the polymer chains and generates a large quantity of free volume compared to conventional polyimides.

Although PIM polyimides have only a single bond between monomeric units, rigidity is reinforced in PIM-PI-1 and PIM-PI-8 through bulky substituents groups adjacent to the imide linking bond, preventing rotation of polymer segments. Even though PIM-PI-3 has more flexibility in the chain, the hexafluoroisopropylidene unit provides a site of contortion leading to free volume. This enhanced rigidity is reflected in the BET surface areas measured: 480, 600 and 700  $\text{m}^2 \text{g}^{-1}$  for PIM-PI-3, PIM-PI-1 and PIM-PI-8 respectively. Each of these polymers were formed at moderate to high molecular weight and displayed excellent film forming properties. Membrane permeation experiments revealed permeabilities higher than conventional polyimides and selectivities higher than conventional PIMs<sup>89</sup>. Exceptional performance was obtained for PIM-PI-8 which demonstrates that when a site of contortion is present in both polymer segments and rotational freedom is restricted, higher surface areas and membrane permeabilities can be achieved.

### 1.8.3: Ladder Polymers

#### 1.8.3.1: PIM-1

PIM-1 is a spiro-polymer derived from the dibenzodioxane forming polymerisation reaction between the commercially available 2,3,5,6-tetrafluoroterephthalonitrile and 5,5',6,6'-tetrahydroxy-3,3',3',3'-tetramethyl-1,1'-spirobisindane (Scheme 1.8.3.1a)<sup>73</sup>.



Scheme 1.8.3.1a. Synthesis of PIM-1.

The resulting polymer is obtained as an amorphous fluorescent yellow powder of high molecular mass ( $M_w=140,000 \text{ g mol}^{-1}$ )<sup>64</sup>. The polymer is soluble in solvents such as tetrahydrofuran and chloroform from which it can be precipitated as a powder or cast into a robust self-standing film (Fig 1.8.3.1a<sup>90</sup>). The polymer exhibits a high BET surface area of  $860 \text{ m}^2 \text{ g}^{-1}$  and a micropore distribution in the range of 0.4-0.8 nm<sup>64</sup> (Fig 1.8.3.1a<sup>64</sup>). This is attributed to the awkward structure imposed by the rigid spirobisindane units and a rigid backbone comprised entirely of fused five and six membered rings, giving rise to highly contorted polymer chains that pack space inefficiently (Fig 1.8.3.1a<sup>90</sup>).

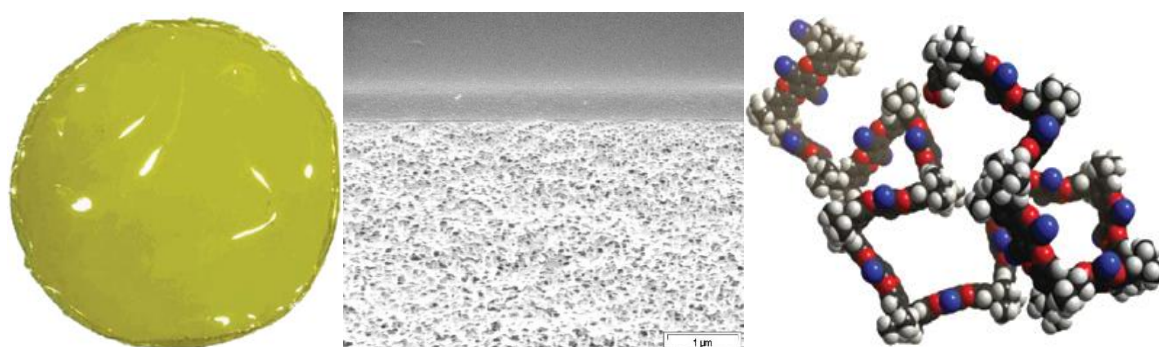


Fig 1.8.3.1a A PIM-1 membrane cast from THF (left), SEM cross-section image of a PIM-1 thin film membrane on a polyacrylonitrile support (middle), of model of a fragment of PIM-1 to illustrate contorted structure (left).

Initial gas permeation measurements on PIM-1 membranes revealed extremely high permeabilities and selectivities for several gas pairs and were only exceeded by high free volume polymers such as PTMSP<sup>91</sup>. In 2008, it was demonstrated that permeability may be substantially improved by removing the casting solvent and reversing physical ageing with

methanol treatment<sup>6</sup>. These impressive properties have attracted interest in a number of applications such as gas separation<sup>92</sup>, pervaporation<sup>8</sup> and sensors<sup>12</sup>.

There have been a number of investigations into tuning the gas transport properties of PIM-1 membranes by various research groups. In 2009, Guiver and co-workers reported the hydrolysis of pendent nitrile groups in a PIM-1 film forming a carboxylated PIM<sup>93</sup> (Fig 1.8.3.1b). It was shown that the polymer, with various degrees of hydrolysis with sodium hydroxide, has similar thermal and mechanical properties as PIM-1 but shows enhanced selectivity for a number of gas pairs (with a corresponding decrease in permeability).

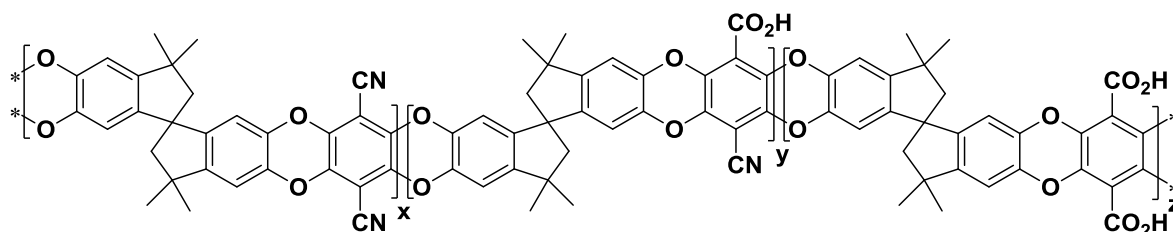
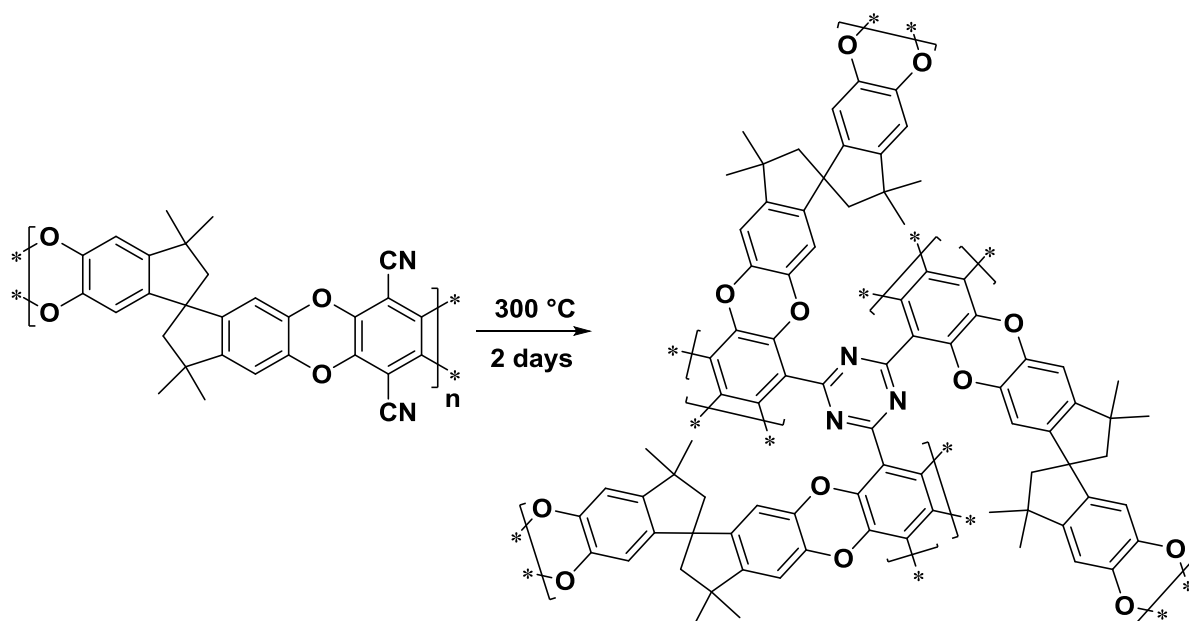


Fig1.8.3.1b. Structure of carboxylated PIM-1 with varying degrees of hydrolysis.

A research group at the University of Singapore reported in 2012 that PIM-1 can undergo a self-cross-linking reaction under thermal conditions forming triazine rings from pendent nitrile groups (Scheme 1.8.3.1b)<sup>94</sup>.

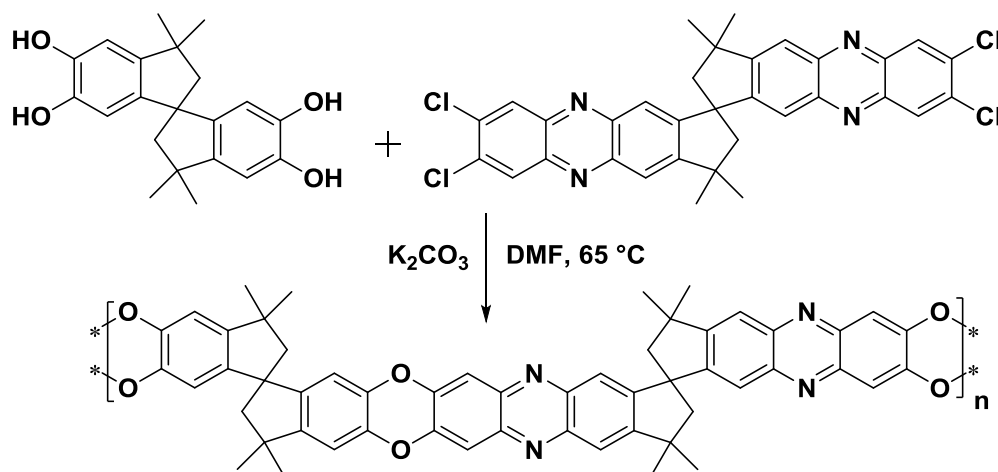


Scheme 1.8.3.1b. Synthesis of PIM-1.

The thermal cross-linking was found to enhance selectivity for a number of gas pairs (with a consistent decrease permeability). Most notable was an almost four fold increase in CO<sub>2</sub>/CH<sub>4</sub> selectivity over the parent PIM-1 membrane.

### 1.8.3.2: PIM-7

PIM-7 is a soluble ladder polymer derived from the dibenzodioxane forming polymerisation reaction between 5,5',6,6'-tetrahydroxy-3,3,3',3'-tetramethyl-1,1'-spirobisindane and a tetra-chloro functionalised spirobisindane bisphenazine monomer<sup>75</sup> (Scheme 1.8.3.2a).



Scheme 1.8.3.2a. Synthesis of PIM-7.

Like PIM-1, this polymer has a rigid and contorted backbone except both monomers contain a spiro-centred site of contortion. Replacement of the phthalonitrile units of PIM-1 with the phenazine units of PIM-7, does not have a considerable impact on the contorted structure of PIM-7 and has a similar but somewhat lower surface area of  $680 \text{ m}^2 \text{ g}^{-1}$ <sup>95</sup>. The presence of phenazine units does however offer the possibility of metal ion coordination. Addition of bis(benzonitrile)palladium (II) chloride solution to a yellow PIM-7 solution resulted in an immediate precipitation of a red powder which was found to contain over 20 % by mass of  $\text{Pd}^{2+}$  and remained microporous (BET surface area  $650 \text{ m}^2 \text{ g}^{-1}$ )<sup>75</sup>. It was inferred that that a palladium cross-linked polymer had been formed (Fig 1.8.3.2a). It was found that this material was an effective heterogeneous catalyst for Suzuki cross-coupling reactions<sup>64</sup>. It has also been shown that a PIM-7 film can be successfully cross-linked with  $\text{Pd}^{2+}$  ions, demonstrating a potential for reactive catalytic PIM membrane applications (Fig 1.8.3.2a)<sup>75</sup>.

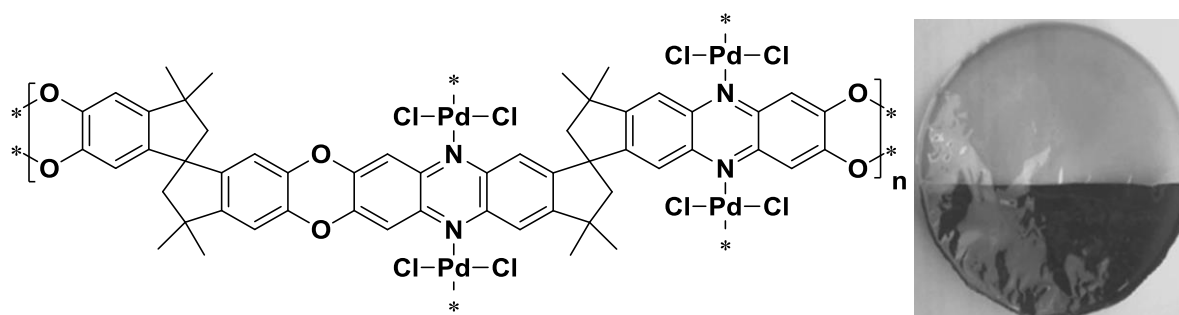


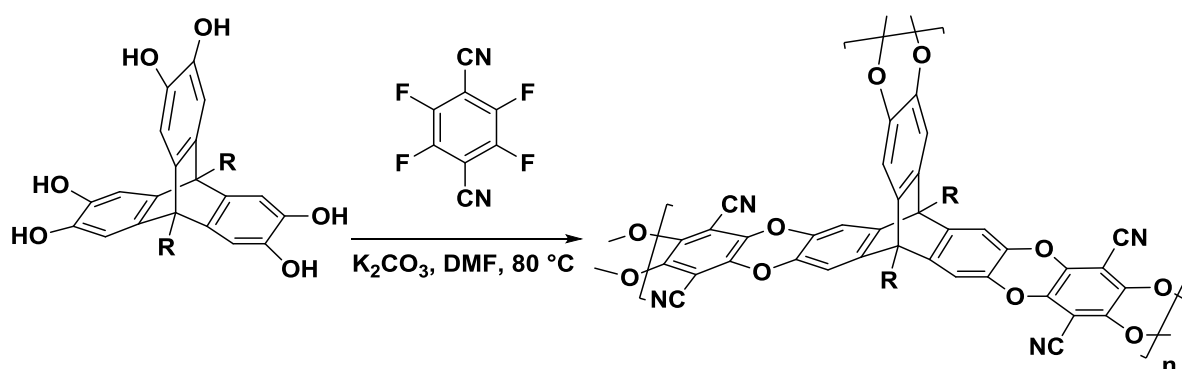
Fig 1.8.3.2a Structure of palladium cross-linked PIM-7 (left), a PIM-7 film in which the darker portion has been treated with (benzonitrile)palladium (II) chloride solution (right).



## 1.8.4: Network Polymers

### 1.8.4.1: Triptycene Network PIMs

The previously described triptycene molecules can be utilised as monomers in the formation of insoluble microporous network PIMs. A series of triptycene network polymers were reported in 2010 that demonstrate the ability to tune network PIMs for gas adsorption<sup>76</sup>. These network PIMs were constructed from catechol functionalised triptycene units with varying lengths of alkyl chains attached to the bridgehead position (R) which were polymerised with tetrafluorophthalonitrile linking groups at each of its three vertices (Scheme 1.8.4.1a).



Scheme 1.8.4.1a Synthesis of triptycene network PIMs. R = H, Me, Et, Pr, <sup>i</sup>Pr, Bu, <sup>i</sup>Bu, Pent, Oct, Bz.

The directions imposed by the three-fold symmetry of the triptycene units form a planar, ribbon-like structure that frustrates space efficient packing of the polymer chains. The "face-to-face" association of these ribbon-like fragments are further disrupted by the bridgehead alkyl groups acting as perpendicular struts (Fig 1.8.4.1a)<sup>76</sup>. It was found that short alkyl chains (H, Me, Et, Pr) lead to highly porous materials with Trip-Me-PIM giving the highest BET surface area of 1760 m<sup>2</sup>g<sup>-1</sup>. Increasing the length of the alkyl chains further caused a decrease in surface area due to an increasing proportion of the generated free volume becoming occupied by the flexible side chains (Fig 1.8.4.1a).

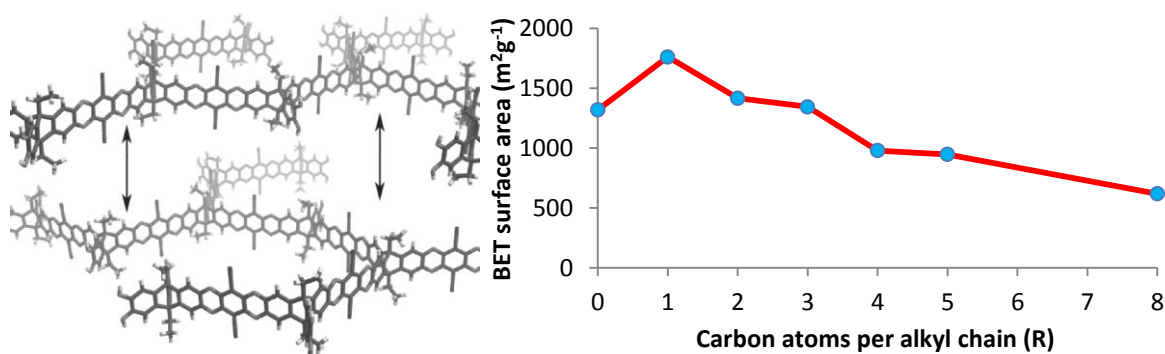
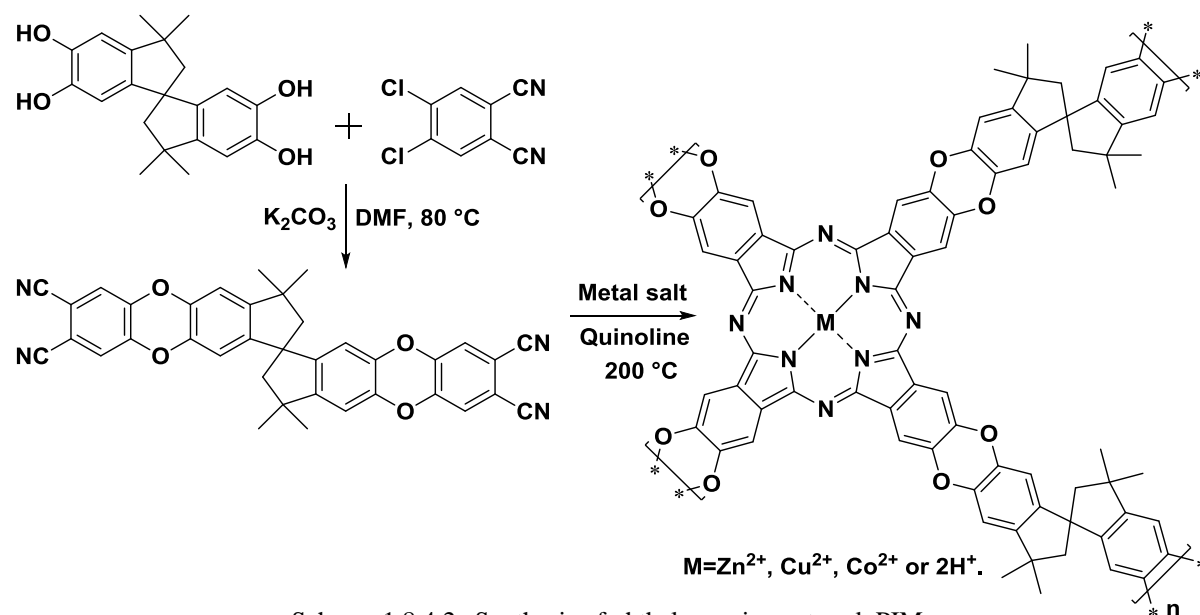


Fig 1.8.4.1a. Planar ribbon structure of Trip-Et-PIM (left), BET surface area Vs bridgehead alkyl chain length in triptycene network PIMs (0 = H, 1 = Me, 2 = Et, 3 = Pr etc.) (right).

### 1.8.4.2: Phthalocyanine Network PIMs

Phthalocyanines (Pcs) are rigid and thermally stable macrocycles that can bind a wide variety of guest cations inside a central cavity. A number of metal Pcs are well-established catalysts in applications such as the removal of thiols from gas streams by oxidation to disulfides with cobalt-Pcs<sup>96</sup>. While Pcs are known to be effective homogeneous catalysts, heterogeneous systems simplify recovery and reduce degradation/deactivation of the catalysts. To be utilised as a heterogeneous catalyst, a Pc must be immobilised in a porous solid such as a zeolite<sup>97</sup> or polymer<sup>98</sup>. Previous attempts to form Pc-network polymers resulted in non-porous materials due to the strong tendency of Pcs to aggregate resulting from non-covalent interactions<sup>99</sup>. Pc-network PIMs are formed from a spirobisindane bis(phthalonitrile) precursor which is synthesised from the dibenzodioxane forming reaction of 4,5-dichlorophthalonitrile with 5,5',6,6'-tetrahydroxy-3,3,3',3'-tetramethyl-1,1'-spirobisindane. Facilitated by a metal template, the bis(phthalonitrile) monomer undergoes a high temperature cyclotetramerisation reaction forming a network polymer (Scheme 1.8.4.2a) as a blue or green insoluble powder<sup>77</sup>.



Scheme 1.8.4.2a Synthesis of phthalocyanine network PIMs.

Pc-network PIMs have high BET surface areas ranging from 450-950 m<sup>2</sup> g<sup>-1</sup>, depending on the metal cation. This is attributed to the contorted spirobisindane linking units that prevent reorganisation of the Pc units into their preferred  $\pi$ -stacked configurations. Catalytic studies of the cobalt Pc-network polymer indeed demonstrated enhanced activity over lower molecular mass Pc catalyst analogues for a number of reactions such as the decomposition of hydrogen peroxide, the oxidation of cyclohexene and the oxidation of hydroquinone<sup>100</sup>.

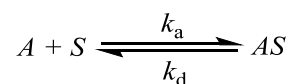
## **Chapter 2: Background Theory**

### **2.1: Determination of Surface Area**

Surface area determination of a well-defined and regular object such as a piece of paper is a simple task that requires no more than measurement with a ruler. If the shape of the object is irregular, ill-defined and possesses internal surface area such as a crumpled-up piece of paper, the measurement of surface area is no longer such a straight forward task. It becomes an even greater challenge when the surface to be measured is in the microscopic scale. There are a number of methods for quantifying the surface area of a material (i.e. the total area of the material that is accessible to a probe). These include: optical methods<sup>101</sup> and porosimetry using a non-wetting liquid such as mercury<sup>102</sup>. The most widely used technique for estimating the surface area of a material is gas adsorption.

The reversible physisorption of gas onto the irregular internal and external surfaces of a material can be exploited to quantify surface area. If the effective cross-sectional area of one gas molecule is known and a measured volume of the gas is adsorbed onto the surface of a microporous material, sufficient to form a monolayer, the surface area of the material can be calculated. To measure the surface area of a material, the sample is placed into a closed system of known volume and the adsorbate gas is adsorbed onto the surface of the sample at the saturation pressure and temperature of the adsorbate. A popular and convenient gas to use as the adsorbate is nitrogen, although in special cases hydrogen, carbon dioxide, argon and krypton may be used. To calculate the number of molecules adsorbed to a surface, a number of mathematical models have been developed to understand the processes that occur on the surface of a sample:

The free nitrogen gas molecules ( $A$ ), free surface sites ( $S$ ) and the adsorbed nitrogen ( $AS$ ) exist in a dynamic equilibrium in the system. The position of this equilibrium depends on the relative stabilities of the species, the temperature and pressure of the system. High pressure and low temperature are necessary to keep the surface saturated with gas molecules.



The extent of surface coverage can be expressed as a fraction i.e. fractional surface coverage ( $\theta$ ).

$$\theta = \frac{\text{Sites occupied}}{\text{Sites available}} = \frac{V_a}{V_m} \quad (2.1a)$$

Where  $V_a$  = Volume of gas adsorbed and  $V_m$  = Volume of gas in one monolayer. The fractional coverage of the surface depends on the pressure ( $P$ ) of the system. Variation of  $\theta$  with pressure at constant volume and temperature is known as an *adsorption/desorption isotherm*.

The Langmuir adsorption isotherm (developed by Irving Langmuir in 1916<sup>103</sup>) is the simplest physically plausible isotherm model which relates the number of molecules adsorbed to a surface at constant temperature. The rate of adsorption depends on the pressure ( $P$ ) and the number of empty sites ( $N(1-\theta)$ ) and the rate of desorption depends on the number of occupied sites ( $N\theta$ ). The rate of change of fractional surface coverage is given by:

$$\frac{d\theta}{dt} = k_a PN(1-\theta) - k_d N\theta \quad (2.1b)$$

At the point of equilibrium:  $\frac{d\theta}{dt} = 0$  and hence:

$$\theta = \frac{KP}{1 + KP} \quad (2.1c) \quad \text{Where: } K = \frac{k_a}{k_d}$$

This equation is generally presented in the  $y = mx + c$  form such that measurable data (volume of gas adsorbed,  $V_a$  and partial pressure,  $P$ ) can be plotted to allow  $V_m$  to be calculated by extrapolation of a straight line plot:

$$\frac{1}{V_a} = \frac{1}{KV_m} \left( \frac{1}{P} \right) + \frac{1}{V_m} \quad (2.1d)$$

The Langmuir adsorption isotherm is based on a number of assumptions:

- 1.) Adsorption cannot proceed beyond monolayer coverage.
- 2.) All surface sites are equivalent and can accommodate, at most, one adsorbed molecule.
- 3.) There are no adsorbate-adsorbate interactions.
- 4.) An adsorbed molecule is immobile.
- 5.) In the gas phase, the adsorbate behaves ideally.

The last assumption is usually reasonable but the remaining assumptions are seldom true and one would expect this model to be unreliable. However, ignoring surface non-uniformity results in an over estimation of average adsorption enthalpy while ignoring adsorbate-adsorbate interactions results in an under estimation of adsorption enthalpy. These two

opposite effects largely cancel out and the Langmuir isotherm generally gives results better than would be expected<sup>104</sup>.

In 1938, Brunauer, Emmett, and Teller<sup>105</sup> modified Langmuir's theory to allow for multilayer adsorption while retaining the other original assumptions (BET Theory).

BET theory makes the following assumptions:

- 1.) Gas molecules can physically adsorb to a surface in an infinite number of layers.
- 2.) There are no interactions between each adsorption layer.
- 3.) The Langmuir theory can be applied to each separate layer.

The resulting BET equation given by Brunauer, Emmett, and Teller is:

$$V_a = \frac{V_m CP}{P_0 - P \left( 1 + \frac{(c-1)P}{P_0} \right)} \quad (2.1e)$$

Which can be rearranged into the  $y = mx + c$  form:

$$\frac{P}{V_a(P - P_0)} = \frac{C-1}{CV_m} \left( \frac{P}{P_0} \right) + \frac{1}{CV_m} \quad (2.1f)$$

Where:  $V_m$  = Volume of gas in one monolayer (ml),  $V_a$  = Volume of gas adsorbed at (ml),  $P$  = Partial vapour pressure of the adsorbate gas in equilibrium with the surface at 77K (Pa),  $P_0$  = Saturation pressure of the adsorbate gas (Pa) and  $C$  is the BET constant (dimensionless) which is approximately given by:

$$C = \exp\left(\frac{E_1 - E_L}{RT}\right) \quad (2.1g)$$

$E_1$  is the heat of adsorption for the first layer and  $E_L$  is the heat of adsorption for second and higher layers and is approximately equal to the heat of liquefaction.

A plot of  $P/V_a(P-P_0)$  against  $P/P_0$  has been shown experimentally<sup>105</sup> to give a linear plot over the range  $0.05 \leq P/P_0 \leq 0.35$ . From this plot, the intercept ( $i$ ) and the gradient ( $m$ ) can be used to calculate the monolayer volume ( $V_m$ ) and the BET constant  $C$  as follows:

$$V_m = \frac{1}{m + i} \quad (2.1h)$$

$$C = \left( \frac{m}{i} \right) + 1 \quad (2.1i)$$

The specific BET surface area ( $S_{BET}$  ( $\text{m}^2\text{g}^{-1}$ )) of the sample is then calculated from  $V_m$  using the following equation:

$$S_{BET} = \frac{V_m N_A \sigma}{M V_{STP}} \quad (2.1j)$$

Where:  $N_A$  = Avogadro's constant ( $6.022 \times 10^{23} \text{ mol}^{-1}$ ),  $V_{STP}$  = Molar volume occupied by a gas at 273.15 K and 1 atm (22414 ml),  $M$  = Mass of sample,  $\sigma$  = Effective cross-sectional area of one nitrogen molecule ( $16.2 \text{ \AA}^2$ )<sup>106</sup>.

The specific BET surface area of the sample is calculated from at least three points in the  $0.05 \leq P/P_0 \leq 0.35$  region. The data points and subsequent calculations such as surface area and total pore volume are produced automatically by the BET surface area analyser apparatus (Fig 2.1a).



Fig 2.1a. A Coulter SA300 BET Surface Area Analyser

Due to the assumptions made in BET theory, there are a number of discrepancies between theoretical and experimental isotherms on which a number of papers have been published<sup>107</sup>. There is also an error in the measurement of sample mass, depending on the precision of the balance and therefore using a larger sample quantity will give a more accurate result. The surface areas obtained using this method are not “true” surface areas as adsorption is strongly influenced by micropore filling effects<sup>5</sup> such as capillary action giving higher than “actual” surface areas. The size of the gas molecules can also affect results if the molecule is too large to access smaller pores and so for example, nitrogen isotherms would not give comparable results to hydrogen isotherms. For these reasons, it is prudent to consider a surface area obtained by a BET isotherm as an “*apparent surface area*” and results should be treated with caution. BET isotherm experiments are however a convenient and very useful method for

measuring preliminary surface area characteristics and for comparison of the apparent microporosity between materials.

Each class of material (according to their pore size: microporous (< 2 nm), mesoporous (2-50 nm) and macroporous (>50 nm)) has a different adsorption isotherm profile. Six types of adsorption isotherms have been classified by IUPAC<sup>108</sup> (Fig 2.1b<sup>109</sup>).

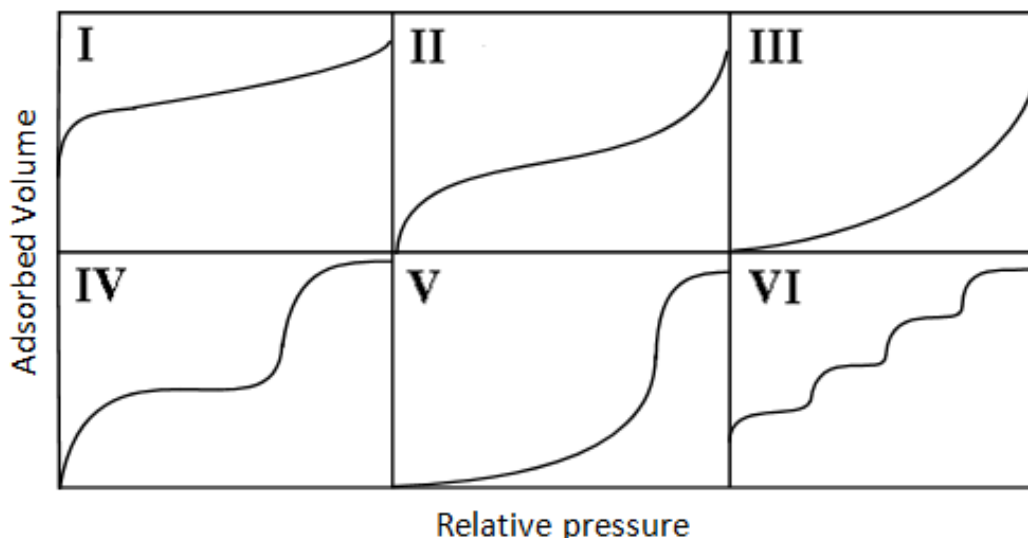


Fig 2.1b The IUPAC classification of adsorption isotherms.

Microporous materials show type I isotherms in which high surface areas allows a large gas uptake at low partial pressures, resulting in the isotherm climbing the y-axis until the surface becomes largely covered with adsorbate molecules. The plot then passes through an almost linear region from  $0.05 \leq P/P_0 \leq 0.35$  where the first monolayer is completed. Continuing past this region, more layers are built on top of the first layer and the pores fill up with the adsorbate until a saturation point is reached at  $P/P_0=1$ .

Mesoporous materials show type IV and V isotherms and macroporous materials show type II, III and VI isotherms. The steps in these isotherms correspond to step-wise formation of monolayers and the absence of steps indicates multilayer formation. Type IV and V isotherms also show a plateau at a partial pressure below the saturation pressure ( $P_0$ ) of the adsorbate gas. This can be explained capillary condensation of gas in the pores due to an increased number of Van Der Waals interactions between gas molecules inside the confined space of a pore. Desorption of a gas from a material can either be completely reversible (types I, II, III and VI) or not fully reversible (types IV and V). This results in hysteresis in the desorption isotherm which is associated with capillary condensation.

## **2.2: Membrane Technology**

Membranes formed from PIMs have many potential applications in industry and two important examples are pervaporation and gas separation:

Pervaporation is a separation process where one side of a membrane is in contact with a feed liquid and on other side, a vacuum is applied. The permeate vaporises from the feed liquid between the two sides of the membrane and the permeate is obtained as a vapour. This process has been used to break the water-alcohol azeotrope in the preparation of anhydrous alcohol and saves 60% energy over azeotropic distillation<sup>110</sup>.

Gas separation membranes have become increasingly more important in industry over the last 30 years since the company Monsanto launched the first commercial polysulfone “Prism<sup>®</sup>” hydrogen separating membrane in 1980<sup>4</sup>. Membranes have since been fabricated from a wide range of polymers such as polyacetylenes and polycarbonates<sup>111</sup>. Gas separation membranes have been widely used in industry to separate naturally occurring gas mixtures such as carbon dioxide from shale gas and industrial separation of nitrogen from air. This process involves a high pressure feed gas mixture which is forced through a membrane module that is designed to selectively retain one component. Gas separation processes operate with a pressure difference of up to 20 atm and the membrane material must be capable of withstanding such pressures. Dip-coating methods are used to prepare asymmetric membranes that consist of a thin layer of the active membrane material supported by a durable porous structure. For example GKSS (Geesthacht, Germany) has fabricated thin-film composite membranes consisting of a PIM-1 layer (yellow) on a porous polyacrylonitrile (PAN) support (Fig 2.2a)<sup>92</sup>.



Fig 2.2a. PIM-1/PAN Thin-Film Composite Membrane of 80 cm width.



Typical asymmetric membranes are 50 to 200  $\mu\text{m}$  thick with a 0.1 to 1  $\mu\text{m}$  active membrane layer. These asymmetric membranes can then be housed in a membrane module suitable for the intended application. There are a number of membrane module designs such as hollow fibre and plate/frame modules but the most popular design is the spiral wound membrane module (Fig 2.2b<sup>112</sup>).

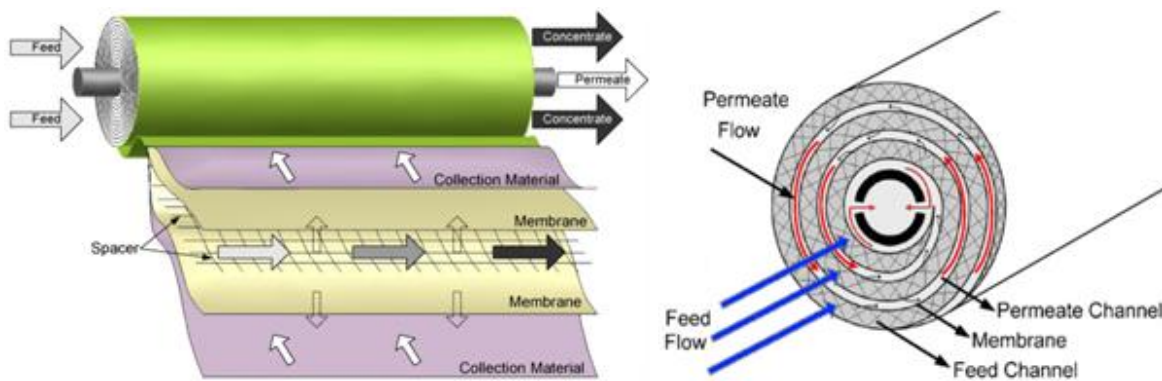


Fig 2.2b. Construction and Function of a Typical Spiral Wound Membrane Module.

A spiral wound membrane module consists of two asymmetric membrane sheets with a feed spacer sandwiched in between. This is then placed in between two sheets of a porous collection material and rolled around a perforated collection pipe into a spiral. The feed gas is passed down the axis of the module and passes in between the two membranes through the feed spacers. The gas then diffuses through the membrane material where it is enriched into the porous collection material. The permeate spirals down through the collection material to the centre of the module into a perforated collection pipe where the permeate is collected. The concentrate and permeate may then be passed into another module in series or in a cyclic flow of modules connected in parallel for further enrichment. An example of this technology is the UOP Separex™ membrane system in Egypt processing over 550 Million cubic feet per day of natural gas (Fig 2.2c<sup>113</sup>).



Fig 2.2c. UOP Separex™ membrane system in Egypt. Two of five racks shown (left), A single module (right).

## **2.3: Membrane Theory**

### **2.3.1: Mass Transport Through Membranes**

The most general definition of a membrane is “A *phase or a group of phases that lies between two different phases which is physically and/or chemically distinctive from both of them and which, due to its properties and force field applied, it is able to control mass transport between these phases*”<sup>114</sup>. The applied “force field” refers to the driving force that causes the permeate to flow through the membrane. This driving force may be a difference in pressure, temperature, concentration or electric potential across the membrane<sup>115</sup>. The ability of membranes to control mass transport of the permeate facilitates separation of mixtures into separate components or enrichment of one of these components. Separation membranes are usually solid materials that possess both physical and chemical properties which can be predicted solely from the chemical structure of the material<sup>115</sup>. These properties determine important characteristics of the membrane such as the membrane lifetime, permeability or flux, chemical and thermal stability and the interfacial interactions between the membrane and permeate, which lead to the selectivity of the membrane.

For gases, there are a number mechanisms<sup>116</sup> through which separation of permeate mixtures may be facilitated based on pore size (Fig 2.3.1a).

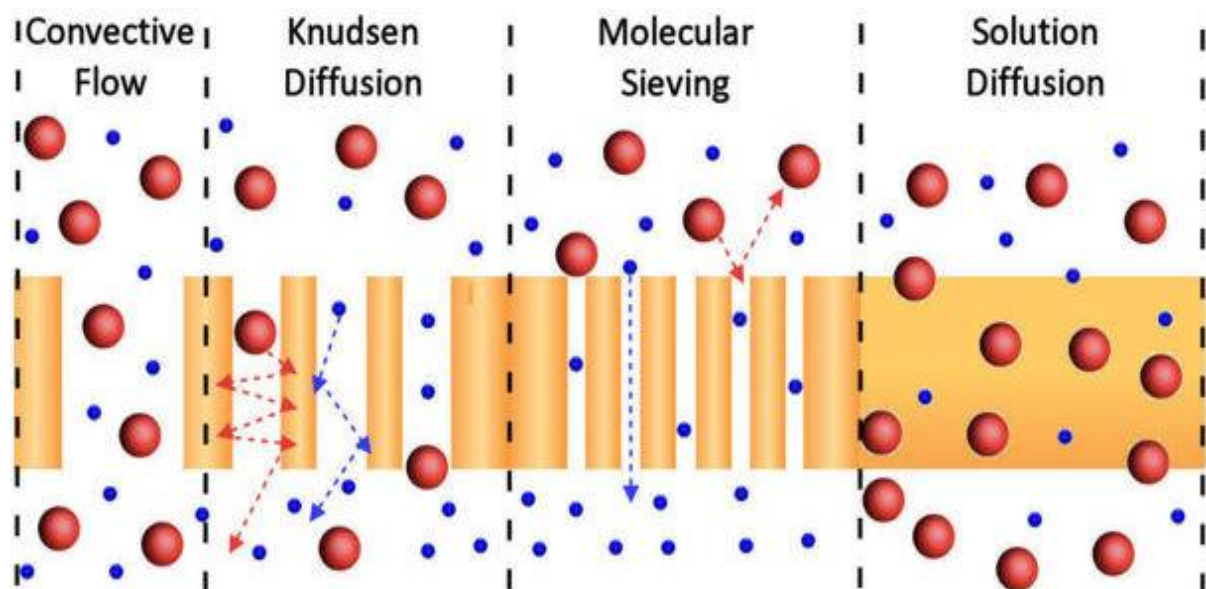


Fig 2.3.1a. Membrane Separation Mechanisms for Gases.

For relatively large pore sizes (0.1-10  $\mu\text{m}$ ), gases permeate the membrane by convection flow and there is no separation of the permeate mixture.

For pore sizes of 0.002-0.1  $\mu\text{m}$ , Knudsen diffusion occurs. The pores are large enough to accommodate both components of the gas mixture however, there is a difference in the mean free path for each component in the mixture based on the size of the molecule. This is due to larger molecules colliding with the pore walls with a greater frequency than smaller molecules. The transport rate for each component is inversely proportional to the square root of the molecular weight<sup>116</sup> (Graham's law of diffusion) and so smaller molecules (higher diffusion coefficient) permeate preferentially.

If the pore size is extremely small (0.0005-0.002  $\mu\text{m}$ ), molecular sieving occurs and separation is achieved through size exclusion. The surface pore size of the membrane blocks molecules over a certain kinetic diameter access to the pore channels and allows only smaller molecules to pass through the membrane. Transport through molecular sieve membranes involves both diffusion in the gas phase and diffusion of species adsorbed onto the surface of the pore walls (surface diffusion<sup>117</sup>).

For a membrane fabricated from a dense material such as a polymer, a process first proposed in 1866<sup>118</sup> known as solution-diffusion occurs. Separation is first facilitated by the differential solubility of components into the membrane surface from the gas phase on the feed side. There is then a difference in the rates of diffusion of each component through the dense regions of the membrane down a concentration and pressure gradient to the downstream surface (Fig 2.3.1b)<sup>119</sup>. There is a subsequent difference in the ability of components to evaporate from the membrane surface into the gas phase on the permeate side due to the difference in solubility<sup>111</sup>. This type of sorption obeys Henry's law of solubility<sup>114</sup> where the solubility of a gas in the polymer is directly proportional to the partial pressure of the gas.

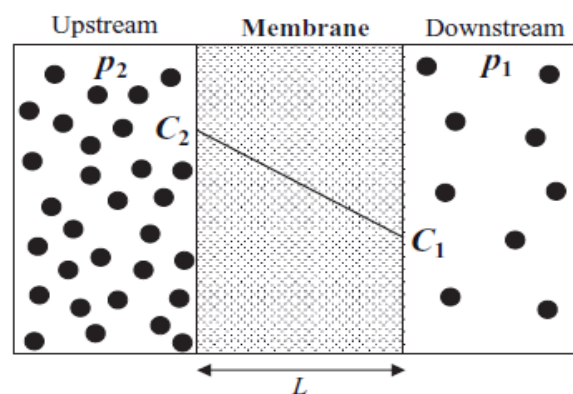


Fig 2.3.1b. A gas separation membrane with at concentration gradient across the membrane thickness  $L$ .

Unlike rubbery polymers, the structure of glassy polymers such as PIMs are not homogenised and contain a distribution of unrelaxed free volume elements. This results in significant deviation from Henry's law such as the dependence of the permeability, solubility and diffusion coefficients on permeate concentration, pressure and temperature<sup>120</sup>.

To explain this difference the dual-mode sorption model was proposed in 1976<sup>121</sup>. The dual-mode sorption model combines both Henry's law and Langmuir sorption models to explain the differences seen in experimental results between rubbery and glassy polymers. The model postulates that the permeate gas dissolved in the polymer can be divided into two phases, each with different diffusive properties in equilibrium (Fig 2.3.1c).

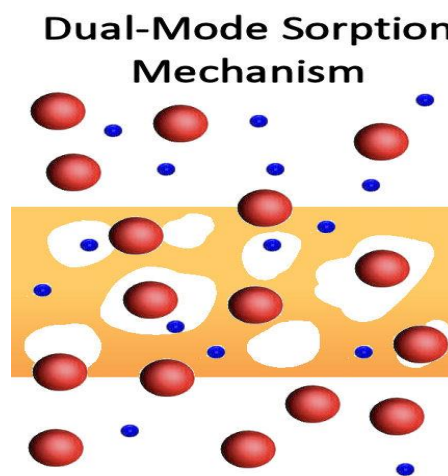


Fig 2.3.1c. Dual-Sorption model showing two sorption modes.

In glassy polymers, permeate dissolves in the bulk polymer (Henry's law type sorption) where diffusion may take place and there is also immobilised permeate inside a number of transient microvoids distributed throughout the polymer (Langmuir type sorption). The number of Langmuir sorption sites is then directly related to the free volume of the polymer. Diffusion takes place through a "hopping" type mechanism<sup>119</sup> where penetrant molecules are trapped inside free volume elements until they find enough energy to "hop" into the next free volume element. The energy barrier to achieve this depends on a number of factors such as the size of penetrant molecule, temperature, concentration, polymer rigidity and the degree of the interconnectivity of free volume elements.

### 2.3.2: Transport Parameters

The permeability coefficient  $P$  is defined as the ratio between the flux  $J$  (volume of the permeate passing through a unit area of the membrane per unit time) and its concentration gradient  $\Delta_C$  over the membrane of thickness  $l$  and is measured in "Barrer" (1 Barrer =  $10^{-10}$  (cm<sup>3</sup>(STP)/cm s cmHg).

$$P = \frac{J}{\Delta_C / l} \quad (2.3.2a)$$

The solution-diffusion model postulates that the permeability coefficient  $P$  of a gas passing through a membrane is the product of the solubility coefficient and the diffusion coefficient.

$$P = SD \quad (2.3.2b)$$

Where the solubility coefficient  $S$  is an equilibrium component and is a measure of the volume of dissolved gas per unit volume of polymer per unit pressure (cm<sup>3</sup> cm<sup>-3</sup> bar<sup>-1</sup>). The diffusion or diffusivity coefficient  $D$  is a dynamic component and is a measure of the rate which the permeate moves through volume of the porous material ( $10^{-12}$  m<sup>2</sup> s<sup>-1</sup>).

The selectivity or "permselectivity" ( $\alpha$ ) is a measurement of the potential gas separating ability of the membrane. The ideal selectivity of a gas pair is obtained as the ratio of the permeability coefficient for each of the two gases.

$$\alpha_{XY} = \frac{P_x}{P_y} \quad (2.3.2c)$$

The selectivity of a membrane has a contribution from both the solubility and diffusion coefficients and so the selectivity for a gas pair can be decoupled into solubility-selectivity and diffusivity-selectivity:

$$\alpha_{XY} = \frac{S_x}{S_y} \cdot \frac{D_x}{D_y} \quad (2.3.2d)$$

It is customary to report the selectivity values for each gas with respect to the permeability of nitrogen ( $\alpha (P_x/PN_2)$ ), ( $\alpha (S_x/SN_2)$ ) and ( $\alpha (D_x/DN_2)$ ) as it is usually the least permeable of the gases.

The basis for selectivity lies in the chemical and physical properties of the material from which the membrane is fabricated and how the material interacts with different gases. For example the addition of polar functional groups to a polymer will increase the interactions

between the polymer and the permeate via dipole/dipole or induced dipole moments. This in turn will change the order in which different gases permeate the membrane preferentially. The selectivity of a membrane can give insight into the mechanisms of separation occurring by studying order of permeability coefficients for each gas.

Molecular sieving type materials are more permeable to gas molecules with smaller kinetic diameters ( $d_k(\text{\AA})$ ) than to larger diameters and so the order of gas permeabilities are typically: He (2.6)>H<sub>2</sub> (2.89)>CO<sub>2</sub> (3.3)>O<sub>2</sub> (3.46)>N<sub>2</sub> (3.64)>CO (3.76)>CH<sub>4</sub> (3.8)<sup>122</sup>. This type of membrane is known as "*forward selective*". For membranes working under the solution-diffusion mechanism, the orders of gas permeabilities are typically: CO<sub>2</sub>>H<sub>2</sub>>O<sub>2</sub>>He>CH<sub>4</sub>>CO>N<sub>2</sub>. This type of membrane is known as "*reverse selective*". The reason for this order stems from the relative differences in solubility and diffusion coefficients of the gases. For example, below is a plot (Fig 2.3.2a<sup>123</sup>) of the Lennard-Jones collision diameter of a number of gases Vs the solubility and diffusion coefficients for a natural rubber membrane.

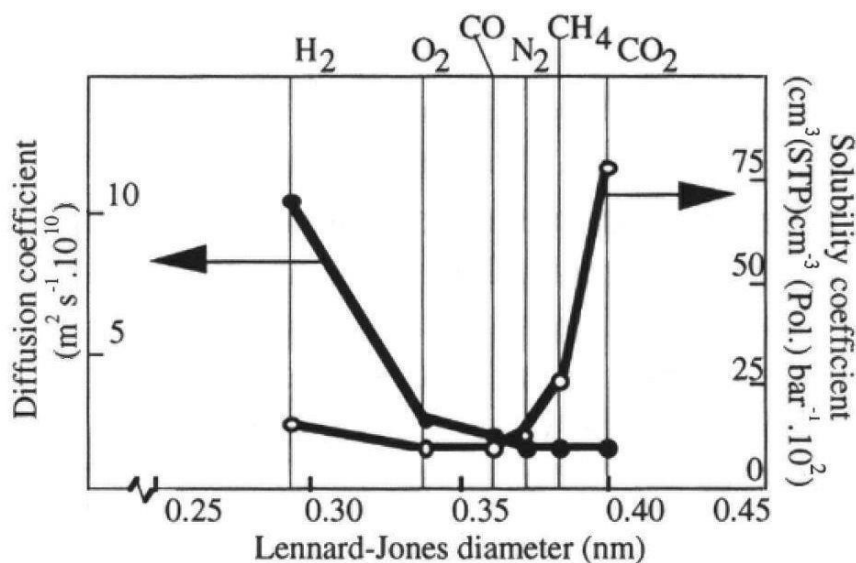


Fig 2.3.2a. Lennard-Jones Diameter of Gases Vs Solubility & Diffusion Coefficients for a Natural Rubber Membrane.

In many cases, as the diameter of the penetrant gases increase, the diffusion coefficients decrease. As the diameter of the penetrant gas increases, the "condensability" (critical temperature increases) of the gas generally increases, along with the solubility coefficient. Using the solution-diffusion model ( $P = SD$ ), a plot below of the Lennard-Jones collision diameter Vs the permeability coefficients for the same natural rubber membrane (Fig

2.3.2b<sup>123</sup>) shows the relative permeability of the gases in the order  $\text{CO}_2 > \text{H}_2 > \text{O}_2 > \text{CH}_4 > \text{CO} > \text{N}_2$ .

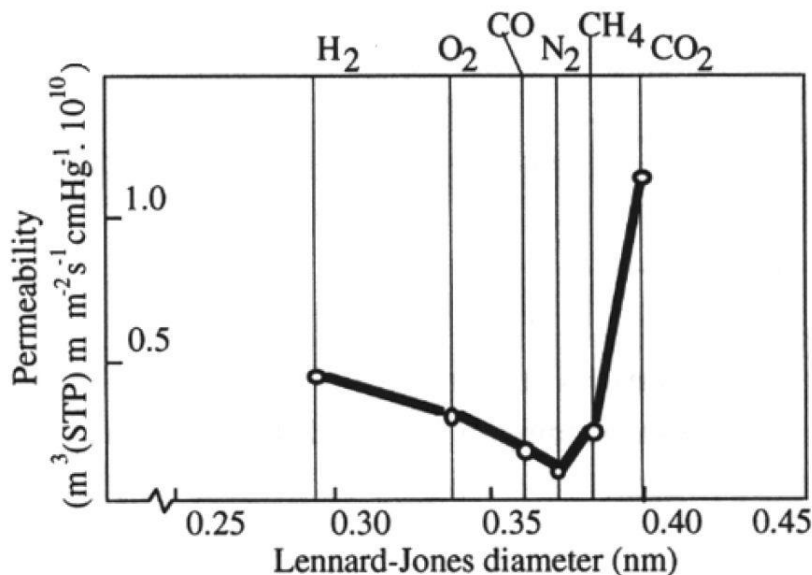


Fig 2.3.2b. Lennard-Jones Diameter of Gases Vs Permeability Coefficients for a Natural Rubber Membrane.

This trend is seen for a wide range of polymers such as polytrimethylsilylpropyne (PTSMPP) and polydimethylsiloxane (PDMS) most of which contain a minima for nitrogen which is due to combined low solubility and diffusivity<sup>124</sup>.

For high free-volume rubbery polymers, the solubility selectivities tend to be high and are more useful for separating larger permeates such as organic vapours<sup>82</sup>. The rigid nature of conventional low free-volume glassy polymers decreases the mobility of gases. The diffusion selectivities become dominant and are more useful for separating light gases<sup>82</sup>. Conventional low free-volume glassy polymers however, lack the permeability required for practical applications. It has been found that attempts to modify polymers to improve the permeability leads to a commensurate decrease in selectivity and increasing selectivity tends to decrease permeability<sup>125</sup>. This inverse relationship between permeability and selectivity is common for all polymers. Lloyd Robeson suggested there was an upper limit for this trade off relation in 1991<sup>126</sup>. Robeson visually demonstrated this by plotting the selectivity Vs permeability transport parameters collected from a large number of polymers in double logarithmic plots for a number of binary gas pairs (Fig 2.3.2c<sup>127</sup>). Robeson projected a semi-empirical upper limit onto the plot above which no values existed; currently known as the "*Robeson (1991) upper bound*". In 1991 this upper bound represented the maximum performance of known

membrane materials and any membrane performing to the upper right of this limit was an advancement over the present technology. Over the next 17 years there were a number of advancements in membrane technology with the appearance of materials such as PIMs. With their ultra-high free-volumes, PIMs combine high selectivities with high permeabilities which transcend Robeson's 1991 upper bound.

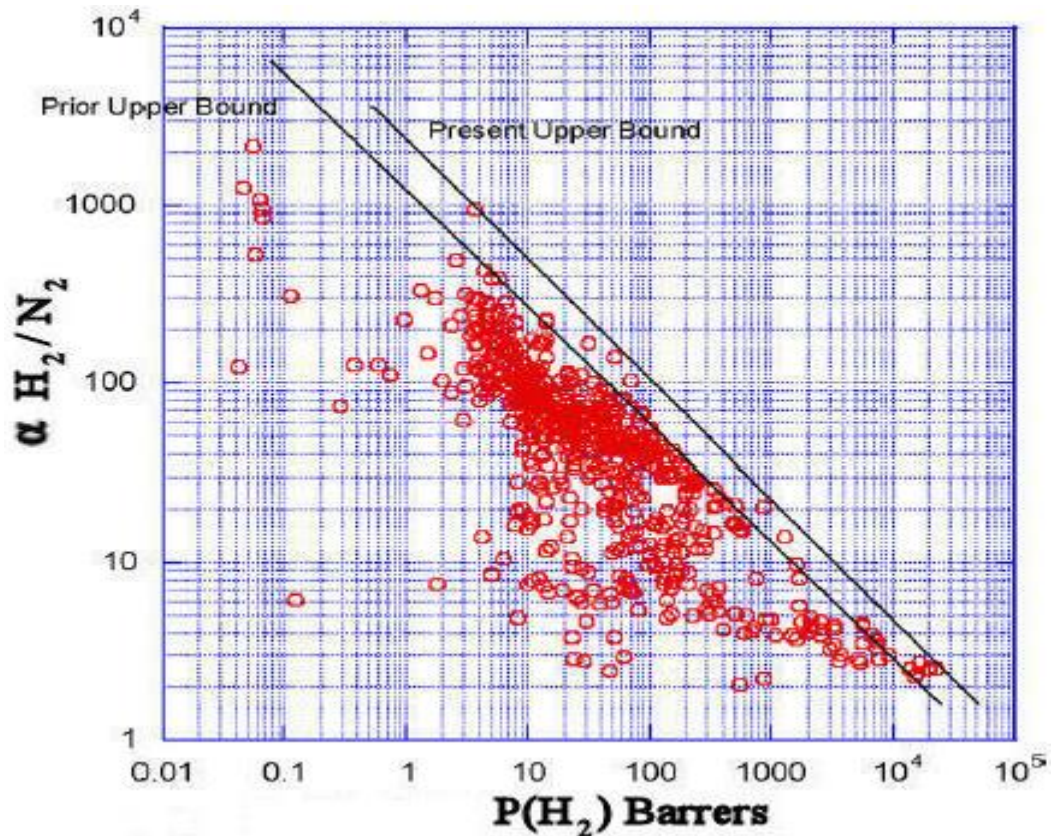


Fig 2.3.2c. Robeson Plot for  $H_2/N_2$  Showing Present and Prior Upper-Bound.

Due to these advancements, Robeson revisited the upper-bound in 2008<sup>127</sup> and updated the plot with a new upper limit known as the "*Robeson (2008) upper bound*". This is still the present day upper limit of membrane performance with few membrane materials performing over this upper-bound. In addition to reporting transport parameters for a membrane material in literature, it is also very common to communicate the performance characteristics graphically in a Robeson Plot to characterise a membrane material. Placing the results of permeation tests on the Robeson plot allows comparison of performance to other known materials. One factor, among many, that determines if a new membrane material will be a viable replacement for industrial separation of gas mixtures such as  $O_2/N_2$ ,  $CO_2/CH_4$ ,  $H_2/CH_4$  and  $He/H_2$ , is that its performance must circumvent the present day Robeson threshold<sup>126</sup>.



## 2.4: Measurement of Transport Parameters

Low pressure single gas permeation experiments were carried out in a fixed volume/pressure increase instrument (Fig 2.4a) by ITM CNR (Calabria, Italy), constructed by GKSS (Geesthacht, Germany), a schematic of which is shown in (Fig 2.4b)<sup>128</sup>. This apparatus allows determination of all three fundamental transport parameters  $P$ ,  $S$  and  $D$ .

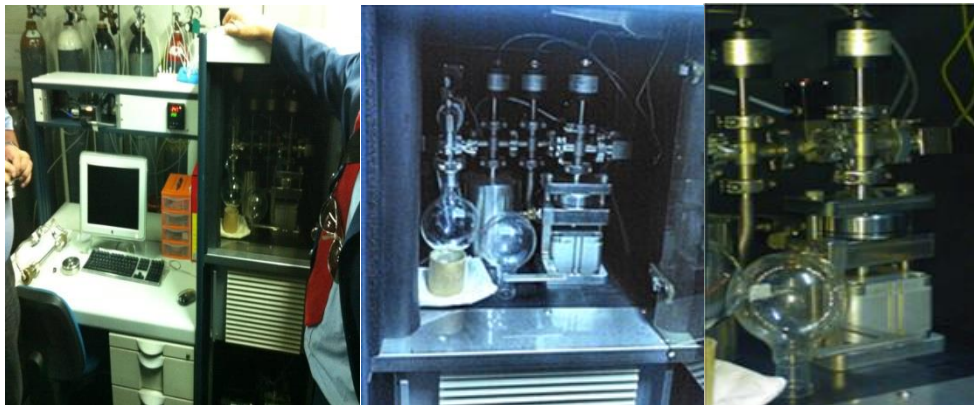


Fig 2.4a. Fixed volume/pressure increase apparatus used at ITM CNR.

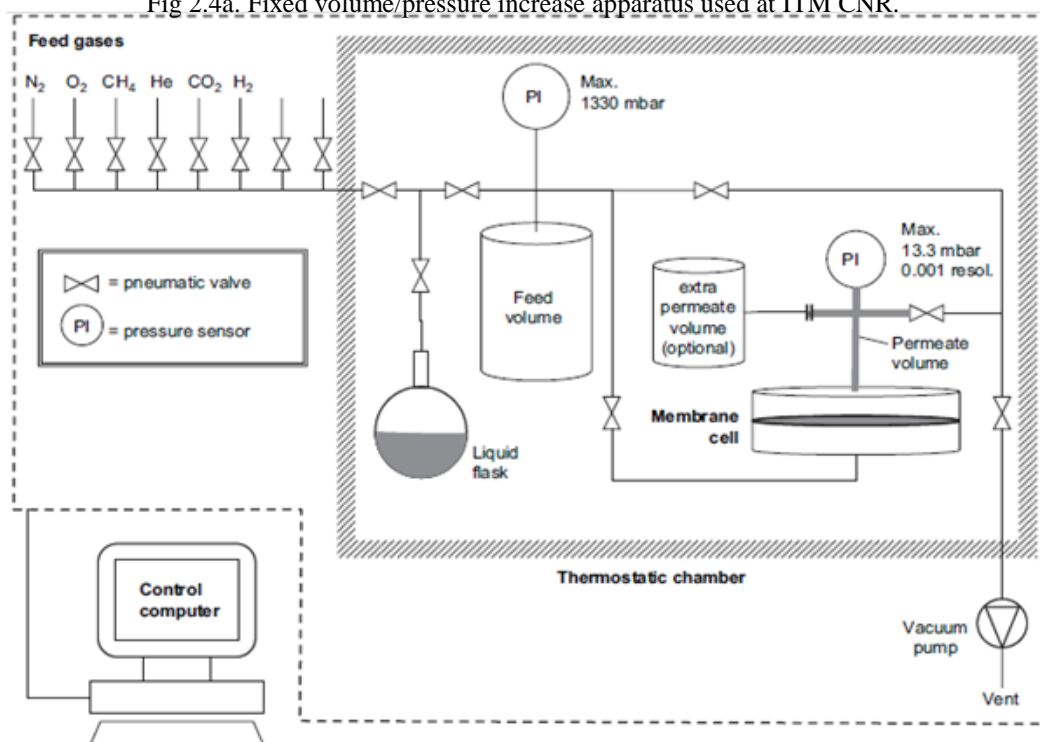


Fig 2.4b. Schematic diagram of fixed volume/pressure increase apparatus used at ITM CNR

The apparatus consists of a membrane cell in which the membrane is placed and a series of valves and pressure sensors which serve to pass a range of gases through the membrane while monitoring the pressure changes on one side of the sample. The crucial parts of the setup are

placed in a thermostatic chamber which allows measurements at a chosen constant temperature.

The measurement of transport parameters is based on the determination of the pressure increase rate of the fixed permeate volume upon exposure of the membrane to the pure gas.

The system is first evacuated using a two stage rotary vacuum pump for 10-20 min to remove dissolved gases and vapours from the membrane and rubber seals. The feed volume is then filled with the gas under study and closed off. The experiment is then started by a computer which simultaneously opens a valve to expose the membrane to the feed volume while monitoring the pressure of the fixed permeate volume. The computer will then plot a permeate pressure against time curve (Fig 2.4c<sup>128</sup>). If a closed feed volume is used then the feed pressure decreases according to the amount of permeating gas. When the feed volume and pressure is much larger than that of the permeate, a constant feed pressure can be assumed. For a constant feed pressure, the permeate pressure will increase asymptotically to the feed pressure (Fig 2.4c left).

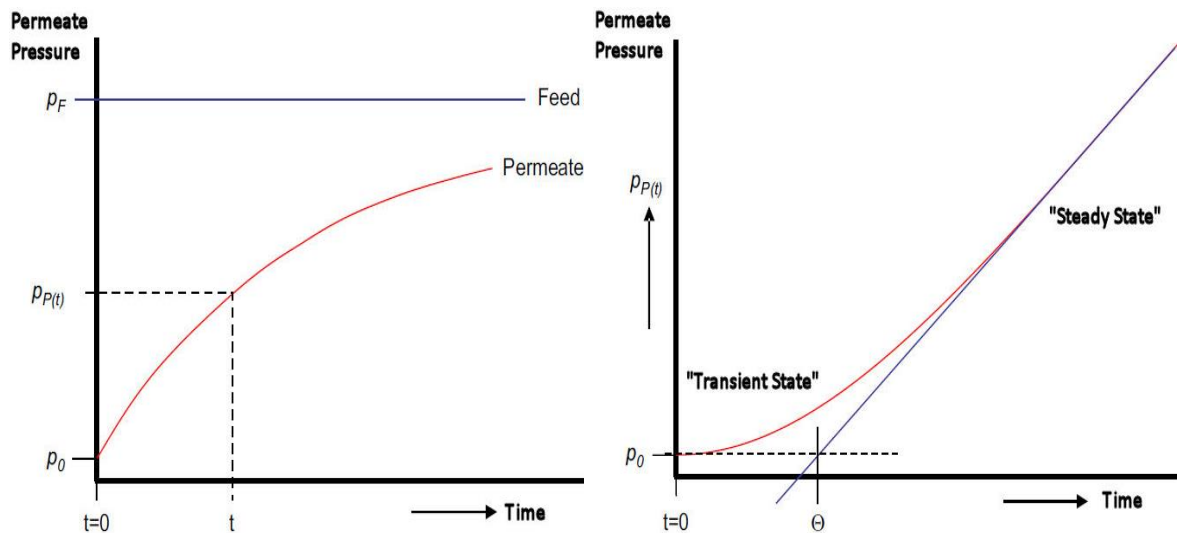


Fig 2.4c. Permeate pressure increase curve (left) and time-lag curve with steady state tangent line (right).

At the beginning of the experiment, the permeate pressure/time curve passes through two distinct regions (Fig 2.4c right). The first region is known as a "transient state" where there is a time-lag from the when the membrane is exposed to the feed volume to when the permeate pressure starts to increase into a linear region known as the "steady state". A straight line tangent can be extrapolated which obeys the following "quasi steady state condition"<sup>129</sup>

$$P_t = P_0 + \left( \frac{dP}{dt} \right)_0 \cdot t + \left( \frac{RT \cdot A}{V_p V_m} \cdot \frac{P_f \cdot P}{l} \right) \left( t - \frac{l^2}{6D} \right) \quad (2.4a)$$

Where:  $P_t$  is the permeate pressure at time  $t$ ,  $P_0$  the starting pressure,  $(dP/dt)_0$  the baseline gradient (accounts for the starting pressure and the baseline slope and is normally negligible in the case of well evacuated defect free samples),  $P_f$  the feed pressure,  $P$  the permeability coefficient,  $R$  the universal gas constant ( $8.3144 \text{ JK}^{-1}\text{mol}^{-1}$ ),  $T$  the absolute temperature ( $298.15 \text{ K}$ ),  $A$  the exposed membrane area ( $2.14 \text{ cm}^2$ ),  $V_p$  the permeate volume,  $V_m$  the molar volume of the permeating gas at standard temperature and pressure ( $0 \text{ }^\circ\text{C}$  and  $1 \text{ atm}$ ) and  $l$  is the membrane thickness.

Extrapolation of the tangent line to the time axis gives the time-lag ( $\theta$ ) from which the diffusion coefficient ( $D$ ) can be calculated:

$$D = \frac{l^2}{6\theta} \quad (2.4b)$$

The permeability coefficient ( $P$ ) can then be calculated from the steady state pressure increase rate:

$$P = \frac{V_p \cdot V_m \cdot l}{RT \cdot A \cdot P_f} \cdot \left[ \left( \frac{dp}{dt} \right) \cdot \left( \frac{dp}{dt} \right)_0 \right] \quad (2.4c)$$

The solubility coefficient ( $S$ ) can then be calculated assuming the validity of the solution-diffusion transport mechanism:

$$S = \frac{P}{D} \quad (2.4d)$$

It is important to note that the permeabilities and selectivities determined by this method are not for "real" gas mixtures since only a single gas is tested per experiment. A real gas mixture may behave differently, for example, if a polymer has a high affinity for a certain gas, liquid or vapour which causes the membrane to swell, the permeability of other penetrants may be affected<sup>130</sup>. Other, more advanced methods may be used to determine gas transport parameters for mixed gases such as reverse-phase gas chromatography<sup>131</sup> although single gas permeation measurements provide very useful information for preliminary characterisation of membrane materials. Until pilot tests using true mixed-gas feed streams containing real impurities such as moisture and hydrogen sulfide are successful, the likelihood of commercial application remains limited.

## Chapter 3: Research Aims

Incorporation of polar functional groups into gas separation membranes has been known to dramatically alter mass transport properties<sup>119, 132, 133</sup>. One avenue of research has focused on using amine functionality to increase polymer affinity towards CO<sub>2</sub> for carbon capture applications.

Recently in 2014, Budd and co-workers<sup>132</sup> reported reducing the nitrile groups on PIM-1 to primary amines. The result was an increase in CO<sub>2</sub> affinity which lowers CO<sub>2</sub> diffusion and permeability, placing data for H<sub>2</sub>/CO<sub>2</sub> over the present Robeson upper bound. Primary amine functionality however, often decreases free volume in porous materials due to hydrogen bonding. Polymers containing neutral tertiary amine functionality such as thermally rearranged polyimides<sup>134, 135</sup> (TR polymers) eliminate this effect while maintaining high selectivity towards CO<sub>2</sub>.

The aim of the research reported in this thesis is to synthesise a number of novel soluble polymers of intrinsic microporosity containing tertiary amine functionality. These polymers can then be cast into films and their membrane gas transport parameters evaluated by our collaborators at The Institute of Membrane Technology (ITM) CNR (Calabria, Italy).

The synthesis of five classes of tertiary amine polymers was attempted, each containing a range of different monomeric units (Fig 3a).

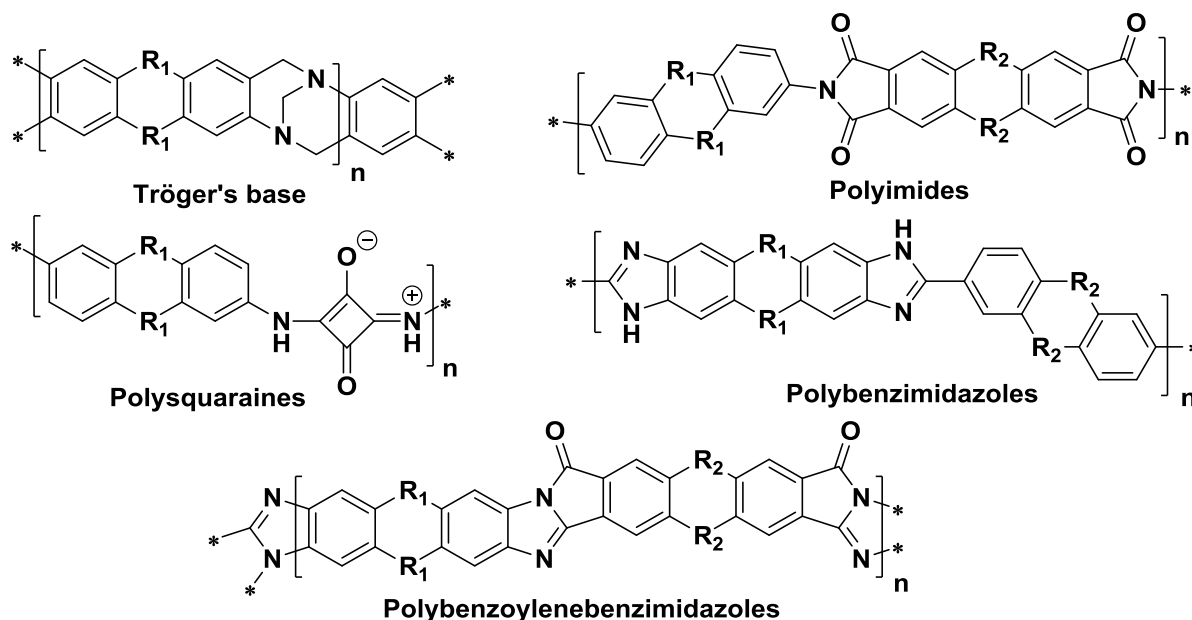


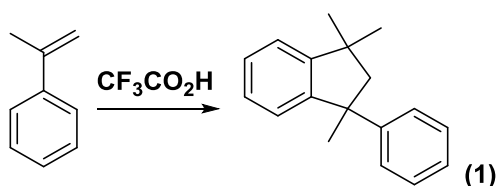
Fig 3a General structures of the five classes of polymer reported in this thesis. R<sub>1</sub> & R<sub>2</sub> are moieties contained within a range of different monomers used for this research.

## **Chapter 4: Monomer Synthesis**

While a small number of polymers reported in this thesis are synthesised from monomers purchased from commercial sources, the majority were formed from monomers that were prepared specifically for the project. The synthetic monomers were based on anthracene, ethanoanthracene, phenylindane and spirobisindane. The general synthetic strategy for the formation of these monomers was first, formation of the hydrocarbon skeleton, followed by post-functionalisation of the preformed units. Depending on the type of polymer in question, there are a number different functionalities that the monomers described in this thesis possess, all of which are aromatic in nature. The target monomers can be separated into four groups by functionality: diamines, tetraamines, dianhydrides, and dicarboxylic acids. A number of these monomers are also used for more than one class of polymer.

All reactions were judged to be complete using thin layer chromatography on silica or alumina TLC plates. All compounds were fully characterised to confirm structure and purity using melting or boiling points, infrared spectroscopy, proton and carbon nuclear magnetic resonance, mass spectrometry and where possible X-ray diffraction crystallography.

### **4.1: 1,3,3-trimethyl-1-phenylindane**

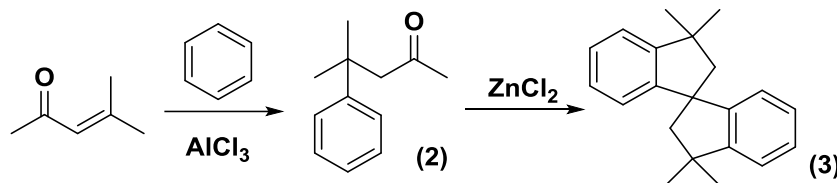


Scheme 4.1a Synthesis of 1,3,3-trimethyl-1-phenylindane.

The acid-catalysed dimerisation of  $\alpha$ -methyl styrene to form 1,3,3-trimethyl-1-phenylindane (1) was based on a modified procedure from literature<sup>136</sup>. Reactive styrene monomers are known to undergo violent, autocatalytic self-polymerisation reactions at room temperature<sup>137</sup>. To inhibit this reaction, manufacturers add up to 0.002% 4-*tert*-butylcatechol as an initiator scavenger which was removed by filtration through basic alumina. The purified  $\alpha$ -methyl styrene was then reacted with TFA at room temperature over 10 min by which time the reaction was complete. The crude product contained a distribution of products so it was purified by distillation under reduced pressure to afford pure 1,3,3-trimethyl-1-phenylindane (1) in 73% yield as a colourless liquid that crystallised on standing.

## 4.2: Spirobisindanes

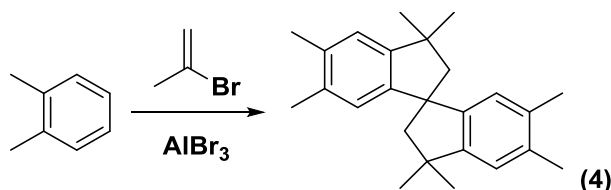
### 3,3,3',3'-tetramethyl-1,1'-spirobisindane



Scheme 4.2a Synthesis of 3,3,3',3'-tetramethyl-1,1'-spirobisindane.

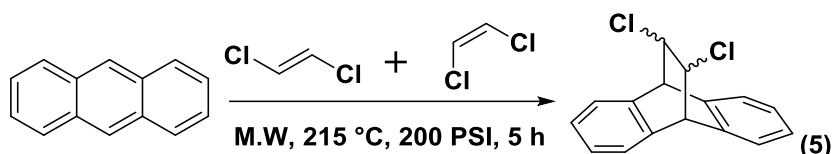
The synthesis of 3,3,3',3'-tetramethyl-1,1'-spirobisindane (3) was based on a procedure from literature<sup>138</sup>. First, 4-methyl-3-pentene-2-one is reacted with benzene using aluminium trichloride as a catalyst at 0 °C. The crude tar-like product was distilled under reduced pressure to afford pure 4-methyl-4-benzyl-2-pentanone (2) in 78% yield as a colourless liquid.

The self-condensation reaction of 4-methyl-4-benzyl-2-pentanone (2) using zinc chloride to form 3,3,3',3'-tetramethyl-1,1'-spirobisindane (3) occurs in a spectacular fashion. A suspension of zinc chloride and 4-methyl-4-benzyl-2-pentanone (2) were heated to exactly 180 °C. At this temperature, a rapid effervescent reaction occurred over a period of about 1 min and two distinct layers separate. It was found that if the reaction mixture was not removed from heat immediately following this reaction, more tar-like impurities were formed, decreasing the yield and making purification difficult. It was also found that using 4-methyl-4-benzyl-2-pentanone without purification resulted in a sluggish reaction that required higher temperatures and concluded with diminished yield. The clear top layer was extracted with hot *n*-hexane from which it was recrystallised multiple times to give pure 3,3,3',3'-tetramethyl-1,1'-spirobisindane (3) in 21% yield as colourless crystals. It should be noted that the structure and formula of this product was assigned incorrectly in literature<sup>138</sup> although, a subsequent study<sup>139</sup> confirmed that 3,3,3',3'-tetramethyl-1,1'-spirobisindane was indeed formed from this procedure.

**3,3,3',3',6,6',7,7'-octamethyl-1,1'-spirobisindane**

Scheme 4.2b Synthesis of 3,3,3',3',6,6',7,7'-octamethyl-1,1'-spirobisindane.

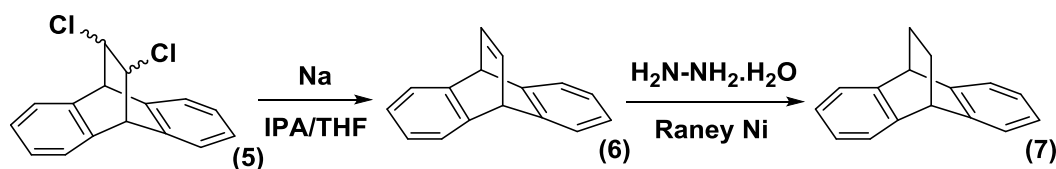
The synthesis of 3,3,3',3',6,6',7,7'-octamethyl-1,1'-spirobisindane (4) was based on a literature procedure for the preparation of substituted 3,3,3',3'-tetramethyl-1,1'-spirobisindanes<sup>140</sup>. The original literature procedure reports a Friedel-Crafts reaction that takes place between benzene or toluene and 2-bromopropene using aluminium tribromide as a catalyst to yield 6,6',7,7'-unsubstituted and 7,7'-dimethyl-substituted spirobisindanes. It was found that replacing the benzene or toluene used in the original procedure with *o*-xylene, that the 6,6',7,7' tetramethyl-substituted spirobisindane can be produced. A reaction time of 72 h at 60 °C was required for a complete reaction, yielding a crude dark-red oil. Purification of this oil using column chromatography and subsequent recrystallisation of the first eluted fraction afforded pure 3,3,3',3',6,6',7,7'-octamethyl-1,1'-spirobisindane (4) in 32% yield as colourless crystals. The authors of the original procedure recommend using freshly distilled 2-bromopropene however, it was found that this only marginally improves yields.

**4.3: Ethanoanthracenes****4.3.1: Ethanoanthracene Compounds Derived from Anthracene****9,10-dihydro-11,12-*cis*(*trans*)dichloro-9,10-ethanoanthracene**Scheme 4.3.1a Synthesis of 9,10-dihydro-11,12-*cis*(*trans*)dichloro-9,10-ethanoanthracene.

The synthesis of 9,10-dihydro-11,12-*cis*(*trans*)dichloro-9,10-ethanoanthracene (5) was based on a modified procedure from literature<sup>141</sup>. The original procedure involved heating *cis* or *trans* 1,2-dichloroethylene and anthracene in a sealed glass tube under pressure to 200-210 °C for 24h. Opting for a safer procedure, the Diels-Alder reaction was conducted with a cheaper 1,2-dichloroethylene *cis/trans* (1:1) mixture and using a microwave reactor, set to vent over 200 PSI. It was found that the reaction mixture did not easily reach the set temperature of 215

°C, even when setting the microwave to the maximum 300 W fixed power. After trial and error it was found that the maximum possible scale of reaction on a power of 300W was using 2.00g anthracene and 3.0 ml 1,2-dichloroethylene. The end point of the reaction was found to be after 5 h but unreacted anthracene remained in the mixture that was not possible to remove using column chromatography. The crude mixture was then reacted with furan-2,5-dione (maleic anhydride) to convert unreacted anthracene into the more polar Diels-Alder adduct. The crude mixture was then subjected to column chromatography and subsequent recrystallisation of the first eluted fraction afforded pure 9,10-dihydro-11,12-*cis(trans)*dichloro-9,10-ethanoanthracene (5) in 50% yield as colourless crystals.

### 9,10-dihydro-9,10-ethanoanthracene

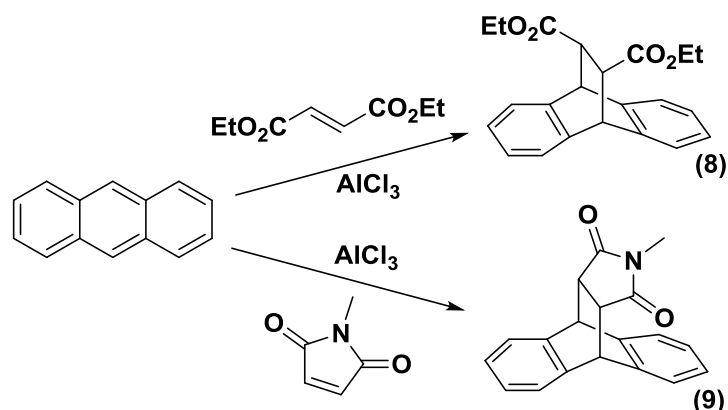


Scheme 4.3.1b Synthesis of 9,10-dihydro-9,10-ethanoanthracene.

The route from 9,10-dihydro-11,12-*cis(trans)*-dichloro-9,10-ethanoanthracene (5) to 9,10-dihydro-9,10-ethanoanthracene (7) was partially based a procedure from literature<sup>141</sup>. The first step involved dehalogenation using an excess of sodium metal in refluxing anhydrous isopropyl alcohol (IPA). It was found that the starting material demonstrated poor solubility in IPA alone and so an equal quantity of anhydrous THF was required to achieve total dissolution. The reaction was judged to be complete after the sodium had been consumed and after a single recrystallisation afforded pure 9,10-dihydro-9,10-ethanoanthracene (dibenzobarrelene) (6) in 71% yield as colourless crystals. From the same literature procedure, the second step involved hydrogenation of the bridge alkene using hydrogen gas and platinum oxide. This was attempted without the use of a dedicated hydrogenation apparatus. Instead, hydrogenation was attempted using a hydrogen filled balloon using catalysts such as platinum oxide, palladium on carbon and Raney nickel, however all attempts failed to produce a detectable quantity of alkane. Another attempt using the catalytic decomposition of hydrazine monohydrate over Raney nickel was however, much more successful, producing the pure desired product 9,10-dihydro-9,10-ethanoanthracene (7) without need for purification in a quantitative yield as colourless crystals.



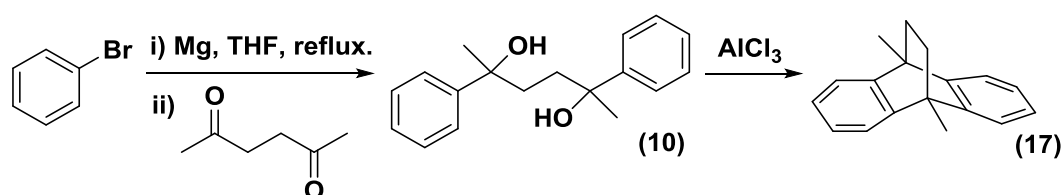
### Diels-Alder Adducts of Anthracene with Diethyl Fumarate and N-Methylmaleimide



Scheme 4.3.1c Synthesis of 9,10-dihydro-9,10-ethanoanthracene-11,12-*trans*-diethyl ester and N-methyl-9,10-dihydro-9,10-ethanoanthracene-11,12-*cis*-dicarboximide.

Both Diels-Alder adducts were synthesised based on a procedure from literature<sup>142</sup>. Both adducts 9,10-dihydro-9,10-ethanoanthracene-11,12-*trans*-diethyl ester (8) and N-methyl-9,10-dihydro-9,10-ethanoanthracene-11,12-*cis*-dicarboximide (9) were formed by the Diels-Alder reaction of anthracene with diethyl fumarate and N-methylmaleimide respectively using aluminium trichloride as a catalyst. It was found that the diethyl fumarate adduct reaction was complete within 6 h and with N-methylmaleimide, 16 h at room temperature. It was found that increasing the reaction temperature to increase the rate of both reactions had a severe detrimental effect to the purity of the crude products. Both reactions at room temperature produced colourless oils and after crystallisation from methanol, afforded colourless needle-shaped crystals in 83% and 60% yields of the diethyl fumarate (8) and N-methylmaleimide (9) adducts respectively.

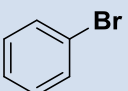
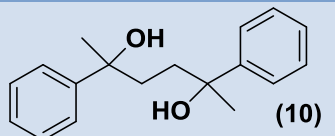
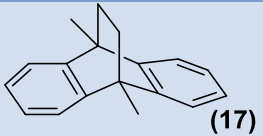
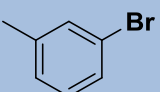
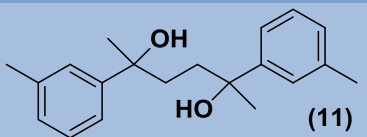
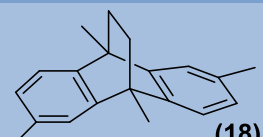
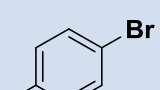
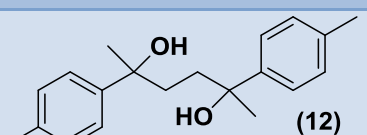
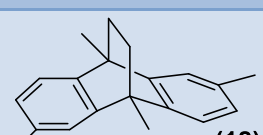
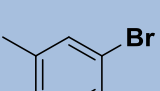
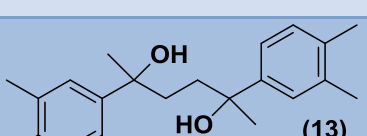
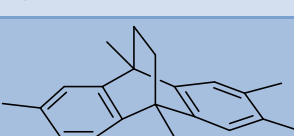
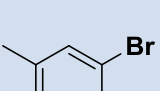
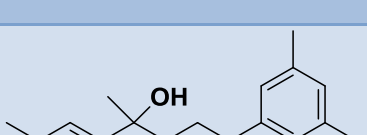
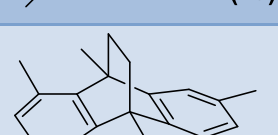
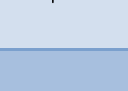
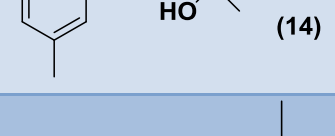
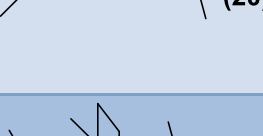
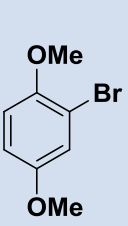
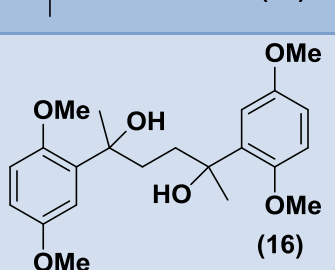
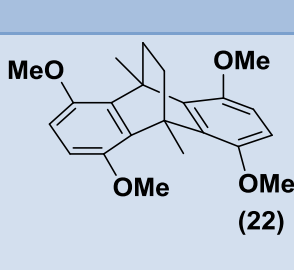
#### 4.3.2: Ethanoanthracene Compounds Derived from Diols



Scheme 4.3.2a Synthesis of 9,10-dimethyl-9,10-dihydro-9,10-ethanoanthracene.

The synthesis of ethanoanthracene compounds from diols was based on a modified procedure from literature<sup>143</sup> (Scheme 4.3.2a). Bromobenzene was first reacted with magnesium turnings under reflux to form a Grignard reagent. Once the magnesium turnings had been consumed, 2,5-hexanedione was added under reflux and after an aqueous work-up, 2,5-diphenylhexane-

2,5-diol was isolated. The diol was then reacted with aluminium trichloride in a double electrophilic aromatic substitution reaction to form 9,10-dimethyl-9,10-dihydro-9,10-ethanoanthracene. This procedure was used to form a number of aromatic-substituted diols and ethanoanthracenes summarised in Table 4.3.2a.

Table 4.3.2a				
Bromo-Reagent	Diol Derivative	% Yield	Ethanoanthracene Derivative	% Yield
		65		36
		86		37
		81		0
		95		18
		91		1.4
		77		0
		59		0

Synthesis of the diol compounds (10-16) was relatively straightforward, following the general Grignard method however, cyclisation of the diols to form ethanoanthracenes was more challenging. The original method reported a 59% yield (compound 17) along with 40% of isomeric tetrahydrofurans but it was found that yields can vary greatly between batches. An effort was made to optimise the procedure using various solvents, Lewis and Brønsted acids however, the only modifications that offered an improvement was using toluene instead of benzene and a larger scale reaction. One contributing factor to the low yield is the formation of a number of unidentified non-polar compounds (no tetrahydrofurans were isolated) that possess the same retention factor as the desired product in column chromatography of the crude tar-like product. This fraction obtained from column chromatography takes the appearance of a light green oil and the yield depends on the ability of the desired product to crystallise out from a solution of this oil and a solvent. With these modifications, the highest yield achieved was 36% for compound 17 from which a crystal structure was obtained (Fig 4.3.2a).

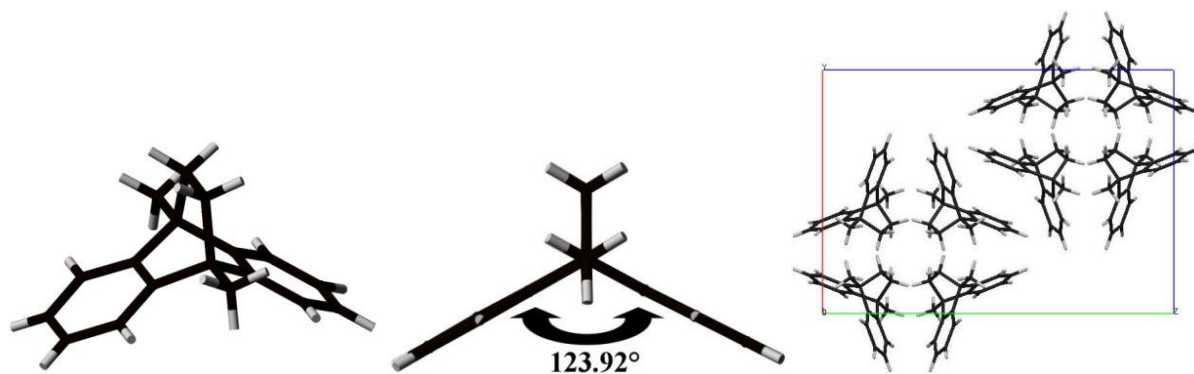


Fig 4.3.2a Crystal structure of compound 17 (left), side view illustrating dihedral angle (middle) and unit cell (right).

Compound 18 can be theoretically formed from either diol 11 or 12 however, compound 18 failed to crystallise when diol 12 was used (possibly due to isomer formation). When diol 11 was used, compound 18 was isolated in 37% yield from which a crystal structure was obtained (Fig 4.3.2b)

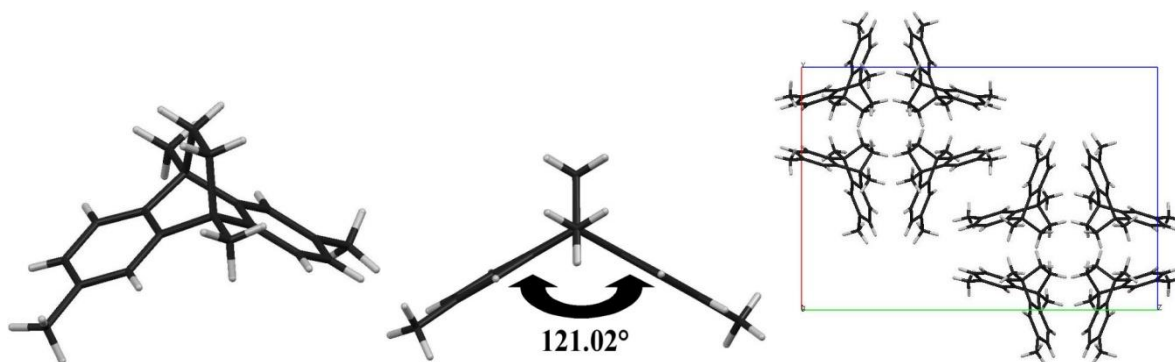


Fig 4.3.2b Crystal structure of compound 18 (left), side view illustrating dihedral angle (middle) and unit cell (right).

Compound 19 was consistently formed in a lower 18% yield, possibly due to the four methyl groups increasing the solubility during recrystallisation. Compound 20 was isolated in an extremely poor yield of 1.4% which is again possibly due to methyl groups increasing solubility and also isomers that disrupt the crystallisation process. A number of solvents were tested in the crystallisation procedure for compound 20 however, only acetonitrile successfully produced crystals after one week.

Cyclisation of diols 15 and 16 failed to produce compounds 21 and 22 respectively, although an unexpected compound (23) was isolated from the reaction involving diol 15 that may provide insight into the side products that have not yet been identified (Fig 4.3.2c).

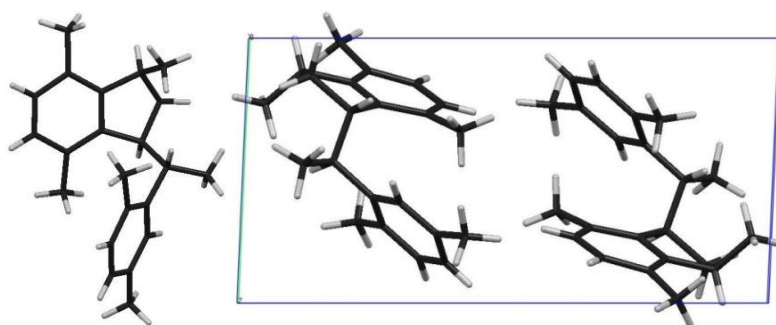
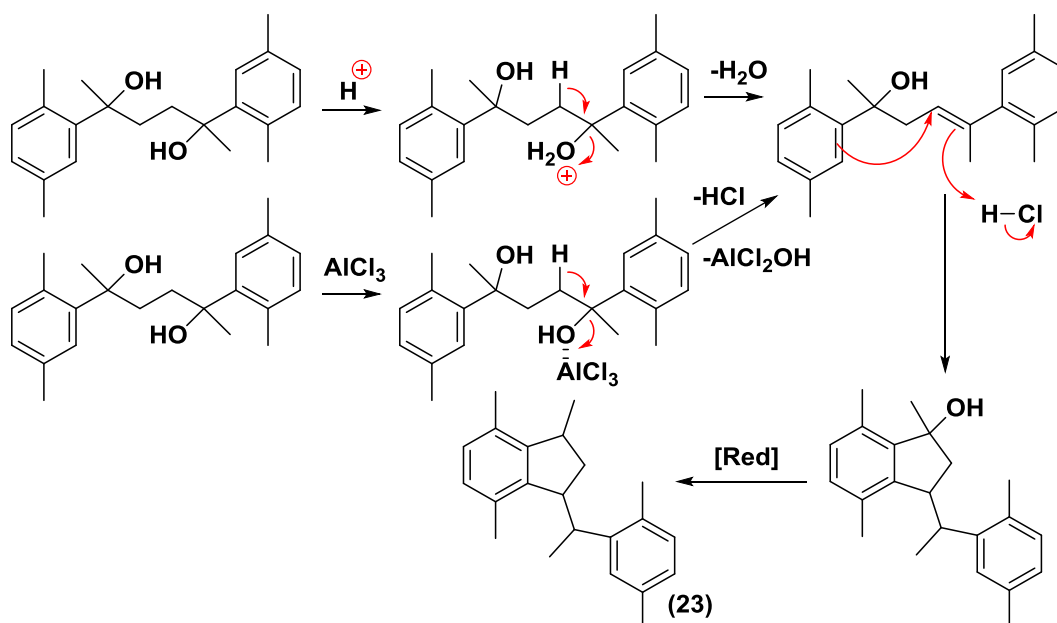


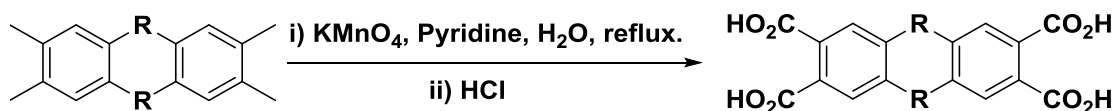
Fig 4.3.2c Crystal structure of compound 23 (left) and unit cell (right).

The formation of a five instead of a six-membered ring may be due to the elimination of an alcohol to form an alkene which is then attacked by the benzene ring (Scheme 4.3.2b). The second step involves a formal reduction of an alcohol to an alkane. This step is very difficult to explain under the reaction conditions used, especially when a second alcohol elimination seems to be much more likely.



Scheme 4.3.2b Possible mechanism (partial) for the formation of compound 23.

#### 4.4: Carboxylic Acid Compounds

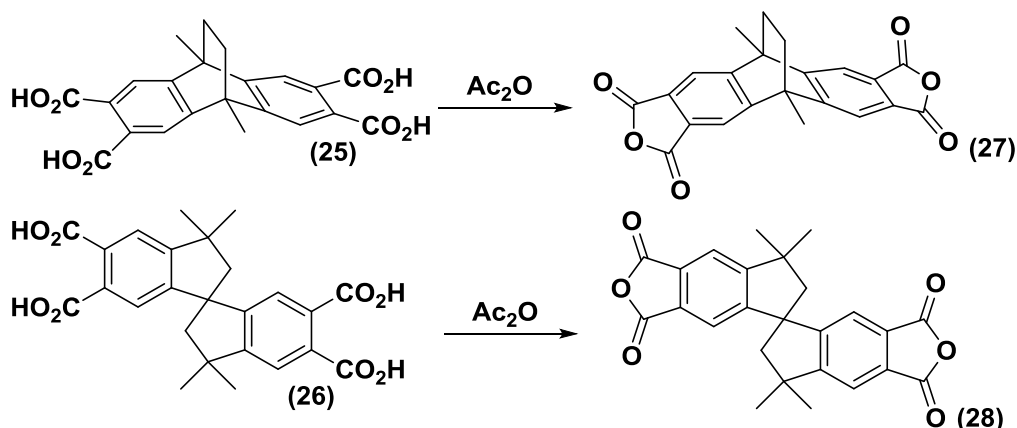


Scheme 4.4a Synthesis of carboxylic acid compounds.

The oxidation of aromatic methyl groups to carboxylic acids using potassium permanganate was based on a procedure from literature<sup>144</sup>. The corresponding dimethyl or tetramethyl compound was reacted with potassium permanganate, using an equal mixture of pyridine and deionised water as a solvent system. It was found that approximately 10 equivalents of potassium permanganate per methyl group were required to fully oxidise the starting material. The pyridine and manganese dioxide were removed and the residue was then neutralised with hydrochloric acid to precipitate the carboxylic acid. It was found that yields were adversely affected if the pyridine was not completely removed, possibly due to the formation of water soluble protonated pyridine/carboxylate salts. This procedure was used to form three carboxylic acids summarised in table 4.4a.

Table 4.4a		
Aromatic Methyl Compound	Carboxylic Acid Derivative	% Yield
 (18)	 (24)	<b>92</b>
 (19)	 (25)	<b>83</b>
 (4)	 (26)	<b>97</b>

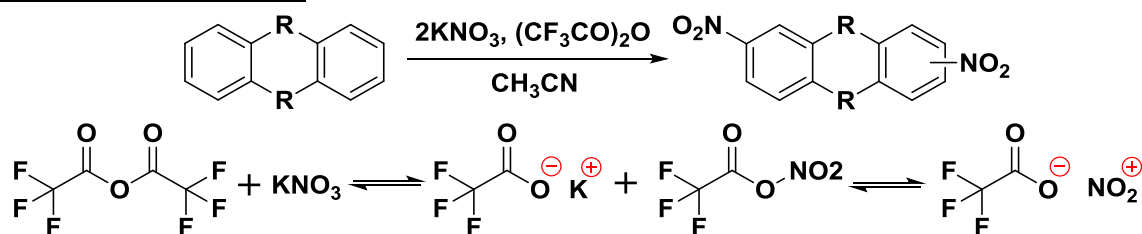
#### 4.5: Dianhydride Compounds



Scheme 4.5a Synthesis of dianhydride compounds.

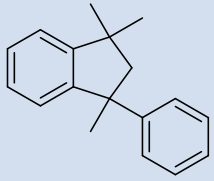
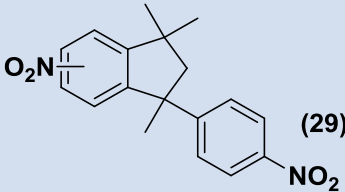
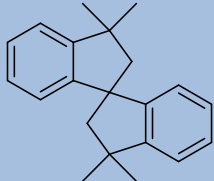
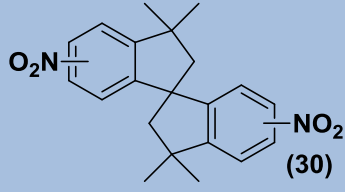
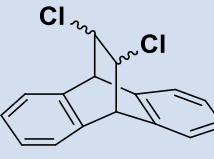
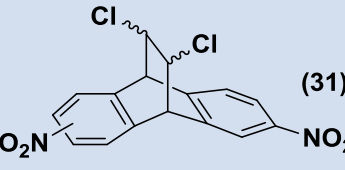
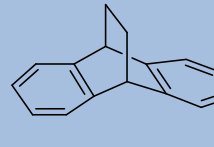
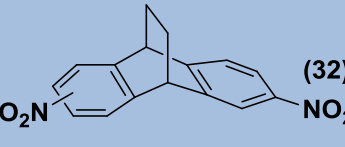
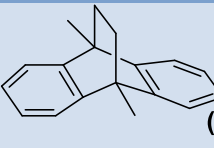
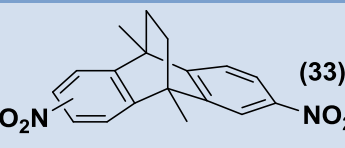
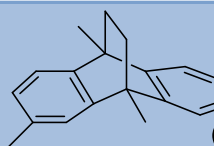
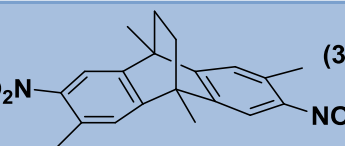
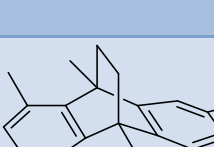
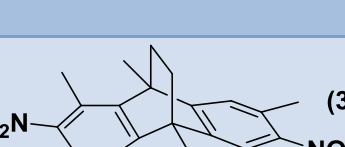
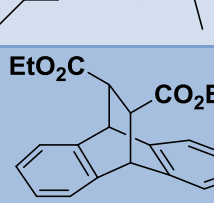
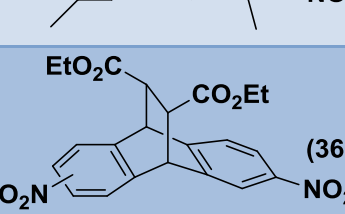
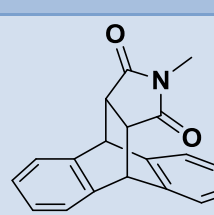
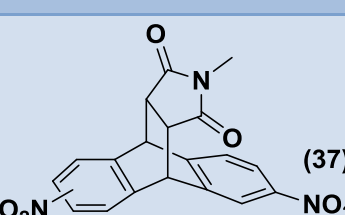
The formation of 9,10-dimethyl-9,10-dihydro-2,3,6,7-tetracarboxyl-9,10-ethanoanthracene (27) and 3,3,3',3'-octamethyl-6,6',7,7'-tetracarboxyl-1,1'-spirobisindane (28) was achieved by refluxing the corresponding tetra-carboxylic acid in acetic anhydride for 12 h. Both reactions produced impure crude products that required a number of recrystallisations to achieve pure products in 46% and 89% yields for compounds 27 and 28 respectively. It was found that removal of the acetic acid formed in the reaction by distillation did not improve the purity of the crude products or increase isolated yields.

#### 4.6: Dinitro Compounds



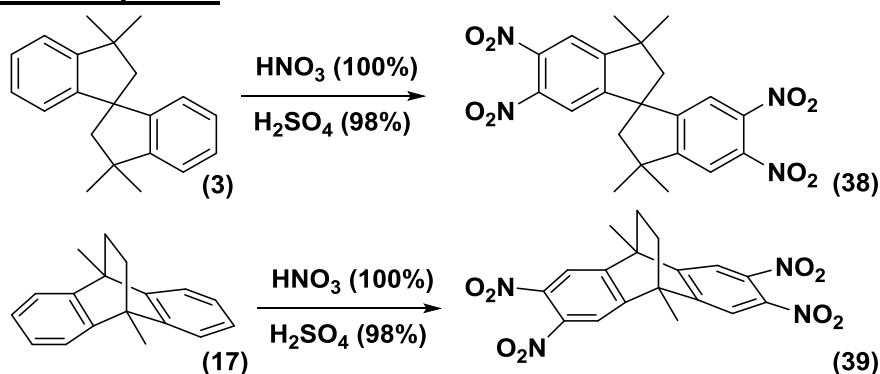
Scheme 4.6a Synthesis of dinitro compounds and formation of trifluoroacetyl nitrate from trifluoroacetic anhydride and potassium nitrate.

The synthesis of all dinitro compounds was based on a procedure from literature<sup>145</sup> that reported a nitration reaction using a metal nitrate and trifluoroacetic anhydride to form the nitrating agent trifluoroacetyl nitrate. A number of common nitration methods were tested, many of which produced moderate yields and impurities that were difficult to separate. The procedure from literature<sup>145</sup> however, afforded higher product yields with only small quantities of impurities that could be easily separated. This method was used to nitrate a number of hydrocarbon substrates summarised in table 4.6a and all were obtained as regioisomers except compound 34.

Table 4.6a		
Substrate	Dinitro Derivative	% Yield
 (1)	 (29)	<b>71</b>
 (3)	 (30)	<b>91</b>
 (5)	 (31)	<b>93</b>
 (7)	 (32)	<b>99</b>
 (17)	 (33)	<b>92</b>
 (18)	 (34)	<b>98</b>
 (20)	 (35)	<b>63</b>
 (8)	 (36)	<b>100</b>
 (9)	 (37)	<b>100</b>

This nitration reaction can be carried out in a number of solvents although, it was found that nitrations in acetonitrile were more homogeneous due to greater solubility of the inorganic salts. The nitration may also be carried out using a number of nitrate salts, however potassium nitrate was chosen because it was the least hygroscopic of the most common nitrates. It was found that heating the reaction to 60 °C to increase the reaction rate produces a larger quantity of impurities and lowers yields. For this reason, all reactions were carried out at room temperature over 24 h. The crude products were then purified by column chromatography. The polar impurities were retained at the baseline of the silica, simplifying the purification procedure to a filtration through silica, affording pure products.

#### 4.7: Tetranitro Compounds



Scheme 4.7a Synthesis of tetranitro derivatives.

The synthesis of 6,6',7,7'-tetranitro-3,3,3',3'-tetramethyl-1,1'-spirobisindane (38) and 9,10-dimethyl-9,10-dihydro-2,3,6,7-tetranitro-9,10-ethanoanthracene (39) was based on a procedure from literature<sup>146</sup>. It was found that nitrations using 100% "fuming" nitric acid alone produced a mixture of di and tri-nitrated products and increasing the temperature of the reactions to 80 °C produced low yields of tetra-nitrated products. Yields were substantially increased using a nitration mixture consisting of equal quantities of nitric acid (100%) and sulfuric acid (98%). The nitration procedure was conducted in three stages. First, the addition of the substrate to the nitration mixture produced a vigorous reaction that required cooling at 0 °C. The vigorous reaction was allowed to subside at room temperature and the temperature was then raised to 80 °C for 3h to complete the nitration. The crude products contained major tetra-nitrated products with minor tri-nitrated products. Increasing the reaction times did not improve yields any further. The tetra-nitrated fractions were separated using column



chromatography to give pure products in 91% and 79% yields for compounds 38 and 39 respectively and for the latter, a crystal structure was obtained (Fig 4.7a).

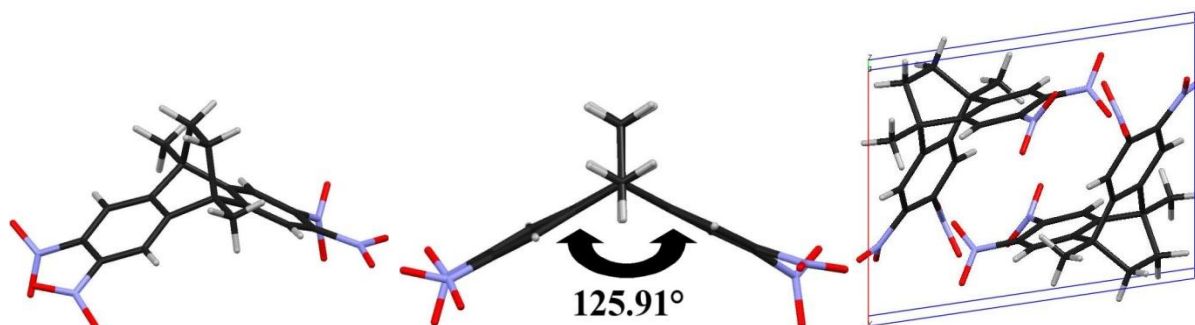
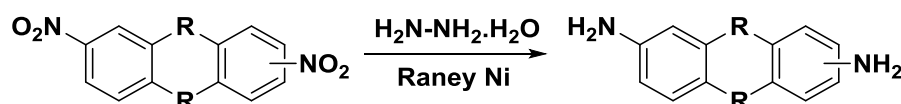


Fig 4.7a Crystal structure of compound 39 (left), side view illustrating dihedral angle (middle) and unit cell (right).

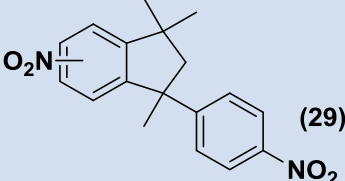
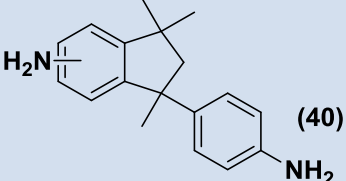
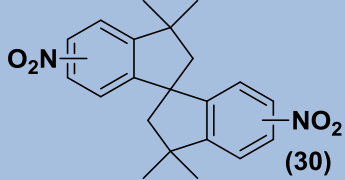
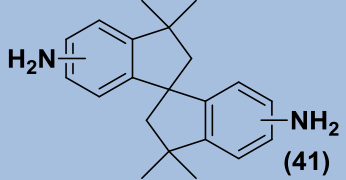
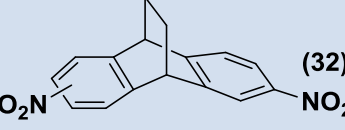
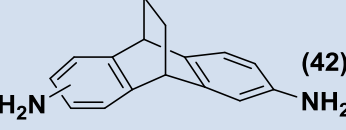
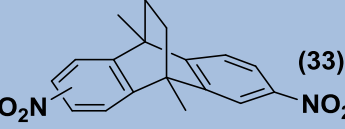
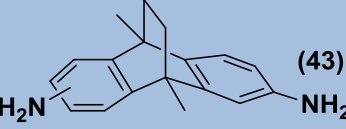
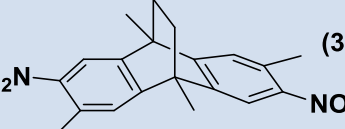
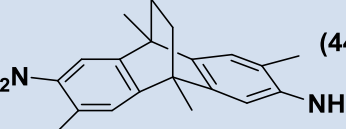
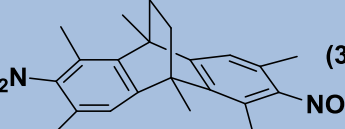
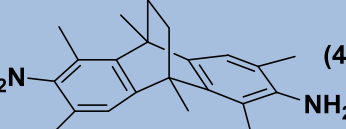
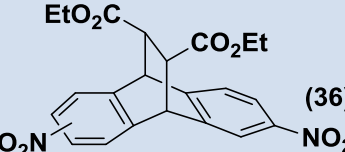
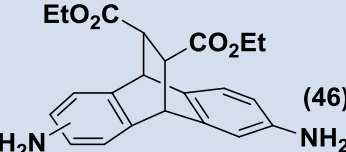
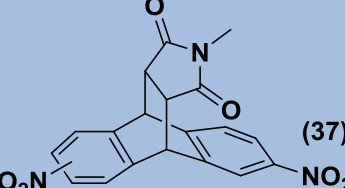
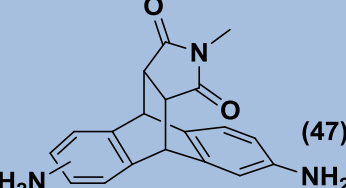
#### 4.8: Diamino Compounds

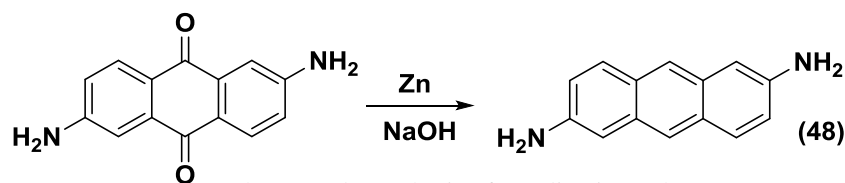


Scheme 4.8a Synthesis diamino derivatives from dinitro compounds.

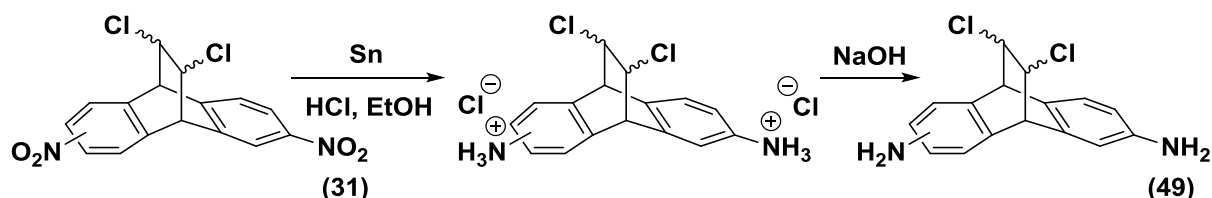
The synthesis of all diamino compounds was based on a modified procedure from literature<sup>147</sup>. A number of common methods for the reduction of aromatic nitro groups to amines were tested but it was found that reduction using hydrazine monohydrate and a catalytic quantity of Raney nickel produced the highest purity amines. The reduction may be carried out at room temperature, however it may also be conducted under reflux, allowing a shorter reaction time. An important factor that influences the product purity is that the reduction must be conducted under an inert atmosphere using solvents that have been thoroughly deoxygenated. It was found that the choice of solvent was also an important factor that determines the purity of the product, with some derivatives changing colour during the reaction in certain solvents. The choice of solvent (ethanol, tetrahydrofuran or diethyl ether) for each derivative was made by trial and error.

Aromatic amines are known to be air sensitive<sup>146</sup> and it was found that the diamines described in this thesis were all sensitive when dissolved (changing from colourless to a dark yellow, brown or pink colour) but are relatively stable in the solid state. All diamine monomers were found to be pure by NMR and were used without purification. This method was used to form a number of aromatic diamino derivatives, all of which were obtained in quantitative yields summarised in Table 4.8a.

Dinitro Derivative	Diamino Derivative
 (29)	 (40)
 (30)	 (41)
 (32)	 (42)
 (33)	 (43)
 (34)	 (44)
 (35)	 (45)
 (36)	 (46)
 (37)	 (47)

**2,6-diaminoanthracene**

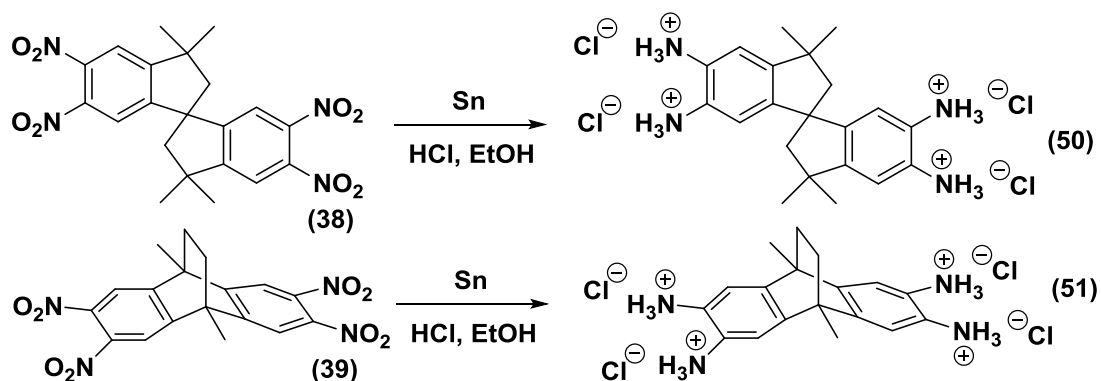
The reduction of 2,6-diaminoanthraquinone to 2,6-diaminoanthracene (48) using zinc was based on a procedure from literature<sup>148</sup>. The reaction of 2,6-diaminoanthraquinone with zinc mesh in aqueous sodium hydroxide was achieved by refluxing under an inert atmosphere for 48 h. Ethanol was added both to increase the solubility of the starting material and to inhibit excessive foaming due to the formation of hydrogen gas. Purification of the crude brown product was found to be problematic due to low solubility in a range of solvents, although the product appeared to be moderately soluble in acetone, leaving a sodium zincate residue that could be removed by filtration. The crude product was then subjected to soxhlet extraction over one week using acetone under a nitrogen atmosphere. Recrystallisation of the extract afforded the desired product 2,6-diaminoanthracene in 28% yield as bright yellow crystals. The product was found to be extremely air sensitive.

**9,10-dihydro-2(3),6(7)-diamino-11,12-*cis(trans)*dichloro-9,10-ethanoanthracene**

Synthesis of 9,10-dihydro-2(3),6(7)-dinitro-11,12-*cis(trans)*dichloro-9,10-ethanoanthracene (49) was achieved using tin (II) chloride which was generated in situ by the reaction between granulated tin metal and concentrated hydrochloric acid. Ethanol was added to improve the solubility of the starting material and was found to substantially increase the rate of reaction. Although the acidic environment protects the amine product from oxidation, the reaction was conducted under an inert environment. With the addition of granulated tin metal, a vigorous reaction occurred immediately and after 30 min the colourless mixture changed to a light yellow colour and then back to a colourless homogeneous solution after 16h. After removal of the ethanol from the solvent system, the mixture was neutralised with sodium hydroxide

solution to precipitate the freebase amine. Since the freebase amine was found to be air sensitive, the product was dried under a stream of nitrogen gas. The precipitate was washed with tetrahydrofuran to extract the product from residual tin salts ( $\text{SnO}\cdot\text{H}_2\text{O}$  and  $\text{NaSn}(\text{OH})_3$ ). This procedure afforded pure 9,10-dihydro-2(3),6(7)-diamino-11,12-*cis(trans)*dichloro-9,10-ethanoanthracene (49) as a colourless powder in a quantitative yield

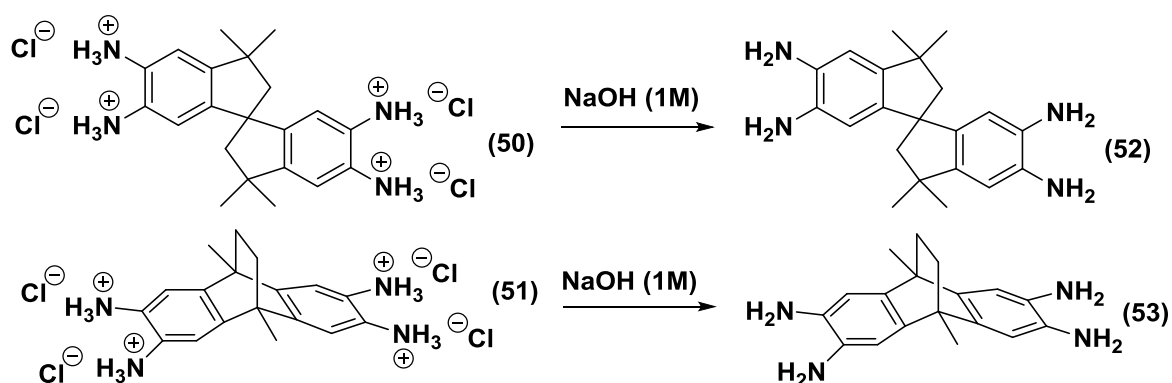
#### 4.9: Tetraamine Hydrochloride Salts



Scheme 4.9a Synthesis of tetraamine hydrochloride salts from tetranitro compounds.

Aromatic tetraamines are exceptionally air and light sensitive so are commonly synthesised as salts to protect the amine groups from oxidation<sup>146</sup>. The synthesis of 6,6',7,7'-tetraamino-3,3,3',3'-tetramethyl-1,1'-spirobisindane hydrochloride (50) and 9,10-dimethyl-9,10-dihydro-2,3,6,7-tetraamino-9,10-ethanoanthracene hydrochloride (51) was based on a procedure from literature<sup>149</sup>. As with the previous procedure, the tetranitro derivatives were reduced to amine hydrochloride salts by tin (II) chloride generated in situ under a nitrogen atmosphere. A vigorous reaction occurred immediately with the addition of tin and after 30 min the colourless mixture changes to a dark orange colour and then back to a colourless homogeneous solution after 16 h. Apart from the colour change, this procedure differs from the previous, where cooling the reaction back to room temperature resulted in the complete precipitation of the corresponding tetraamine salt. This salts were found to be heat sensitive when wet and so the products were dried under a stream of nitrogen gas. This procedure afforded the pure tetraamine salts 50 and 51 in 97% and 99% yields respectively. Both salts were found to be stable at room temperature for extended time periods.

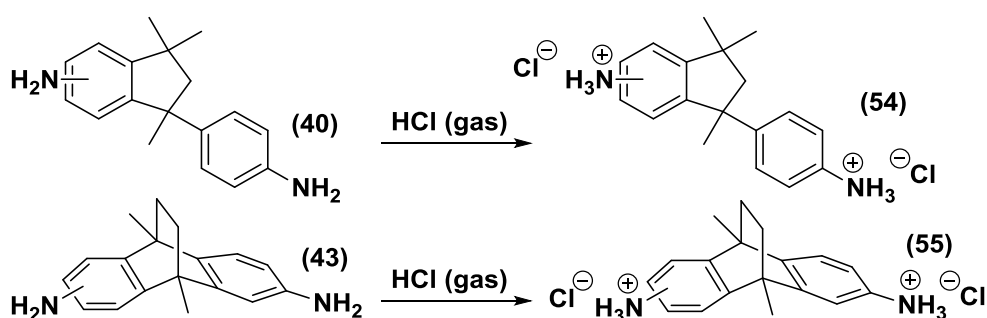
#### 4.10: Tetraamino Compounds



Scheme 4.10a Synthesis of freebase tetraamines from tetraamine hydrochloride salts.

The freebase amines 6,6',7,7'-tetraamino-3,3,3',3'-tetramethyl-1,1'-spirobisindane (52) and 9,10-dimethyl-9,10-dihydro-2,3,6,7-tetraamino-9,10-ethanoanthracene (53) were formed by the neutralisation of the corresponding hydrochloride salt. The hydrochloride salts were found to be highly soluble in water from which the freebase amines were precipitated by the addition of sodium hydroxide solution. It was found that deoxygenation of the deionised water was not a necessity due to the freebase amine being directly formed as a solid, however, it was decided that the use of a deoxygenated solvent would be prudent. Due to the air sensitivity of the products, the precipitates were dried under a stream nitrogen gas to afford the desired freebase tetraamines in quantitative yields. The tetraamines were found to be extremely unstable when dissolved in a solvent (changing to a red colour within 1 h) but were found to be relatively stable in the solid form for up to a week.

#### 4.11: Diamine Hydrochloride Salts

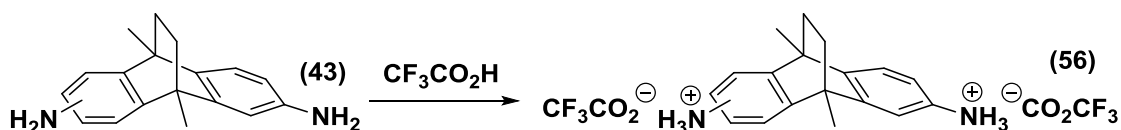


Scheme 4.11a Synthesis of diamine hydrochloride salts.

As previously mentioned, the diamines reported in this thesis were found to be unstable if stored for extended periods of time. Diamines 40 and 43 were converted to 6,(7)-amino-

1,3,3-trimethyl-1-(4-aminophenyl)indane hydrochloride (54) and 9,10-dimethyl-9,10-dihydro-2,6(7)-diamino-9,10-ethanoanthracene hydrochloride (55) respectively to test if the salts were air stable and also if hydrochloride salts could be used in place of freebase amines in Tröger's base polymerisations. The hydrochloride salts were obtained by dissolving the corresponding diamine compound in deoxygenated diethyl ether and passing a stream of dry hydrogen chloride gas (generated from calcium chloride and concentrated hydrochloric acid) through the solution to form a white precipitate. The precipitates were found to be heat sensitive when wet and so the products were dried under a stream of nitrogen gas to afford pure hydrochloride salts 54 and 55 in quantitative yields. Both salts were found to be stable under ambient conditions but the salts appeared to be moderately hygroscopic.

#### **4.12: 9,10-dimethyl-9,10-dihydro-2,6(7)-diamino-9,10-ethanoanthracene trifluoroacetate**



Scheme 4.12a Synthesis of 9,10-dimethyl-9,10-dihydro-2,6(7)-diamino-9,10-ethanoanthracene trifluoroacetate.

As for the previously described diamine hydrochloride salts, diamine 43 was also converted to the trifluoroacetate salt to test stability and possible use in Tröger's base polymerisations. The trifluoroacetate salt was obtained by the addition of a stoichiometric quantity of trifluoroacetic acid to a solution of diamine 43 in deoxygenated diethyl ether to form a yellow precipitate. The trifluoroacetate salt was found to be heat sensitive when wet and so the precipitate was dried under a stream of nitrogen gas to afford the desired product 9,10-dimethyl-9,10-dihydro-2,6(7)-diamino-9,10-ethanoanthracene trifluoroacetate (56) as a yellow powder in a quantitative yield. The trifluoroacetate salt was found to be stable under ambient conditions however, the salt was found to be extremely hygroscopic, forming a liquid after two weeks. The salt was also found to show instability towards heat, decomposing at 62-63 °C.

## **Chapter 5: Polymer Synthesis**

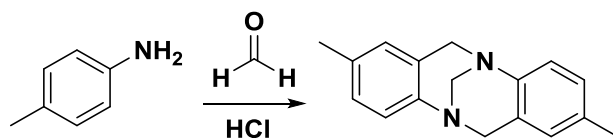
All polymers reported in this thesis were synthesised with the intention of casting defect-free films, durable enough for membrane gas permeation experiments. Formation of such a film can be a challenging undertaking. The polymer must first be soluble, pre-disposed to film formation and free of insoluble cross-linked particles. Generally, minimum molecular weights of approximately  $40\text{-}50 \text{ Kg mol}^{-1}$  are required to form self-standing, flexible PIM films. Low molecular weight polymers typically form fragile and discontinuous films. The presence of oligomeric material in high molecular weight samples can cause films to become brittle. All procedures were optimised with a view to producing high molecular weight soluble polymers without the formation of insoluble cross-linked material. Polymer solubility was tested in a range of common solvents such as acetone, acetonitrile, chloroform, DCM, DMAc, DMF, DMSO, hexane, NMP, THF and toluene. Purification of polymer samples was achieved using a re-precipitation procedure involving the addition of a polymer solution into a solvent in which the polymer shows poor solubility. The higher molecular weight polymer fraction precipitates as a solid or gel while the solvent retains the more soluble lower molecular weight fraction. This procedure may be repeated as needed.

Non-absolute molecular weights ( $M_n$  = number average,  $M_w$  = weight average) of polymer samples were determined by gel permeation chromatography (GPC) calibrated against polystyrene standards. Since the structure of PIMs are by definition more rigid and disordered than polystyrene, GPC which correlates hydrodynamic volume, may over-estimate the molecular weight of PIM samples. GPC can also provide an indication of the distribution of molecular weights within a polymer sample known as the *polydispersity index* ( $M_w/M_n$ ). Visual inspection of the peaks in a GPC trace may also reveal the presence of impurities and oligomeric material. All polymer samples were fully characterised to confirm structure and purity using FTIR spectroscopy, thermal gravimetric analysis (TGA) and nuclear magnetic resonance ( $^1\text{H}$  &  $^{13}\text{C}$ ). Analysis of low molecular weight oligomeric material removed from crude polymer samples by acetone washing and re-precipitation procedures using MALDI-TOF may also provide additional information. A MALDI spectrum may reveal the presence of oligomers of different chain lengths, differing by multiples of the repeat monomeric unit. The mass of the individual chains can also reveal if the structures are linear (containing end groups) or cyclic in nature, which can provide insight into the polymerisation reaction itself.

## Chapter 6: Tröger's Base Polymers

### 6.1: Tröger's Base

Tröger's base (TB) was first isolated by the German chemist Julius Tröger in 1887 while studying an acid mediated reaction of *p*-toluidine with formaldehyde<sup>150</sup> (Scheme 6.1a).



Scheme 6.1a Synthesis of Tröger's Base.

Tröger isolated a basic compound with the formula  $C_{17}H_{18}N_2$  but failed to elucidate the true structure. The correct structure was assigned in 1935 by M. A. Spielman<sup>151</sup> and confirmed almost 100 years after its discovery by single crystal X-ray diffraction in 1986<sup>152</sup>. TB is well known for containing two stereogenic nitrogen atoms in its rigid twisted V-shaped structure (Fig 6.1a<sup>153</sup>). Enantiomers containing stereogenic N-centres often cannot be resolved due to rapid inversion at room temperature but the rigid TB structure is an exception to this rule as inversion is prevented by ring strain<sup>154</sup>.

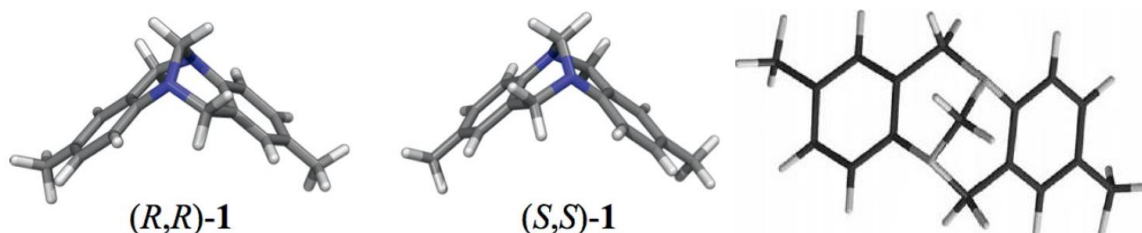
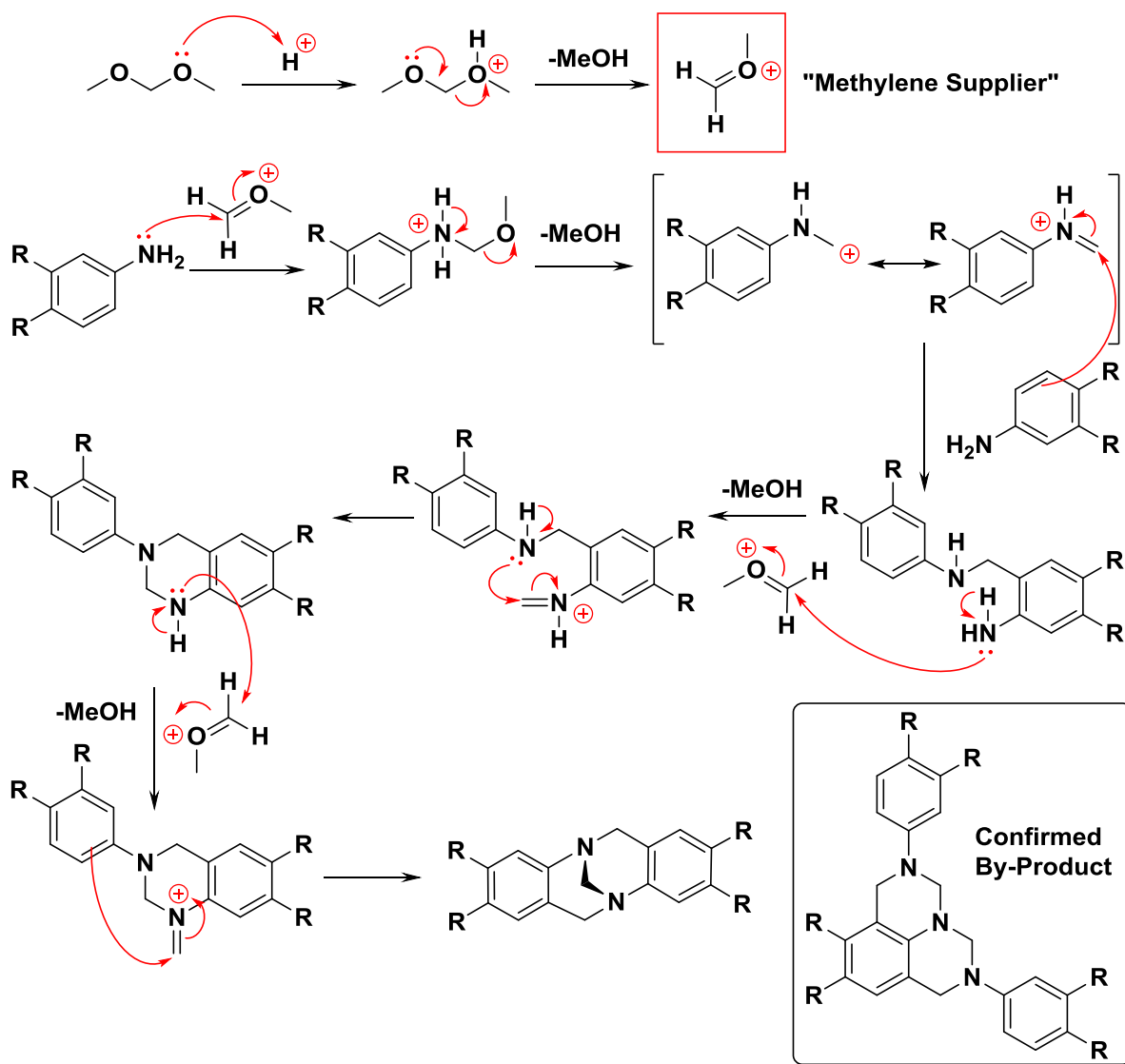


Fig 6.1a MMFFs-Optimized geometry of the two enantiomers of Tröger's base (left), overhead view (right).

TB was initially estimated to be only weakly basic<sup>155</sup>, however, a study on the hydrogen bonding acceptor strength in 2004 reported that TB is strongly basic compared to other aromatic amines ( $pK_{HB}(N) = 1.15$ )<sup>156</sup>. The relatively high basicity is thought to be due to the rigid structure forcing the nitrogen lone pairs into an orientation where there is little orbital overlap with the connected aromatic ring system and hence conjugation is disrupted<sup>157</sup>. The basic nature of TB has recently been exploited in heterogeneous catalysis<sup>158, 159</sup> and also suggests an opportunity for use in  $CO_2$  capture materials, where basic amine functionality has demonstrated an increased affinity for  $CO_2$ <sup>160</sup>. The rigid bicyclic shape of TB presents an attractive unit to incorporate into a PIM as a site of contortion and facilitates the incorporation of basic amine functionality. In their neutral form, the tertiary amines also ensure hydrogen bonding does not occur, which would otherwise result in a reduced surface area of the material.



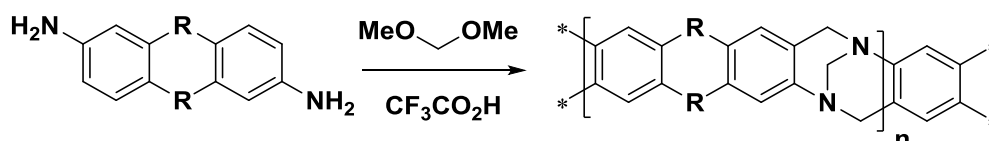
Since its discovery, a number of methodologies have been reported for TB synthesis, all of which remain analogous to the original procedure<sup>157</sup>. An aromatic amine derivative is reacted with a "methylene supplier" under acidic conditions to form TB. The "methylene supplier" is a synthetic equivalent of methylene such as formaldehyde<sup>150</sup> or a methylene precursor such as paraformaldehyde<sup>161</sup>, hexamethylenetetramine<sup>162</sup>, and dimethoxymethane<sup>163</sup>. An acid, such as hydrochloric acid<sup>150</sup>, methanesulfonic acid<sup>164</sup> and trifluoroacetic acid<sup>162</sup>, serves as a solvent as well as a catalyst for the formation of the "methylene supplier" and TB. The reaction takes place *via* a mechanism proposed by Wagner<sup>165, 166</sup> and Farrar<sup>167</sup> (Scheme 6.1b) that is supported by Eberlin and Coelho<sup>168</sup> who studied the reaction intermediates using mass spectrometry. A number of by-products are known to form, one of which is of interest to this research<sup>157</sup>.



Scheme 6.1b Mechanism of Tröger's Base formation proposed by Wagner and Farrar using dimethoxymethane as an example of a methylene precursor and a confirmed by-product.

## 6.2: Tröger's Base Polymerisation

Early attempts within our research group (Dr. Mariolino Carta) to incorporate preformed TB units into PIMs using dibenzodioxane chemistry did not give polymers with satisfactory film forming properties unless only small percentages of TB units were used in co-polymers. A different approach however, using TB formation as the linking reaction between monomers in a polymerisation was much more successful. Replacing *p*-toluidine with a “dianiline”, as the starting material in Tröger’s base formation, a novel polymerisation reaction will result (Scheme 6.2a).



Scheme 6.2a Synthesis of Tröger's Base polymers.

Previous work within our research group (now patented<sup>169</sup>) has determined that the highest molecular weight polymers are formed when dimethoxymethane is used as a methylene precursor and trifluoroacetic acid (TFA) is used both as the acid catalyst and solvent. Comparing more recent work with research group members has led to the conclusion that a general procedure is not adequate to satisfy the requirements of all monomers and the polymerisation of each monomer must be optimised individually. The reasons for this will be discussed in specific cases later in this chapter. We have however, agreed on a general procedure that is a good starting point when dealing with new monomers and produces high molecular weight polymers in the majority of cases.

A typical procedure is as follows: One equivalent of a pure (determined by NMR) aromatic diamine is mixed with five equivalents of dimethoxymethane (two equivalents excess) and cooled to ice temperature. TFA (approximately 10 ml per gram of monomer) is then slowly added drop-wise over 30 minutes. In some cases, if the addition is slow enough a gel will form that dissolves with the addition of more TFA. This mixture is then stirred at room temperature under a static inert atmosphere until the solution achieves the desired viscosity (determined arbitrarily by the impulse response of a magnetic stirrer bar to changes in speed). At this time the colour of the solution will typically change to an orange or dark red colour. The mixture is then slowly poured into aqueous ammonium hydroxide solution to quench the reaction and precipitate the polymer (Fig 6.2a) as an amorphous solid. The polymer is filtered and washed with acetone to remove oligomeric material and then purified by a re-precipitation procedure.



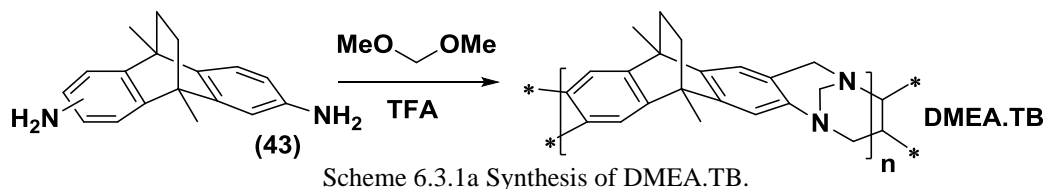
Fig 6.2a TB polymerisation of DMEA.TB (left), precipitation into  $\text{NH}_4\text{OH}$  solution (middle & right). Optimisation of a TB polymerisation has so far been a challenging undertaking of trial and error. The polymerisation may be optimised by varying concentration and rate of TFA addition. If a mixture fails to become viscous in a reasonable time (more than five days), it is usually due to an inadequately low concentration and the product is formed as low molecular weight linear and cyclic oligomers. In many cases, a slightly higher concentration or a slower TFA addition rate can result in the formation of insoluble "jelly" like particles or a "rubber" like material at the end point of the polymerisation. It is likely that the insoluble products are the result of cross-chain reactions from which a number the reactive intermediates proposed in Scheme 6.1b may be responsible. TB polymerisations appear to be highly sensitive to changes in concentration and the rate of TFA addition. In extreme cases, by changing the TFA addition time from 30 to 40 minutes for example, a polymerisation can change from a low viscosity liquid to a rubbery solid in a matter of seconds without warning at an unpredictable time from the start of the reaction. For a select few cases however, polymerisations can be relatively predictable, yielding soluble polymers with repeatable molecular weights and surface areas.

There has so far been limited use of TB as a component in polymer architecture<sup>159, 170</sup> but the synthesis of TB oligomers was reported recently in 2012, that feature a small number of successive TB links between benzene units<sup>171</sup>. Previous to the research described in this thesis, there were no reports on the use of TB formation as a polymerisation reaction. The following sections of this chapter will discuss the synthesis and properties of a number of novel examples from this new class of microporous polymers.

## 6.3: Tröger's Base Polymers from Synthetic Monomers

### 6.3.1: DMEA.TB

DMEA.TB was synthesised in 76% yield from the TB polymerisation of 9,10-dimethyl-9,10-dihydro-2,6(7)-diamino-9,10-ethanoanthracene at a concentration of 8.33 ml of TFA per gram of monomer over 48 h (Scheme 6.3.1a) and was isolated as a white powder.



Thermal gravimetric analysis shows the polymer is stable up to 260 °C with an initial 10% decrease in mass, consistent with the loss of an ethylene fragment from the ethanoanthracene unit via a retro Diels-Alder reaction<sup>172</sup>. Differential scanning calorimetry did not reveal the presence of a glass transition under its decomposition temperature.

Analysis of the acetone washings from the crude polymer using MALDI-TOF revealed multiples of the presumed polymeric repeating unit ( $C_{21}H_{20}N_2$ ) (Fig 6.3.1a). The values obtained show the presence cyclic oligomers from dimers to pentadecamers with dimers, trimers and hexamers being particularly favoured. Ring strain resulting from a hexameric unit suggests either a twisted cyclic structure or that of a catenane (two interlocked trimer rings).

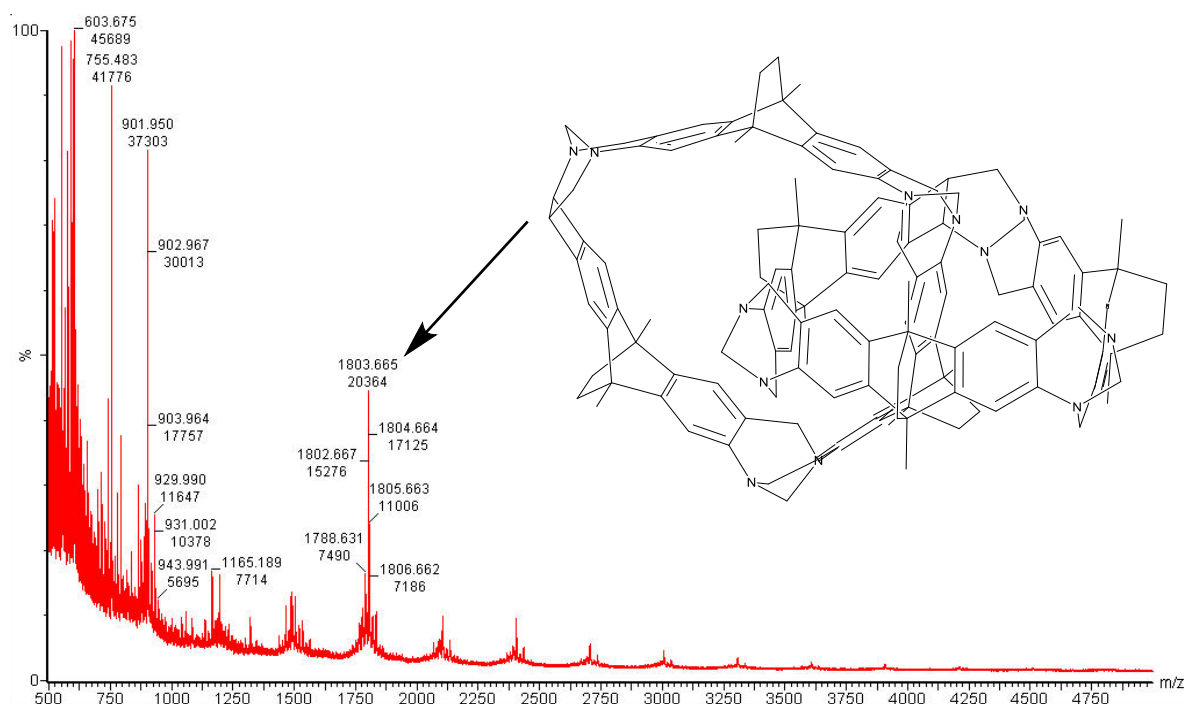


Fig 6.3.1a MALDI-TOF spectrum of acetone soluble oligomers of DMEA.TB showing the repeating unit of the polymer resulting from cyclic oligomers and a catenane hexamer is illustrated.

Nitrogen adsorption shows DMEA.TB has an unusually high BET surface area of 1028 m<sup>2</sup>/g which is the highest recorded for any soluble polymer to date. This can be attributed to the extreme structural rigidity of both the ethanoanthracene and the TB linking units. Both structures also host a site of contortion that impose a series of kinks into the stiff polymer chain (Fig 6.3.1b<sup>173</sup>).

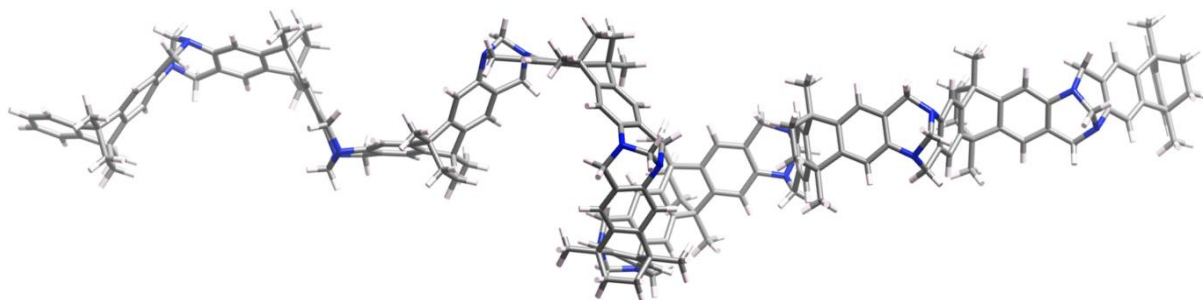


Fig 6.3.1b Molecular model of DMEA.TB illustrating its highly contorted and rigid polymer chain. It was found by varying the polymerisation concentration, that while it is certainly possible for DMEA.TB to cross-link, it is more resistant to cross-linking than other monomers. This is likely due to the bridgehead methyl groups sterically hindering electrophilic attack of the 1,4 and 5,8 aromatic positions from reactive TB intermediates. This allows the formation of a high molecular weight polymer (GPC:  $M_n = 40,700$ ,  $M_w = 155,800$ ) without insoluble gel formation. DMEA.TB was found to have exceptional film forming properties and a number of films were formed for membrane gas permeation studies (Fig 6.3.1c).

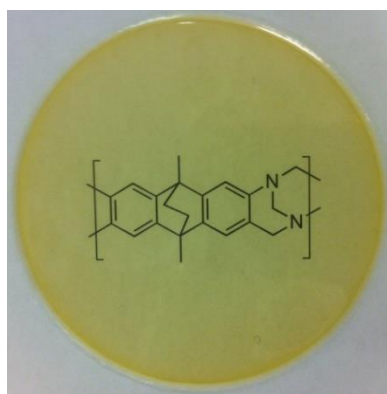


Fig 6.3.1c An optically clear chloroform-cast film (10 cm x 181  $\mu\text{m}$ ) of DMEA.TB, through which is visible its molecular structure printed on a piece of paper.

Before the first permeation measurements were carried out on a new class of polymer, it was important to determine if TB polymers respond to methanol treatment in the same way as other PIMs and if methanol is indeed the best solvent to cancel membrane history. A film was cut into small samples, separately treated with a range of solvents for 2 hours and dried under vacuum at 25 °C for 2 hours. These treatments were designed to reproduce those typically

used before membrane permeability tests at ITM. One sample was left untreated (as cast) and another was dried at 120 °C for 6 hours in a vacuum oven to remove all traces of solvent for comparison. Each of the samples were then assessed for solvent content using TGA (Fig 6.3.1d).

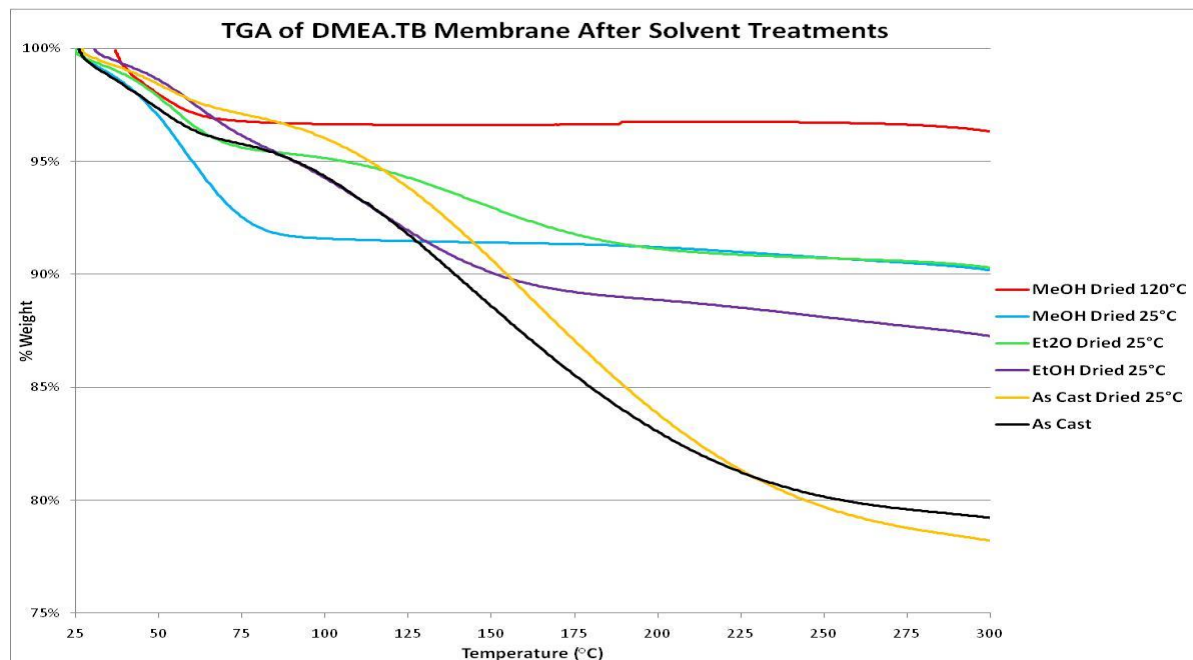


Fig 6.3.1d TGA of DMEA.TB membranes after different solvent and post solvent treatments.

The results show that the casting solvent (chloroform) is held tenaciously by the membrane and is only fully removed by heating to near the decomposition temperature of the polymer. Ethanol and diethyl ether effectively remove the casting solvent but are also both held strongly by the membrane, being fully removed at ~170 °C and ~ 200 °C respectively. Methanol also effectively removes casting solvent but is however easily removed by heating to just ~80 °C. This study confirms that like other PIMs, methanol is the best solvent to be used for cancelling membrane history and conveniently allows direct permeability comparisons with other PIMs. With this information in hand, researchers at ITM conducted permeability experiments using a number of membranes: untreated 178  $\mu\text{m}$  (As cast), methanol treated 181  $\mu\text{m}$  (expanded from 178  $\mu\text{m}$  with methanol swelling), a thinner 95  $\mu\text{m}$  membrane (treated with methanol) and the same methanol treated 181  $\mu\text{m}$  membrane aged for 24 hours. The calculated transport parameters for DMEA.TB are shown in table 6.3.1a along with PIM-1 data (120  $\mu\text{m}$  methanol treated, collected at ITM) for comparison.

Table 6.3.1a :DMEA.TB Membrane Permeability Measurements

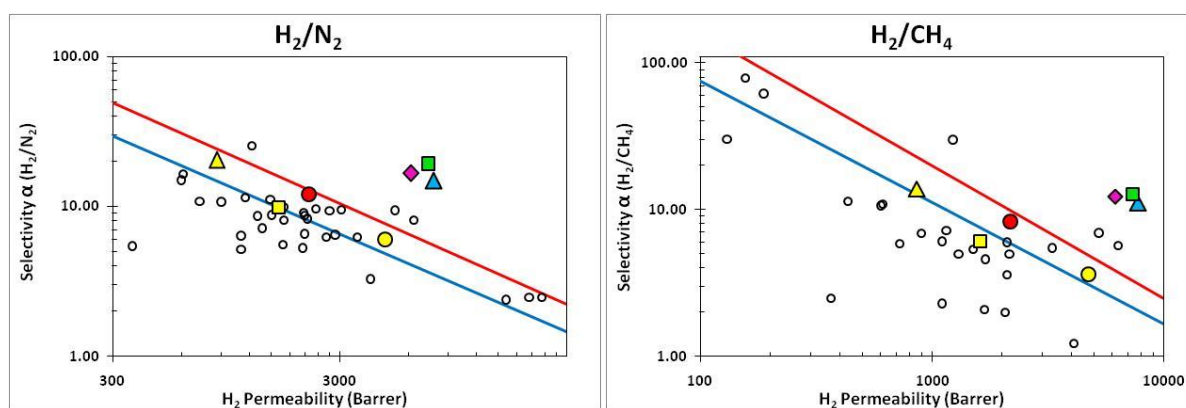
Transport parameter	Membrane	N <sub>2</sub>	O <sub>2</sub>	CO <sub>2</sub>	CH <sub>4</sub>	H <sub>2</sub>	He
$P_x$ [Barrer]	178 $\mu\text{m}$ As Cast	178	687	2319	259	2175	779
	181 $\mu\text{m}$ MeOH	525	2150	7140	699	7760	2570
	95 $\mu\text{m}$ MeOH	380	1630	5100	572	7310	2720
	181 $\mu\text{m}$ MeOH 24h	370	1590	4780	502	6155	2070
	120 $\mu\text{m}$ PIM-1 MeOH	773	2135	12775	1281	4711	1830
$\alpha(P_x/PN_2)$	178 $\mu\text{m}$ As Cast	-	3.87	13.05	1.46	12.24	4.39
	181 $\mu\text{m}$ MeOH	-	4.1	13.6	1.3	14.8	4.9
	95 $\mu\text{m}$ MeOH	-	4.3	13.4	1.5	19.2	7.2
	181 $\mu\text{m}$ MeOH 24h	-	4.3	12.9	1.4	16.6	5.6
	120 $\mu\text{m}$ PIM-1 MeOH	-	2.76	16.52	1.66	6.09	2.37
$D_x$ [ $10^{-12} \text{m}^2 \text{s}^{-1}$ ]	178 $\mu\text{m}$ As Cast	36.2	125.46	38.6	12.87	2986.48	5028.48
	181 $\mu\text{m}$ MeOH	99.5	318	87	36	>7000*	>10000*
	95 $\mu\text{m}$ MeOH	40.5	177	41	12	>5000*	>6000*
	181 $\mu\text{m}$ MeOH 24h	49.1	210	60.7	14.9	>5000*	>6000*
	120 $\mu\text{m}$ PIM-1 MeOH	164.6	452.3	199.4	70.0	5763.3	7119.6
$\alpha(D_x/DN_2)$	178 $\mu\text{m}$ As Cast	-	3.47	1.07	0.35	82.50	138.91
	181 $\mu\text{m}$ MeOH	-	3.7	1	0.32	>90*	>116*
	95 $\mu\text{m}$ MeOH	-	4.37	1.01	0.30	>123.4*	>148.1*
	181 $\mu\text{m}$ MeOH 24h	-	4.28	1.24	0.30	>101.8*	>122.2*
	120 $\mu\text{m}$ PIM-1 MeOH	-	2.748	1.211	0.425	35.018	43.259
$S_x$ [ $\text{cm}^3 \text{cm}^{-3} \text{bar}^{-1}$ ]	178 $\mu\text{m}$ As Cast	3.68	4.11	45.07	15.12	0.55	0.12
	181 $\mu\text{m}$ MeOH	4.7	6	57	14.8	<0.8*	<0.2*
	95 $\mu\text{m}$ MeOH	7	6.9	92	35.5	<1.1*	<0.3*
	181 $\mu\text{m}$ MeOH 24h	5.7	6	58.5	25.2	<1.1*	<0.3*
	120 $\mu\text{m}$ PIM-1 MeOH	3.52	3.54	48.06	13.73	0.61	0.19
$\alpha(S_x/SN_2)$	178 $\mu\text{m}$ As Cast	-	1.12	12.25	4.11	0.15	0.03
	181 $\mu\text{m}$ MeOH	-	1.1	12	4.3	<0.06*	<0.02*
	95 $\mu\text{m}$ MeOH	-	0.99	13.14	5.07	<0.16*	<0.04*
	181 $\mu\text{m}$ MeOH 24h	-	1.05	10.26	4.42	0.19	<0.05*
	120 $\mu\text{m}$ PIM-1 MeOH	-	1.004	13.634	3.894	0.174	0.055

\*A time lag (<1 s) allows only an estimation of the minimum limit of D and maximum limit of S.

Consistent with the extremely high BET surface area, the permeabilities for DMEA.TB are particularly high due to combined high diffusion and solubility coefficients. As predicted, methanol treatment significantly improves permeability, for example after treatment the membrane is over ten times more permeable to CO<sub>2</sub>. The thicker 181  $\mu\text{m}$  membrane is more permeable than the thinner 95  $\mu\text{m}$  membrane. This is a known phenomenon<sup>174</sup> that is attributed a higher relative contribution of the less permeable dense surface region of thinner membranes relative to thicker membranes. Measurements of the methanol treated 181  $\mu\text{m}$  membrane 24 hours after the first measurement shows a decrease in permeability due rapid physical ageing (as with all ultra-permeable polymers) with a corresponding increase in selectivity.

The order of gas permeabilities ( $\text{H}_2 > \text{CO}_2 > \text{He} > \text{O}_2 > \text{CH}_4 > \text{N}_2$ ) demonstrates preferential permeation for smaller gas molecules. This is not the usual trend observed for reverse selective PIMs that typically are more permeable to CO<sub>2</sub> than H<sub>2</sub> and more permeable to O<sub>2</sub> than He. This suggests that gas permeation through DMEA.TB operates at least partially on a molecular sieving mechanism. This also suggests that DMEA.TB contains smaller pores than PIM-1 however, positron annihilation lifetime spectroscopy (PALS) data would be more instructive.

According to the Robeson<sup>126</sup> relation, polymers are highly permeable at the expense of selectivity. DMEA.TB however, displays remarkably high selectivities ( $P_x/P_y$ ), especially for gas pairs with smaller kinetic diameters (He, H<sub>2</sub>, and O<sub>2</sub>) over larger diameters (CO<sub>2</sub>, N<sub>2</sub> and CH<sub>4</sub>) due to enhanced diffusivity selectivities ( $D_x/D_y$ ). Data for technologically important gas pairs O<sub>2</sub>/N<sub>2</sub>, H<sub>2</sub>/N<sub>2</sub>, H<sub>2</sub>/CH<sub>4</sub> and H<sub>2</sub>/CO<sub>2</sub> lie far over the present Robeson upper bound and close to the upper bound for CO<sub>2</sub>/CH<sub>4</sub> and He/N<sub>2</sub> (Fig 6.3.1e).





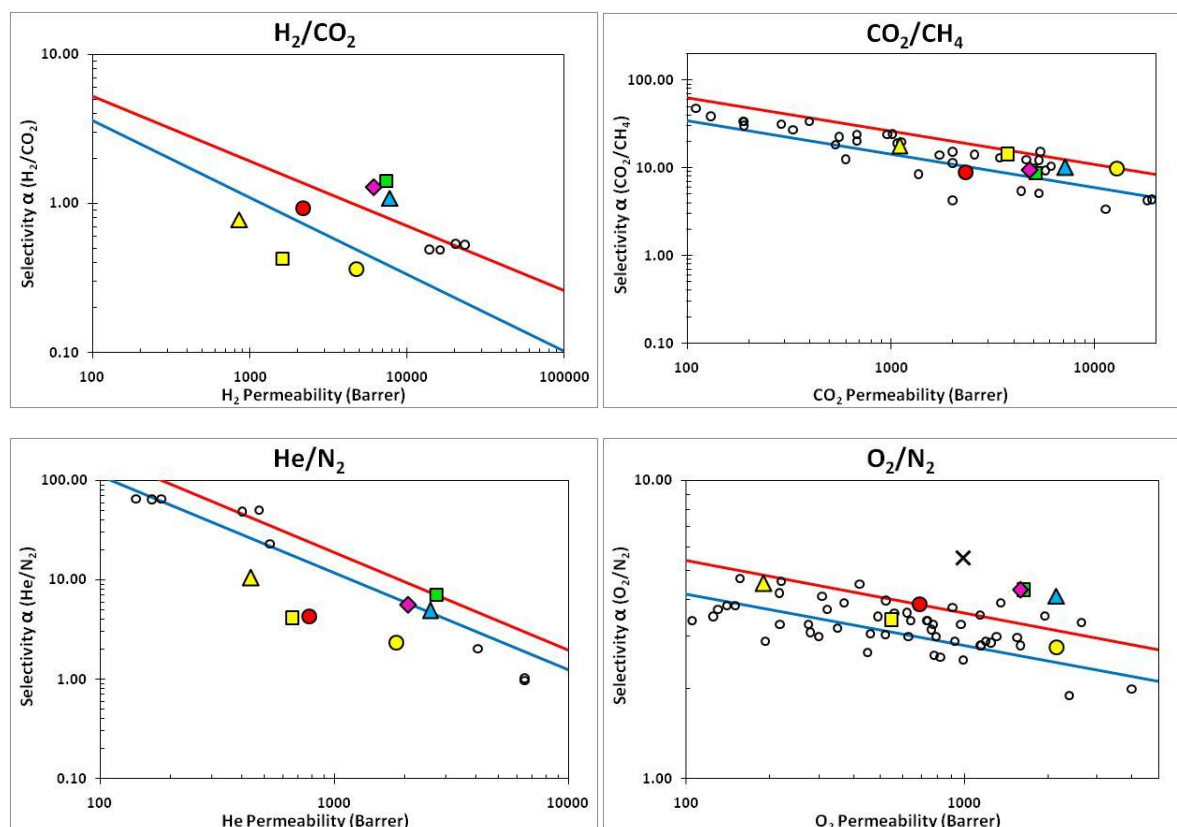


Fig 6.3.1e Robeson plots of selected gas pairs for DMEA.TB with 1991 (—) and 2008 (—) upper bounds : 178  $\mu\text{m}$  As Cast ( $\bullet$ ), 181  $\mu\text{m}$  MeOH ( $\blacktriangle$ ), 95  $\mu\text{m}$  MeOH ( $\blacksquare$ ), 181  $\mu\text{m}$  MeOH 24h ( $\blacklozenge$ ) and 181  $\mu\text{m}$  MeOH average  $\text{O}_2/\text{N}_2$  values obtained for air at variable feed pressures ( $\times$ ) compared to PIM-1 ( $\bullet$ ), PIM-7 ( $\blacktriangle$ )<sup>95</sup>, PIM-PI-8 ( $\blacksquare$ )<sup>89</sup> and Robeson's literature data lying close to the upper bounds ( $\circ$ )<sup>126, 127</sup>.

DMEA.TB was also assessed for the enrichment of  $\text{O}_2$  from air using an aged (3 days) methanol treated membrane over a range of feed pressures up to 7 bar. High permeabilities, almost independent of pressure, ranging from 900-1100 barrer ( $\text{O}_2$ ) and 160-205 barrer ( $\text{N}_2$ ) were observed. These high permeabilities coupled with exceptional selectivities (4.5-6.1) place DMEA.TB substantially over the upper bound for enrichment of  $\text{O}_2$  from air.

The enhanced gas separation characteristics of DMEA.TB are particularly evident for hydrogen paired gases which indicates unparalleled potential for a soluble polymer to separate hydrogen in applications such as Haber–Bosch ammonia production, natural gas purification, and carbon capture from steam reforming of fossil fuels.

Many gas separation processes take place at elevated temperatures and hence data collected at 25  $^\circ\text{C}$  is not directly applicable. A number of similar permeation experiments were performed by Dr. Tim Merkel at Membrane Technology and Research, Inc (MTR), California before and after heat treatment (150  $^\circ\text{C}$ ) of 160  $\mu\text{m}$  (as cast) and 145  $\mu\text{m}$  (MeOH treated) membranes. The results of this study are summarised in table 6.3.1b.

Transport parameter	Membrane	N <sub>2</sub>	CO <sub>2</sub>	CH <sub>4</sub>	H <sub>2</sub>	He
<b><math>P_x</math> [Barrer]</b>	160 $\mu\text{m}$ As Cast	18	770	46	290	120
	160 $\mu\text{m}$ As Cast After 150 °C Exposure	50	1100	110	1300	500
	145 $\mu\text{m}$ MeOH	640	6700	1200	3800	1900
	145 $\mu\text{m}$ MeOH After 150 °C Exposure	460	4900	820	5200	1800
<b><math>\alpha(P_x/PN_2)</math></b>	160 $\mu\text{m}$ As Cast	-	43	2.6	16	6.8
	160 $\mu\text{m}$ After 150 °C Exposure	-	20	1.9	24	9.1
	145 $\mu\text{m}$ MeOH	-	10	1.9	5.9	3.0
	145 $\mu\text{m}$ MeOH After 150 °C Exposure	-	11	1.8	11	4.0
<b>% Change in <math>P_x</math> after 150 °C Exposure</b>	160 $\mu\text{m}$ As Cast	181%	43%	137%	348%	315%
	145 $\mu\text{m}$ MeOH	-28%	-27%	-32%	37%	-5%
<b>% Change in <math>\alpha</math> after 150 °C Exposure</b>	160 $\mu\text{m}$ As Cast	-	-54%	-26%	51%	35%
	145 $\mu\text{m}$ MeOH	-	-7%	4%	95%	33%

The results show that heat treatment of the "as cast" sample increases the permeability of all gases due to partial removal of the casting solvent. The heat treatment of the methanol treated sample however shows a decrease in the permeability of all gases except H<sub>2</sub> with an overall increase in selectivities. Although heat treatment removes residual methanol, increasing permeability, the overall decrease in permeability is due to temperature induced acceleration of physical ageing being a dominant factor. Even after heat treatment, data for H<sub>2</sub>/N<sub>2</sub>, H<sub>2</sub>/CH<sub>4</sub> and H<sub>2</sub>/CO<sub>2</sub> remain over the present Robeson upper bound.

A second experiment was performed by MTR to evaluate the potential of DMEA.TB for hydrogen enrichment and carbon capture at elevated feed temperatures during the steam reforming of fossil fuels.

The permeabilities of H<sub>2</sub> and CO<sub>2</sub> on both as cast and methanol treated membranes were measured as a function of feed temperature at a constant feed pressure of 4.5 bar (Fig 6.3.1f).

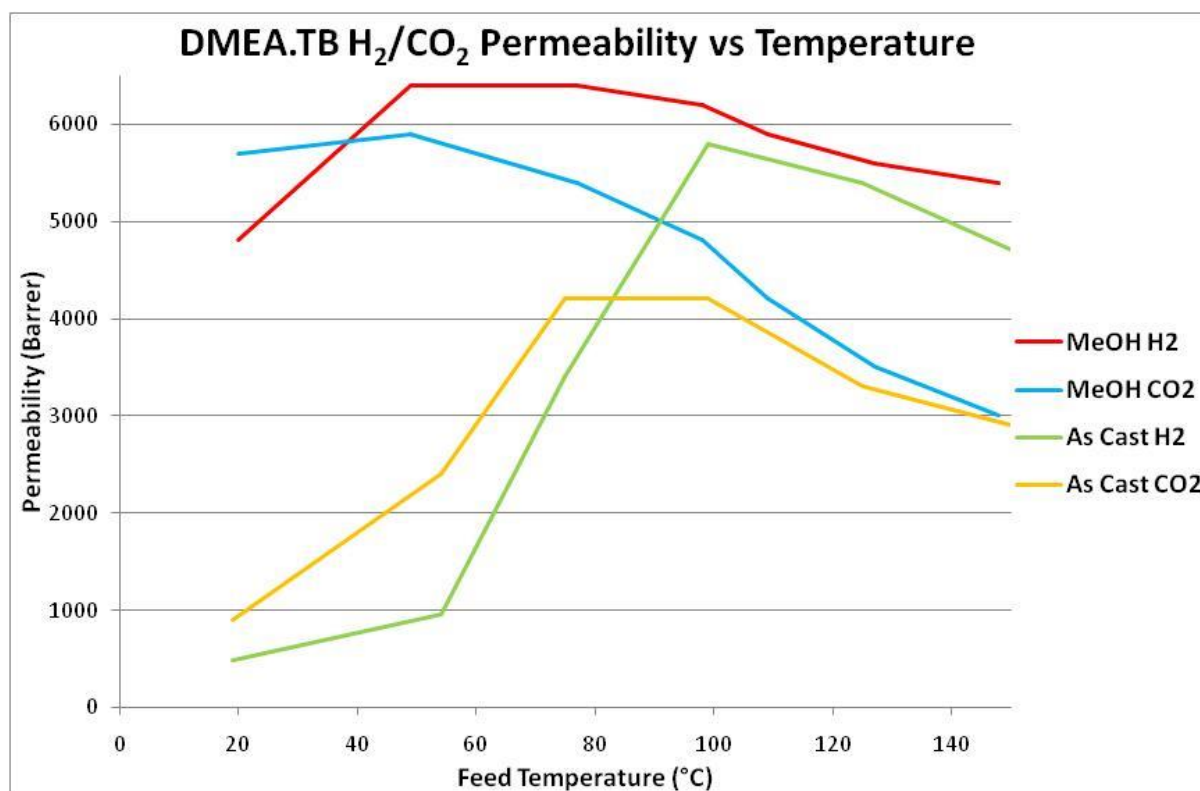


Fig 6.3.1f Permeability of "as cast" and "MeOH treated" DMEA.TB membranes as a function of feed temperature.

As expected, the permeabilities of both gases are higher for the methanol treated membrane and become similar values for both membranes at higher temperatures due to solvent removal. For both samples, CO<sub>2</sub> is initially more permeable than H<sub>2</sub> but the reverse becomes true as solvent is removed. The permeability of both H<sub>2</sub> and CO<sub>2</sub> initially increase with temperature for both samples as solvent is removed from the membranes. According to the dual sorption model, permeate diffusion through a high free volume polymer is a thermally activated process and so the diffusion coefficients increase with temperature which contribute towards initial higher permeabilities. After the initial increase, permeabilities then decrease due to accelerated physical ageing. Another factor decreasing the permeability is that gas solubility in polymers decreases with increasing temperature.

This decrease in solubility affects larger, more condensable gas molecules than smaller, less condensable molecules. As temperature increases, there is then a larger decrease in the solubility of CO<sub>2</sub> than there is for H<sub>2</sub> which is responsible for a larger drop in the observed permeability for CO<sub>2</sub> than H<sub>2</sub>. It follows that as temperature increases, the relative difference in permeabilities of H<sub>2</sub> and CO<sub>2</sub> also increases and so selectivity increases with temperature (Fig 6.3.1g).

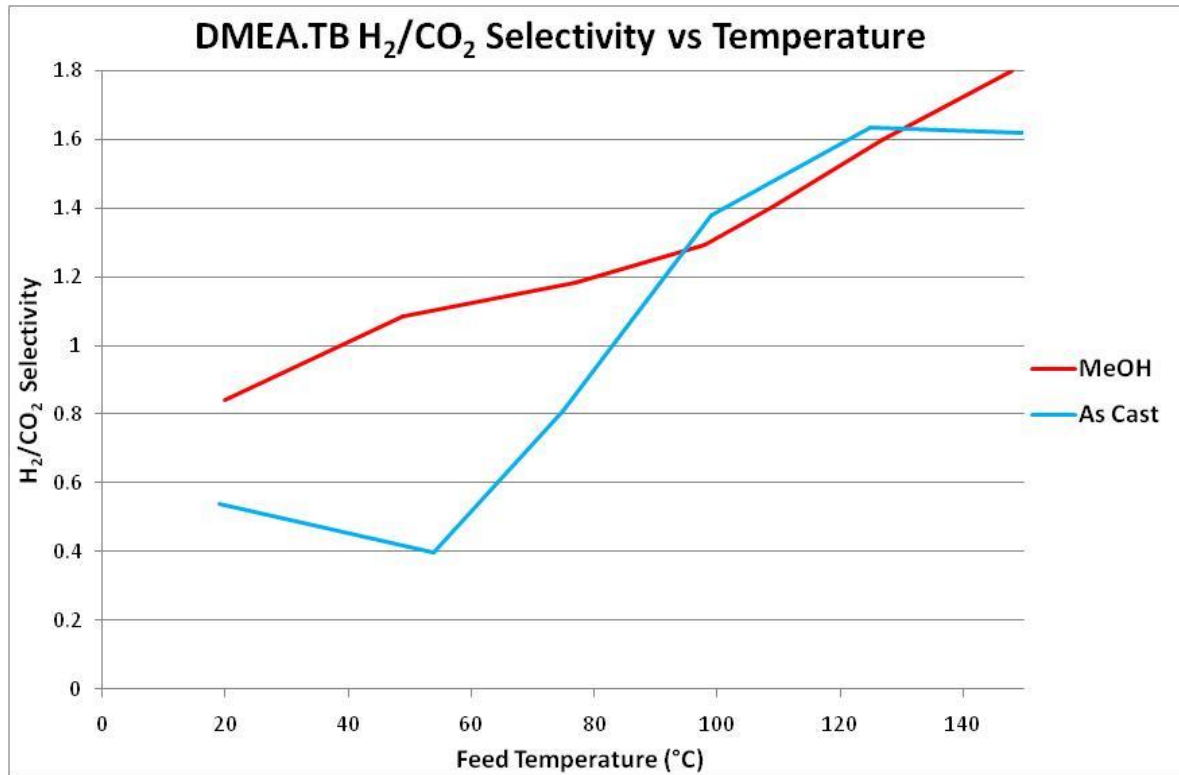


Fig 6.3.1g Selectivity of "as cast" and "MeOH treated" DMEA.TB membranes as a function of feed temperature.

At higher temperatures both samples provide data over the present upper bound (Fig 6.3.1h) indicating that DMEA.TB has potential in high temperature separation of H<sub>2</sub>/CO<sub>2</sub>.

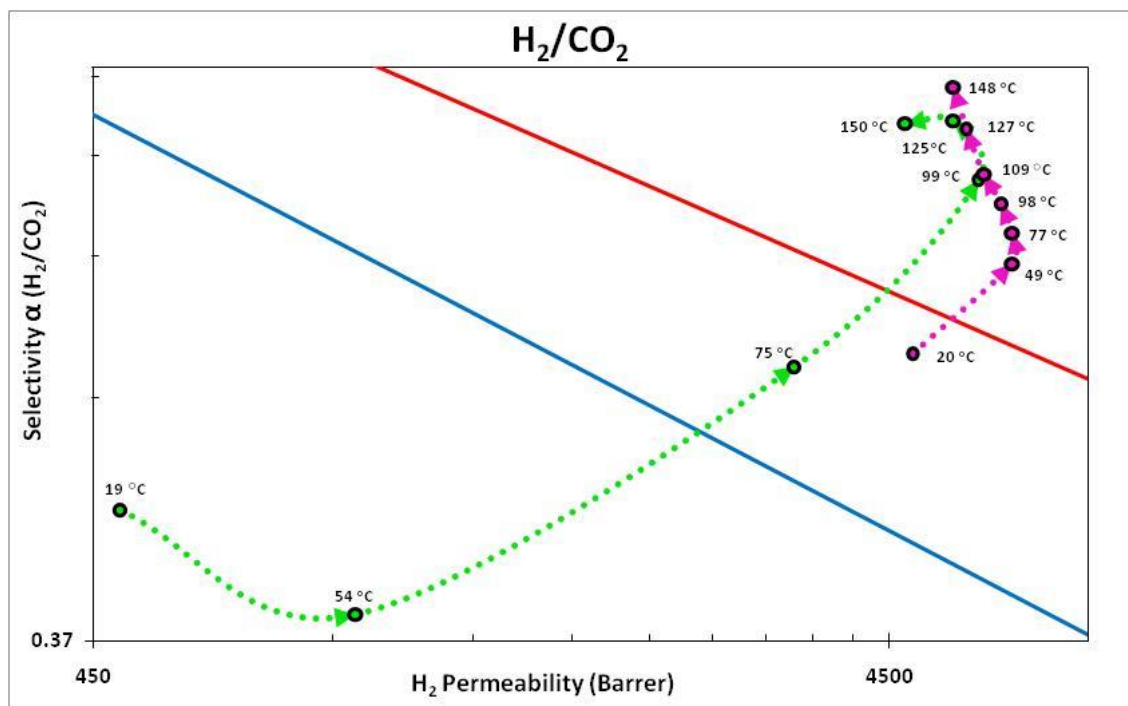
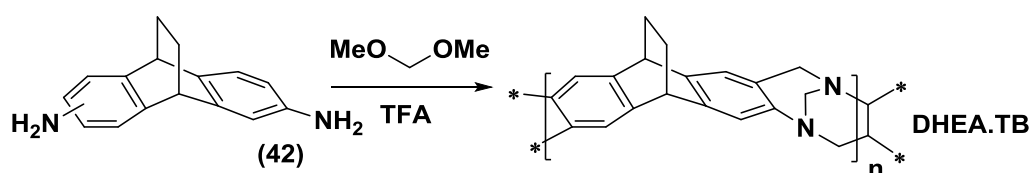


Fig 6.3.1h Robeson plot of H<sub>2</sub>/CO<sub>2</sub> with 1991 (—) and 2008 (—) upper bounds: as cast (●) and MeOH treated (●) DMEA.TB membranes at different temperatures.

### 6.3.2: DHEA.TB

With the success of DMEA.TB for gas permeation due to its enhanced rigidity, it was speculated that the methyl groups may be acting as rotors that impede or accelerate the passage of permeate molecules. It was theorised that selectivity could be improved by preparing an analogue polymer, DHEA.TB, lacking these bridgehead methyl groups to increase structural rigidity even further.

DHEA.TB was synthesised in 91% yield from the TB polymerisation of 9,10-dihydro-2,6(7)-diamino-9,10-ethanoanthracene at a concentration of 8.33 ml of TFA per gram of monomer over 2 h (Scheme 6.3.2a) and was isolated as a white powder.



Scheme 6.3.2a Synthesis of DHEA.TB.

Thermal gravimetric analysis shows the polymer is stable up to 260 °C with an initial 10% decrease in mass, consistent with the loss of an ethylene fragment from the ethanoanthracene unit via a retro Diels-Alder reaction<sup>172</sup>. Differential scanning calorimetry did not reveal the presence of a glass transition below its decomposition temperature. Analysis of the acetone washings from the crude polymer using MALDI-TOF failed to reveal an oligomeric pattern.

Nitrogen adsorption shows DHEA.TB has a high BET surface area of 843 m<sup>2</sup>/g which again, can be attributed to the extreme structural rigidity of both the ethanoanthracene and the TB linking units. The somewhat lower BET surface area of DHEA.TB compared to DMEA.TB confirmed our suspicion that the bridgehead methyl groups in DMEA.TB serve as struts that further disrupt polymer chain packing in a similar manner to the previously described bridgehead alkylated triptycene network polymers<sup>76</sup>.

It was found by varying the polymerisation concentration, that DHEA.TB is much less resistant to cross-linking than DMEA.TB. This is likely due to the 1,4 and 5,8 aromatic positions being less sterically protected from electrophilic attack of the from reactive TB intermediates compared to DMEA.TB. For this reason a shorter reaction time of 2h was required to produce a high molecular weight polymer (GPC:  $M_n = 9,200$ ,  $M_w = 49,300$ ) before the onset of insoluble gel formation. DHEA.TB was found to have almost identical film forming properties to DMEA.TB and a number of membranes were formed (Fig 6.3.2a) for gas permeation studies by ITM. The results of permeation tests on a 128  $\mu\text{m}$  as cast and a

130  $\mu\text{m}$  MeOH treated membrane are summarised in table 6.3.2a along with results from a 181  $\mu\text{m}$  DMEA.TB methanol treated membrane for comparison.

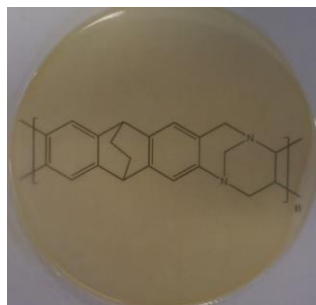


Fig 6.3.2a An optically clear chloroform-cast film (10 cm x 128  $\mu\text{m}$ ) of DHEA.TB, through which is visible its molecular structure printed on a piece of paper.

Table 6.3.2a DHEA.TB Membrane Permeability Measurements							
Transport parameter	Membrane	N <sub>2</sub>	O <sub>2</sub>	CO <sub>2</sub>	CH <sub>4</sub>	H <sub>2</sub>	He
$P_x$ [Barrer]	128 $\mu\text{m}$ As Cast	29	94	495	64	262	118
	130 $\mu\text{m}$ MeOH	369	1673	6097	469	6088	1938
	DMEA.TB 181 $\mu\text{m}$ MeOH	525	2150	7140	699	7760	2570
$\alpha(P_x/PN_2)$	128 $\mu\text{m}$ As Cast	-	3.23	17.05	2.20	9.01	4.05
	130 $\mu\text{m}$ MeOH	-	4.68	17.05	1.28	17.02	5.42
	DMEA.TB 181 $\mu\text{m}$ MeOH	-	4.1	13.6	1.3	14.8	4.9
$D_x$ [ $10^{-12}$ m <sup>2</sup> s <sup>-1</sup> ]	128 $\mu\text{m}$ As Cast	16.27	40.41	13.68	6.35	802.6	2006.8
	130 $\mu\text{m}$ MeOH	47.64	216.42	66.44	15.06	5634.2	7822.1
	DMEA.TB 181 $\mu\text{m}$ MeOH	99.5	318	87	36	>7000*	>10000*
$\alpha(D_x/DN_2)$	128 $\mu\text{m}$ As Cast	-	2.48	0.84	0.39	49.33	123.34
	130 $\mu\text{m}$ MeOH	-	4.54	1.39	0.32	118.27	164.19
	DMEA.TB 181 $\mu\text{m}$ MeOH	-	3.7	1	0.32	>90*	>116*
$S_x$ [cm <sup>3</sup> cm <sup>-3</sup> bar <sup>-1</sup> ]	128 $\mu\text{m}$ As Cast	1.34	1.73	27.13	7.54	0.24	0.04
	130 $\mu\text{m}$ MeOH	5.63	5.80	68.83	22.83	0.81	0.19
	DMEA.TB 181 $\mu\text{m}$ MeOH	5.7	6	58.5	25.2	1.1	0.3
$\alpha(S_x/SN_2)$	128 $\mu\text{m}$ As Cast	-	1.29	20.28	5.63	0.18	0.03
	130 $\mu\text{m}$ MeOH	-	1.03	12.22	4.05	0.14	0.03
	DMEA.TB 181 $\mu\text{m}$ MeOH	-	1.1	12	4.3	<0.06*	<0.02*

\*A time lag (<1 s) allows only an estimation of the minimum limit of D and maximum limit of S.

As with DMEA.TB, methanol treatment of the DHEA.TB membrane results in a significant increase in permeability. The permeabilities of all gases are lower for DHEA.TB than DMEA.TB which is consistent with the lower surface area of DHEA.TB. These permeabilities are however still relatively high. The order of gas permeabilities for DHEA.TB ( $\text{CO}_2 > \text{H}_2 > \text{He} > \text{O}_2 > \text{CH}_4 > \text{N}_2$ ) is slightly different to that of DMEA.TB where  $\text{CO}_2$  is marginally more permeable than  $\text{H}_2$  (differing by only 9 barrer). DHEA.TB however demonstrates analogous molecular sieving type permeation observed for DMEA.TB. In accordance with the Robeson trade off relation, the less permeable DHEA.TB displays higher selectivities ( $P_x/P_y$ ), than DMEA.TB due to higher diffusivity selectivities ( $D_x/D_y$ ). Larger selectivities are again observed for gas pairs with smaller kinetic diameters ( $\text{He}$ ,  $\text{H}_2$ , and  $\text{O}_2$ ) over larger diameters ( $\text{CO}_2$ ,  $\text{N}_2$  and  $\text{CH}_4$ ). Data for technologically important gas pairs  $\text{H}_2/\text{N}_2$ ,  $\text{H}_2/\text{CH}_4$ , and  $\text{O}_2/\text{N}_2$ , lie far over the present Robeson upper bound and close to the upper bound for  $\text{H}_2/\text{CO}_2$  (Fig 6.3.2b).

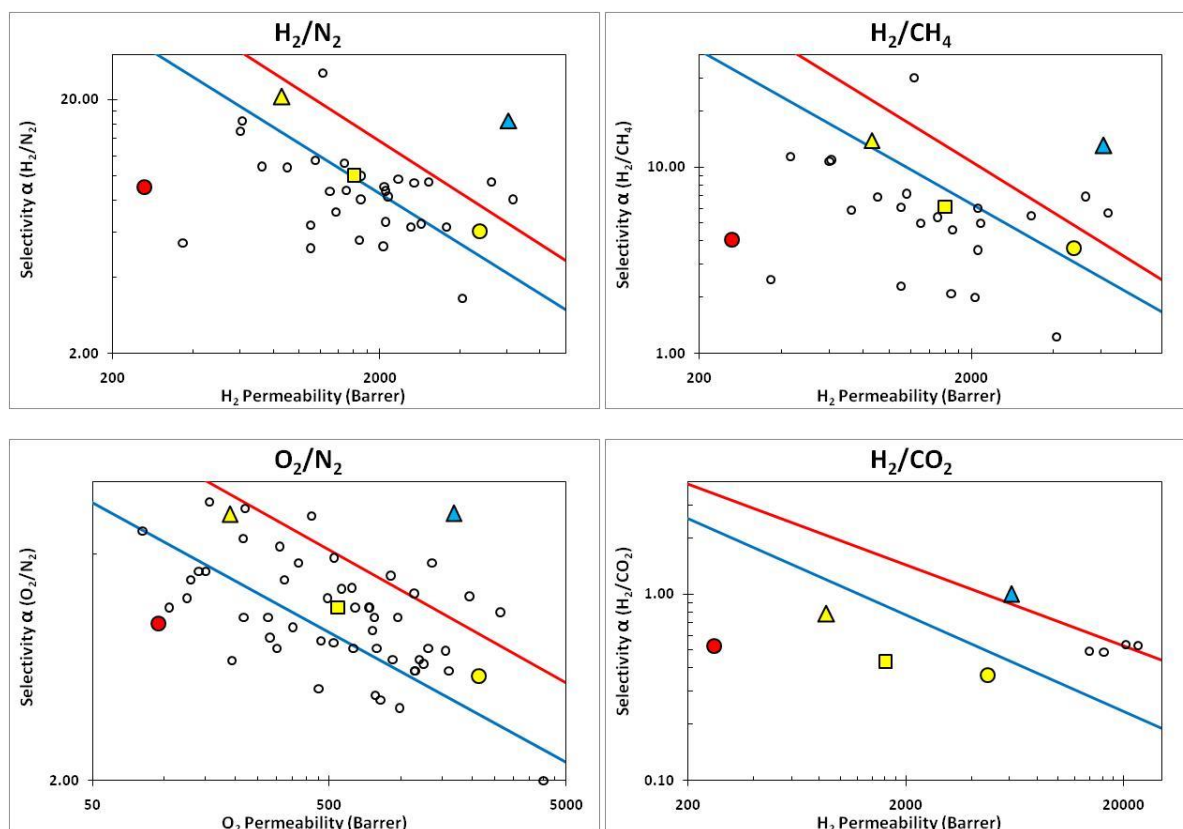
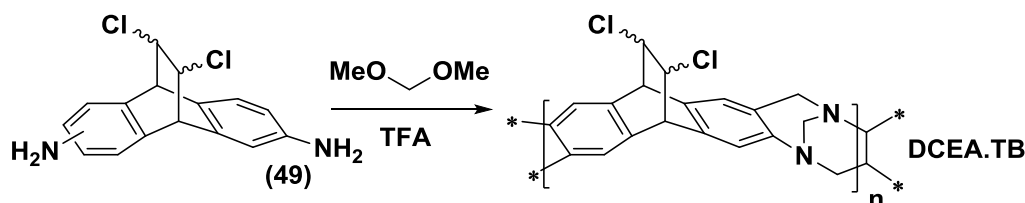


Fig 6.3.2b Robeson plots of selected gas pairs for DMEA.TB with 1991 (—) and 2008 (—) upper bounds : 128  $\mu\text{m}$  As Cast (●) and 130  $\mu\text{m}$  MeOH (▲) compared to PIM-1 (○), PIM-7 (▲)<sup>95</sup>, PIM-PI-8 (■)<sup>89</sup>, and Robeson's literature data lying close to the upper bounds (○)<sup>126, 127</sup>.

### 6.3.3: DCEA.TB

Incorporation of polar functional groups into microporous polymers has been known to improve gas solubility and selectivity by increasing electrostatic interactions<sup>119</sup>. As an intermediate in the synthesis of the DHEA.TB monomer, 9,10-dihydro-11,12-*cis(trans)*-dichloro-9,10-ethanoanthracene presented an opportunity to introduce chlorine functionality into a TB polymer and test the functional group tolerance of the TB polymerisation.

DCEA.TB was synthesised in 88% yield from the TB polymerisation of 9,10-dihydro-2(3),6(7)-diamino-11,12-*cis(trans)*-dichloro-9,10-ethanoanthracene at a concentration of 8.33 ml of TFA per gram of monomer over 3 days (Scheme 6.3.3.a) and was isolated as a light brown powder.



Scheme 6.3.3.a Synthesis of DCEA.TB.

Thermal gravimetric analysis shows the polymer is stable up to 250 °C with an initial 20% decrease in mass, consistent with the loss of Cl<sub>2</sub> from the bridge unit to form dibenzobarrelene units. Differential scanning calorimetry did not reveal the presence of a glass transition below its decomposition temperature. Analysis of the acetone washings from the crude polymer using MALDI-TOF failed to reveal an oligomeric pattern.

Nitrogen adsorption shows DHEA.TB has only a modest BET surface area = 360 m<sup>2</sup>/g. The chlorine atoms were initially expected to act as struts that separate polymer chains, however it is likely that the large chlorine atoms fill any pore space that is created.

The molecular weight of DCEA.TB remains undetermined as it was not soluble in a solvent suitable for GPC analysis. It can be said however, that the polymerisation afforded a highly viscous solution which suggests a high molecular weight polymer had been formed. The only solvent that DCEA.TB was found to be soluble in was DMSO, which is unsuitable for film formation and hence no permeability measurements were made.

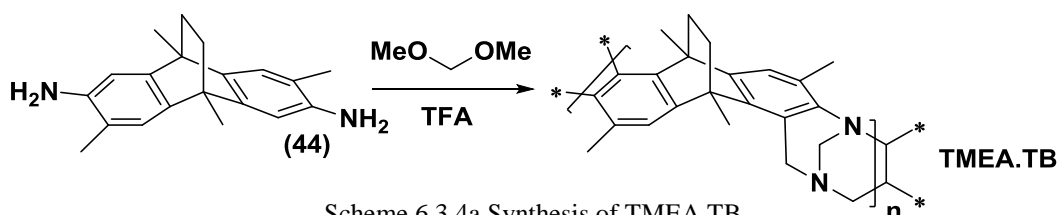
In possible future studies, the chlorine functionality can be removed post-polymerisation by heating the polymer to 250 °C, forming dibenzobarrelene units throughout the polymer chain, further enhancing structural rigidity and thermal stability.



### 6.3.4: TMEA.TB

The design of the TMEA.TB monomer was expected to serve a number of functions. The aromatic methyl groups placed adjacent to the amine groups prevent reactions at these positions and offer only a single free position for TB formation. This reduces the number of possible cross-linking sites on the aromatic rings and further hinders the remaining sites from attack. It also forces the polymer into a more contorted "zigzag" conformation with extra methyl group struts that further disrupt efficient chain packing. It was also expected that the directions of polymer growth imposed by the methyl groups would prevent the formation of cyclic structures, while simultaneously increasing amine nucleophilicity, both having a positive contribution to molecular weight.

The synthesis of TMEA.TB was attempted from the TB polymerisation of 2,6,9,10-tetramethyl-9,10-dihydro-3,7-diamino-9,10-ethanoanthracene at a concentration of 5 ml of TFA per gram of monomer over 7 days (Scheme 6.3.4a).



The TB polymerisation did not achieve a high viscosity, even at higher concentrations, temperatures or prolonged reaction times, suggesting only oligomeric material had formed. A large proportion of the material recovered was acetone soluble, leaving only a small quantity (43% yield) of higher molecular weight oligomers as a white powder. Purification of the oligomeric material was unsuccessful due to high solubility preventing the precipitation of higher oligomers.

The reason a high molecular weight polymer did not form is likely due to the only free position available for TB formation being too sterically hindered by the bridgehead methyl groups, resulting in a greatly reduced reaction rate. A possible solution to the problem would be to use a monomer lacking bridgehead methyl groups, although a lower surface area is a possible consequence.

Thermal gravimetric analysis shows the material is stable up to 260 °C, consistent with other TB polymers based on ethanoanthracenes. Differential scanning calorimetry did not reveal the presence of a glass transition below its decomposition temperature.

Analysis of the recovered material using MALDI-TOF revealed multiples of the presumed polymeric repeating unit ( $C_{23}H_{24}N_2$ ) with the additional weight of two amine end groups (Fig 6.3.4a).

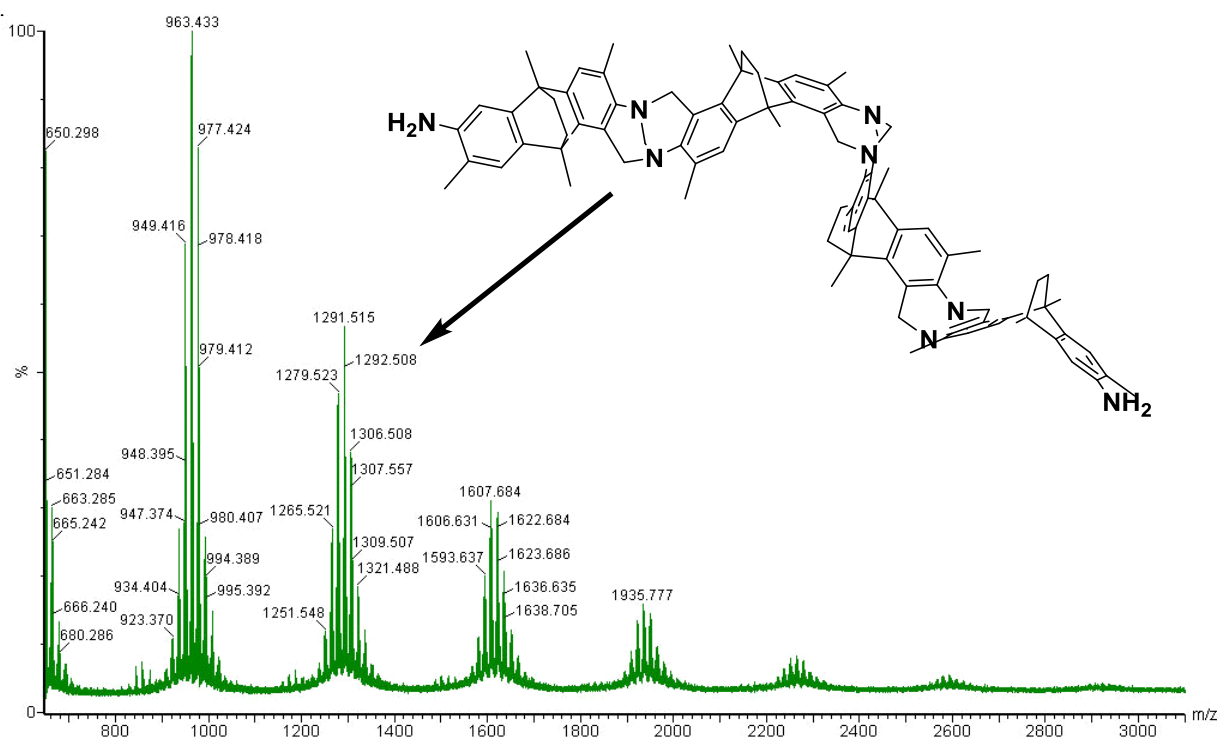


Fig 6.3.4a MALDI-TOF spectrum of recovered TMEA.TB oligomers showing the repeating unit of the polymer resulting from linear oligomers and a linear tetramer is illustrated.

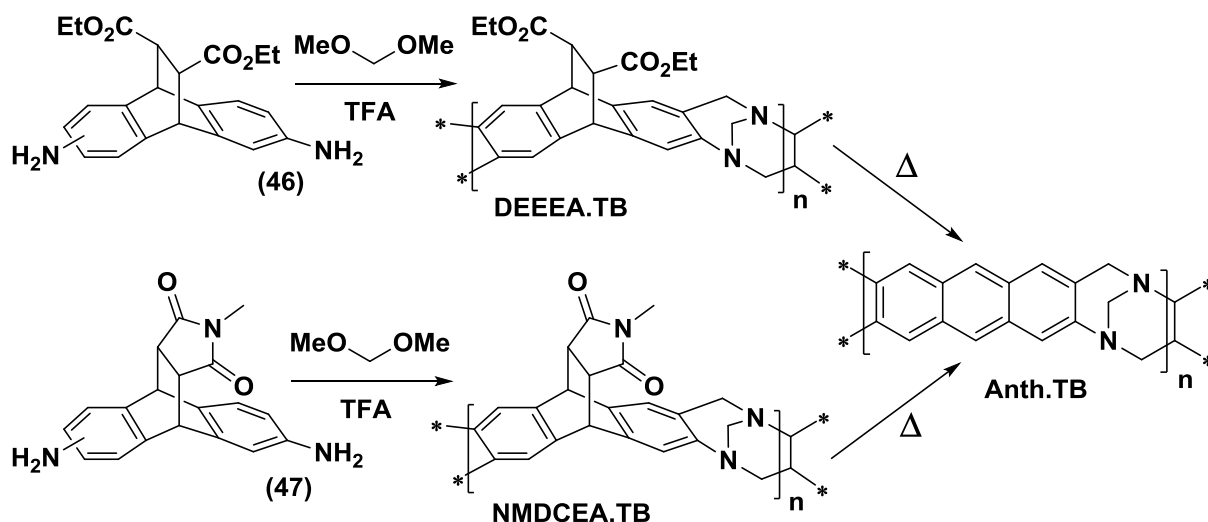
The values obtained show the presence of linear oligomers from trimers to octamers and possibly higher oligomers. The absence of cyclic structures confirms the earlier presumption that cyclic oligomers would be prevented from forming due to the imposed directions of polymer growth.

Nitrogen adsorption shows that the low molecular weight material has a low BET surface area of only  $70 \text{ m}^2/\text{g}$ . This may be attributed to the oligomeric nature of the material and the inability to remove impurities using a re-precipitation method. It may also be the case that the extra methyl groups fill pore space and reduce free volume. Without measurements from a high molecular weight sample, it is difficult to determine the reason for such a relatively low surface area compared to other EA.TB analogues.

### 6.3.5: Anth.TB

The rigid extended rod-like structure of anthracene has previously been incorporated into polymers such as polyesters<sup>175</sup> and polyimides<sup>148, 176</sup>. Polymers incorporating planar anthracene structures tend to be insoluble due to aggregation of anthracene units resulting from non-covalent interactions. Such a trait can make the processing of these polymers problematic. A solution to this problem is to first synthesise a soluble precursor polymer that can be processed into the required form such as a film. This film can be subsequently converted into the required aromatic anthracene polymer via a simple reaction such as thermal treatment. This “precursor-polymer” approach was utilised by Hodge<sup>148</sup> and co-workers in 1996 to produce polyimides containing anthracene units. Hodge and co-workers prepared a number of precursor polyimides from monomers that were Diels-Alder adducts of diaminoanthracene with dienophiles such as dimethyl fumarate and N-methylmaleimide. These soluble precursor polymers were then formed into films and subsequently heated to 220 °C to convert them to anthracene polyimides by a thermal retro Diels-Alder reaction that removes the dieneophile bridge units.

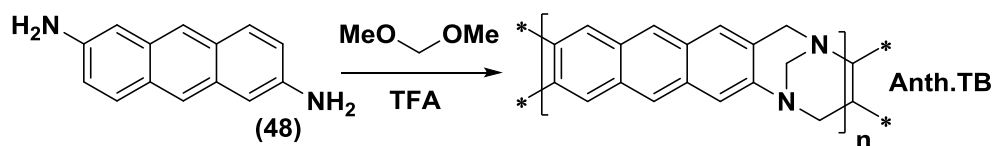
This precursor polymer approach was applied in an attempt to synthesise Anth.TB. Diels-Alder adducts of diaminoanthracene with diethyl fumarate and N-methylmaleimide were used as TB monomers to form precursor polymers that could be subsequently converted to Anth.TB by thermal treatment (Scheme 6.3.5a).



Scheme 6.3.5a Synthesis of precursor polymers DEEEA.TB, NMDCEA.TB and subsequent thermal treatment to form Anth.TB

The synthesis of both precursor polymers DEEEA.TB and NMDCEA.TB was attempted from the TB polymerisation of 9,10-dihydro-2(3),6(7)-diamino-9,10-ethanoanthracene-11,12-*trans*-diethyl ester and N-methyl-9,10-dihydro-2(3),6(7)-diamino-9,10-ethanoanthracene-11,12-*cis*-dicarboximide respectively. Both polymerisation reactions were conducted at a concentration of 10 ml of TFA per gram of monomer over 3 days (Scheme 6.3.5a). Both polymerisations failed to achieve a high viscosity, even at higher concentrations, temperatures or prolonged reaction times, suggesting only oligomeric material had formed. This may be due to electron withdrawing effects of the bridge substituents reducing amine nucleophilicity. A large proportion of the material recovered was acetone soluble, leaving only a small quantity of higher molecular weight oligomers as a white powder. Purification of the oligomeric material was unsuccessful due to high solubility preventing the precipitation of higher oligomers. Analysis of the oligomers using MALDI-TOF failed to reveal an oligomeric pattern. Nitrogen adsorption shows that both materials were not microporous, having BET surface areas of 0 and 2 m<sup>2</sup>/g for DEEEA.TB and NMDCEA.TB respectively. This may be attributed to the oligomeric nature of the material and the inability to remove impurities using a re-precipitation method.

A second route was also tested to form Anth.TB directly from the TB polymerisation of 2,6-diaminoanthracene at a concentration of 10 ml of TFA per gram of monomer over 3 days (Scheme 6.3.5b).



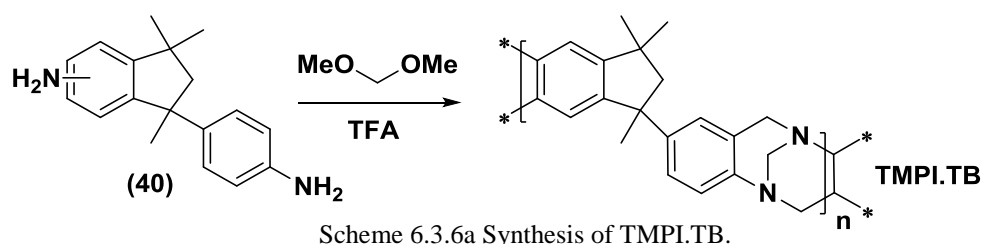
Scheme 6.3.5b Synthesis of Anth.TB.

This polymerisation also failed to achieve a high viscosity and instead, precipitated a dark brown powder that was insoluble in all common solvents and acids. This is likely due to extensive cross-linking at a number of free aromatic positions on the monomer. Nitrogen adsorption shows that the material was not microporous, having BET surface area of 1 m<sup>2</sup>/g. This may be attributed to non-covalent interactions between anthracene units enabling efficient packing of polymer chains. Since Anth.TB has been shown to be thermally stable up to 377 °C by TGA, it is possible that an Anth.TB film could be formed directly from the thermal treatment of a DHEA.TB film. The low BET surface area observed for Anth.TB however, does not indicate that this material would be suitable for gas separation membrane applications.

### 6.3.6: TMPI.TB

The TMPI.TB monomer is the same diaminophenylindane used for the previously described Matrimid®<sup>85</sup> polyimide. The phenylindane skeleton contains a single carbon-carbon bond between the phenyl and indane unit that can freely rotate. While this is not a usual feature of a PIM monomer, the connected tetrahedral carbon provides a site of contortion.

The synthesis of TMPI.TB was attempted from the TB polymerisation of 6,(7)-amino-1,3,3-trimethyl-1-(4-aminophenyl)indane at a concentration of 30 ml of TFA per gram of monomer over 16 h (Scheme 6.3.6a) and was isolated as a white powder.



Thermal gravimetric analysis shows the polymer is stable up to 349 °C. Differential scanning calorimetry did not reveal the presence of a glass transition below its decomposition temperature.

It was found that TMPI.TB is extremely sensitive to changes in the concentration of polymerisation, even only using three equivalents of dimethoxymethane. At concentrations higher than 30 ml of TFA per gram of monomer, the polymer cross-links at an unpredictable time from the start of the reaction. This is likely due to a number of free positions on the benzene rings that are vulnerable to cross-linking reactions. At lower concentrations a low molecular weight polymer is formed (GPC:  $M_n = 200$ ,  $M_w = 1,700$ ) (Fig 6.3.6a).

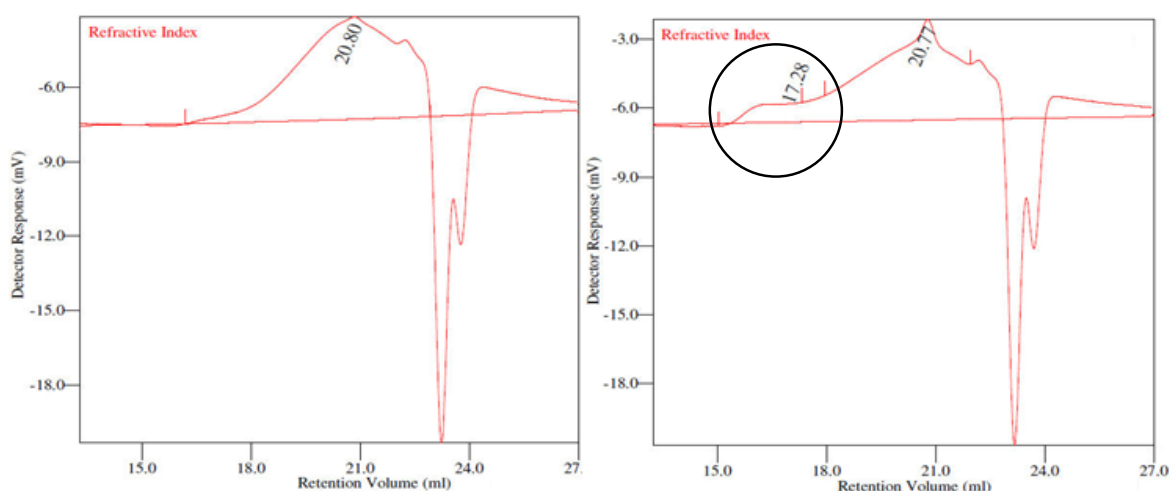


Fig 6.3.6a Gel permeation chromatography (chloroform) traces of TMPI.TB: Crude polymer (left) and polymer purified by three re-precipitation procedures with second peak highlighted (right).

After the polymer had been subjected to three re-precipitation purification procedures, a second, less intense peak became visible (GPC retention volume  $\sim 16$  ml) (Fig 6.3.6a). This second peak suggests the material contains a small proportion of high molecular weight polymer but a much larger proportion of low molecular weight oligomers.

Analysis of the crude polymer using MALDI-TOF revealed multiples of the presumed polymeric repeating unit ( $C_{21}H_{22}N_2$ ) as sharp intense peaks (Fig 6.3.6b).

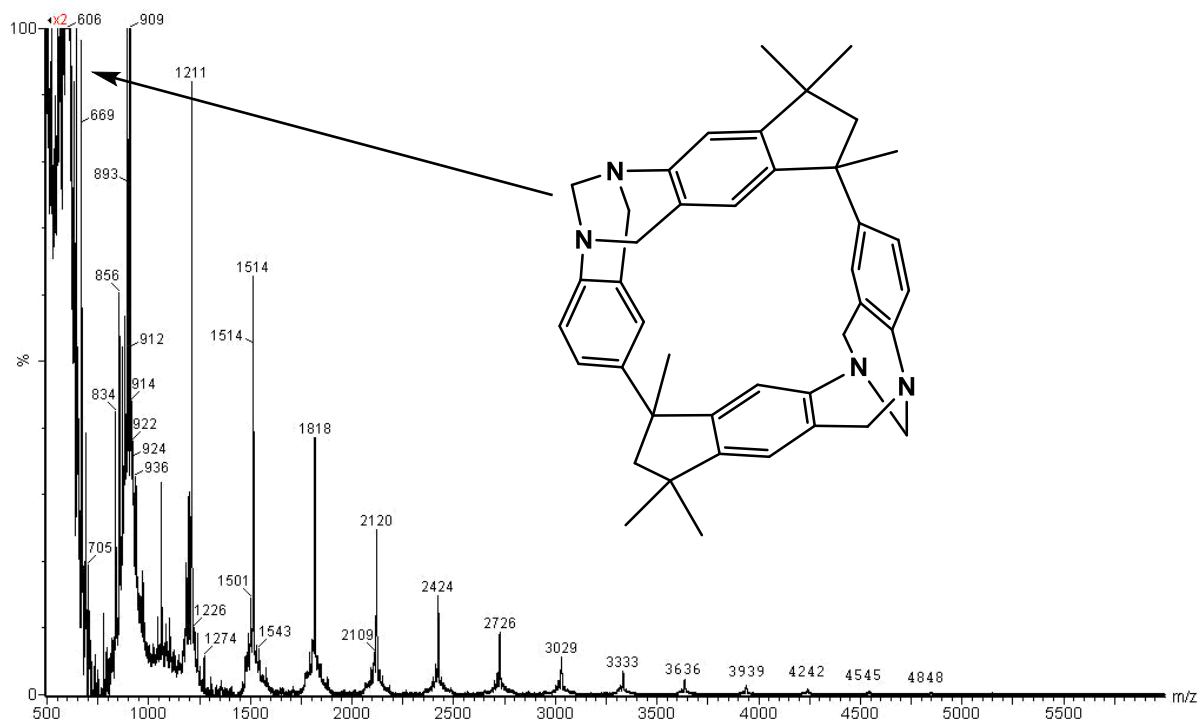


Fig 6.3.6b MALDI-TOF spectrum of TMPI.TB oligomers showing the repeating unit of the polymer resulting from cyclic oligomers and a cyclic dimer is illustrated.

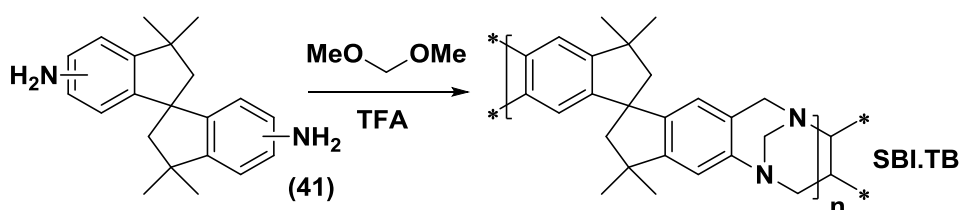
The values obtained show the presence of cyclic oligomers from dimers to heptadecamers. The rotatable single carbon-carbon bond between the phenyl and indane unit provides the monomer enough flexibility to twist and bend into the correct conformation to form cyclic structures. It is likely that this is the reason for the formation of such a large proportion of oligomeric material compared to high molecular weight polymer.

Nitrogen adsorption shows TMPI.TB has a high BET surface area of  $535 \text{ m}^2/\text{g}$ . This relatively high surface area is somewhat surprising considering the polymer contains rotatable bonds. It demonstrates however, that a single carbon-carbon bond connected to a tetrahedral carbon in a five membered ring can provide an effective site of contortion in PIM design.

### 6.3.7: SBI.TB

The spirobisindane architecture has been previously described in its use in the synthesis of a number of PIMs, most notably PIM-1. Similar to the TMPI.TB phenylindane monomer, the SBI.TB monomer differs where a tetrahedral carbon is shared by two five membered rings. This structure, known as a spiro unit, is significantly more shape persistent than the phenylindane structure and offers increased structural rigidity compared to TMPI.TB.

SBI.TB was synthesised in 73% yield from the TB polymerisation of 6,(7),6',(7')-diamino-3,3,3',3'-tetramethyl-1,1'-spirobisindane at a concentration of 8.33 ml of TFA per gram of monomer over 48 h (Scheme 6.3.7a) and was isolated as a white powder.



Scheme 6.3.7a Synthesis of SBI.TB.

Thermal gravimetric analysis shows the polymer is stable up to 435 °C. Differential scanning calorimetry did not reveal the presence of a glass transition below its decomposition temperature. Analysis of the acetone washings from the crude polymer using MALDI-TOF failed to reveal an oligomeric pattern.

Nitrogen adsorption shows SBI.TB has a high BET surface area of 745 m<sup>2</sup>/g. As expected this value is higher than TMPI.TB due to enhanced structural rigidity. This value is however lower compared to TB polymers containing ethanoanthracene units, suggesting that spirobisindane units are relatively flexible in comparison.

It was found by varying the polymerisation concentration, that SBI.TB is significantly more resistant to cross-linking than other all other TB monomers discussed in this thesis. This is likely due to the 5,5' aromatic positions being sterically protected from reactive TB intermediates by two methyl groups each and the 8,8' positions being protected by both monomer geometry and one methylene group each. This increased resistance to cross-linking enabled the polymerisation reaction to proceed for a longer time of 48 h before the onset of insoluble gel formation. The longer reaction time enabled SBI.TB to be obtained as a very high molecular weight polymer (GPC:  $M_n = 96,000$ ,  $M_w = 360,000$ ), which is the highest so far obtained for a TB polymer. In addition, the geometry and enhanced rigidity of the SBI structure compared to the phenylindane unit is likely to inhibit the formation of cyclic

structures, leading to an increase in molecular weight. SBI.TB was found to have excellent film forming properties and a number of films were formed (Fig 6.3.7a) for membrane gas permeation studies by ITM. The results of permeation tests on a 193  $\mu\text{m}$  as cast, a 157  $\mu\text{m}$  MeOH and a 128  $\mu\text{m}$  MeOH treated membrane are summarised in Table 6.3.7a.

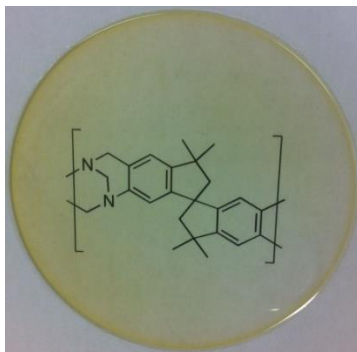


Fig 6.3.7a An optically clear chloroform-cast film (10 cm x 193  $\mu\text{m}$ ) of SBI.TB, through which is visible its molecular structure printed on a piece of paper.

Table 6.3.7a SBI.TB Membrane Permeability Measurements							
Transport parameter	Membrane	N <sub>2</sub>	O <sub>2</sub>	CO <sub>2</sub>	CH <sub>4</sub>	H <sub>2</sub>	He
$P_x$ [Barrer]	193 $\mu\text{m}$ As Cast	71	269	1056	121	1036	471
	157 $\mu\text{m}$ MeOH	232	720	2900	450	2200	878
	128 $\mu\text{m}$ MeOH	215	657	2720	406	2110	858
$\alpha(P_x/PN_2)$	193 $\mu\text{m}$ As Cast	-	3.78	14.82	1.69	14.54	6.60
	157 $\mu\text{m}$ MeOH	-	3.1	12.5	1.9	9.4	3.8
	128 $\mu\text{m}$ MeOH	-	3.1	12.7	1.9	9.8	4
$D_x$ [ $10^{-12}$ m <sup>2</sup> s <sup>-1</sup> ]	193 $\mu\text{m}$ As Cast	30.8	94.24	36.52	11.68	>2116*	>3980*
	157 $\mu\text{m}$ MeOH	75.2	201	74	31.5	3500	>5000*
	128 $\mu\text{m}$ MeOH	70.1	187	66	19.1	>3000*	>5000*
$\alpha(D_x/DN_2)$	193 $\mu\text{m}$ As Cast	-	3.06	1.19	0.38	>68.70*	>129.2*
	157 $\mu\text{m}$ MeOH	-	2.7	1	0.35	45	>69*
	128 $\mu\text{m}$ MeOH	-	2.67	0.94	0.27	>42.8*	>71.33*
$S_x$ [cm <sup>3</sup> cm <sup>-3</sup> bar <sup>-1</sup> ]	193 $\mu\text{m}$ As Cast	1.74	2.14	21.7	7.75	<0.37*	<0.09*
	157 $\mu\text{m}$ MeOH	2.3	2.7	29.4	10.7	0.47	<0.12*
	128 $\mu\text{m}$ MeOH	2.3	2.6	30.7	10.5	<0.5*	<0.12*
$\alpha(S_x/SN_2)$	193 $\mu\text{m}$ As Cast	-	1.23	12.47	4.45	<0.21*	<0.05*
	157 $\mu\text{m}$ MeOH	-	1.35	13	4.6	0.20	<0.05*
	128 $\mu\text{m}$ MeOH	-	1.13	13.35	4.57	<0.22*	<0.05*

\*A time lag (<1 s) allows only an estimation of the minimum limit of D and maximum limit of S.



As with other TB polymers, methanol treatment of the membrane results in a significant increase in permeability. The permeabilities of all gases are drastically lower for SBI.TB than DMEA.TB and DHEA.TB due to lower diffusion and solubility coefficients. The lower permeabilities are consistent with the lower surface area of SBI.TB. The order of gas permeabilities for SBI.TB are the same as for DHEA.TB ( $\text{CO}_2 > \text{H}_2 > \text{He} > \text{O}_2 > \text{CH}_4 > \text{N}_2$ ) but  $\text{H}_2$  is considerably less permeable than  $\text{CO}_2$  (by 700 barrer for the 157  $\mu\text{m}$  membrane). DHEA.TB also displays lower selectivities ( $P_x/P_y$ ), than DMEA.TB and DHEA.TB due to combined lower diffusivity ( $D_x/D_y$ ) and solubility ( $S_x/S_y$ ) selectivities. Selectivity is also generally lower for the methanol treated membranes compared to the "as cast" samples where the opposite was observed for DMEA.TB and DHEA.TB. All data for technologically important gas pairs lie below the present Robeson upper bound and data for most gas pairs lie below the 1991 upper bound. Data for  $\text{O}_2/\text{N}_2$ ,  $\text{H}_2/\text{N}_2$ ,  $\text{H}_2/\text{CH}_4$  and  $\text{H}_2/\text{CO}_2$  however, lie close to or above the 1991 upper bound. In the case of  $\text{H}_2/\text{CO}_2$ , SBI.TB marginally exceeds the performance of PIM-1, PIM-7 and PIM-PI-8 (Fig 6.3.7b).

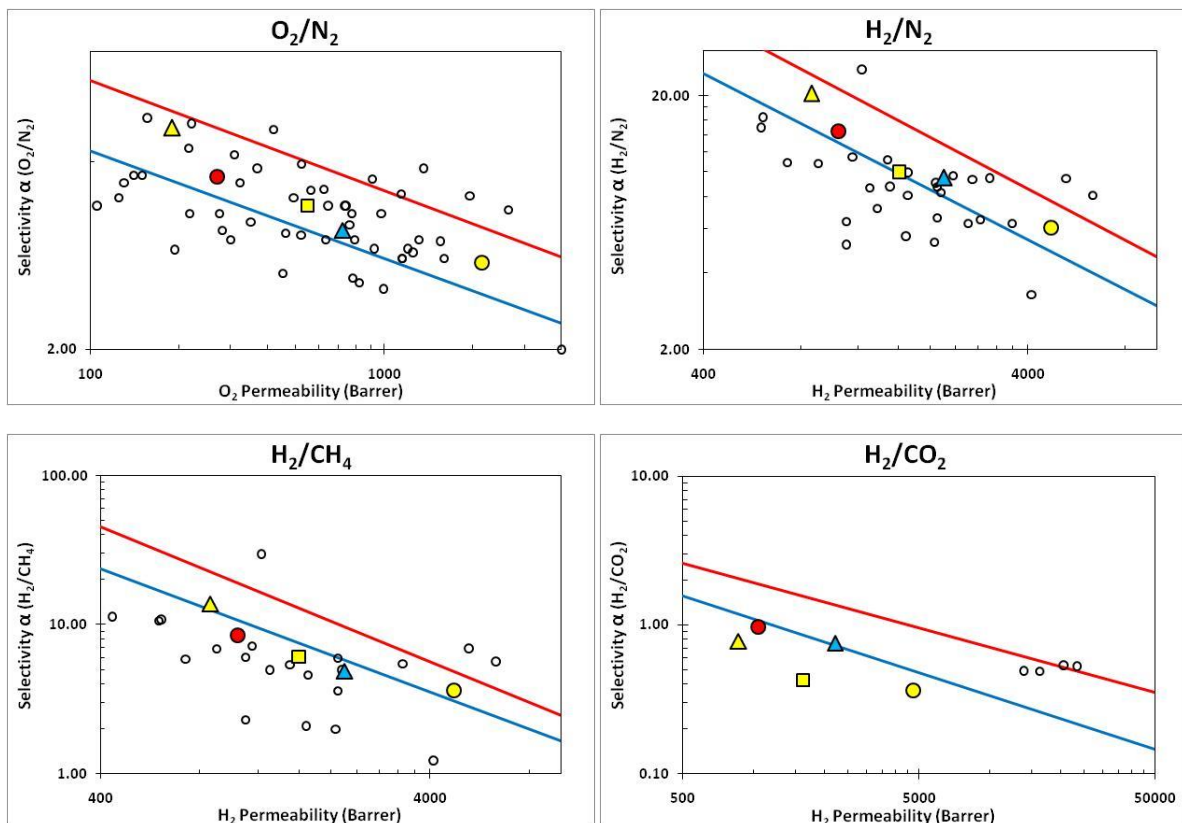
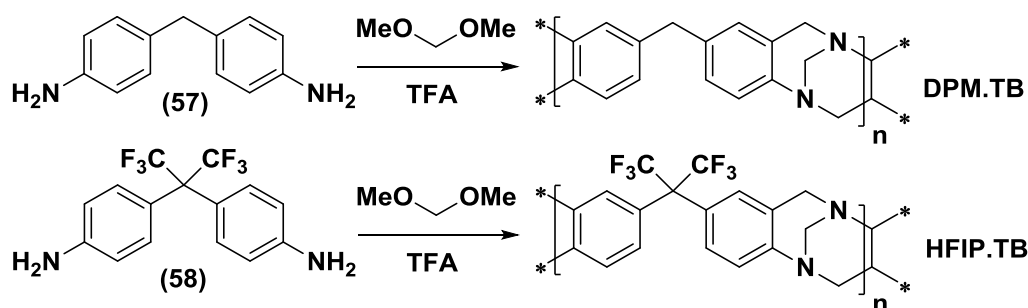


Fig 6.3.7b Robeson plots of selected gas pairs for SBI.TB with 1991 (—) and 2008 (—) upper bounds : 193  $\mu\text{m}$  As Cast (●) and 157  $\mu\text{m}$  MeOH (▲) compared to PIM-1 (○), PIM-7 (▲)<sup>95</sup>, PIM-PI-8 (■)<sup>89</sup>, and Robeson's literature data lying close to the upper bounds (○)<sup>126, 127</sup>.

#### 6.4: Tröger's Base Polymers from Commercial Monomers

There are a number of cheap commercially available aromatic diamine compounds that can be used in the formation of Tröger's base polymers. Three such monomers based on a diphenylmethane (DPM) structure were tested. While the DPM skeleton which contains rotatable carbon-carbon bonds, does not conform to the PIM design concept, it was the intention that these monomers would offer a cheap and convenient route to TB polymers that may be used for further experimentation such as amine quaternerisation (chapter 7). The synthesis of DPM.TB and HFIP.TB was attempted from the TB polymerisation of 4,4'-diaminophenylmethane and 4,4'-(hexafluoroisopropylidene)dianiline respectively at a concentration of 8.33 ml of TFA per gram of monomer (Scheme 6.4a).



Scheme 6.4a Synthesis of DPM.TB and HFIP.TB.

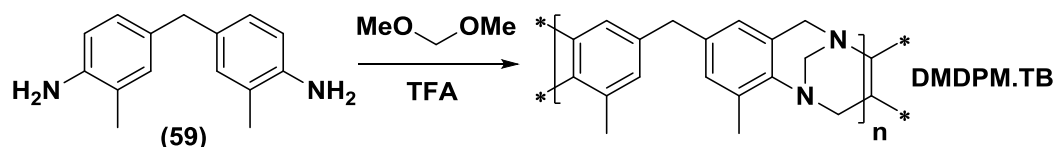
It was found that both polymerisations inevitably result in cross-linking, even at lower concentration, temperature and using only three equivalents of dimethoxymethane. This is likely due to a number of free positions on the benzene rings that are vulnerable to cross-linking reactions.

In the case of DPM.TB, the onset of gel formation occurred after a reaction time of 1 h, while in contrast, gel formation of HFIP.TB onset occurred after a reaction time of 6h. The reduced reaction rate of HFIP.TB may be attributed to the electron withdrawing effects of the two  $\text{CF}_3$  groups reducing amine nucleophilicity. It does however suggest for future studies that incorporation of polar  $\text{CF}_3$  groups into TB polymers is at least possible.

Nitrogen adsorption shows that both DPM.TB and HFIP.TB are not microporous, having BET surface areas of 0.82 and 20  $\text{m}^2/\text{g}$  respectively. This can be attributed to both the rotatable carbon-carbon bonds providing flexibility in the DPM skeleton and cross-linking bonds locking polymer chains in close proximity.

A third DPM monomer was also tested, featuring an aromatic methyl group adjacent to each amine, offering protection of aromatic positions from cross-linking reactions.

DMDPM.TB was synthesised in 88% yield from the TB polymerisation of 4,4'-diamino-3,3'-dimethylphenylmethane at a concentration of 8.33 ml of TFA per gram of monomer over 3 d (Scheme 6.4b) and was isolated as an off-white powder.



Scheme 6.4b Synthesis of DMDPM.TB.

Thermal gravimetric analysis shows the polymer is stable up to 357 °C. Differential scanning calorimetry did not reveal the presence of a glass transition under its decomposition temperature. Nitrogen adsorption shows that DMDPM.TB has a low BET surface area of 38 m<sup>2</sup>/g which can be attributed to the rotatable carbon-carbon bonds.

Analysis of the acetone washings from the crude polymer using MALDI-TOF revealed multiples of the presumed polymeric repeating unit (C<sub>18</sub>H<sub>18</sub>N<sub>2</sub>) (Fig 6.4a).

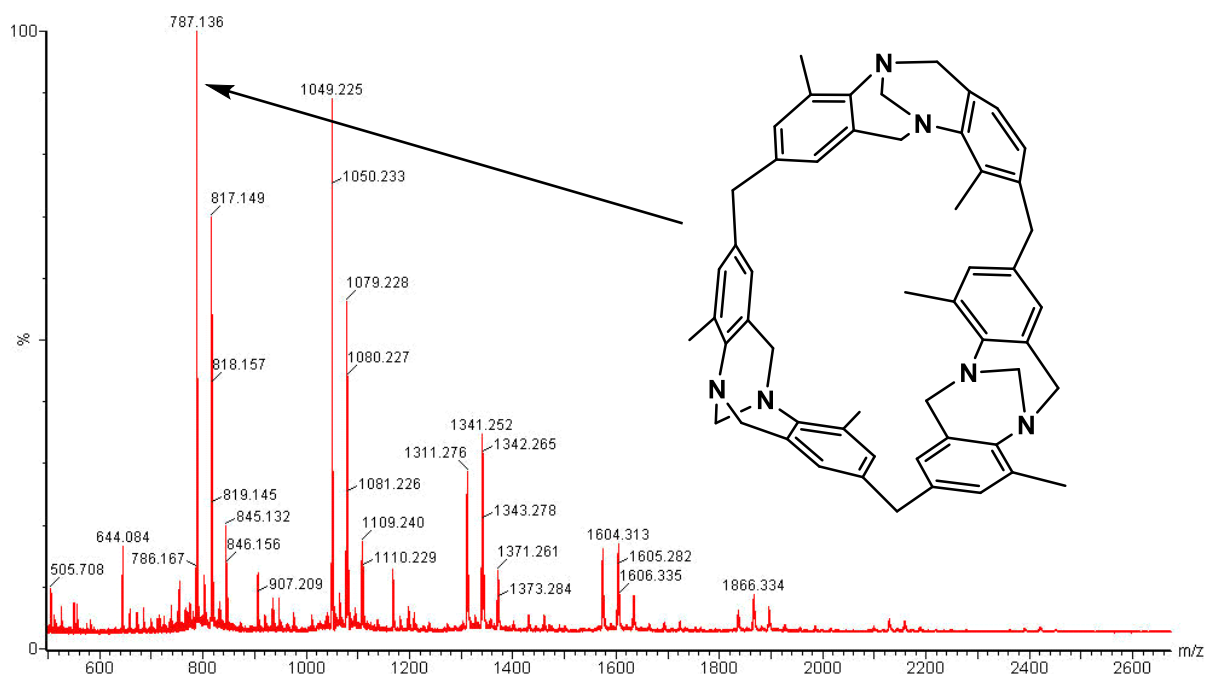


Fig 6.4a MALDI-TOF spectrum of DMDPM.TB oligomers showing the repeating unit of the polymer resulting from cyclic oligomers and a cyclic trimer is illustrated.

The values obtained show the presence cyclic oligomers from trimers to octamers. The rotatable single carbon-carbon bonds between the phenyl units provides the monomer enough

flexibility to twist and bend into the correct conformation to form cyclic structures which is detrimental to the formation of high molecular weight polymer.

It was found that DMDPM.TB is highly resistant to gel formation by virtue of the protecting aromatic methyl groups. This allows the formation of a high molecular weight polymer (GPC:  $M_n = 49,600$ ,  $M_w = 94,600$ ) despite the apparent ease of the monomer to form cyclic structures.

DMDPM.TB was found to have exceptional film forming properties and a number of films were formed (Fig 6.4b) for further experimentation (chapter 7).

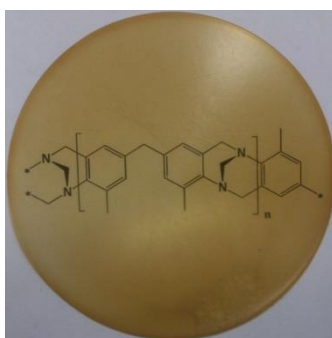


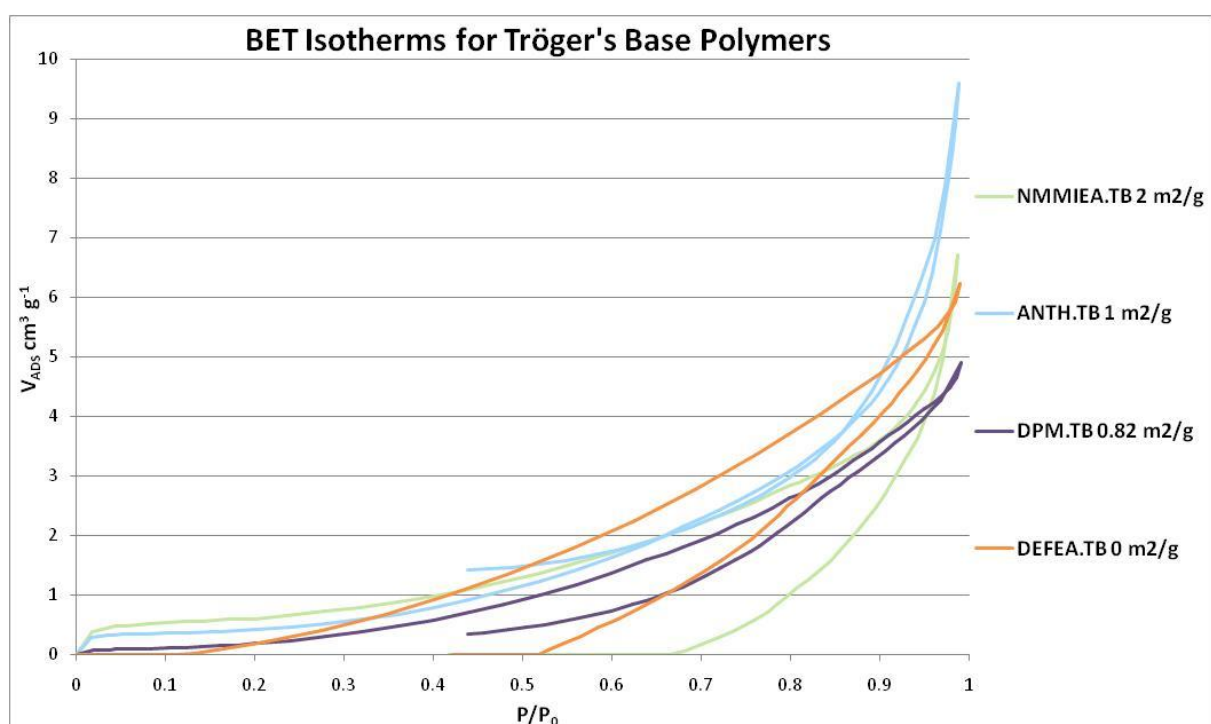
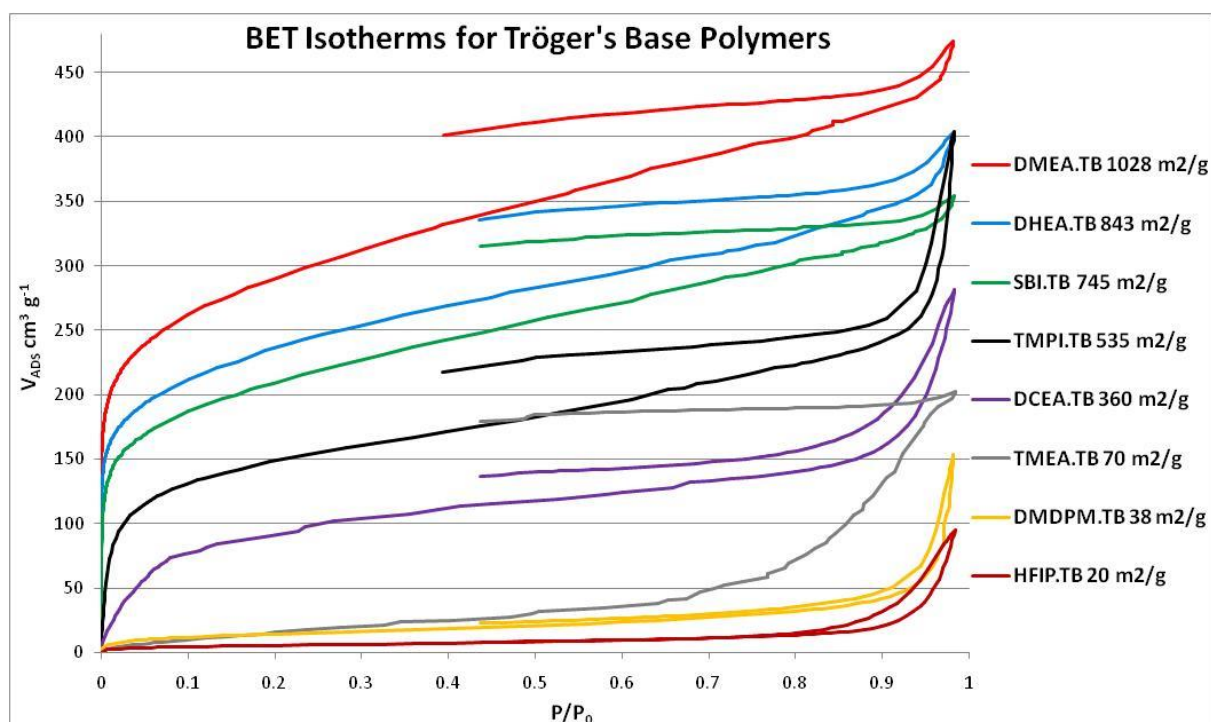
Fig 6.4b An optically clear chloroform-cast film of DMDPM.TB, through which is visible its molecular structure printed on a piece of paper.

Below is a table summarising the some of the physical characteristics of the TB polymers reported in this thesis.

Tröger's Base Polymers	BET Analysis		GPC			TGA	Film Formation
	BET Surface Area ( $\text{m}^2 \text{g}^{-1}$ )	Pore Volume ( $\text{cm}^3 \text{g}^{-1}$ )	$M_w$	$M_n$	$M_w/M_n$ (PDI)	$T_{DEC}$ ( $^{\circ}\text{C}$ )	
DMEA.TB	1028	0.75	155,800	40,700	3.83	260	✓
DHEA.TB	843	0.6178	49,300	9,200	5.35	260	✓
SBI.TB	745	0.542	360,000	96,000	3.75	435	✓
TMPI.TB	535	0.9814	4,200	700	5.93	349	✗
DCEA.TB	360	0.4246	*	*	*	250	✗
TMEA.TB	70	0.3069	-	-	-	260	✗
DMDPM.TB	38	0.1378	94,600	49,600	1.91	357	✓
HFIP.TB	20	0.9814	X	X	X	280	✗
NMDCEA.TB	2	0.009	-	-	-	300	✗
Anth.TB	1	0.0131	X	X	X	377	✗
DPM.TB	0.82	0.007	X	X	X	362	✗
DEEEA.TB	0	0.009	-	-	-	360	✗

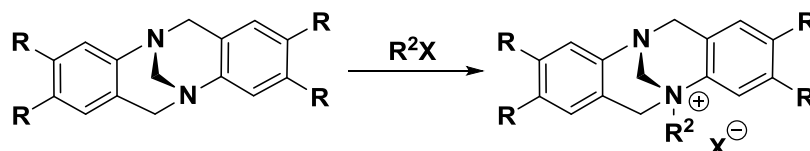
GPC values: X indicates polymer is cross-linked, - indicates oligomeric material, \* indicates the polymer is not soluble in a solvent suitable for GPC

Below are the BET isotherms from which the BET surface areas were calculated for the TB polymers reported in this thesis.



## Chapter 7: Quaternerised Tröger's Base Polymers

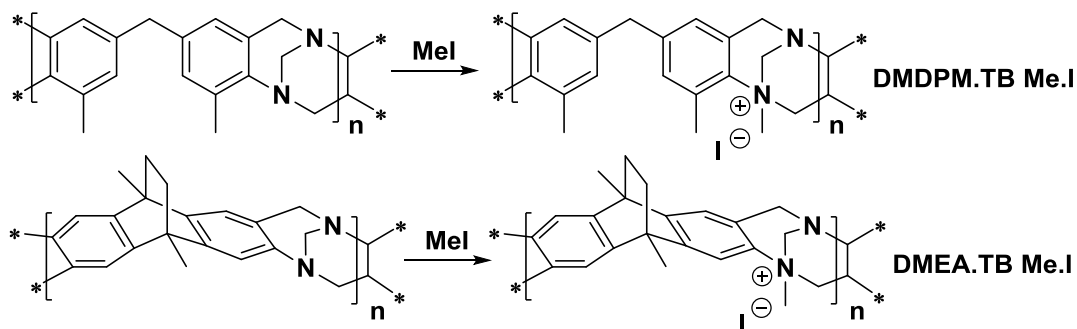
The basic tertiary amine functionality contained in TB polymers provides an obvious target for functionalisation to produce microporous ionic polymers. Ionic polymers have found a number of important applications in ion exchange<sup>55</sup>, catalysis<sup>64, 177</sup> and solid polymer electrolyte<sup>178</sup> applications. The nitrogen atoms contained in the methanodiazocine ring are easily quaternerised to form monoquaternary TB salts using alkyl or benzyl halides<sup>157</sup> (Scheme 7a).



Scheme 7a Quaternerisation of Tröger's Base where  $R^2$  = alkyl or benzyl and  $X = Cl, Br$  or  $I$ . Formation of the first quaternary nitrogen on the methanodiazocine ring significantly reduces the nucleophilicity of the second nitrogen atom due to a strong negative inductive effect<sup>157</sup>. For this reason, chemistry on TB nitrogen atoms has been effectively limited to monoquaternary salts<sup>179</sup> but in 2006, Lenev and co-workers<sup>179</sup> successfully formed dimethylated TB analogues using dimethyl sulfate. The anion may then be exchanged with a vast range of counterions to tailor physical and chemical properties.

### 7.1: Tröger's Base Polymer Methylation

The methylation of two TB polymers DMDPM.TB and DMEA.TB was carried out using an excess of methyl iodide at room temperature over 16 h to form DMDPM.TB Me.I and DMEA.TB Me.I respectively in quantitative yields as dark brown powders (Scheme 7.1a).



Scheme 7.1a Quaternerisation of DMDPM.TB and DMEA.TB with methyl iodide.

Both quaternerised polymers were found to be only soluble in dimethyl sulfoxide and so this solvent was used in the methylation procedure to ensure a complete reaction. Alternatively,

methylation of preformed a film is also possible by soaking in a mixture of methyl iodide and methanol however, these methylated films tend to become less robust.

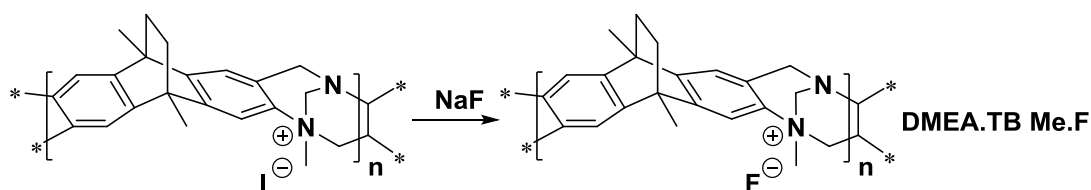
Thermal gravimetric analysis shows that both polymers are only stable up to 100 °C with an initial decrease in mass consistent with the loss of one equivalent of methyl iodide per repeating unit.

Nitrogen adsorption shows that DMDPM.TB Me.I has a BET surface area of 74 m<sup>2</sup>/g which is higher than its parent polymer DMDPM.TB (38 m<sup>2</sup>/g). This is possibly due to the large iodide counterions separating polymer chains to create extra void space which moderately increases free volume from a somewhat poor starting point. The BET surface area of DMEA.TB Me.I was found to be significantly lower (116 m<sup>2</sup>/g) than the parent polymer DMEA.TB (1028 m<sup>2</sup>/g). This is likely due to the large iodide counterions filling pore space with a decrease in free volume. The low surface areas observed for both polymers limit their applicability in gas separations but exchange of the iodide counterion offers the ability to tune the properties of the materials.

## **7.2: Ion Exchange**

### **7.2.1: Exchange with Fluoride**

In an effort to increase the free volume of the quaternerised DMEA.TB Me.I polymer, the large iodide counterion was exchanged with fluoride to form DMEA.TB Me.F (Scheme 7.2.1a).



Scheme 7.2.1a Ion exchange of DMEA.TB Me.I with NaF to form DMEA.TB Me.F.

The ion exchange was carried out by stirring powdered DMEA.TB Me.I in a sodium fluoride solution (1 M) for 24 h after which time the mixture had changed from a dark brown to a light brown colour to afford DMEA.TB Me.F in a quantitative yield.

Thermal gravimetric analysis shows that the polymer is stable up to 165 °C with a loss of mass below consistent with one equivalent of methyl fluoride.

Nitrogen adsorption shows that DMEA.TB Me.F has a BET surface area of 454 m<sup>2</sup>/g which is lower than the parent polymer DMEA.TB (1028 m<sup>2</sup>/g) but significantly higher than the

iodide analogue DMEA.TB Me.I (116 m<sup>2</sup>/g). This can be attributed to the fluoride counterion filling relatively less pore space than the iodide.

DMEA.TB Me.F was found to be soluble in methanol from which a number of films were cast (Fig 7.2.1a) for membrane gas permeation studies by ITM. The membranes were however not mechanically robust enough to withstand the permeation tests and were damaged during analysis.

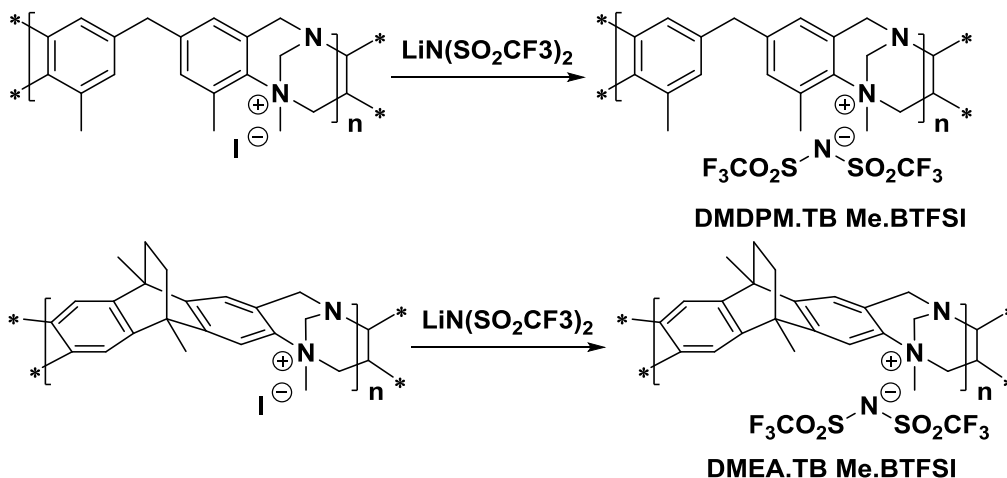


Fig 7.2.1a An optically clear methanol-cast film of DMEA.TB Me.F.

### **7.2.2: Exchange with Bistrifluoromethanesulfonimide (Bistriflimide)**

Research conducted by Johannes Jansen (at ITM) and co-workers has shown that a poly(vinylidene fluoride-*co*-hexafluoropropylene) membrane containing up to 80 wt % of the ionic liquid 1-ethyl-3-methylimidazolium bistriflimide improves gas permeability over the pure polymer, most notably for CO<sub>2</sub><sup>180</sup>. Addition of an ionic liquid to a polymer however, results in a significant reduction of the mechanical strength of the membrane.

Inspired by this work, an ion exchange was carried out on DMDPM.TB Me.I and DMEA.TB Me.I with the bistriflimide anion to form DMDPM.TB Me.BTFSI and DMEA.TB Me.BTFSI respectively (Scheme 7.2.2a)



Scheme 7.2.2a Ion exchange of DMDPM.TB Me.I and DMEA.TB Me.I with lithium bistriflimide.



The ion exchange was carried out by refluxing the corresponding powdered methyl iodide quaternerised TB polymer in a methanol solution of lithium bistriflimide for 16 h by which time the mixture had changed from a dark brown to a light orange colour.

Thermal gravimetric analysis shows that DMDPM.TB Me.BTFSI and DMEA.TB Me.BTFSI are stable up to 300 and 260 °C respectively, with the latter showing initial decrease in mass consistent with the loss of an ethylene fragment via a retro Diels-Alder reaction<sup>172</sup>. Nitrogen adsorption shows that DMDPM.TB Me.BTFSI and DMEA.TB Me.BTFSI have BET surface areas of 0 and 24 m<sup>2</sup>/g respectively. This large reduction in surface area over the parent polymers may be attributed to the large and flexible bistriflimide anion filling pore space and reducing free volume. Both polymers were found to be soluble in acetone although, attempts to cast films resulted in cracked samples. Using 2-butanone as a less volatile solvent however, resulted in the formation of films (Fig 7.2.2a) that were more robust for membrane gas permeation studies by ITM.

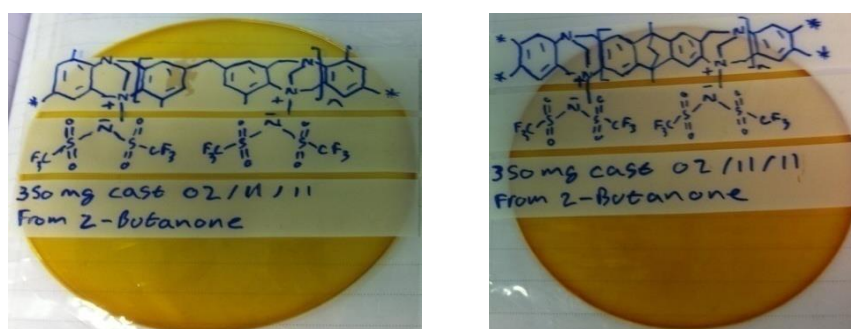


Fig 7.2.2a Optically clear 2-butanone-cast films of DMDPM.TB Me.BTFSI (left) and DMEA.TB Me.BTFSI (right).

Since DMDPM.TB Me.BTFSI was found to be non-porous, only a 86  $\mu\text{m}$  DMEA.TB Me.BTFSI sample was tested, the results of which are summarised in table 7.2.2a. Unfortunately, methanol treatment caused the membrane to fragment and only "as cast" data could be collected.

Transport parameter	N <sub>2</sub>	O <sub>2</sub>	CO <sub>2</sub>	CH <sub>4</sub>	H <sub>2</sub>	He
$P_x$ [Barrer]	1.06	6.57	53.48	4.5	40.43	41.30
$\alpha(P_x/PN_2)$	-	6.22	50.6	4.25	38.2	39.1
$D_x$ [ $10^{-12}$ m <sup>2</sup> s <sup>-1</sup> ]	3.40	11.23	3.96	0.37	188.78	326.10
$\alpha(D_x/DN_2)$	-	3.30	1.16	0.11	55.52	95.91
$S_x$ [cm <sup>3</sup> cm <sup>-3</sup> bar <sup>-1</sup> ]	0.23	0.44	10.14	9.16	0.16	0.09
$\alpha(S_x/SN_2)$	-	1.91	44.09	39.83	0.70	0.39

The permeabilities of all gases are drastically lower for DMEA.TB Me.BTFISI than the parent polymer DMEA.TB due to lower diffusion and solubility coefficients. The lower permeabilities are consistent with the lower surface area of DMEA.TB Me.BTFISI. The order of gas permeabilities for DMEA.TB Me.BTFISI ( $\text{CO}_2 > \text{He} > \text{H}_2 > \text{O}_2 > \text{CH}_4 > \text{N}_2$ ) is slightly different to that of DMEA.TB where He is marginally more permeable than  $\text{H}_2$  (differing by less than 1 barrer).

DMEA.TB Me.BTFISI also displays lower selectivities ( $P_x/P_y$ ), than DMEA.TB due to combined lower diffusivity ( $D_x/D_y$ ) and solubility ( $S_x/S_y$ ) selectivities however, the selectivity of  $\text{CO}_2/\text{N}_2$  displays a potentially interesting value of 50.6.

All data for technologically important gas pairs lie far below the 1991 and present upper bounds except for  $\text{O}_2/\text{N}_2$  that lies close to the 1991 upper bound (Fig 7.2.2b).

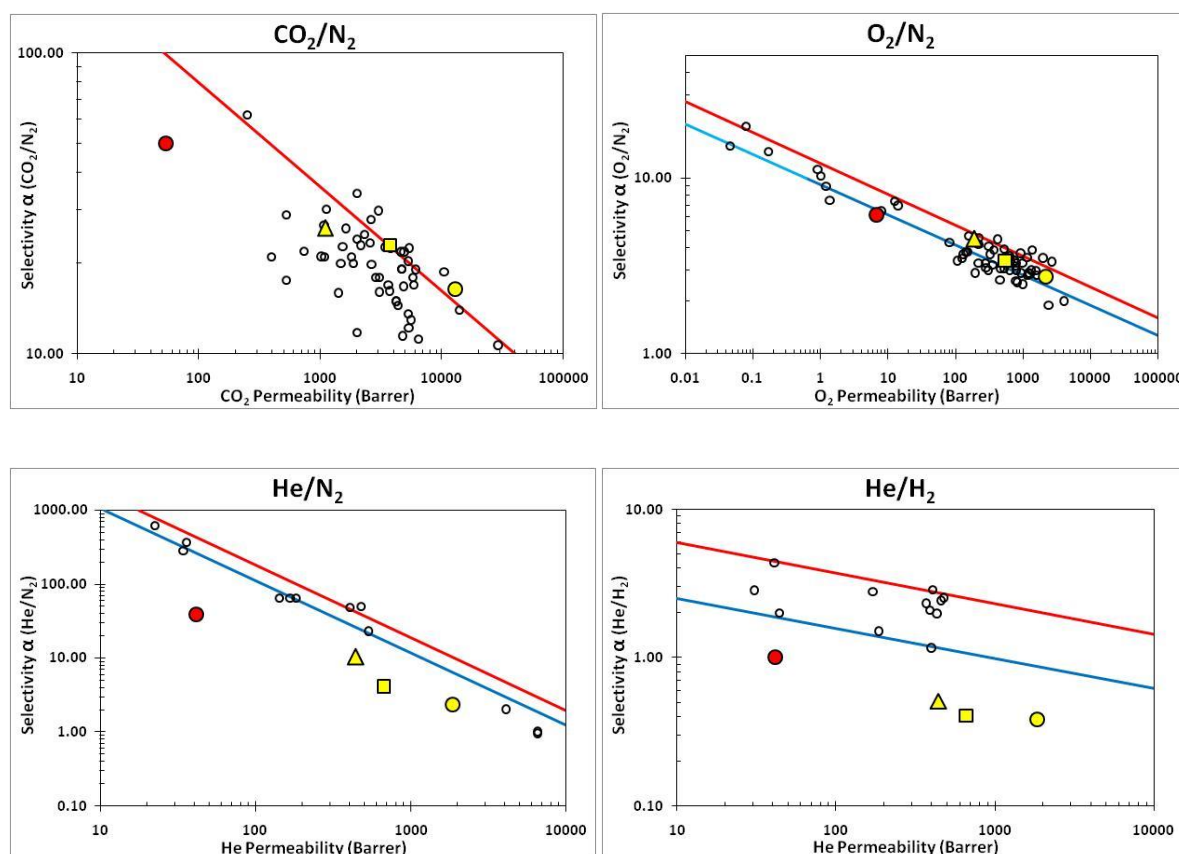
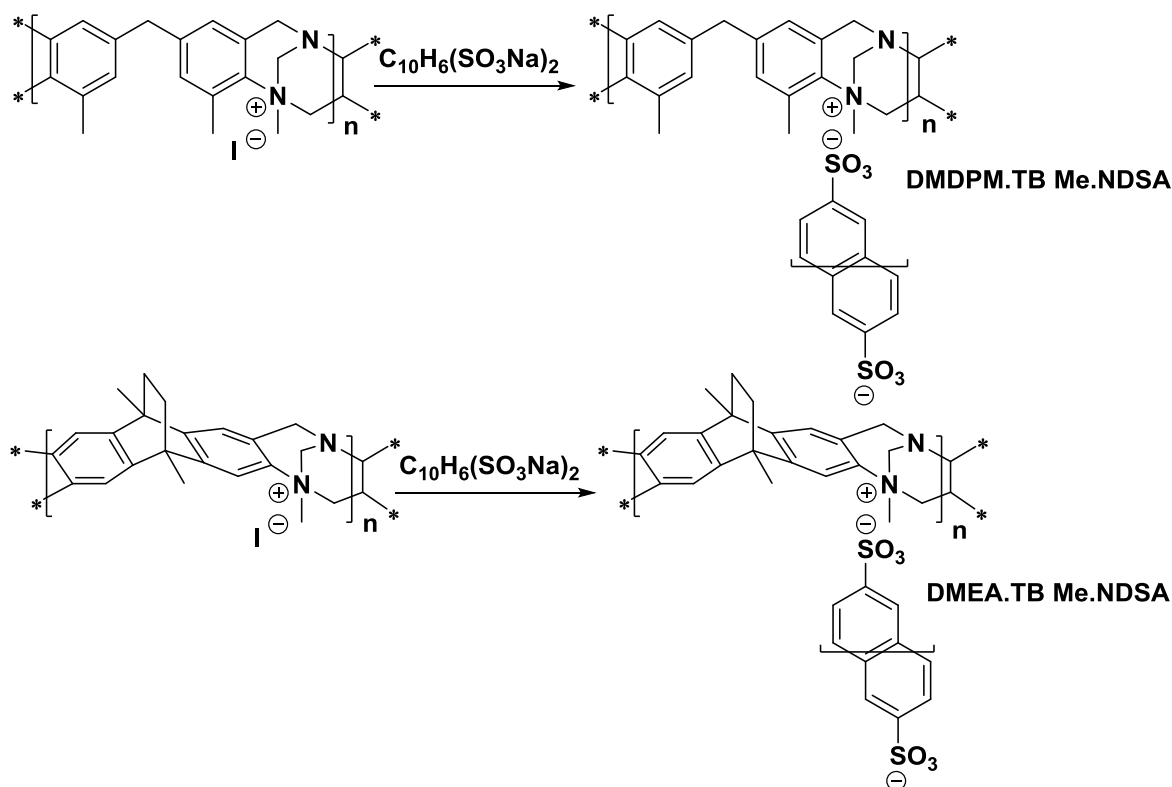


Fig 7.2.2b Robeson plots of selected gas pairs for DMEA.TB Me.BTFISI with 1991 (—) and 2008 (—) upper bounds : 86  $\mu\text{m}$  As Cast (●) compared to PIM-1 (●), PIM-7 (▲)<sup>95</sup>, PIM-PI-8 (■)<sup>89</sup>, and Robeson's literature data lying close to the upper bounds (○)<sup>126, 127</sup>.

### 7.2.3: Exchange with 2,6-Naphthalene Disulfonic acid

As previously mentioned, cross-linking of a polymer can improve solvent resistance and reduce physical ageing. Ion exchange on TB polymers offers the possibility of exchanging the iodide anion for a dianionic (or polyanionic) species that will form ionic bridges between polymer chains that function as "pseudo cross-links". Since these cross-links are not covalent in nature, such polymers may be soluble in polar solvents that are suitable for film formation. Two polymers DMDPM.TB Me.NDSA and DMEA.TB Me.NDSA were tested using 2,6-naphthalene disulfonic acid as the bridging unit (Scheme 7.2.3a).



Scheme 7.2.3a Ion exchange of DMDPM.TB Me.I and DMEA.TB Me.I with 2,6-naphthalenedisulfonic acid disodium salt .

The ion exchange was carried out by refluxing the corresponding powdered methyl iodide quaternerised TB polymer in a solution of 2,6-naphthalenedisulfonic acid disodium salt in deionised water. After refluxing for 16 h, the mixture had changed from a dark brown to an off white colour.

Thermal gravimetric analysis shows that DMDPM.TB Me.NDSA and DMEA.TB Me.NDSA are stable up to 300 and 260 °C respectively; with the latter showing initial decrease in mass consistent with the loss of an ethylene fragment via a retro Diels-Alder reaction<sup>172</sup>.

Nitrogen adsorption shows that DMDPM.TB Me.NDSA and DMEA.TB Me.NDSA have BET surface areas of 0 and 3 m<sup>2</sup>/g respectively. These extremely low surface areas may be attributed the naphthalene cross-linking unit filling pore space and forcing adjacent chains into close proximity to each other which reduces free volume. A possible improvement may be to use larger linking units or units that are also sites of contortion.

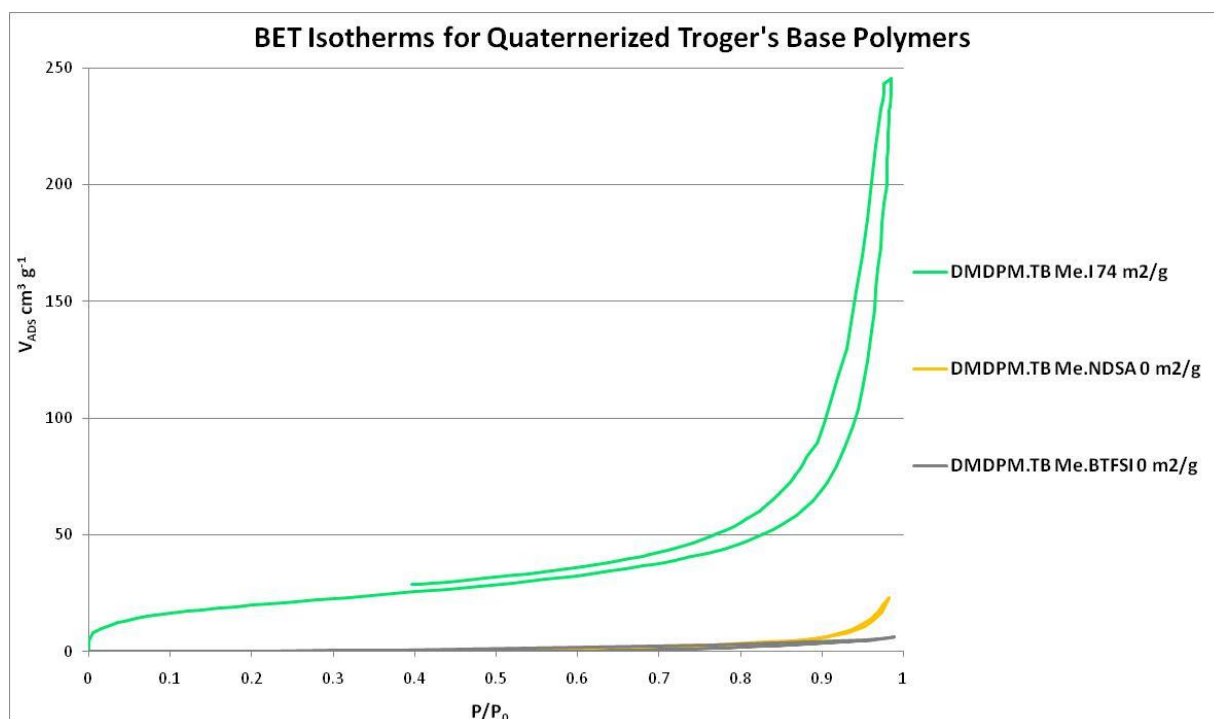
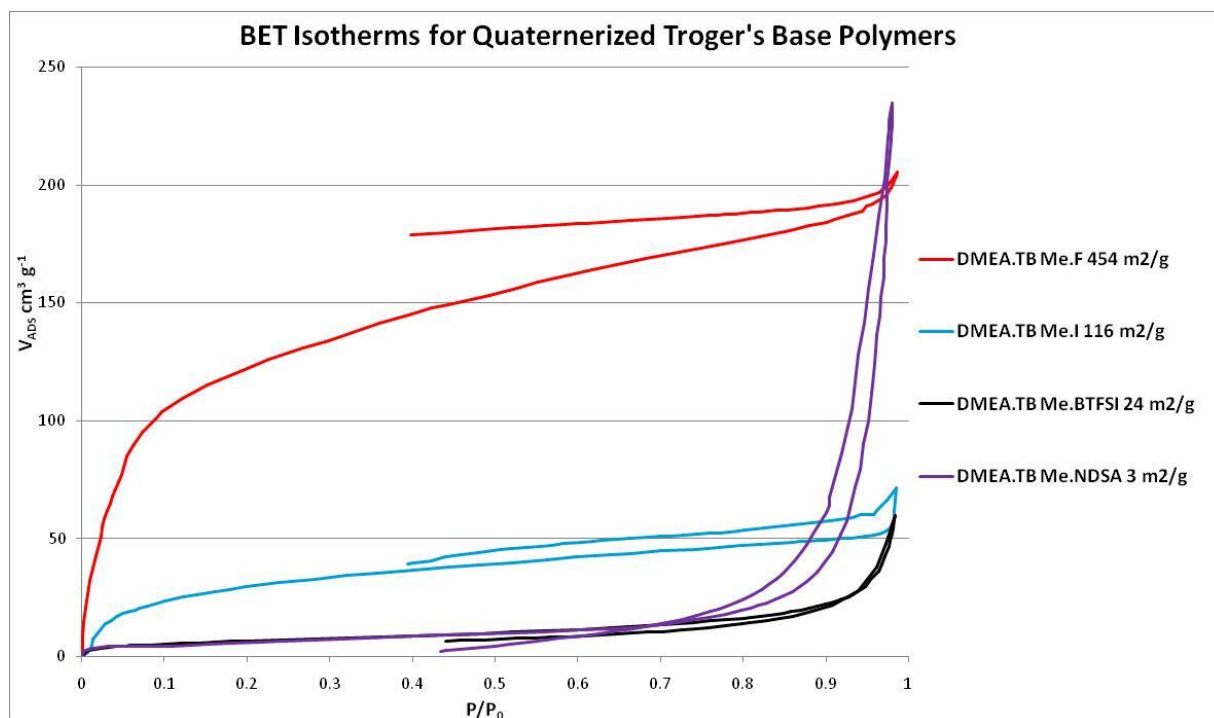
DMDPM.TB Me.NDSA was found to be only sparingly soluble in DMSO while DMEA.TB Me.NDSA was found to be insoluble and hence films could not be formed for membrane gas permeation tests. Films could be obtained from quaternerisation and subsequent ion exchange on preformed films but the low surface areas observed for these materials limit their applicability in gas separations.

It is clear from these experiments that quaternerisation of TB polymers significantly changes the physical properties such as solubility, surface area and gas transport parameters. The vast range of possible counterions available provides almost endless possibilities for tailoring these physical properties. Quaternerised TB polymers are currently being investigated by our collaborators for use as catalysis and solid polymer electrolytes for alkaline fuel cell applications.

Below is a table summarising the some of the physical characteristics of the quaternerised TB polymers reported in this thesis.

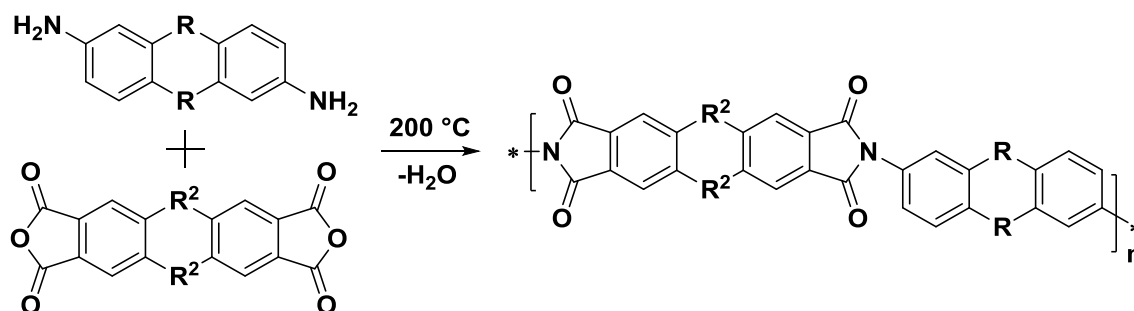
Quaternerised Tröger's Base Polymers	BET Analysis		TGA	Suitable Solvent	Film Formation From Powder
	Polymer	BET Surface Area (m <sup>2</sup> g <sup>-1</sup> )	Pore Volume (cm <sup>3</sup> g <sup>-1</sup> )		
DMEA.TB Me.F	454	0.3096	165	MeOH	✓
DMEA.TB Me.I	116	0.1013	100	DMSO	✗
DMDPM.TB Me.I	74	0.3400	100	DMSO	✗
DMEA.TB Me.BTFSI	24	0.0842	260	2-butanone, acetone	✓
DMEA.TB Me.NDSA	3	0.3542	260	-	✗
DMDPM.TB Me.NDSA	0	0.0336	300	DMSO	✗
DMDPM.TB Me.BTFSI	0	0.0089	300	2-butanone, acetone	✓

Below are the BET isotherms from which the BET surface areas were calculated for the quaternerised TB polymers reported in this thesis.



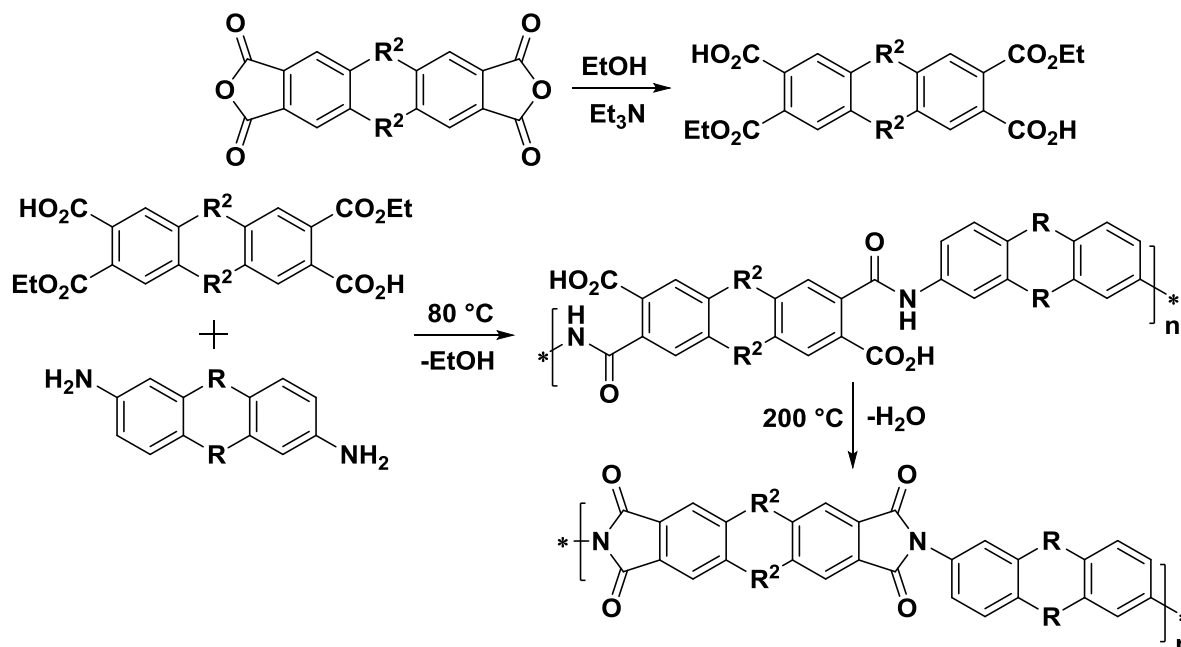
## Chapter 8: Polyimides

The importance of polyimides in gas separation membrane technology has been discussed previously. Also discussed, was the effect of polymer rigidity and hindered rotation around the imide linking bonds on gas transport properties. The dimethyl ethanoanthracene unit has been proved to be a highly effective TB monomer due to its enhanced rigidity and contorted shape. The dimethyl ethanoanthracene unit was also tested in the synthesis of polyimides. Polyimides are classically synthesised by a cycloimidisation polycondensation reaction between bis-carboxylic anhydride and diamine monomers (Scheme 8a).



Scheme 8a Synthesis of polyimides by high temperature cycloimidization.

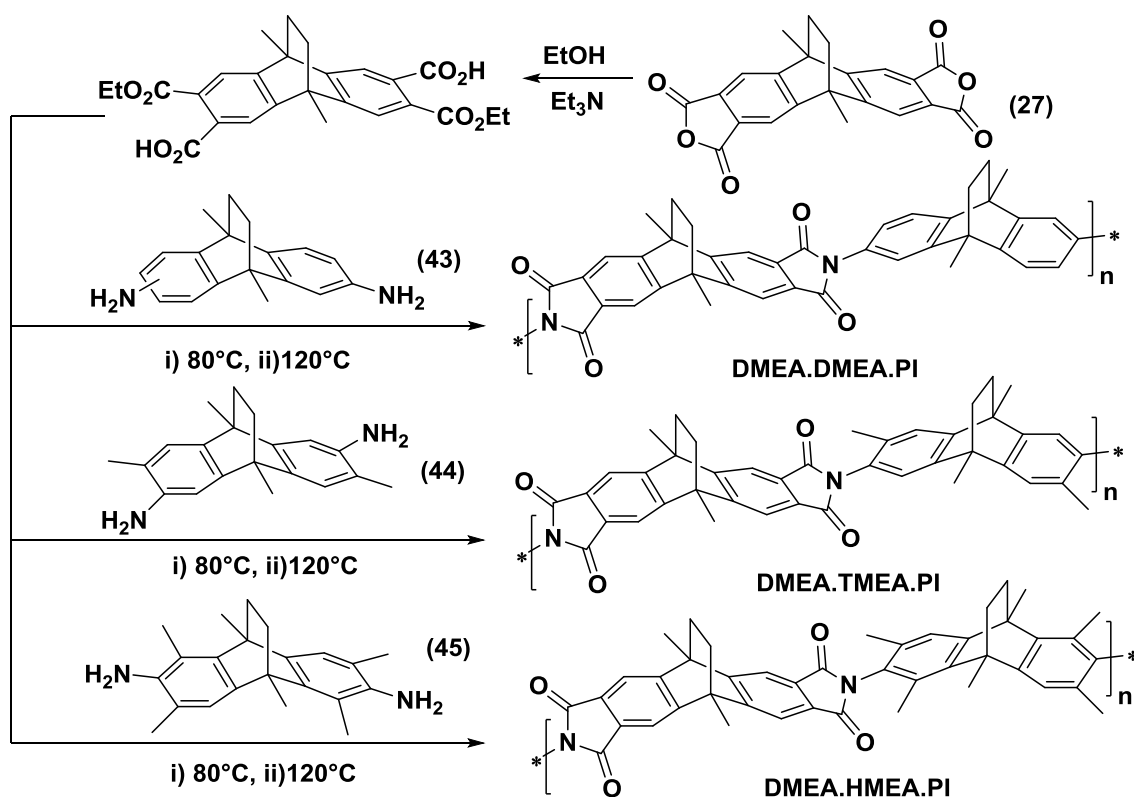
The synthesis of the polyimides described in this thesis was achieved using a similar procedure known as the "ester acid" route<sup>181</sup> that produces high molecular weight soluble polyimides with a high degree of imidisation (Scheme 8b).



Scheme 8b Synthesis of polyimides using the ester acid route.

This procedure first involves conversion of the bis-carboxylic anhydride monomer to a diester-diacid by reacting the monomer with refluxing ethanol in the presence of triethylamine. The residual ethanol and triethylamine are then removed under heating and the diamine is added along with N-methyl-2-pyrrolidone (NMP) as a solvent. The diamine is then reacted with the ester groups under a nitrogen atmosphere at low temperature (80 °C) to form a high molecular weight polyamic acid. The polyamic acid is then heated to 200 °C where it undergoes an imidisation reaction to form a polyimide. On larger scale polymerisations, 1,2-dichlorobenzene may also be added to form an azeotrope with the water produced, which can then be extracted using a reverse Dean-Stark trap. It was found that for small scale reactions, removal of water was more efficient by simply removing a stopper from the two-necked reaction flask and allowing a stream of nitrogen to remove evaporated water. This modified method requires heating of the sides of the reaction flask with a heat gun and replacement of evaporated NMP as needed.

Using this method, three ethanoanthracene diamine analogues (43, 44, 45) containing different numbers of aromatic methyl groups adjacent to each amine were reacted with an ethanoanthracene bis-carboxylic anhydride monomer (27) (Scheme 8c).



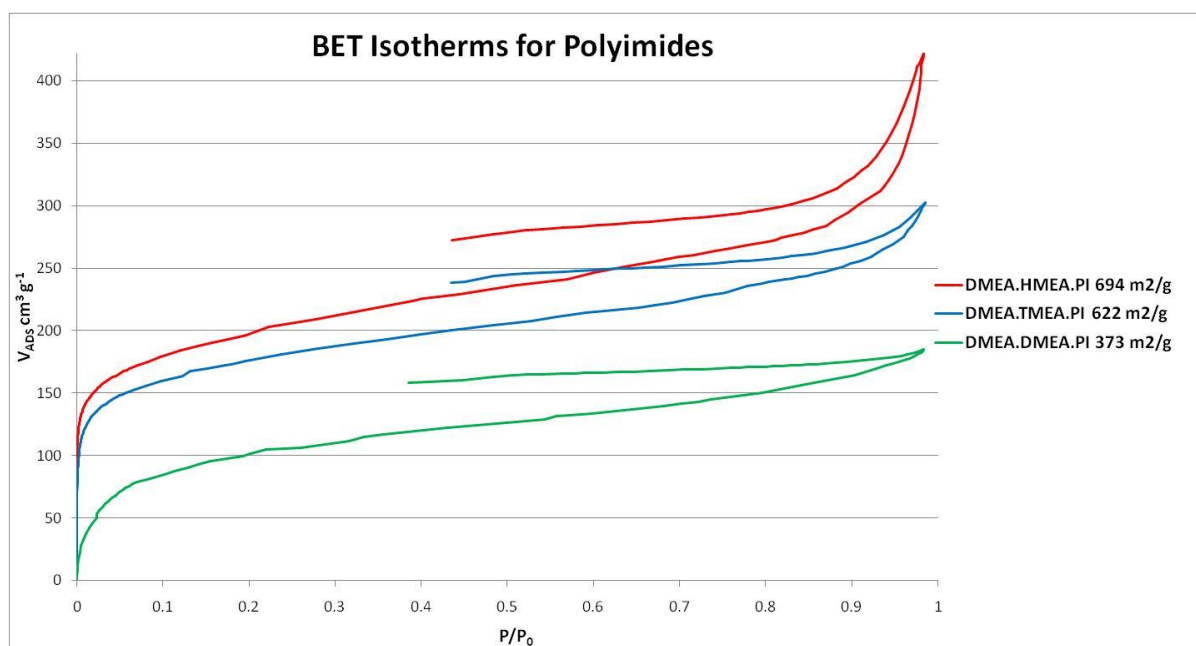
Scheme 8c Synthesis of polyimides using the ester acid route.

Three polyimides DMEA.DMEA.PI, DMEA.TMEA.PI and DMEA.HMEA.PI were synthesised in yields of 90, 73 and 86 % respectively as light brown powders.

Solid state FTIR spectroscopy of all three polymers revealed similar absorption bands at:  $\sim 1775$  (C=O asymm),  $\sim 1720$  (C=O symm),  $\sim 1360$  (C-N stretch) and  $\sim 745$  (imide ring deformation) ( $\text{cm}^{-1}$ ) which are due to the imide structure. Absorption bands due to polyamic acid structures:  $\sim 2700$  (OH stretch),  $\sim 1720$  (acid C=O),  $\sim 1660$  (amide C=O), and  $\sim 1535$  (C-N stretch)<sup>182, 183</sup> ( $\text{cm}^{-1}$ ) were not visible. The absence of polyamic acid structures was also confirmed using  $^1\text{H}$  NMR, indicating a high degree of imidisation.

Thermal gravimetric analysis shows that all three polyimides are stable up to  $260^\circ\text{C}$  with all polymers showing an initial decrease in mass consistent with the loss of an ethylene fragment via a retro Diels-Alder reaction<sup>172</sup>. Differential scanning calorimetry did not reveal the presence of glass transitions below the decomposition temperatures. Analysis of the acetone washings from the crude polymer using MALDI-TOF failed to reveal an oligomeric pattern.

Nitrogen adsorption shows that DMEA.DMEA.PI, DMEA.TMEA.PI and DMEA.HMEA.PI have high BET surface areas of 373, 622 and  $694\text{ m}^2/\text{g}$  respectively. The high surface areas can be partially attributed to the enhanced rigidity of the ethanoanthracene monomeric units.



DMEA.DMEA.PI contains no aromatic methyl groups adjacent to the imide linking bonds and polymer segments can freely rotate. For this reason, DMEA.DMEA.PI is the least rigid polymer of the series and displays the lowest BET surface area.



DMEA.TMEA.PI contains one aromatic methyl group adjacent to the imide linking bonds which restricts full rotation of polymer segments and is hence more rigid than DMEA.DMEA.PI. For this reason DMEA.TMEA.PI displays a much higher BET surface area than DMEA.DMEA.PI.

DMEA.HMEA.PI contains two aromatic methyl groups adjacent to the imide linking bonds which further restricts polymer segment rotation. For this reason, DMEA.HMEA.PI possesses the greatest rigidity of the polymer series and displays the highest BET surface area.

DMEA.DMEA.PI and DMEA.TMEA.PI were formed as relatively high molecular weight polymers (GPC:  $M_n = 21,700$ ,  $M_w = 67,000$  and  $M_n = 49,400$ ,  $M_w = 63,900$  respectively) however, many attempts to form DMEA.HMEA.PI resulted in only a moderate molecular weight (GPC:  $M_n = 19,300$ ,  $M_w = 28,100$ ). The relatively low molecular weight of DMEA.HMEA.PI may be due to the two aromatic methyl groups adjacent to each amine sterically hindering the polymerisation reaction. DMEA.DMEA.PI and DMEA.TMEA.PI were found to have excellent film forming properties and a number of films were formed (Fig 8a) for membrane gas permeation studies by ITM. Attempts to cast a film from DMEA.HMEA.PI however, resulted in brittle films that were unsuitable for gas permeation tests.

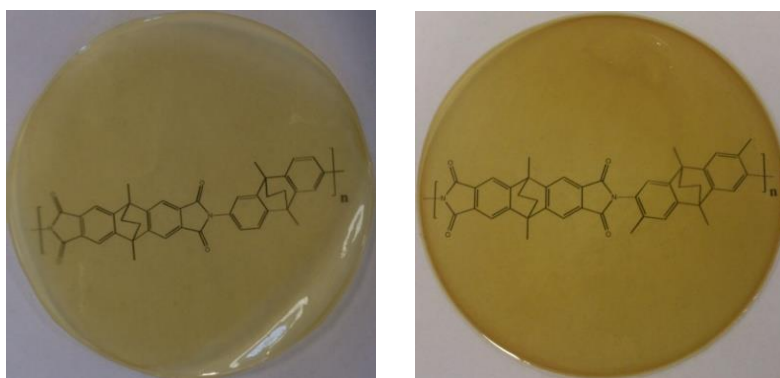


Fig 8a Optically clear chloroform-cast films of DMEA.DMEA.PI (10 cm x 108  $\mu\text{m}$ ) (left) and DMEA.TMEA.PI (10 cm x 137  $\mu\text{m}$ ) (right) through which is visible the molecular structures printed on a piece of paper.

The results of permeation tests on a DMEA.DMEA.PI 108  $\mu\text{m}$  As Cast and a 106  $\mu\text{m}$  MeOH treated film along with a DMEA.TMEA.PI 137  $\mu\text{m}$  As Cast and a 143  $\mu\text{m}$  MeOH treated film are summarised in Table 8a.

Table 8a Polyimide Membrane Permeability Measurements							
Transport parameter	Membrane	N <sub>2</sub>	O <sub>2</sub>	CO <sub>2</sub>	CH <sub>4</sub>	H <sub>2</sub>	He
<b><math>P_x</math> [Barrer]</b>	DMEA.DMEA 108 μm As Cast	11.76	36.17	267.58	21.98	105.81	61.69
	DMEA.TMEA 137 μm As Cast	42.72	110.10	954.70	88.39	259.46	134.44
	DMEA.DMEA 106 μm MeOH	93.56	331.82	1825.19	128.24	1233.14	514.79
	DMEA.TMEA 143 μm MeOH	429	1211	6168	673	3325	1213
<b><math>\alpha(P_x/PN_2)</math></b>	DMEA.DMEA 108 μm As Cast	-	3.78	27.98	2.20	11.07	6.45
	DMEA.TMEA 137 μm As Cast	-	2.86	27.29	2.32	7.42	3.84
	DMEA.DMEA 106 μm MeOH	-	3.55	19.51	1.37	13.18	5.50
	DMEA.TMEA 143 μm MeOH	-	2.82	14.38	1.57	7.75	2.83
<b><math>D_x</math> [<math>10^{-12}</math> m<sup>2</sup>s<sup>-1</sup>]</b>	DMEA.DMEA 108 μm As Cast	14.0	36.9	12.0	5.8	592.4	2015
	DMEA.TMEA 137 μm As Cast	31.2	62.7	29.3	13.8	1027.9	2526.2
	DMEA.DMEA 106 μm MeOH	22.0	77.7	26.8	7.4	1937.9	3043.0
	DMEA.TMEA 143 μm MeOH	88.6	253.7	88.8	35.8	4127.6	5772.8
<b><math>\alpha(D_x/DN_2)</math></b>	DMEA.DMEA 108 μm As Cast	-	2.63	0.85	0.41	42.18	143.46
	DMEA.TMEA 137 μm As Cast	-	2.01	0.94	0.44	32.98	81.05
	DMEA.DMEA 106 μm MeOH	-	3.531	1.219	0.338	88.049	138.259
	DMEA.TMEA 143 μm MeOH	-	2.86	1.00	0.40	46.61	65.18
<b><math>S_x</math> [cm<sup>3</sup> cm<sup>-3</sup> bar<sup>-1</sup>]</b>	DMEA.DMEA 108 μm As Cast	0.511	0.736	16.738	2.744	0.134	0.023
	DMEA.TMEA 137 μm As Cast	0.84	1.20	24.47	4.41	0.19	0.04
	DMEA.DMEA 106 μm MeOH	3.1886	3.2029	51.0255	12.9357	0.4773	0.1269
	DMEA.TMEA 143 μm MeOH	3.63	3.58	52.09	14.07	0.60	0.16
<b><math>\alpha(S_x/SN_2)</math></b>	DMEA.DMEA 108 μm As Cast	-	1.44	32.78	5.37	0.26	0.04
	DMEA.TMEA 137 μm As Cast	-	1.42	29.07	5.23	0.22	0.05
	DMEA.DMEA 106μm MeOH	-	1.004	16.002	4.057	0.150	0.040
	DMEA.TMEA 143 μm MeOH	-	0.99	14.34	3.87	0.17	0.04

Consistent with the high BET surface areas, the permeabilities of both polyimides are relatively high due to combined high diffusion and solubility coefficients. Consistent with the higher surface area and polymer rigidity, DMEA.TMEA.PI displays significantly higher permeabilities than DMEA.DMEA.PI due to enhanced diffusion coefficients. As with other polyimide samples, methanol treatment drastically improves permeability of both samples. The order of gas permeabilities for both samples ( $\text{CO}_2 > \text{H}_2 > \text{He} > \text{O}_2 > \text{CH}_4 > \text{N}_2$ ) show the typical trend observed for reverse selective PIMs working under the solution diffusion mechanism.

Both polyimides display high selectivities ( $P_x/P_y$ ) with DMEA.DMEA.PI displaying proportionately higher selectivities than DMEA.TMEA.PI due to enhanced diffusivity selectivities ( $D_x/D_y$ ), consistent with the Robeson<sup>126</sup> relation. All data for technologically important gas pairs lie below the present Robeson upper bound however, data for  $\text{O}_2/\text{N}_2$ ,  $\text{H}_2/\text{N}_2$  and  $\text{H}_2/\text{CH}_4$  lie above the 1991 upper bound and close to the 1991 upper bound for  $\text{H}_2/\text{CO}_2$ . Data for  $\text{H}_2/\text{N}_2$ ,  $\text{H}_2/\text{CH}_4$  and  $\text{H}_2/\text{CO}_2$  surpass that of PIM-PI-8 (Fig 8b).

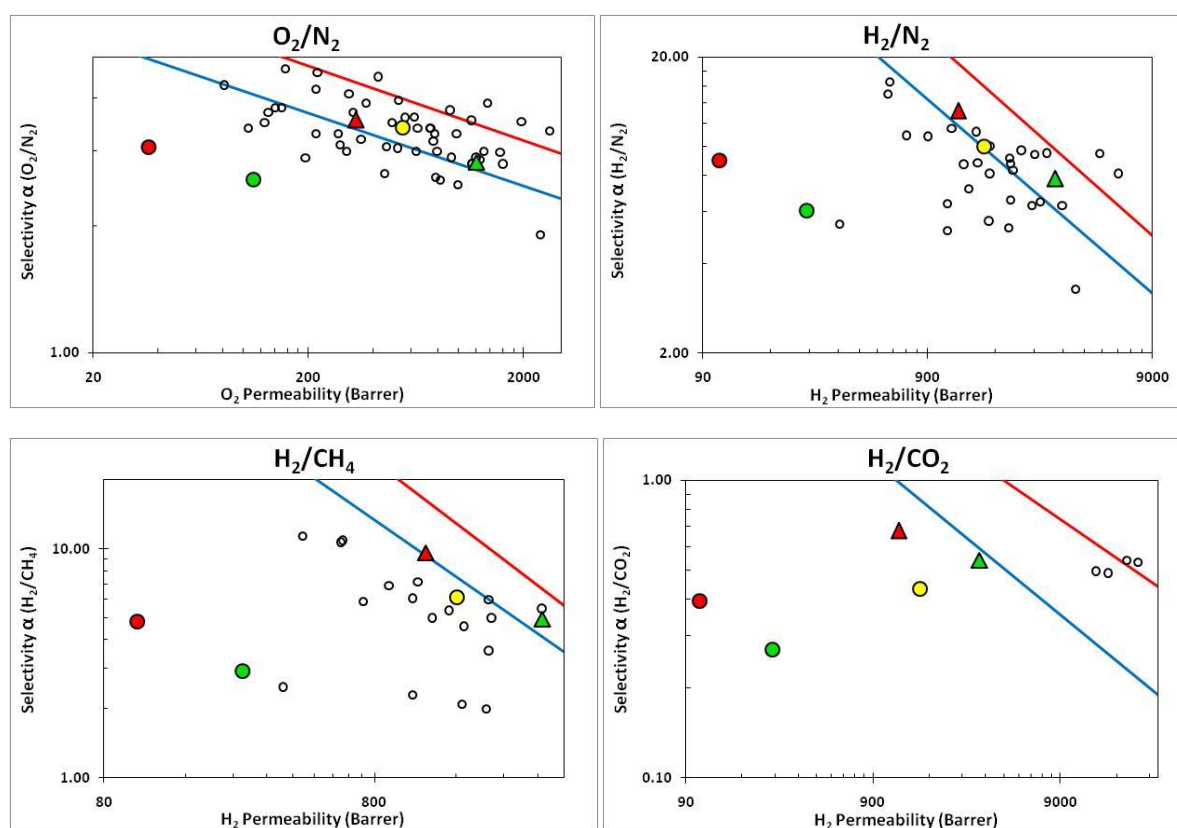
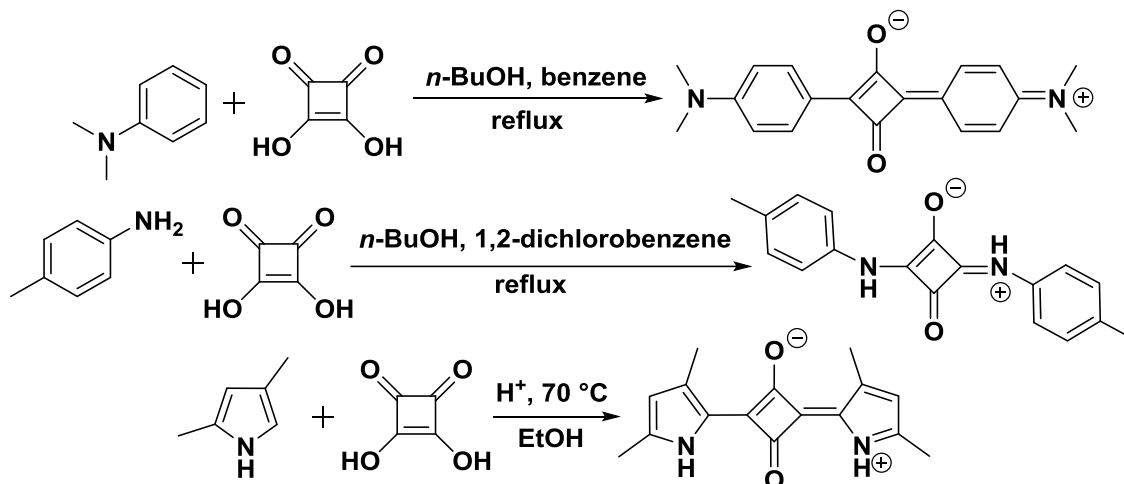


Fig 8b Robeson plots of selected gas pairs for DMEA.DMEA.PI and DMEA.TMEA.PI with 1991 (—) and 2008 (—) upper bounds: DMEA.DMEA.PI 108µm As Cast (●), 106µm MeOH (▲), DMEA.TMEA.PI 137µm As Cast (●), 143µm MeOH (▲) compared to PIM-PI-8 (■)<sup>89</sup> and Robeson's literature data lying close to the upper bounds (○)<sup>126, 127</sup>.

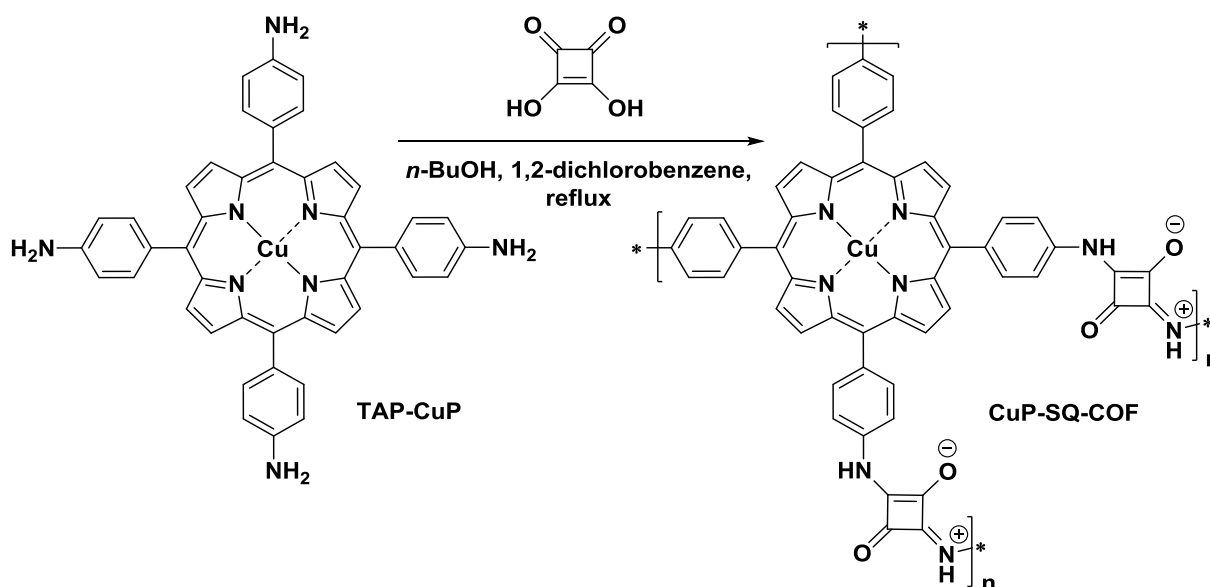
## Chapter 9: Polysquaraines

Squaraines are formally polycondensation products of squaric acid (3,4-dihydroxy-3-cyclobutene-1,2-dione) with a wide range of aromatic<sup>184, 185</sup> or heteroaromatic compounds<sup>186</sup> (Scheme 9a) and are usually highly coloured materials with zwitterionic resonance structures.



Scheme 9a Synthesis of various squaraines.

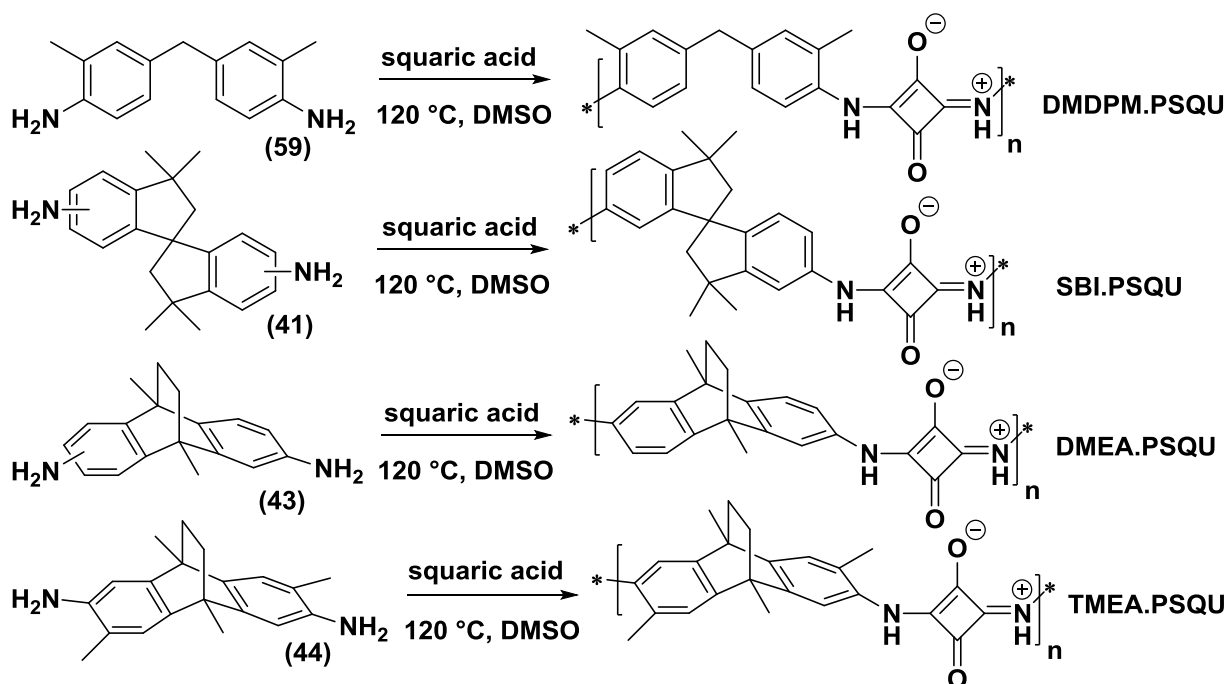
Squaraines were first reported in 1965<sup>186</sup> and due to the intense colours of the materials, they have since been used as organic dyes<sup>187</sup> and fluorescent probes<sup>188</sup>. Recently in 2013, a copper(II) porphyrin based, squaraine-linked, mesoporous COF (CuP-SQ-COF) was reported<sup>185</sup>. The COF was prepared by refluxing TAP-CuP and squaric acid in a mixture of *n*-butanol and 1,2-dichlorobenzene (Scheme 9b).



Scheme 9b Synthesis of CuP-SQ-COF.

CuP-SQ-COF has a reported BET surface area of  $539 \text{ m}^2/\text{g}$  which can be attributed to the rigid structure of both the porphyrin and the squaraine units. Squaraines formed from aromatic primary amines possess a rigid planar "zigzagged" skeleton with extended  $\pi$ -conjugation<sup>189</sup> that presents an attractive unit to incorporate into a PIM. The zwitterionic nature of squaraines also offers the possibility to form ionic PIMs without the need for counterions that have been previously shown to fill pore space and reduce free volume.

Fully conjugated linear squaraine polymers (polysquaraines) have attracted attention most notably as electrically conducting polymers since 1993<sup>190</sup>. Polysquaraines have been previously synthesised from the polymerisation reaction between appropriately di-functionalised monomers such as bis-pyrroles<sup>191</sup> and squaric acid but no examples of linear polymers formed from aromatic primary amines and squaric acid could be found in literature to date. Inspired by the chemistry used to form CuP-SQ-COF, a number of diamine monomers were polymerised with squaric acid to form a new class of linear polysquaraines (Scheme 9c).



Preliminary experimentation with the new polymerisation reaction using the *n*-butanol/1,2-dichlorobenzene solvent mixture reported for CuP-SQ-COF, resulted in the precipitation of a bright yellow powders after refluxing for 2 h. Analysis of these materials by FTIR and NMR spectroscopy confirmed the expected structure of the polymers consistent with characterisation of CuP-SQ-COF and discrete squaraines from literature<sup>192</sup>. FTIR

spectroscopy revealed a characteristic squaraine C=O vibration band at  $\sim 1600\text{ cm}^{-1}$  while NMR spectroscopy revealed both secondary NH and tertiary N<sup>+</sup>H peaks with equal integration and no protonated oxygen peaks.

All products displayed poor solubility in all solvents except DMSO and for this reason, estimation of molecular weight by GPC was not possible although, all the isolated materials displayed low viscosities when dissolved which is characteristic of low molecular weight material.

An improved method was then devised involving heating the corresponding diamine monomer with squaric acid to 120 °C under a nitrogen atmosphere using anhydrous DMSO as a solvent. Replacing the *n*-butanol/1,2-dichlorobenzene solvent mixture with DMSO allowed the polymer to remain dissolved and to continue polymerising without precipitating out of solution as oligomers. After a reaction time of 12 h, bright yellow and highly viscous solutions were obtained from diamine monomers 59, 41, 43 and 44. The polymers were obtained as intense yellow powders by the addition of the reaction mixture to a large excess of ethanol and subsequent filtration of the product. After purification by re-precipitation from DMSO, the desired polymers DMDPM.PSQU, SBI.PSQU, DMEA.PSQU and TMEA.PSQU were obtained in 96, 99, 99 and 95 % yields respectively.

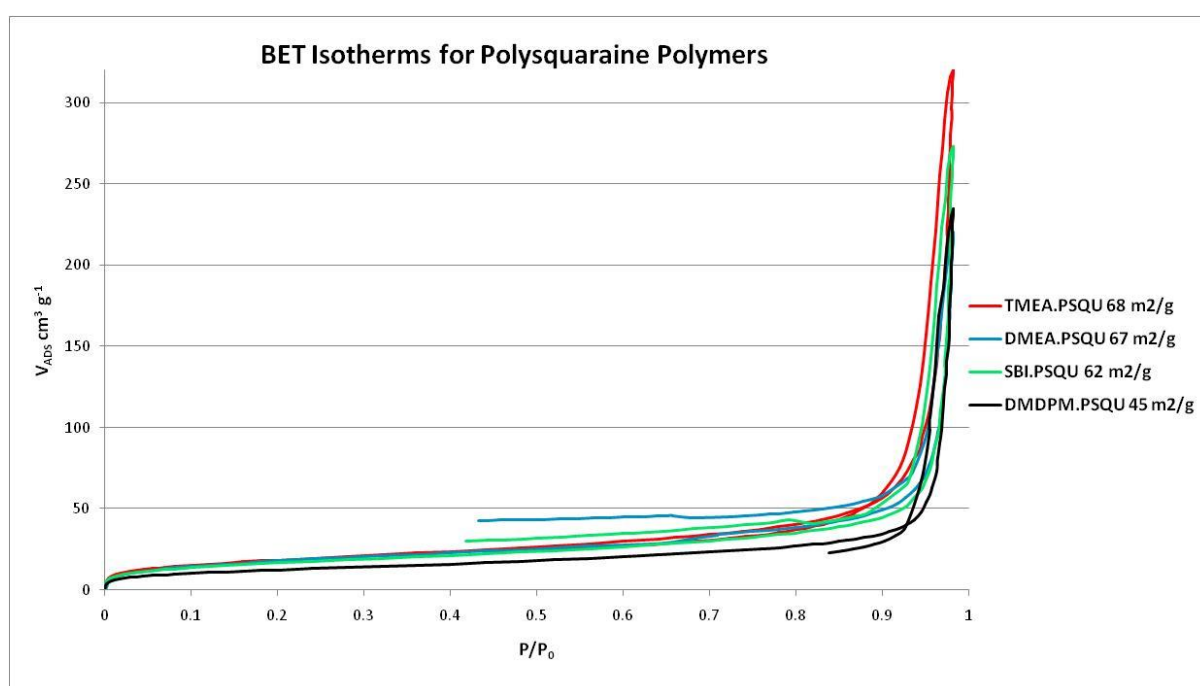
Thermal gravimetric analysis shows that DMDPM.PSQU and SBI.PSQU are both stable up to 300 °C while DMEA.PSQU and TMEA.PSQU are both stable up to 260 °C showing an initial decrease in mass consistent with the loss of an ethylene fragment via a retro Diels-Alder reaction<sup>172</sup>. Differential scanning calorimetry did not reveal the presence of glass transitions below the decomposition temperatures. Analysis of the ethanol washings from the crude polymers using MALDI-TOF failed to reveal an oligomeric pattern.

Nitrogen adsorption shows that DMDPM.PSQU, SBI.PSQU, DMEA.PSQU and TMEA.PSQU have low BET surface areas of 45, 62, 67 and 68 m<sup>2</sup>/g respectively. The low surface areas may be attributed to hydrogen bonding between secondary amine groups, ionic bonding and rotation of polymer segments around aromatic amine bonds. The relative order of observed BET surface areas appear to correlate with the with monomer rigidity although, the difference between the values of SBI.PSQU, DMEA.PSQU and TMEA.PSQU are within BET experimental error and for practical purposes, can be considered equal. It appears in the case of PIM polysquaraines, that increasing monomer and polymer segment rigidity has little effect on the resulting free volume of the polymer. A possible explanation may be that

polysquaraines do not respond to methanol treatment in such a dramatic manor as observed with other PIMs and physical ageing cannot be so easily cancelled. The obtained yields also suggest that little oligomeric material or impurities were removed by the re-precipitation procedures and this could affect the observed surface areas.

Unfortunately, films could not be formed from the isolated polysquaraines as DMSO is unsuitable for film formation using previously outlined laboratory methods although, other methods such as "dual bath coagulation"<sup>193</sup> could be utilised to obtain films.

Below are the BET isotherms from which the BET surface areas were calculated for the polysquaraines reported in this thesis.

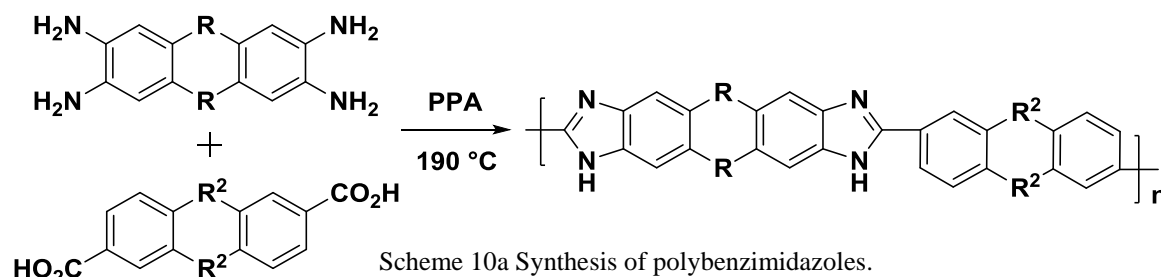


Below is a table summarising the some of the physical characteristics of the polysquaraines reported in this thesis.

Polysquaraine Polymers	BET Analysis		TGA
	BET Surface Area ( $\text{m}^2 \text{g}^{-1}$ )	Pore Volume ( $\text{cm}^3 \text{g}^{-1}$ )	$T_{\text{DEC}}$ ( $^{\circ}\text{C}$ )
TMEA.PSQU	68	0.4792	260
DMEA.PSQU	67	0.3264	260
SBI.PSQU	62	0.4036	300
DMDPM.PSQU	45	0.3366	300

## Chapter 10: Polybenzimidazoles

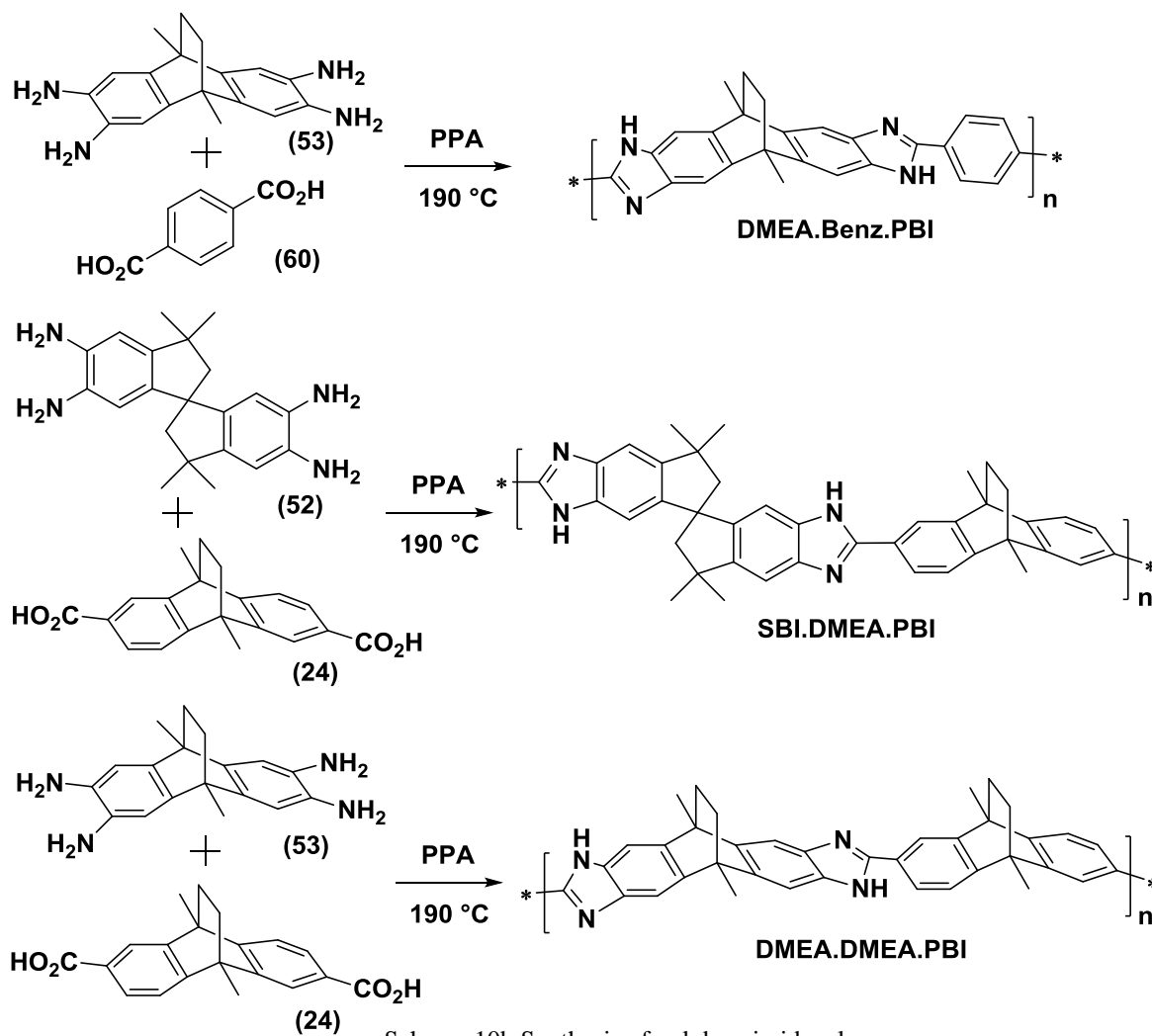
Aromatic polybenzimidazoles (PBI) are formed from the polycondensation of aromatic tetraamines with aromatic dicarboxylic acids<sup>194</sup> or diphenylesters<sup>195</sup>. The polymerisations are conducted at high temperature, either as a solvent free melt condensation<sup>194</sup> or in polyphosphoric acid (PPA) (190 °C)<sup>196</sup> (Scheme 10a).



The first aromatic polybenzimidazoles were reported in 1961 by Marvel and Vogel<sup>194</sup> and due to their exceptional chemical and thermal stability, have since been used primarily as heat resistant coatings and synthetic fibres to fabricate thermally protective apparel<sup>197</sup>. Polybenzimidazole membranes have found a number of uses in applications such as reverse osmosis<sup>198</sup> and solid polymer electrolytes in proton exchange membrane fuel cells<sup>196</sup>. Polybenzimidazoles have also been tested as gas separation membranes, displaying enhanced selectivity towards H<sub>2</sub>/CO<sub>2</sub> at elevated temperatures<sup>199</sup>. The measured permeabilities however, have been shown to be very low especially at lower temperatures. This is likely due to the dense, close chain packing structure of polybenzimidazoles resulting from rotation around the single linking bonds, cohesive interactions of planar monomers and hydrogen bonding of the secondary amine groups. Due to their high thermal stability, polybenzimidazoles remain a promising material for membrane applications that require elevated feed temperatures such as carbon capture from flue gas or steam reforming of fossil fuels. By applying the PIM design concept and introducing sites of contortion into the polybenzimidazole chains, the permeability of resulting membranes could be improved.

Three such polybenzimidazoles, DMEA.Benz.PBI, SBI.DMEA.PBI, and DMEA.DMEA.PBI were synthesised from tetraamines 53 and 52 and dicarboxylic acids 24 and 60 (commercially available) (Scheme 10b).





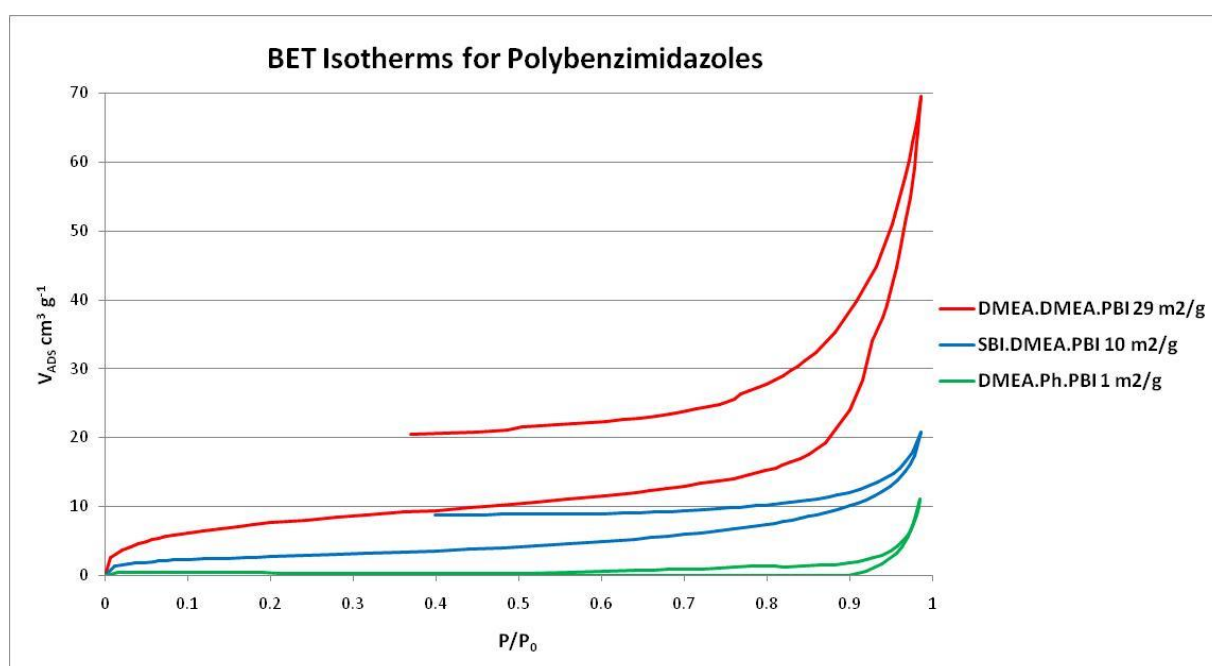
Scheme 10b Synthesis of polybenzimidazoles.

Due to the sensitivity of the tetraamine monomers to air and heat, the polyphosphoric acid method<sup>196</sup> was used instead of the solvent free melt method. The polyphosphoric acid requires a lower temperature, catalyses the reaction and also protects the tetraamine from oxidation by protonation of the amine groups. The polymerisations were carried out under a nitrogen atmosphere by slowly heating a mixture of corresponding tetraamine monomer and dicarboxylic acid in polyphosphoric acid to 190 °C, over 1h. The mixtures were then stirred at this temperature for a further 16h to form dark brown viscous mixtures. The mixtures were then poured into crushed ice and neutralised with saturated sodium bicarbonate solution to afford light brown precipitates. The precipitates were filtered and washed with hot acetone to afford the desired polymers DMEA.Benz.PBI, SBI.DMEA.PBI, and DMEA.DMEA.PBI in 97, 94 and 96 % yields respectively as dark brown powders. The isolated products were found to be insoluble in all common solvents but were soluble in sulfuric and trifluoroacetic acid. For this reason, estimation of molecular weight by GPC was not possible although, all

the isolated materials displayed high viscosities when dissolved in TFA which is characteristic of high molecular weight material.

Thermal gravimetric analysis shows that all three polymers are stable up to 200 °C. Differential scanning calorimetry did not reveal the presence of glass transitions below the decomposition temperatures. Analysis of the acetone washings from the crude polymers using MALDI-TOF failed to reveal an oligomeric pattern.

Nitrogen adsorption shows that DMEA.Benz.PBI, SBI.DMEA.PBI, and DMEA.DMEA.PBI have low BET surface areas of 1, 10 and 29 m<sup>2</sup>/g respectively. The low surface areas can be attributed to polymer segment rotation around the single C-C linking bonds and hydrogen bonding of the secondary amine groups. It can be concluded that incorporation of rigid and contorted polymer segments in polybenzimidazoles to induce microporosity is counteracted by the overbearing polymer cohesive interactions. The relative order of observed BET surface areas does however appear to correlate with monomer rigidity. DMEA.Benz.PBI contains only one site of contortion from the ethanoanthracene unit and has the lowest BET surface area of the series. SBI.DMEA.PBI contains two sites of contortion from ethanoanthracene and somewhat less rigid spirobisindane units which generates a slightly higher BET surface area than DMEA.Benz.PBI. DMEA.DMEA.PBI has the highest BET surface area of the series resulting from both sites of contortion being provided by highly rigid ethanoanthracene units.



Polybenzimidazoles are commonly soluble in dimethylacetamide from which films may be cast<sup>199</sup> however, all isolated products were insoluble in this solvent. A number of attempts were made to cast films from trifluoroacetic acid however, this resulted in the polymers precipitating as a powder before complete evaporation of the solvent.

Another method, used for fabricating conductive proton exchange membranes doped with phosphoric acid for fuel cell applications<sup>196</sup>, was also attempted. This method involves forming a film directly from a polymerisation mixture in polyphosphoric acid and allowing the slow hydrolysis of the polyphosphoric acid to phosphoric acid by ambient moisture. The polymer then slowly precipitates forming a solid film containing phosphoric acid. The phosphoric acid may then be washed out with water leaving a polybenzimidazole film. This method was attempted with all three polymers by slow hydrolysis over two months however, the result in all cases was a jelly like material. In an effort to obtain solid materials, the PTFE casting containers were carefully immersed in water to remove phosphoric acid. The isolated materials were found to be non-flexible, brittle and subsequently crumbled into powders upon removal from the casting containers.

It is clear that further experimentation is required to form films suitable for gas permeation studies however, due to the low surface areas observed, it is likely that permeabilities would be extremely low. As previously mentioned, the permeability of polybenzimidazole membranes increases with temperature and the applications of potential interest operate at elevated temperatures. All three polymers DMEA.Benz.PBI, SBI.DMEA.PBI, and DMEA.DMEA.PBI are only stable up to 200 °C which limits their potential in high temperature processes. This could be potentially solved using monomers with higher thermal stability such as triptycene, spirobisindane and spirobifluorene.

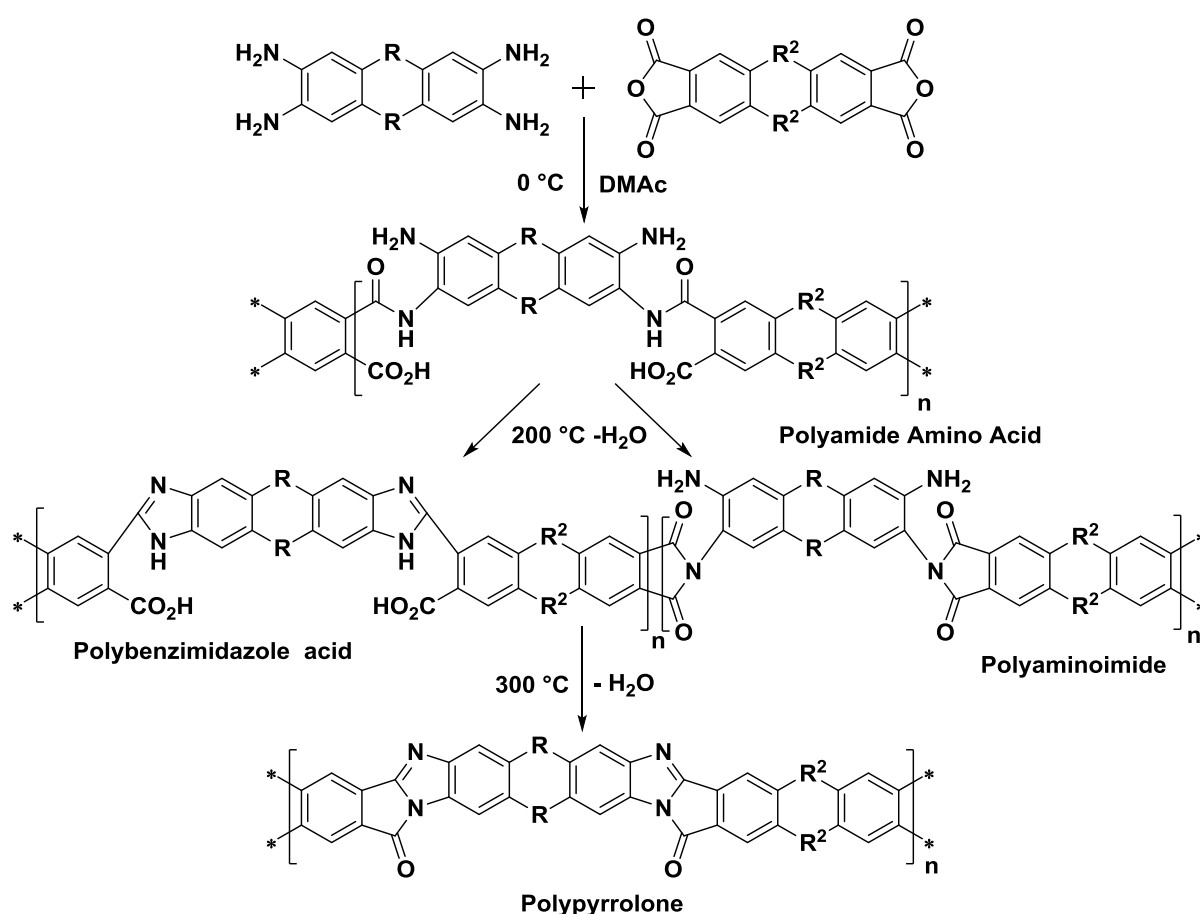
Below is a table summarising the some of the physical characteristics of the polybenzimidazoles reported in this thesis.

Polybenzimidazole Polymers	BET Analysis		TGA
	Polymer	BET Surface Area (m <sup>2</sup> g <sup>-1</sup> )	Pore Volume (cm <sup>3</sup> g <sup>-1</sup> )
DMEA.DMEA.PBI	29	0.0990	200
SBI.DMEA.PBI	10	0.0289	200
DMEA.Benz.PBI	1	0.0140	200

## Chapter 11: Polypyrrolones

Polypyrrolones (PPy) were first reported by Dawans and Marvel in Oct 1965<sup>200</sup> in which they referred to their new class of polymer as *polybenzimidazolimides*. Other researchers in the field later referred to these polymers as *polyimidazopyrrolones* (Bell and Pezdirtz, Dec 1965<sup>201</sup>) or *polybenzoylenebenzimidazoles* (Colson, Michel and Paufler, 1966<sup>202</sup>). For the purpose of consistency, these polymers shall be referred to in this thesis as *polypyrrolones*, which appears to be the most common name used in present day literature.

Polypyrrolones are insoluble step-ladder polymers derived from the polycondensation of aromatic tetraamines and aromatic dianhydrides in a two-step synthesis (Scheme 11a<sup>203</sup>).



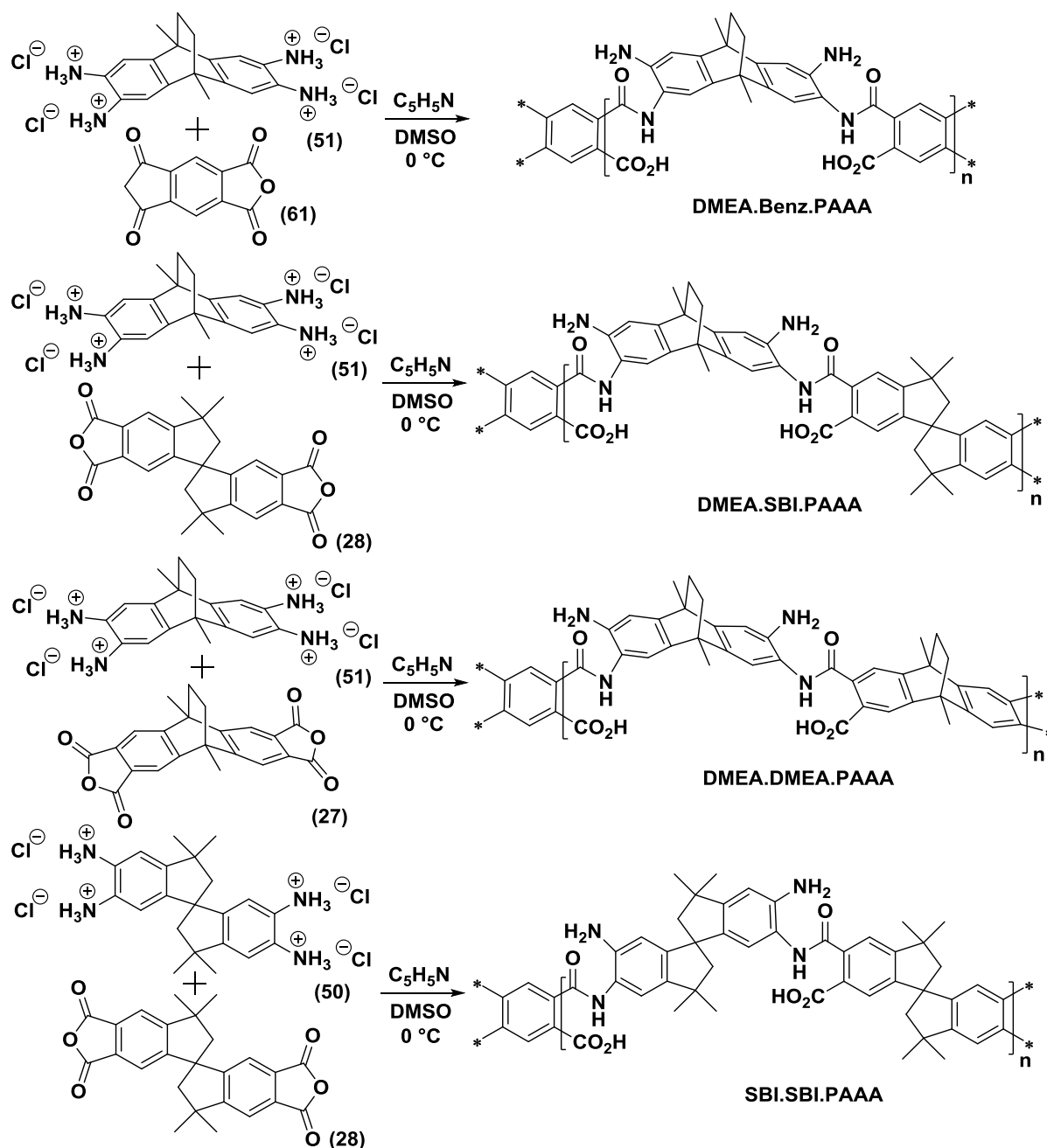
Scheme 11a Synthesis of polypyrrolones via polyamide amino acids.

The first step involves a polycondensation reaction at 0 °C by the slow addition of a solution of the dianhydride monomer to a solution of the tetraamine monomer to form a polyamide amino acid (PAAA) precursor polymer. The polymerisation requires a polar aprotic solvent such as dimethylformamide (DMF) although dimethylacetamide (DMAc) is most commonly used. The use of a tetraamine monomer is known to make this polymerisation notoriously

difficult<sup>203</sup> as it can potentially react with four equivalents of the dianhydride monomer, forming a network polymer. This often results in an instantaneous insoluble gel formation during the polymerisation reaction which cannot be further processed. To avoid network formation, low temperatures, high monomer purity, slow monomer addition and precise monomer stoichiometry are required. Once a soluble polyamide amino acid is formed, this precursor polymer may then be processed into the required form such as a coating or solvent-cast film. The second step involves a staged thermal curing of the precursor polymer at 150-200 °C to convert the polyamide amino acid to a polybenzimidazole acid/polyaminoimide copolymer. The temperature is then increased up to 290-300°C<sup>204, 205</sup> to form the polypyrrolone structure. During the thermal curing process, cross-chain reactions inevitably occur, forming cross-links between chains, resulting in an insoluble polymer. The final dehydration reaction is known to be often incomplete, leaving a partial "imide/imidazole character" within the polymer structure<sup>203</sup>.

Polypyrrolones, similar to polybenzimidazoles, are thermally stable polymers due to the inherent stability of their fused ring systems and have been intensely studied as heat and radiation resistant laminates by NASA<sup>206</sup>. The few examples of polypyrrolones studied as gas separation membranes<sup>204, 205, 207</sup> show data above the Robeson 1991 upper bound for O<sub>2</sub>/N<sub>2</sub> and CO<sub>2</sub>/CH<sub>4</sub> although the measured permeabilities were found to be relatively low. The permeability of polypyrrolones has been shown to improve for high temperature (200 °C) gas separations<sup>207</sup> which combined with their thermal stability, makes these polymers potential candidates for high temperature applications. The permeability of polypyrrolone membranes can likely be improved further by applying the PIM design concept and incorporating contorted polymer segments. The pyrrolone linking unit is likely to be more successful at maintaining intrinsic microporosity than the previously described benzimidazoles because pyrrolone linkages are comprised of highly rigid fused ring units and tertiary nitrogen atoms that will not decrease free volume by hydrogen bonding.

To investigate polypyrrolones formed from PIM-type monomers, four polyamide amino acid precursor polymers DMEA.Benz.PAAA, DMEA.SBI.PAAA, DMEA.DMEA.PAAA and SBI.SBI.PAAA were formed from tetraamine hydrochlorides 50 and 51 with dianhydrides 27, 28 and 61 (commercially available) using a modified procedure from literature<sup>206</sup> (Scheme 11b).



Scheme 11b Synthesis of polyamide amino acid precursor polymers.

The most common methods of preparing polyamide amino acid precursor polymers use a freebase tetraamine monomer. A method first reported by Bell and Pezdirtz<sup>201</sup> offers an alternative procedure when particularly sensitive tetraamines are involved by using the less sensitive tetraamine hydrochloride salt along with pyridine to convert the hydrochloride to the freebase *in situ*. Preliminary experimentation with this method using DMAc as a solvent resulted in instantaneous gel formation after only half an equivalent of the dianhydride monomer had been added. This was due to the poor solubility of the tetraamine monomers in

DMAc which resulted in only a small proportion of solvated tetraamine that changed the stoichiometry of the polymerisation. Both tetraamine hydrochlorides 50 and 51 were found to be most soluble in DMSO and remained in solution after the addition of pyridine. The polymerisations were then conducted using DMSO as the solvent. Under a nitrogen atmosphere, the corresponding tetraamine hydrochloride salt was dissolved in anhydrous DMSO and the solution was cooled in an ice bath. A solution of the corresponding dianhydride monomer in anhydrous pyridine and DMSO was added drop-wise over 2 h to produce a viscous bright yellow mixture. It was found that if these mixtures were allowed to stir for more than one hour after the addition, they were likely to form insoluble gels. The polymerisations were quenched in deionised water and washed with water and ethanol to remove pyridine hydrochloride. The polymers were then dried under nitrogen to afford DMEA.Benz.PAAA, DMEA.SBI.PAAA, DMEA.DMEA.PAAA and SBI.SBI.PAAA as bright yellow powders in 98, 98, 98 and 99 % yields respectively. It has been reported that precursor polymers of this type are commonly air sensitive and will rapidly turn green if not stored under a nitrogen atmosphere<sup>203</sup>. The isolated products were only found to be air sensitive when being dried from a solvent and were subsequently air stable when dry.

Nitrogen adsorption shows that all the isolated products are non-porous, possessing BET surface areas of 0 m<sup>2</sup>/g with irregular isotherms. This can be attributed to rotation around amide linkages and extensive hydrogen/ionic bonding.

PAAA precursor polymers are commonly soluble in DMAc, DMF, NMP and DMSO<sup>203</sup> however, once precipitated from the DMSO polymerisation solution, the isolated products were found to be insoluble in all common solvents, including DMSO. The products were only soluble in pure TFA, from which a number of attempts were made to cast films but this resulted in the polymers precipitating as a powder before complete evaporation of the solvent. A possibility for future work is to cast a film directly from the polymerisation solution and allow the polymer to form a cross-linked gel. Thermal treatment under vacuum would then form the polypyrrolone structure while removing the reaction solvent.

Thermal gravimetric analysis of each precursor polymer reveals a loss of mass between 150 and 400 °C, approximately equal to that calculated for predicted thermal reactions (Fig 11a) and are summarised in Table 11a. The precursor polymer dehydrates forming two molecules of H<sub>2</sub>O per repeating unit to form a polybenzimidazole acid/polyaminoimide co-polymer. A higher temperature dehydration then forms two molecules of H<sub>2</sub>O per repeating unit to form a

polypyrrolone. Polymers containing dimethyl ethanoanthracene units, also undergo the loss of an ethylene fragment unit via a retro Diels-Alder reaction<sup>172</sup> at approximately 260 °C to form dimethyl anthracene units. All polymers appear to decompose above 400 °C.

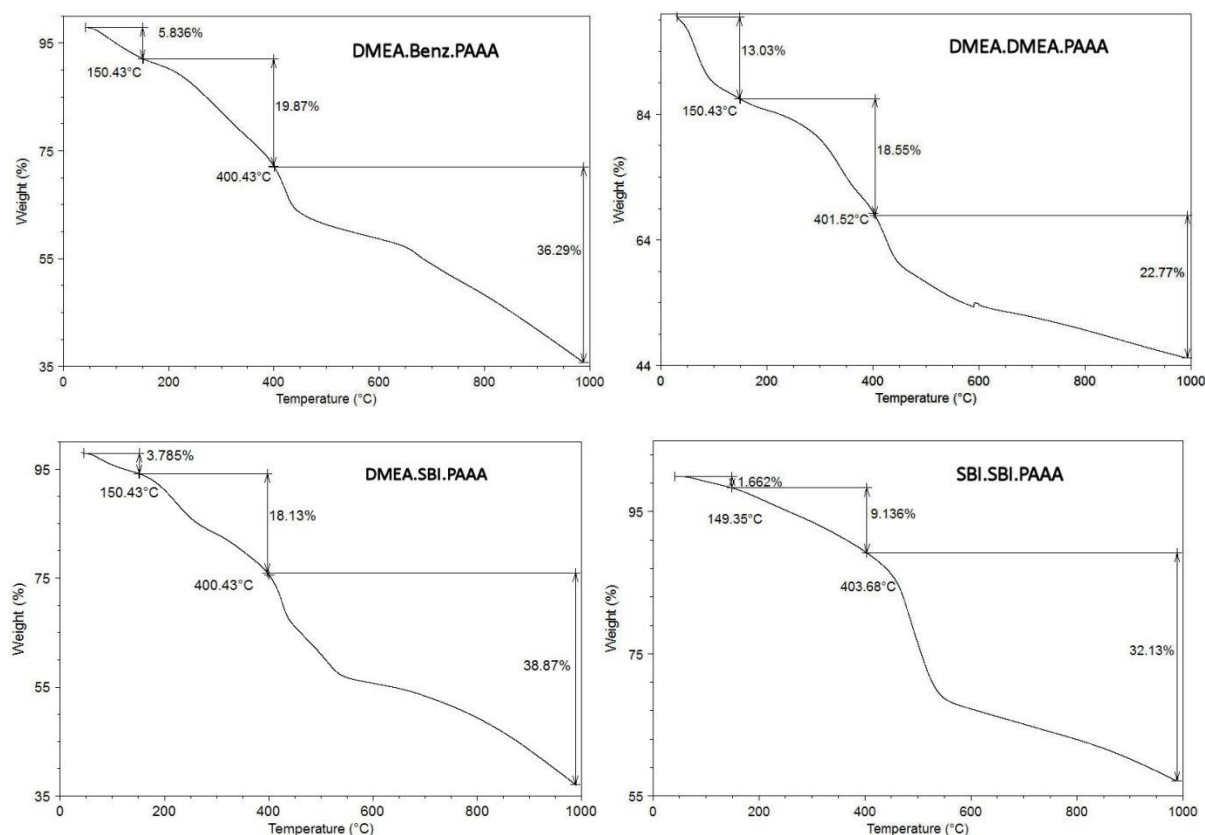


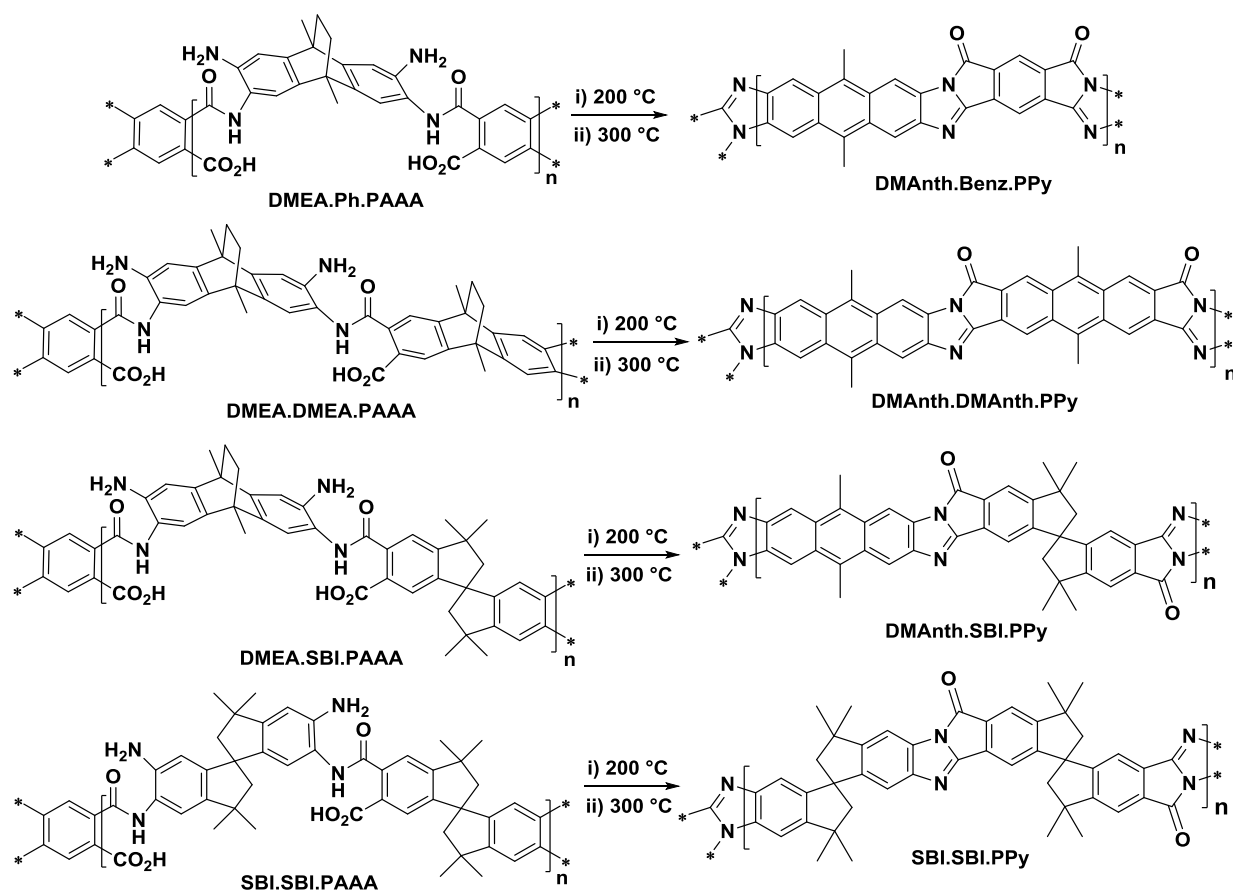
Fig 11a Thermal gravimetric analysis of polyamide amino acid precursor polymers.

Table 11a Polyamide Amino Acid Thermal Gravimetric Analysis			
Precursor Polymer	Species Lost Per Repeating Unit	Calculated Loss of Mass	TGA Loss of Mass
DMEA.Benz.PAAA	4 H <sub>2</sub> O, C <sub>2</sub> H <sub>4</sub>	19.53%	19.87%
DMEA.SBI.PAAA	4 H <sub>2</sub> O, C <sub>2</sub> H <sub>4</sub>	14.08%	18.13%
DMEA.DMEA.PAAA	4 H <sub>2</sub> O, 2 C <sub>2</sub> H <sub>4</sub>	19.17%	18.55%
SBI.SBI.PAAA	4 H <sub>2</sub> O	9.57%	9.14%

The precursor polymers were then converted to the corresponding polypyrrolone polymers using a tube furnace. Under a nitrogen atmosphere the corresponding powdered precursor polymers were placed in a ceramic boat crucible and positioned inside a wire wound single zone tube furnace. The furnace was ramped 10°C /min to 200 °C for 1 h, then 10°C /min to



300 °C for 4 h and cooled to room temperature to produce DMAAnth.Benz.PPy, DMAAnth.DMAAnth.PPy, DMAAnth.SBI.PPy and SBI.SBI.PPy in 98, 99, 98 and 99 yields respectively as dark brown powders (Scheme 11c).



Scheme 11c Synthesis of polypyrrolones from polyamide amino acids.

Thermal gravimetric analysis (Fig 11b) shows DMAAnth.Benz.PPy, DMAAnth.DMAAnth.PPy, DMAAnth.SBI.PPy and SBI.SBI.PPy are stable up to ~ 382, 477, 400 and 480 °C respectively.

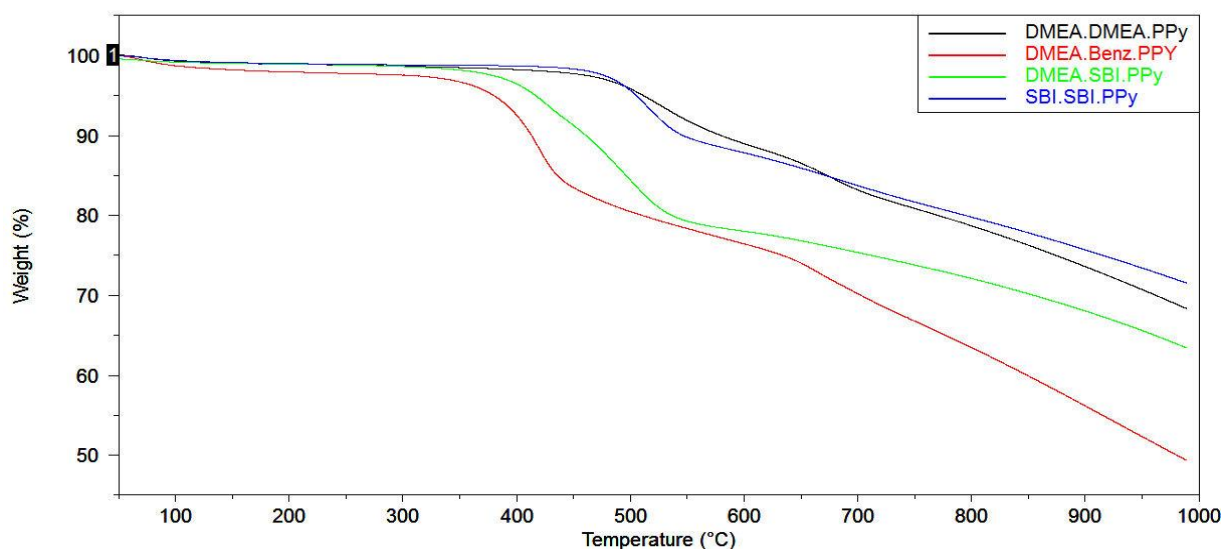
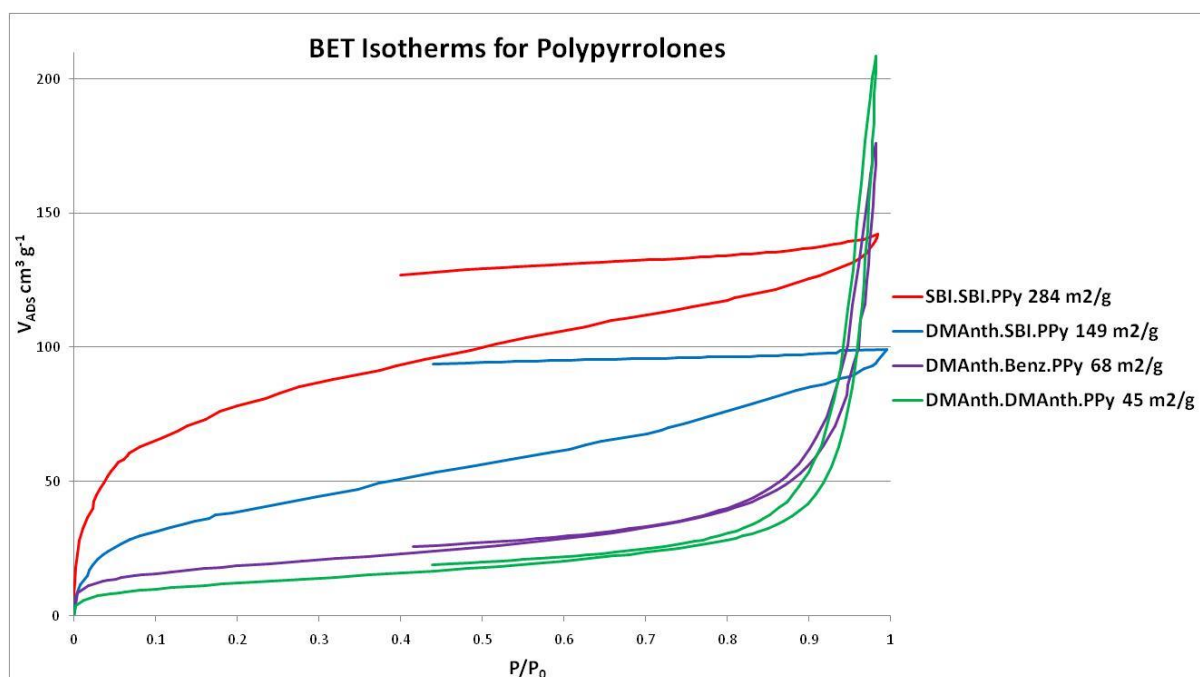


Fig 11b Thermal gravimetric analysis of thermally cured polypyrrolones.

NASA reports that PAAA precursor polymers are fusible materials at the temperatures required for pyrrolone formation and that sufficient flow is a requirement to form high strength films and laminates<sup>203</sup>. The products were isolated as powders which suggests, the precursor polymers were infusible and differential scanning calorimetry of the precursor polymers did not reveal the presence of glass transitions below 400 °C.

The insoluble polypyrrolones were characterised using FTIR spectroscopy and solid state <sup>13</sup>C NMR. FTIR spectroscopy revealed absorption bands at ~1775 (C=O asymm), ~1720 (C=O symm), 1615 (C=N stretch), ~1360 (C-N stretch), 745 (imide ring deformation) (cm<sup>-1</sup>). Absorption bands due to C=O, C=N and C-N are ambiguous and could be assigned to either pyrrolone, imide or imidazole structures however, absorption bands at ~745 cm<sup>-1</sup> are characteristic of imide ring deformation. This suggests that all four isolated products have at least a partial imide/imidazole character that may have resulted from branching in the precursor polymer and cross-chain reactions during thermal curing.

Nitrogen adsorption shows that thermally cured DMAnth.DMAnt.PPy, DMAnth.Benz.PPy, DMAnth.SBI.PPy and SBI.SBI.PPy possess relatively low BET surface areas of 45, 68, 149 and 284 m<sup>2</sup>/g respectively.



Preceding the removal of carboxylic acid groups by the first dehydration reaction of the non-porous PAAA precursor polymers, a portion of free volume is conceivably gained from the release of ionic ( $-\text{NH}_3^+/-\text{CO}_2^-$ ) bonding. This likely followed by thermally accelerated ageing

and finally the polymer is locked into this state by cross-chain reactions during the higher temperature dehydration. It is possible that the surface areas may then change depending on the thermal curing procedure and could be optimised with a view to producing high surface area materials rather than dense and tough laminates.

For the polymers containing planar anthracene units, one would expect dense solids with a surface area of 0 m<sup>2</sup>/g however, corresponding ethanoanthracene units contained in the precursor polymers presumably create a pore structure in the intermediate co-polymer that, to some degree, remains after thermal cross-linking. DMAnth.DMAnt.PPy has a lower BET surface area than DMAnth.Benz.PPy due to the incorporation of two anthracene units that enforce polymer chain cohesion by non-covalent interactions. Substantially higher surface areas are observed for the polymers containing thermally stable spirobisindane units that remain intact after thermal treatment. SBI.SBI.PPy has a higher BET surface area than DMAnth.SBI.PPy due to the incorporation of two spirobisindane units that act as sites of contortion between the planar pyrrolone linkages.

SBI.SBI.PPy appears to be the most promising polypyrrolone of the series for high temperature gas separations although the inability to process the insoluble and infusible precursor polymer into films is a problem that may be challenging to overcome.

A report published by NASA in 1969<sup>203</sup> contains what appears to be a similar example of a precursor polymer that was insoluble in commonly used solvents and infusible. The authors attribute this behaviour to strong electrostatic interactions between ionic sites (-NH<sub>3</sub><sup>+</sup>/-CO<sub>2</sub><sup>-</sup>) of a postulated zwitterionic form of a PAAA. This ionic cross-linking renders the polymer insoluble and increases the melting temperature. It is unclear if a "neutral" polymer results from impurities contained in the solvents acting as counterions or direct interaction with the polymerisation solvents. It is likely that the precursor polymers described in this thesis were obtained as a rarely observed ionised form instead of the more common "neutral" form. This may also be the reason for the apparent higher stability towards air of the isolated products compared with examples from literature. The authors of the study also report a simple solution to this problem that could be attempted in future work. By using a tetra-ester instead of a bisanhydride monomer, the resulting polymerisation will produce a polyamide where ionisable -CO<sub>2</sub>H groups are replaced with -CO<sub>2</sub>R groups. The addition of ester groups to the precursor polymer may also enhance solubility in less polar solvents that are more easily removed during film formation.

## **Chapter 12: Preliminary Study of Cross-Linking DHEA.TB with PIM-1**

Cross-linking of polymeric membranes is an important aspect of membrane technology as it can improve solvent resistance, reduce polymer plasticisation and decrease physical ageing. In chapter 7.2.3, it was shown that it is possible to cross-link Tröger's base polymers by ion exchange of methyl iodide quaternerised TB polymers with a dianionic counterion. It was also shown that the presence of counterions significantly decreases free volume by filling pore space. The reduction of free volume has shown to be minimised using a small counterion and it is also plausible that using a very large counterion may separate polymer chains and maintain porosity. Another option is to use an anionic species which is itself, intrinsically microporous.

A species that fits this description was described previously in chapter 1.8.3.1. In 2009, Guiver and co-workers reported the hydrolysis of pendent nitrile groups in a PIM-1 film forming a carboxylated PIM<sup>93</sup>. As a result, the permeability and solubility of the material was significantly reduced due to extensive hydrogen bonding of the pendent carboxylic acid groups. Carboxylated PIM-1 can be incorporated into a Tröger's base polymer membrane to act as a microporous pseudo cross-linking counterion by virtue of a salt formation between the acidic carboxylic acid groups on carboxylated PIM-1 with the basic nitrogen atoms on the TB polymer.

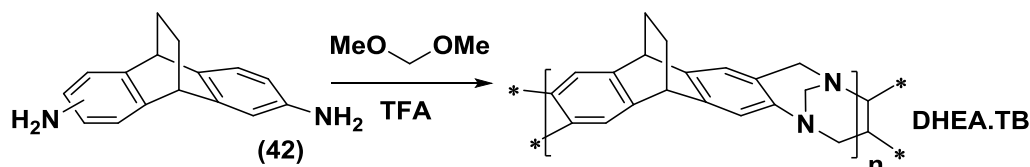
This chapter reports a short preliminary investigation into the cross-linking of the most commercially applicable TB polymer, DHEA.TB, using carboxylated PIM-1 as a counterion. The approach involved the casting of a film from a chloroform solution consisting of a mixture of non-hydrolysed PIM-1 and DHEA.TB. The film obtained was then hydrolysed, converting the PIM-1 portion to carboxylated PIM-1, which subsequently formed ionic bonds with the DHEA.TB portion achieving a cross-linked film.

Samples of all polymers and polymer mixtures were synthesised separately as powders for characterisation and BET surface area analysis. Film samples were then cast separately and compared.

## Polymer Synthesis

### DHEA.TB

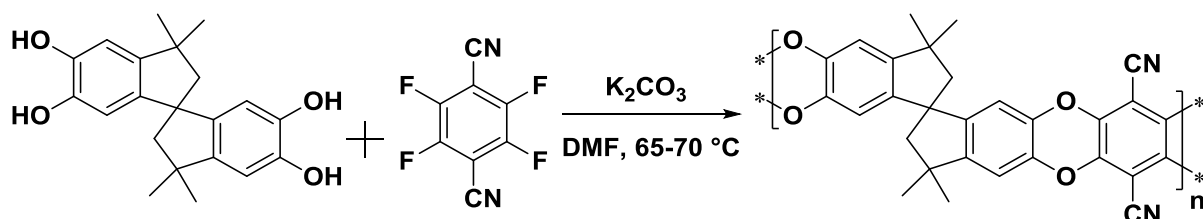
DHEA.TB was synthesised as previously described (Scheme 12a) with a high molecular weight (GPC:  $M_n = 9,200$ ,  $M_w = 49,300$ ) and a BET surface area of  $843 \text{ m}^2/\text{g}$ . A sample was refluxed in an equal mixture of ethanol and saturated sodium hydroxide solution for 24 h and it was confirmed by NMR the polymer was stable in basic conditions.



Scheme 12a Synthesis of DHEA.TB.

### PIM-1

PIM-1 was synthesised according to a procedure from literature<sup>73</sup> (Scheme 12b) by stirring mixture of 3,3,3',3'-tetramethyl-1,1'-spirobisindane-5,5',6,6'-tetrol and 2,3,5,6 tetrafluorophthalonitrile in anhydrous dimethylformamide with anhydrous potassium carbonate at  $65\text{-}70 \text{ }^\circ\text{C}$  for 72 h.



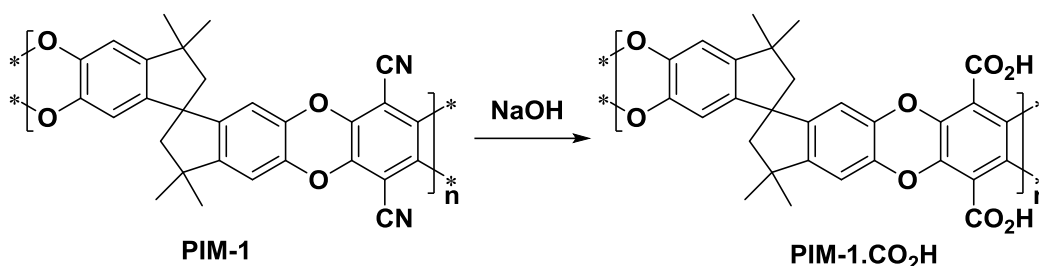
Scheme 12b Synthesis of PIM-1.

The bright yellow mixture was quenched in water and stirred for 1 hr. The solid was collected by filtration, washed with water and then acetone until the washings were clear. The resulting powder was dried, and purified by re-precipitation from tetrahydrofuran into a mixture of methanol and acetone to afford PIM-1 in 92% yield. PIM-1 was obtained as a high molecular weight polymer (GPC:  $M_n = 60,400$ ,  $M_w = 194,700$ ) with a BET surface area of  $812 \text{ m}^2/\text{g}$ . Thermal gravimetric analysis shows that the sample is stable up to  $500 \text{ }^\circ\text{C}$ .

### PIM-1.CO<sub>2</sub>H

PIM-1.CO<sub>2</sub>H was synthesised according to a procedure from literature<sup>93</sup> by refluxing a suspension of PIM-1 in an equal mixture of ethanol and saturated sodium hydroxide solution for 24 h (Scheme 12c). The dark grey mixture was filtered, washed with deionised water and

then refluxed in deionised water containing a few drops of hydrochloric acid (pH 4) for 1h to neutralise the polymer. The light grey mixture was filtered, washed with deionised water and then acetone until washings were clear to afford carboxylated PIM-1 in 94% yield.



Scheme 12c Synthesis of carboxylated PIM-1.

Hydrolysis was confirmed by FTIR spectroscopy and noting the disappearance of the weakly absorbing PIM-1 nitrile C=N band at  $2241\text{ cm}^{-1}$  and the appearance of strong carbonyl absorption bands at  $1672\text{ (C=O asym)}$  and  $1601\text{ (C=O sym)}$ . Thermal gravimetric analysis shows that the sample is less stable than PIM-1 and decomposed above  $200\text{ }^\circ\text{C}$ , possibly with the loss of  $\text{CO}_2$ . Carboxylated PIM-1 has a BET surface area of  $399\text{ m}^2/\text{g}$  which is substantially lower than PIM-1 and can be attributed to extensive hydrogen bonding reducing free volume.

### **PIM-1 10%, DHEA.TB 90% Mixture**

A mixture of PIM-1 10% and DHEA.TB 90% by weight was prepared by dissolving PIM-1 and DHEA.TB in HPLC chloroform and stirring thoroughly for 16h. A film was cast in a 10 cm PTFE dish in the normal manner to give a flexible light yellow film (Fig 12a). The film was refluxed in methanol for 24 h, and dried in a vacuum oven at  $120\text{ }^\circ\text{C}$  for 9 h. A second identical mixture was precipitated into methanol and filtered to afford a light yellow powder which was post treated in the same manner.

Nitrogen adsorption shows that the isolated powder has a BET surface area of  $655\text{ m}^2/\text{g}$  which is lower than that observed from either component in the mixture measured separately. This suggests that a mixture of the two polymers can pack space more efficiently than the pure component polymers. Thermal gravimetric analysis shows that the sample is stable up to  $260\text{ }^\circ\text{C}$  which is due to decomposition of the DHEA.TB component.

A previous attempt was made to cast a film from a PIM-1 50% / DHEA.TB 50% mixture however, the film was non-homogenous and extremely brittle. Placing the film under a

254nm UV lamp revealed phase separation of the fluorescent PIM-1 from DHEA.TB. Reducing the PIM-1 content to 10% produced a homogeneous and flexible film (Fig 12a)

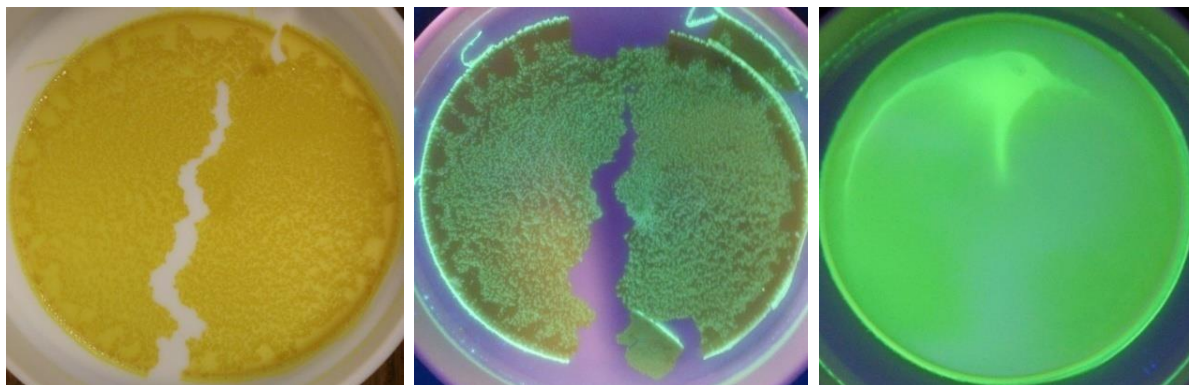
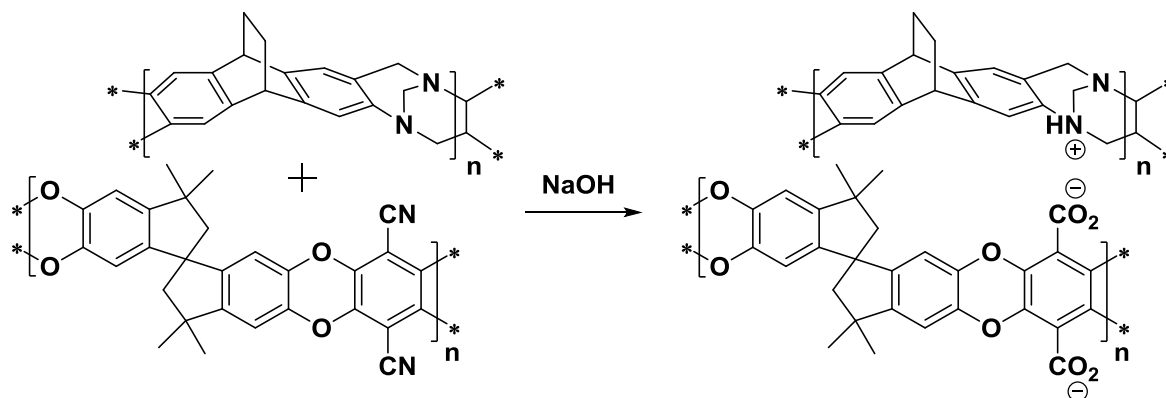


Fig 12a A PIM-1 50%/DHEA.TB 50% film (left), under UV light (middle) and a PIM-1 10%/DHEA.TB 50% film under UV light (right).

### PIM-1.CO<sub>2</sub>H 10%.DHEA.TB 90%

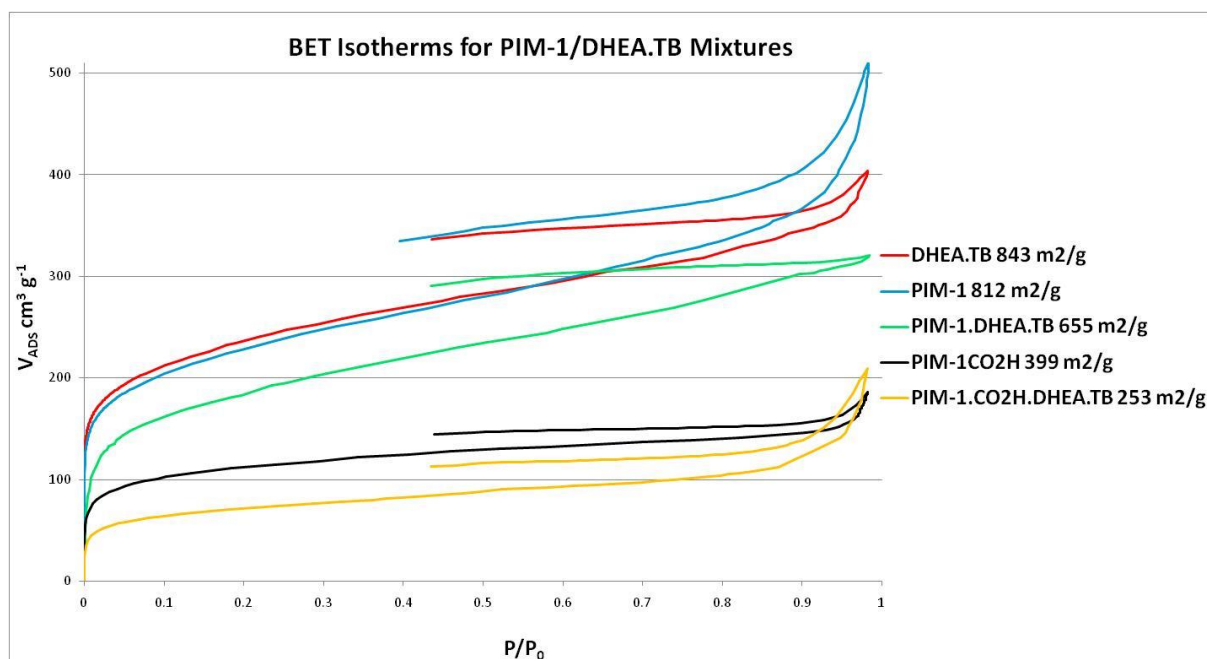
One half of the film containing PIM-1 10% and DHEA.TB 90% was hydrolysed using the same method as with PIM-1.CO<sub>2</sub>H (Scheme 12d) to afford a flexible light orange film.



Scheme 12d Hydrolysis of a PIM-1.CO<sub>2</sub>H 10%, DHEA.TB 90% mixture.

A powdered sample containing PIM-1 10% and DHEA.TB 90% was treated with the same procedure to afford a light orange powder. Hydrolysis could not be confirmed by FTIR spectroscopy as the weakly absorbing PIM-1 nitrile band in the original film and carbonyl absorption bands in the treated film were not visible due to the low PIM-1 content. Thermal gravimetric analysis shows that the sample is stable up to 300 °C. Nitrogen adsorption shows that the isolated powder has a BET surface area of 253 m<sup>2</sup>/g which is lower than that observed for PIM-1.CO<sub>2</sub>H. This is consistent with strong ionic bonding between the two component polymers compared with the weaker hydrogen bonding in PIM-1.CO<sub>2</sub>H.

Below are the BET isotherms from which the BET surface areas were calculated for different PIM-1/DHEA.TB mixtures.



Placing the non-hydrolysed film next to the hydrolysed film under 254nm UV lamp revealed that the treated film appears more brightly fluorescent than the untreated film when pure PIM-1.CO<sub>2</sub>H is non-fluorescent. A piece of each film was cut off and placed in separate vials containing chloroform. The non-hydrolysed sample completely dissolved after 1 h and the hydrolysed sample remained insoluble after 24 h which confirms cross-linking of the film (Fig 12b).

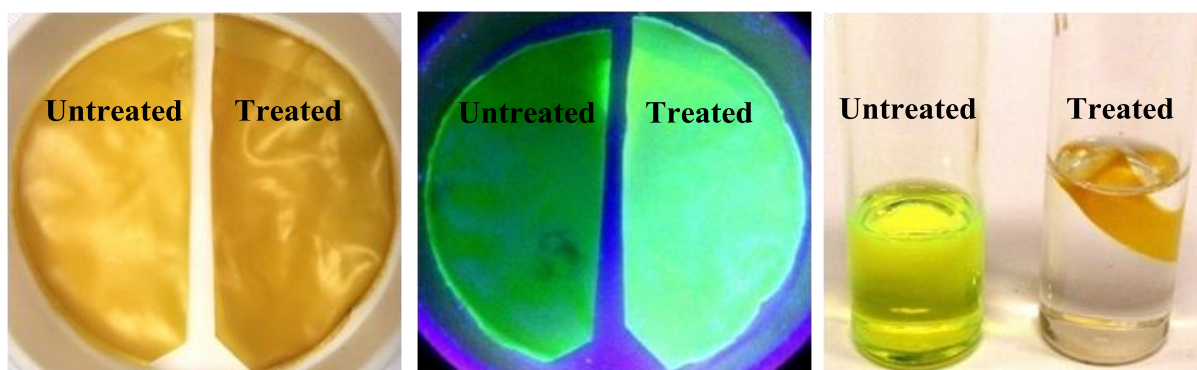


Fig 12b Non-hydrolysed and hydrolysed PIM-1 10%/DHEA.TB 90% films (left), under UV light (middle) and small film pieces placed in vials containing chloroform after 24 h (right).

The film samples were sent for gas permeation studies by ITM but the samples were not mechanically robust enough to withstand the permeation tests and were damaged during analysis. This study has achieved only a proof of concept and it is clear that further work is needed to optimise film strength and free volume. In future work there are a number of variables that can be investigated such as PIM-1.CO<sub>2</sub>H content and degree of hydrolysis.



## **Chapter 13: Conclusions**

Five classes of polymer featuring tertiary amine functionality were synthesised from a range of aromatic diamine, tetraamine, dianhydride, and dicarboxylic acid monomers that conform to the PIM design concept. Structure-property relationships were established between these polymers with BET surface area and gas permeation measurements.

It was found that monomeric units which contain structural features that induce rigidity and contortion, combined with rigid linkers that prevent polymer segment rotation will maximise surface area and increase gas permeability. Chain flexibility and structural features that increase polymer chain cohesive interactions such as planar monomeric units and hydrogen bonding groups serve to decrease surface area and gas permeability.

A novel polymerisation reaction was developed, giving rise to a new class of microporous polymer called Tröger's Base PIMs. These polymers were found to be solution-processable and can possess a wide range of BET surface areas ranging from 0-1028 m<sup>2</sup>/g. The highest BET surface area was observed from DMEA.TB which combines the enhanced structural rigidity of both ethanoanthracene and Tröger's Base units with sites of contortion possessed by both polymer segments. These features bestowed the highest recorded BET surface area for any soluble polymer to date, while placing gas permeation data for technologically important gas pairs far over the present Robeson upper bound. Enhanced molecular sieving type permeability characteristics were found to be particularly evident for gases paired with hydrogen. Quaternisation and subsequent ion exchange of Tröger's Base polymers has shown that the properties of these polymers can be dramatically altered according to the choice of counterion. Ion exchange with polyanionic counterions has also been investigated as a platform for the cross-linking of Tröger's Base polymers. It was found that counterions fill pore space and a compromise in surface area is made however, it was also shown that using counterions that are intrinsically microporous can maintain free volume.

Three polyimides were synthesised from highly rigid and contorted ethanoanthracene monomers containing differing numbers of methyl groups that restrict rotation around polymer segments. It was found that increasing the number of methyl groups next to the imide linkages increased polymer chain rigidity and a subsequent increase in BET surface area and gas permeability was observed. These polyimides were shown to possess a range of BET surface areas from 373-694 m<sup>2</sup>/g although only moderate gas permeation characteristics were displayed.

---

A new class of zwitterionic polysquaraines were synthesised from monomers that conform to the PIM design concept but it was found that these materials were non-porous, possessing BET surface areas in the range of 45-68 m<sup>2</sup>/g. This can be attributed to the polymer linkages containing rotatable bonds and to strong ionic/hydrogen bonding that increases polymer chain cohesion. These materials were found to be soluble only in DMSO and so film formation was not possible with these materials using methods outlined in this research. In future work, films may be attempted to be formed with the use of a dedicated vacuum oven or a dual bath coagulation method.

A number of novel polybenzimidazoles were from synthesised monomers that conform to the PIM design concept but it was found that these materials were non-porous, possessing BET surface areas in the range of 1-29 m<sup>2</sup>/g. This can again be attributed to the polymer linkages containing rotatable bonds and to extensive hydrogen bonding that reduces free volume, forming non porous solids. These polymers were found to be only soluble in acids from which film casting proved to be ineffective. Due to the low surface areas observed, it is not likely that these materials will offer any improvement over present technology.

Various novel polypyrrolones were synthesised *via* polyamide amino acid precursor polymers. The precursor polymers were found to be only soluble in acids from which films could not be effectively formed. The insolubility of all precursor polymers was likely the result of strong electrostatic interactions between ionic sites of a postulated zwitterionic form. After thermal curing of the precursor polymers the resulting polypyrrolones exhibited BET surface areas ranging from 45-284 m<sup>2</sup>/g. The polypyrrolone possessing the highest BET surface area of the series was formed from monomers that both contained spirobisindane architectures, while lower surface areas were observed for polymers containing planar anthracene units. In future work, addition of ester groups to the precursor polymer may enhance solubility and aid film formation. It is also likely that the free volume in these polymers may be altered by adjusting the thermal curing process as to maximise gas permeability characteristics.

This work has shown that microporous polymers containing tertiary amine functionality can be formed using monomers that conform to the PIM design concept and can be tailored to exhibit a wide range of properties. Some of the materials resulting from this research may have little technological significance at present however, there is now a growing interest in the application of Tröger's Base PIMs in gas separation, catalysis and electrochemistry.

---

## **Chapter 14: Experimental**

### **14.1: General Methods and Equipment**

All reactions using air/moisture sensitive reagents were performed in oven-dried apparatus, under a nitrogen atmosphere. TLC analysis refers to analytical thin layer chromatography, using aluminium-backed plates coated with Merck Kieselgel 60 GF<sub>254</sub>. Product spots were viewed either by the quenching of UV fluorescence, or by staining with a solution of Cerium Sulfate in aqueous H<sub>2</sub>SO<sub>4</sub>. Commercially available reagents were used without further purification unless otherwise stated. Anhydrous solvents were obtained by distillation over calcium hydride (dichloromethane), drying over activated molecular sieves (tetrahydrofuran), purchased from Sigma-Aldrich (benzene, dimethylformamide, dimethyl sulfoxide, propan-2-ol and pyridine) or from a solvent purification system (diethyl ether, toluene). Column chromatography was performed over a silica gel (pore size 60 Å, particle size 40-63 µm) stationary phase.

#### **Melting Points (MP)**

Melting points were recorded using a Gallenkamp Melting Point apparatus and are uncorrected. *Dec* refers to the compound decomposing instead of melting at the stated temperature.

#### **Infrared Spectra (IR)**

Infrared adsorption spectra were recorded in the range 4000 - 400 cm<sup>-1</sup> using either a Perkin-Elmer 660 plus FTIR spectrophotometer as a thin film cast from dichloromethane between sodium chloride plates or a Shimadzu IRAffinity-1 FTIR spectrophotometer as a solid film or powder. Broad peaks are further labelled *br*.

#### **Nuclear Magnetic Resonance (NMR)**

<sup>1</sup>H and <sup>13</sup>C NMR spectra were recorded in a suitable deuterated solvent using an Avance Bruker DPX 250, Avance Bruker DPX 400 or Avance Bruker DPX 500 instrument. <sup>19</sup>F NMR spectra were recorded on a Jeol JNM-ECP 300 instrument. Solid state <sup>13</sup>C NMR spectra were recorded by the EPSRC funded solid state NMR service at Durham University.

Chemical shifts ( $\delta$ ) were recorded in parts per million (ppm) and corrected according to solvent peaks listed in Table 14a.

Table 14a Corrected $^1\text{H}$ and $^{13}\text{C}$ chemical shifts of employed deuterated solvents.			
Solvent	Formula	$^1\text{H}$ Corrected $\delta$	$^{13}\text{C}$ Corrected $\delta$
Acetone- $d_6$	$(\text{CD}_3)_2\text{CO}$	2.05	29.90, 206.68
Chloroform- $d$	$\text{CDCl}_3$	7.24	77.23
Deuterium oxide- $d_2$	$\text{D}_2\text{O}$	4.80	-
DMSO- $d_6$	$(\text{CD}_3)_2\text{SO}$	2.50	39.51
Methanol- $d_4$	$\text{CD}_3\text{OD}$	3.31	49.15
Trifluoroacetic acid - $d$	$\text{CF}_3\text{CO}_2\text{D}$	11.50	116.60, 164.20

Multiplicity is reported as singlet (*s*), doublet (*d*), doubled-doublet (*dd*), doubled-triplet (*dt*), triplet (*t*), quartet (*q*), pentet (*p*) or multiplet (*m*). Broad peaks are further labelled *br*. Coupling constants (*J*) are quoted in Hz.

### Mass Spectrometry

Small molecule ( $\text{MW} < 1000 \text{ g mol}^{-1}$ ) low-resolution mass spectrometric (LRMS) were obtained using a Fisons VG Platform II quadrupole instrument. High resolution mass spectrometric (HRMS) data were obtained using a Waters GCT Premier E1 instrument, utilising either electron impact (EI), electrospray (ES) or atmospheric pressure chemical ionisation (APCI). Ion peaks are labelled  $[\text{M}^+]$  or  $[\text{M}^-]$  if the spectra was obtained in positive or negative mode respectively. Oligomers ( $\text{MW} \geq 1000 \text{ g mol}^{-1}$ ) low-resolution mass spectrometric data were obtained using a Waters Micromass Q-ToF micro mass spectrometer, utilising matrix assisted laser desorption ionisation (MALDI) and calibrated to poly(ethylene glycol) standards ( $\text{MW} 1000 - 3000 \text{ g mol}^{-1}$ ).

### BET Surface Areas

Low-temperature (77 K) nitrogen adsorption/desorption isotherms were obtained using a Coulter SA3100 surface area analyser. Accurately weighed powdered samples of roughly 0.10 g were degassed for 15 h at 120 °C under high vacuum prior to analysis unless otherwise stated.

### **Thermo-Gravimetric Analysis (TGA) and Differential Scanning Calorimetry**

Thermo-gravimetric and differential scanning calorimetry analyses were performed on a Thermal Analysis SDT Q600 system, heating samples (~ 10 mg) at a rate of 10 °C/min from 50°C to 1000 °C under a nitrogen atmosphere.

### **X-Ray Crystal Structure Determination**

Single crystal X-ray structures were recorded either at Cardiff University using a Bruker-Nonius Kappa CCD area-detector diffractometer equipped with an Oxford Cryostream low temperature cooling device operating at 150(2) K ( $\lambda = 0.71073 \text{ \AA}$ ), or at station I19 of the Diamond Light Source using synchrotron radiation and a Rigaku Saturn 724 CCD diffractometer (graphite monochromated radiation). All structures were solved by direct methods and all calculations were carried out using the SHELX-97 package. All Pictures were obtained using Mercury 2.2 (Build RC5) and solvent molecules were removed for clarity.

### **Gel Permeation Chromatography (GPC).**

Gel permeation chromatography (GPC) analyses were performed on chloroform solutions (2 mg ml<sup>-1</sup>) using a GPC MAX variable loop equipped with two KF-805L SHODEX columns and a RI(VE3580) detector, operating at a flow rate of 1 ml min<sup>-1</sup>. Calibration was achieved using Viscotek polystyrene standards ( $M_w$  1000 – 1,000,000 g mol<sup>-1</sup>).

### **Film Fabrication for Membrane Gas Permeation Studies**

Film formation was achieved by preparing a solution of polymer (e.g. 0.70 g for the 180  $\mu\text{m}$  film and 0.35 g for the 90  $\mu\text{m}$  film) in chloroform (15 ml), which was filtered through glass wool and poured into a 10 cm circular Teflon mould. The film was allowed to form by slow solvent evaporation for 96 h in a desiccator. Membranes were post-treated with MeOH to cancel casting history and to remove traces of residual solvent. This treatment consists in soaking overnight in MeOH and drying for 24h under ambient conditions.

### **Measurement of Membrane Gas Permeabilities**

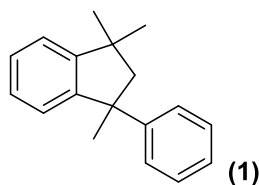
Low temperature measurements were carried out by the Institute on Membrane Technology (ITM-CNR), Calabria, Italy. Gas permeation tests of single gases were carried out at 25 °C and at a feed pressure of 1 bar, using a fixed-volume pressure increase instrument, described in the background theory section. Before analysis, the membrane samples were carefully

evacuated to remove previously dissolved species. The gases were tested in the following order: He, N<sub>2</sub>, O<sub>2</sub>, CH<sub>4</sub> and CO<sub>2</sub>. A total membrane area of 2.14 cm<sup>2</sup> was used and five thickness measurements were made for each membrane sample with a digital micrometer (Mitutoyo). The pressure increase in the permeate volume was monitored by a pressure transducer, starting from the instant of exposure of the membrane to the feed gas. High temperature measurements were carried out by Dr. Tim Merkel at Membrane Technology and Research, Inc (MTR), California using a similar pressure increase instrument. All values were calculated from the slope of the pressure-time curves by methods described in background theory section.

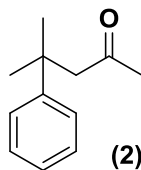
## **14.2: Monomer Synthesis**

### **1,3,3-trimethyl-1-phenylindane**

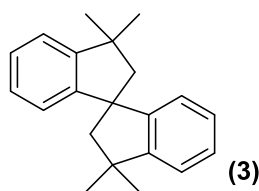
(A modified procedure from literature<sup>136</sup>)



A solution of  $\alpha$ -methyl styrene (20.0 g, 22.0 ml) in *n*-hexane (300 ml) was filtered through basic alumina to remove 4-*tert*-butylcatechol (a self-polymerisation inhibitor) and the solvent was removed under vacuum. Purified  $\alpha$ -methyl styrene (10.0 g, 11.0 ml, 85 mmol) was added drop-wise to trifluoroacetic acid (20.0 ml) with vigorous stirring over 10 min. After stirring for a further 20 min, the mixture was quenched in water (200 ml), extracted with chloroform and washed with saturated sodium hydrogen carbonate solution. The extract was dried over magnesium sulfate and the solvent was removed under vacuum. The crude product was distilled under reduced pressure (1.2 mbar) and the fraction boiling at 112-113 °C was collected to afford the desired product 1,3,3-trimethyl-1-phenylindane (1) (7.26 g, 73%, lit<sup>136</sup> 75%) as a colourless liquid which crystallised on standing. Mp: 50-51 °C (lit<sup>136</sup> 52 °C);  $\nu_{\max}$  (CH<sub>2</sub>Cl<sub>2</sub>/cm<sup>-1</sup>): 3197, 3084, 3060, 3019, 2957, 2924, 2862, 1598; <sup>1</sup>H NMR (400 MHz, CDCl<sub>3</sub>):  $\delta_{\text{H}}$  = 7.56 (m, 9H, Ar *H*), 2.83 (d, *J* = 12.99 Hz, 1H, CH<sub>2</sub>), 2.59 (d, *J* = 12.99 Hz, 1H, CH<sub>2</sub>), 2.08 (s, 3H, CH<sub>3</sub>), 1.74 (s, 3H, CH<sub>3</sub>), 1.44 (s, 3H, CH<sub>3</sub>); <sup>13</sup>C NMR (101 MHz, CDCl<sub>3</sub>):  $\delta_{\text{C}}$  = 152.49, 151.33, 149.03, 128.40, 127.65, 127.05, 125.90, 125.38, 122.93, 59.68, 51.19, 43.24, 31.37, 31.13, 30.83; TOF-LRMS (EI, *m/z*): calculated C<sub>18</sub>H<sub>20</sub> 236.16 found: 236.14 [M<sup>+</sup>].

**4-methyl-4-benzyl-2-pentanone**(Based on a procedure from literature<sup>138</sup>)

Under a nitrogen atmosphere, a suspension of aluminium trichloride (60.00 g, 450 mmol) in anhydrous benzene (140.0 ml) was cooled in an ice bath. With vigorous stirring, 4-methyl-3-pentene-2-one (40.0 ml, 34.16 g, 348 mmol) was injected drop-wise over 30 min. The mixture was stirred for 3 h at 0 °C to form a dark brown solution. The mixture was poured into crushed ice, extracted with diethyl ether and the solvent was removed under vacuum. The crude product was distilled under reduced pressure (2.5 mbar) and the fraction boiling at 98-102 °C (lit<sup>138</sup> 100-101 °C at 5.3 mbar) was collected to afford the desired product 4-methyl-4-benzyl-2-pentanone (2) (47.85g, 78%, lit<sup>138</sup> 80%) as a colourless liquid.  $\nu_{\max}$  (CH<sub>2</sub>Cl<sub>2</sub>/cm<sup>-1</sup>): 3059, 2965, 2877, 1704, 1700; <sup>1</sup>H NMR (500 MHz, CDCl<sub>3</sub>):  $\delta_{\text{H}}$  = 7.31 (d,  $J$  = 7.86 Hz, 2H, Ar  $H$ ), 7.23 (t,  $J$  = 7.58 Hz, 2H, Ar  $H$ ), 6.93 (t,  $J$  = 7.86 Hz, 1H, Ar  $H$ ), 2.64 (s, 2H, CH<sub>2</sub>), 2.68 (s, 3H, C=OCH<sub>3</sub>), 1.37 (s, 6H, 2 CH<sub>3</sub>); <sup>13</sup>C NMR (125 MHz, CDCl<sub>3</sub>):  $\delta_{\text{C}}$  = 206.78, 148.30, 128.25, 125.89, 125.50, 56.43, 37.10, 31.54, 28.92; TOF-HRMS (EI,  $m/z$ ): calculated C<sub>12</sub>H<sub>16</sub>O 176.1201 found: 176.1200 [M<sup>+</sup>].

**3,3,3',3'-tetramethyl-1,1'-spirobisindane**(A modified procedure from literature<sup>138</sup>)

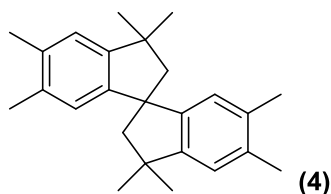
Under a nitrogen atmosphere, a stirred suspension of anhydrous zinc chloride (21.00 g, 154 mmol) in 4-methyl-4-benzyl-2-pentanone (2) (27.14 g, 154 mmol) was heated to 180 °C, at which point a rapid effervescent reaction took place. The mixture was maintained at 180 °C until two distinct phases separated. The mixture was cooled to room temperature and the clear upper phase was extracted from the lower tar-like phase with hot *n*-hexane. The crude product was recrystallised from *n*-hexane multiple times to afford the desired product 3,3,3',3'-tetramethyl-1,1'-spirobisindane (3) (8.91 g, 21%, lit<sup>138</sup> 33%) as colourless needle

shaped crystals . Mp: 126-127 °C (lit<sup>138</sup> 130-131 °C);  $\nu_{\max}$  (CH<sub>2</sub>Cl<sub>2</sub>/cm<sup>-1</sup>): 3063, 3018, 2949, 2922, 2861; <sup>1</sup>H NMR (500 MHz, CDCl<sub>3</sub>):  $\delta_{\text{H}}$  = 7.30 (m, 6H, Ar H), 6.94 (d,  $J$  = 7.54 Hz, 2H, Ar H), 2.49 (d,  $J$  = 13.05 Hz, 2H, CH<sub>2</sub>), 2.39 (d,  $J$  = 13.05 Hz, 2H, CH<sub>2</sub>), 1.54 (s, 6H, 2 CH<sub>3</sub>), 1.49 (s, 6H, 2 CH<sub>3</sub>); <sup>13</sup>C NMR (125 MHz, CDCl<sub>3</sub>):  $\delta_{\text{C}}$  = 152.28, 150.81, 127.24, 127.05, 124.44, 121.89, 59.53, 57.81, 43.62, 31.85, 30.38; TOF-HRMS (EI, m/z): calculated C<sub>21</sub>H<sub>24</sub> 276.1878 found: 276.1875 [M<sup>+</sup>].

Note that the structure and formula of this product was assigned incorrectly in literature<sup>138</sup> but a subsequent study<sup>139</sup> confirmed that 3,3,3',3'-tetramethyl-1,1'-spirobisindane was formed from the above procedure.

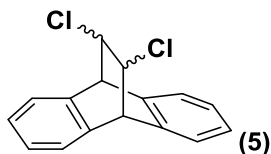
### **3,3,3',3',6,6',7,7'-octamethyl-1,1'-spirobisindane**

(Based on a literature procedure for the preparation of substituted 3,3,3',3'-tetramethyl-1,1'-spirobisindanes<sup>140</sup>)

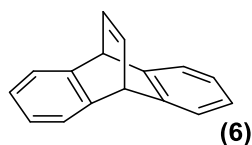


Under a nitrogen atmosphere, aluminium tribromide (5.32 g, 20 mmol) was dissolved in *o*-xylene (180 ml) and freshly distilled 2-bromopropene (33 ml, 24.10 g, 199 mmol) was added drop-wise over 30 min to produce a dark red mixture. The mixture was heated to 60 °C for 72 h, cooled to room temperature and quenched in crushed ice. The mixture was extracted with diethyl ether and subjected to column chromatography (*n*-hexane). The yellow oil obtained was crystallised from an acetone/methanol (4) (1:1) mixture to afford the desired product 3,3,3',3',6,6',7,7'-octamethyl-1,1'-spirobisindane (7.0 g, 32%) as colourless crystals. Mp: 144-145 °C;  $\nu_{\max}$  (cm<sup>-1</sup>): 2952, 2863, 1488, 1448; <sup>1</sup>H NMR (500 MHz, CDCl<sub>3</sub>):  $\delta_{\text{H}}$  = 7.44 (s, 2H, Ar H), 7.12 (s, 2H, Ar H), 2.8 (d,  $J$  = 12.97 Hz, 2H, CH<sub>2</sub>), 2.73 (m, 8H, CH<sub>2</sub> + 2 Ar CH<sub>3</sub>), 2.62 (s, 6H, 2 Ar CH<sub>3</sub>), 1.88 (s, 6H, CH<sub>3</sub>), 1.82 (s, 6H, CH<sub>3</sub>); <sup>13</sup>C NMR (125 MHz, CDCl<sub>3</sub>):  $\delta_{\text{C}}$  = 150.34, 148.84, 135.72, 135.47, 125.70, 123.28, 60.45, 57.68, 43.54, 32.22, 30.92, 20.37, 20.15; TOF-HRMS (EI, m/z): calculated C<sub>25</sub>H<sub>32</sub> 332.2504 found: 332.2509 [M<sup>+</sup>].



**9,10-dihydro-11,12-*cis(trans)*dichloro-9,10-ethanoanthracene**(A modified procedure from literature<sup>141</sup>)

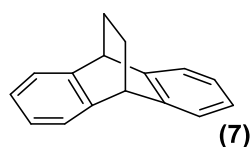
A mixture of *cis/trans* (1:1) 1,2-dichloroethylene (3.0 ml, 3.80 g, 39.1 mmol) and anthracene (2.00 g, 11.2 mmol) were heated to 215 °C at 200 PSI for 5 h under microwave irradiation (300 W fixed). Excess 1,2-dichloroethylene was removed under vacuum and the black residue was dissolved in toluene (50 ml). Furan-2,5-dione (maleic anhydride) (1.00 g, 10 mmol) was added and the mixture was refluxed for 16 h to remove residual anthracene. The mixture was cooled to room temperature and the solvent was removed under vacuum. The black residue subjected to column chromatography (*n*-hexane) and the resulting yellow crystals were recrystallised from ethanol to afford the desired product 9,10-dihydro-11,12-*cis(trans)*-dichloro-9,10-ethanoanthracene (5) (1.54 g, 50%, lit<sup>141</sup> *cis*: 75 %, *trans*: 82%) as colourless crystals. Mp: 190-192 °C (lit<sup>141</sup> *cis*: 203-204 °C, *trans*: 113-114 °C);  $\nu_{\max}$  (cm<sup>-1</sup>): 3074, 3044, 3023, 2972, 1785, 1467, 1458, 1252, 877, 751 ; <sup>1</sup>H NMR (500 MHz, CDCl<sub>3</sub>):  $\delta_{\text{H}}$  = 7.44 (m, 2H, Ar *H*), 7.37 (m, 2H, Ar *H*), 7.30 (m, 2H, Ar *H*), 7.23 (m, 2H, Ar *H*), 4.57 (s, 2H, bridgehead *CH*), 4.52 (s, 2H, bridge *CH*); <sup>13</sup>C NMR (125 MHz, CDCl<sub>3</sub>):  $\delta_{\text{C}}$  = 140.35, 137.87, 127.80, 127.38, 127.19, 126.84, 126.49, 125.25, 1124.64, 58.75, 52.59, 47.99, 45.44; TOF-HRMS (EI, *m/z*): calculated C<sub>16</sub>H<sub>12</sub>Cl<sub>2</sub> 274.0316 found: 274.0313 [M<sup>+</sup>].

**9,10-dihydro-9,10-ethenoanthracene (Dibenzobarrelene)**(Following a procedure from literature<sup>141</sup>)

Under a nitrogen atmosphere, 9,10-dihydro-11,12-*cis(trans)*-dichloro-9,10-ethanoanthracene (5) (6.60 g, 24 mmol) was dissolved in a refluxing mixture of anhydrous tetrahydrofuran (100 ml) and anhydrous propan-2-ol (100 ml). Sodium metal (5.49 g, 240 mmol) was added slowly in small portions and the mixture was refluxed until the sodium had been consumed. The mixture was cooled to room temperature and quenched in water. The white precipitate was filtered, washed with water and dried. The precipitate was recrystallised from methanol

to afford the desired product 9,10-dihydro-9,10-ethenoanthracene (6) (3.50 g, 71%, lit<sup>141</sup> 60%) as colourless crystals. Mp: 125-126°C (lit<sup>141</sup> 118-119 °C);  $\nu_{\max}$  ( $\text{cm}^{-1}$ ): 3068, 3041, 3016, 2974, 1456, 1147, 806 ;  $^1\text{H}$  NMR (500 MHz,  $\text{CDCl}_3$ ):  $\delta_{\text{H}}$  = 7.39 (m, 4H, Ar *H*), 7.11 (m, 2H, =*CH*), 7.06 (m, 4H, Ar *H*), 5.25 (m, 2H, bridgehead *CH*);  $^{13}\text{C}$  NMR (125 MHz,  $\text{CDCl}_3$ ):  $\delta_{\text{C}}$  = 146.23, 139.52, 124.52, 123.15, 51.28; TOF-HRMS (EI,  $m/z$ ): calculated  $\text{C}_{16}\text{H}_{12}$  204.0939 found: 204.0943 [ $\text{M}^+$ ].

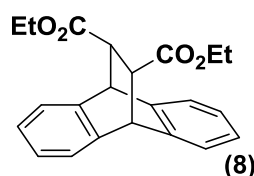
### 9,10-dihydro-9,10-ethanoanthracene



Under a nitrogen atmosphere, 9,10-dihydro-9,10-ethenoanthracene (6) (5.00 g, 24 mmol) was dissolved in tetrahydrofuran (100 ml, de-oxygenated). Raney nickel (~40 mg) and hydrazine monohydrate (24.7 ml, 24.50 g, 490 mmol) was added and the mixture was refluxed for 24 h. The colourless mixture was cooled to room temperature and filtered under nitrogen. The organic phase was extracted with chloroform and the solvent was removed under vacuum to afford the desired product 9,10-dihydro-9,10-ethanoanthracene (7) in a quantitative yield as colourless crystals. Mp: 143-144 °C (lit<sup>141</sup> 142-143 °C);  $\nu_{\max}$  ( $\text{cm}^{-1}$ ): 3020, 2953, 2868, 1456;  $^1\text{H}$  NMR (500 MHz,  $\text{CDCl}_3$ ):  $\delta_{\text{H}}$  = 7.17 (m, 4H, Ar *H*), 7.00 (m, 4H, Ar *H*), 4.23 (s, 2H, bridgehead *CH*), 1.61 (m, 4H, bridge *CH*<sub>2</sub>);  $^{13}\text{C}$  NMR (125 MHz,  $\text{CDCl}_3$ ):  $\delta_{\text{C}}$  = 143.91, 125.63, 123.38, 44.13, 26.76; TOF-HRMS (EI,  $m/z$ ): calculated  $\text{C}_{16}\text{H}_{14}$  206.1096 found: 206.1096 [ $\text{M}^+$ ].

### 9,10-dihydro-9,10-ethanoanthracene-11,12-*trans*-diethyl ester

(Following a procedure from literature<sup>142</sup>)

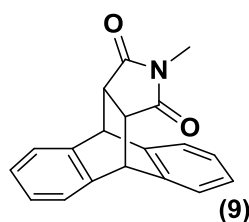


Under a nitrogen atmosphere, anthracene (2.50 g, 14 mmol), diethyl fumarate (3.44 ml, 3.62 g, 21 mmol) and aluminium trichloride (3.73 g, 28 mmol) were dissolved in distilled dichloromethane (100 ml dried over  $\text{CaH}_2$ ). The reaction mixture was stirred at room

temperature for 6 h and then poured into crushed ice. The organic layer was extracted with chloroform and the solvent was removed under vacuum to give a colourless oil. The crude product was recrystallised from methanol to afford the desired product 9,10-dihydro-9,10-ethanoanthracene-11,12-*trans*-diethyl ester (8) (4.1 g, 83%) as colourless, needle-shaped crystals: Mp: 101-103 °C (lit<sup>208</sup> 104 °C);  $\nu_{\max}$  (CH<sub>2</sub>Cl<sub>2</sub>/cm<sup>-1</sup>): 2979, 2953, 1732; <sup>1</sup>H NMR (400 MHz, CDCl<sub>3</sub>):  $\delta_{\text{H}}$  = 7.3 (m, 2H, Ar *H*), 7.2 (m, 2H, Ar *H*), 7.0 (m, 4H, Ar *H*), 4.6 (s, 2H, bridgehead *CH*), 4.0 (m, 4H, CH<sub>2</sub>), 3.4 (s, 2H, bridge *CH*), 1.1 (t, *J* = 7.13 Hz, 6H, CH<sub>3</sub>); <sup>13</sup>C NMR (101 MHz, CDCl<sub>3</sub>):  $\delta_{\text{C}}$  = 172.36, 142.10, 140.43, 126.42, 126.25, 124.62, 123.84, 61.07, 47.77, 46.83, 14.34; TOF-LRMS (EI, *m/z*): calculated C<sub>22</sub>H<sub>22</sub>O<sub>4</sub> 350.15 found: 350.15 [M<sup>+</sup>].

### **N-methyl-9,10-dihydro-9,10-ethanoanthracene-11,12-*cis*-dicarboximide**

(A modified procedure from literature<sup>142</sup>)

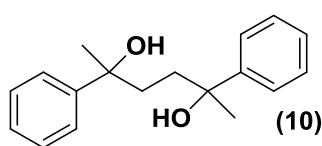


Under a nitrogen atmosphere, anthracene (1.00 g, 6 mmol), N-methylmaleimide (0.93 g, 8 mmol) and aluminium trichloride (1.30 g, 10 mmol) was dissolved in distilled dichloromethane (50 ml dried over CaH<sub>2</sub>). The reaction mixture was stirred at room temperature for 16 h and then poured into crushed ice. The organic layer was extracted with chloroform and the solvent was removed under vacuum to give a colourless oil. The crude product was recrystallised from methanol to afford the desired product N-methyl-9,10-dihydro-9,10-ethanoanthracene-11,12-*cis*-dicarboximide (9) (0.98g, 60%) as colourless, needle-shaped crystals: Mp: 267-268 °C (lit<sup>209</sup> 268-269 °C);  $\nu_{\max}$  (CH<sub>2</sub>Cl<sub>2</sub>/cm<sup>-1</sup>): 2964, 1694, 1129; <sup>1</sup>H NMR (400 MHz, CDCl<sub>3</sub>):  $\delta_{\text{H}}$  = 7.29 (m, 2H, Ar *H*), 7.18 (m, 2H, Ar *H*), 7.09 (m, 2H, Ar *H*), 7.03 (m, 2H, Ar *H*), 4.70 (s, 2H, bridge *CH*), 3.12 (s, 2H, bridgehead *CH*), 2.42 (s, 3H, CH<sub>3</sub>); <sup>13</sup>C NMR (101 MHz, CDCl<sub>3</sub>):  $\delta_{\text{C}}$  = 176.99, 141.45, 138.50, 127.02, 126.75, 124.87, 124.28, 47.02, 45.55, 24.29; TOF-LRMS (APCI, *m/z*): calculated C<sub>19</sub>H<sub>15</sub>NO<sub>2</sub> 289.11 found: 331.15 [M + CH<sub>3</sub>CNH<sup>+</sup>] (solvent).

### **General Procedure (14.2a) for Diol Compounds**

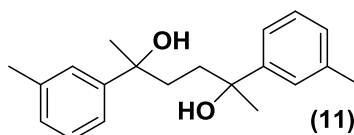
Under a nitrogen atmosphere, magnesium turnings and an iodine crystal (~5 mg) was suspended in dry tetrahydrofuran. With vigorous stirring, the corresponding bromo reagent was injected drop-wise and the mixture was refluxed until the magnesium was consumed. A solution of 2,5-hexanedione was injected drop-wise and the mixture was allowed to reflux for a further hour. The mixture was cooled to room temperature and then poured into crushed ice. The organic layer was extracted with diethyl ether and the solvent was removed under vacuum. The resulting oil was purified appropriately to afford the desired product.

### **2,5-diphenylhexane-2,5-diol**



General procedure 14.2a was followed using magnesium turnings (10.00 g, 411 mmol), tetrahydrofuran (200 ml), bromobenzene (44 ml, 64.6 g, 411 mmol) and 2,5-hexanedione (24 ml, 23.48 g, 206 mmol). The resulting yellow oil was dissolved in boiling acetone (100 ml) and the diol was precipitated with the addition of *n*-hexane (400 ml) and filtered to afford the desired product 2,5-diphenylhexane-2,5-diol (10) (36.10 g, 65%) as a colourless powder Mp: 121-122 °C (lit<sup>210</sup> 121-122 °C) ;  $\nu_{\max}$  (CH<sub>2</sub>Cl<sub>2</sub>/cm<sup>-1</sup>): 3398 (br), 2939, 2864; <sup>1</sup>H NMR (400 MHz, CDCl<sub>3</sub>):  $\delta_{\text{H}}$  = 7.35 (m, 6H, Ar *H*), 7.24 (m, 2H, Ar *H*), 2.43 (s, br, 2H, OH), 1.88 (m, 2H, CH<sub>2</sub>), 1.73 (m, 2H, CH<sub>2</sub>), 1.54 (s, 3H, CH<sub>3</sub>), 1.49 (s, 3H, CH<sub>3</sub>); <sup>13</sup>C NMR (101 MHz, CDCl<sub>3</sub>):  $\delta_{\text{C}}$  = 147.85, 147.60, 128.18, 126.52, 126.50, 124.86, 124.80, 74.53, 74.41, 38.10, 37.95, 31.32, 30.48; TOF-LRMS (EI, m/z): calculated C<sub>18</sub>H<sub>22</sub>O<sub>2</sub> 270.16 found: 252.00 [M - H<sub>2</sub>O<sup>+</sup>].

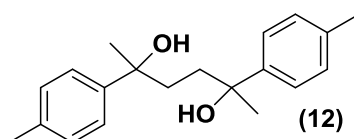
### **2,5-di(3-methylphenyl)hexane-2,5-diol**



General procedure 14.2a was followed using magnesium turnings (10.00 g, 411 mmol), tetrahydrofuran (200 ml), 3-bromotoluene (50 ml, 70.37 g, 411 mmol) and 2,5-hexanedione (24 ml, 23.48 g, 206 mmol). The resulting yellow oil was subjected to column chromatography (dichloromethane) to afford the desired product 2,5-di(3-

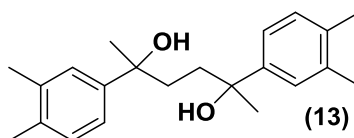
methylphenyl)hexane-2,5-diol (11) (53.72 g, 86%) as a colourless oil. Mp: under 25 °C;  $\nu_{\max}$  ( $\text{cm}^{-1}$ ): 3408 (br), 3020, 2970, 2926, 2868, 1701;  $^1\text{H}$  NMR (500 MHz,  $\text{CDCl}_3$ ):  $\delta_{\text{H}} = 7.07$  (m, 6H, Ar *H*), 6.92 (m, 2H, Ar *H*), 2.88 (s, br, 2H, 2 OH), 2.23 (m, 6H, 2 Ar  $\text{CH}_3$ ), 1.75 (m, 2H,  $\text{CH}_2$ ), 1.63 (m, 2H,  $\text{CH}_2$ ), 1.39 (s, 3H,  $\text{CH}_3$ ), 1.33 (s, 3H,  $\text{CH}_3$ );  $^{13}\text{C}$  NMR (125 MHz,  $\text{CDCl}_3$ ):  $\delta_{\text{C}} = 148.07, 147.82, 137.57, 128.14, 128.01, 127.35, 127.12, 125.64, 125.60, 74.47, 74.35, 38.14, 37.94, 31.32, 30.35, 21.66, 21.63$ ; TOF-HRMS (ES,  $m/z$ ): calculated  $\text{C}_{20}\text{H}_{26}\text{O}_2$  298.1933 found: 298.1924 [M].

### **2,5-di(4-methylphenyl)hexane-2,5-diol**



General procedure 14.2a was followed using magnesium turnings (10.00 g, 411 mmol), tetrahydrofuran (200 ml), 4-bromotoluene (50.6 ml, 70.36 g, 411 mmol) and 2,5-hexanedione (24 ml, 23.48 g, 206 mmol). The resulting yellow oil was subjected to column chromatography (dichloromethane) to afford the desired product 2,5-Di(4-methylphenyl)hexane-2,5-diol (12) (49.6 g, 81%) as a colourless oil. Mp: under 25 °C;  $\nu_{\max}$  ( $\text{cm}^{-1}$ ): 3410 (br), 3140, 2926, 2890 ;  $^1\text{H}$  NMR (500 MHz,  $\text{CDCl}_3$ ):  $\delta_{\text{H}} = 7.15$  (m, 4H, Ar *H*), 7.02 (m, 4H, Ar *H*), 2.67 (s, br, 2H, 2 OH), 2.24 (s, 3H, Ar  $\text{CH}_3$ ), 2.22 (s, 3H, Ar  $\text{CH}_3$ ), 1.75 (m, 2H,  $\text{CH}_2$ ), 1.62 (m, 2H,  $\text{CH}_2$ ), 1.39 (s, 3H,  $\text{CH}_3$ ), 1.34 (s, 3H,  $\text{CH}_3$ );  $^{13}\text{C}$  NMR (125 MHz,  $\text{CDCl}_3$ ):  $\delta_{\text{C}} = 145.11, 144.85, 135.88, 135.83, 128.80, 128.63, 124.84, 124.64, 74.37, 74.25, 38.14, 37.98, 31.26, 30.39, 20.94, 20.92$ ; TOF-HRMS (ES,  $m/z$ ): calculated  $\text{C}_{20}\text{H}_{26}\text{O}_2$  298.1933 found: 333.1626 [M + Cl].

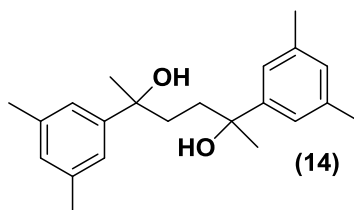
### **2,5-di(3,4-dimethylphenyl)hexane-2,5-diol**



General procedure 14.2a was followed using magnesium turnings (10.00 g, 411 mmol), tetrahydrofuran (200 ml), 4-bromo-1,2-dimethylbenzene (55.6 ml, 76.14 g, 411 mmol) and 2,5-hexanedione (24 ml, 23.48 g, 206 mmol). The resulting yellow semi-solid was triturated in *n*-hexane and filtered to afford the desired product 2,5-di(3,4-dimethylphenyl)hexane-2,5-diol (13) (64.1 g, 95%) as colourless crystals. Mp: 117-120 °C;  $\nu_{\max}$  ( $\text{CH}_2\text{Cl}_2/\text{cm}^{-1}$ ): 3390 (br),

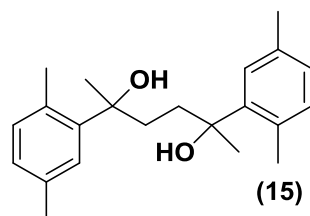
3018, 3018, 2971, 2921, 2864, 1506, 1451 ;  $^1\text{H}$  NMR (500 MHz,  $\text{CDCl}_3$ ):  $\delta_{\text{H}} = 7.02$  (s, 2H, Ar *H*), 6.94 (m, 4H, Ar *H*), 2.83 (s, br, 1H, OH), 2.72 (s, br, 1H, OH), 2.12 (m, 12H, 4 Ar  $\text{CH}_3$ ), 1.73 (m, 2H,  $\text{CH}_2$ ), 1.62, (m, 2H,  $\text{CH}_2$ ), 1.37 (s, 3H,  $\text{CH}_3$ ), 1.32 (s, 3H,  $\text{CH}_3$ );  $^{13}\text{C}$  NMR (125 MHz,  $\text{CDCl}_3$ ):  $\delta_{\text{C}} = 145.69, 145.44, 136.13, 134.54, 134.48, 129.46, 129.44, 126.27, 1216.23, 122.41, 122.35, 74.43, 74.31, 38.17, 37.94, 31.43, 30.45, 20.05, 20.03, 19.35, 19.32$ ; TOF-HRMS (EI,  $m/z$ ): calculated  $\text{C}_{22}\text{H}_{30}\text{O}_2$  326.2246 found: 308.2140 [ $\text{M} - \text{H}_2\text{O}^+$ ].

### **2,5-di(3,5-dimethylphenyl)hexane-2,5-diol**



General procedure 14.2a was followed using magnesium turnings (10.00 g, 411 mmol), tetrahydrofuran (200 ml), 1-bromo-3,5-dimethylbenzene (55.9 ml, 76.14 g, 411 mmol) and 2,5-hexanedione (24 ml, 23.48 g, 206 mmol). The resulting yellow oil was triturated in *n*-hexane to afford the desired product 2,5-di(2,4-dimethylphenyl)hexane-3,5-diol (14) (61.4 g, 91%) as a colourless oil. Mp: under 25 °C;  $\nu_{\text{max}}$  ( $\text{cm}^{-1}$ ): 3400 (br), 3005, 2970, 1918, 1604 1450;  $^1\text{H}$  NMR (500 MHz,  $\text{CDCl}_3$ ):  $\delta_{\text{H}} = 7.07$  (m, 4H, Ar *H*), 6.95 (s, 1H, , Ar *H*), 6.93 (s, 1H, , Ar *H*), 3.04 (s, br, 2H, 2 OH), 2.40 (s, 6H, 2 Ar  $\text{CH}_3$ ), 2.38 (s, 6H, 2 Ar  $\text{CH}_3$ ), 1.95 (m, 2H,  $\text{CH}_2$ ), 1.84 (m, 2H,  $\text{CH}_2$ ), 1.58 (s, 3H,  $\text{CH}_3$ ), 1.53 (s, 3H,  $\text{CH}_3$ );  $^{13}\text{C}$  NMR (125 MHz,  $\text{CDCl}_3$ ):  $\delta_{\text{C}} = 148.18, 147.90, 137.51, 128.13, 128.06, 122.80, 122.77, 74.53, 74.42, 38.14, 37.87, 31.58, 30.43, 21.63, 21.60$ ; TOF-HRMS (EI,  $m/z$ ): calculated  $\text{C}_{22}\text{H}_{30}\text{O}_2$  326.2246 found: 308.2141 [ $\text{M} - \text{H}_2\text{O}^+$ ].

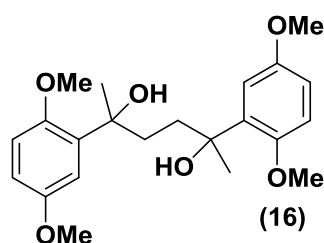
### **2,5-di(2,5-dimethylphenyl)hexane-2,5-diol**



General procedure 14.2a was followed using magnesium turnings (10.00 g, 411 mmol), tetrahydrofuran (200 ml), 2-bromo-1,4-dimethylbenzene (56.8 ml, 76.14 g, 411 mmol) and 2,5-hexanedione (24 ml, 23.48 g, 206 mmol). The resulting yellow oil was subjected to

column chromatography (1:4 EtOAc : *n*-hexane) afford the desired product 2,5-di(2,5-dimethylphenyl)hexane-2,5-diol (15) (51.40 g, 77%) as colourless crystals. Mp: 111-112°C;  $\nu_{\max}$  (cm<sup>-1</sup>): 3522 (br), 3390, 2972, 2925, 2870, 1496, 1458; <sup>1</sup>H NMR (500 MHz, CDCl<sub>3</sub>):  $\delta_{\text{H}}$  = 7.46 (s, 1H, Ar *H*), 7.41 (s, 1H, Ar *H*), 7.10 (m, 4H, Ar *H*), 3.31 (s, br, 2H, 2 OH), 2.48 (m, 6H, 2 CH<sub>3</sub>), 2.44 (m, 6H, 2 CH<sub>3</sub>), 2.10 (m, 2H, CH<sub>2</sub>), 1.94 (m, 2H, CH<sub>2</sub>), 1.73 (s, 3H, CH<sub>3</sub>), 1.68 (s, 3H, CH<sub>3</sub>); <sup>13</sup>C NMR (125 MHz, CDCl<sub>3</sub>):  $\delta_{\text{C}}$  = 144.95, 144.69, 134.90, 134.85, 132.68, 132.08, 131.90, 127.52, 127.29, 127.22, 75.71, 75.67, 36.63, 36.56, 29.92, 29.36, 21.91, 21.85, 21.36, 21.32; TOF-HRMS (EI, *m/z*): calculated C<sub>22</sub>H<sub>30</sub>O<sub>2</sub> 326.2246 found: 326.2223 [M].

### 2,5-di-(2,5-dimethoxyphenyl)hexane-2,5-diol



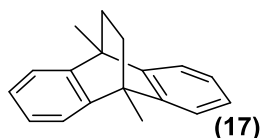
General procedure 14.2a was followed using magnesium turnings (0.6 g, 23 mmol), tetrahydrofuran (100 ml), 2-bromo-1,4 dimethoxybenzene (3.5 ml 5 g, 23 mmol) and 2,5-hexanedione (1.35 ml, 1.3 g, 11.4 mmol). The organic layer was extracted with diethyl ether and the solvent was removed under vacuum. The resulting yellow oil was triturated in *n*-hexane (200 ml) for 24 h and filtered to afford the desired product 2,5-di-(2,5-dimethoxyphenyl)hexane-2,5-diol (16) (2.63 g, 59%) as a colourless powder Mp: 98-100 °C;  $\nu_{\max}$  (CH<sub>2</sub>Cl<sub>2</sub>/cm<sup>-1</sup>): 3434 (br), 2937, 2833, 1489, 1219, 1049; <sup>1</sup>H NMR (500 MHz, CDCl<sub>3</sub>):  $\delta_{\text{H}}$  = 6.94 (s, 2H, Ar *H*), 6.75 (m, 4H, Ar *H*), 4.39 (s, br, 2H, OH), 3.75 (m, 12H, O-CH<sub>3</sub>), 1.99 (m, 2H, CH<sub>2</sub>), 1.84 (m, 2H, CH<sub>2</sub>), 1.54 (s, 3H, CH<sub>3</sub>), 1.50 (s, 3H, CH<sub>3</sub>); <sup>13</sup>C NMR (125 MHz, CDCl<sub>3</sub>):  $\delta_{\text{C}}$  = 153.60, 150.93, 150.85, 136.48, 136.02, 114.16, 113.89, 112.09, 111.41, 75.02, 74.89, 55.67, 36.61, 36.32, 27.98, 27.32; TOF-HRMS (APCI, *m/z*): calculated C<sub>22</sub>H<sub>30</sub>O<sub>6</sub> 390.2042 found: 391.2111 [M + H<sup>+</sup>].

### **General Procedure (14.2b) for Ethanoanthracene Compounds Derived from Diols**

Under a nitrogen atmosphere, the diol was suspended in anhydrous toluene and cooled in an ice bath. Aluminium trichloride was slowly added over 30 min and the mixture was stirred for 1 h and then at room temperature for 1 h. The mixture was then refluxed for 24 h, cooled and poured into crushed ice. The organic layer was extracted with chloroform and the solvent was removed under vacuum. The residue was subjected to column chromatography (*n*-hexane) and the resulting green oil was recrystallised from a suitable solvent to afford the desired product.

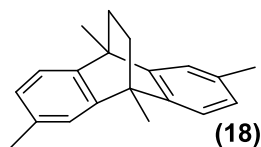
#### **9,10-dimethyl-9,10-dihydro-9,10-ethanoanthracene**

(A modified procedure from literature<sup>143</sup>)

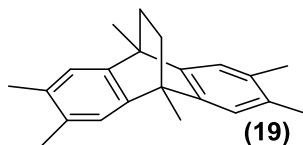


General procedure 14.2b was followed using 2,5-diphenylhexane-2,5-diol (10) (22.00 g, 81 mmol), toluene (70 ml), aluminium trichloride (10.80 g, 81 mmol) and recrystallisation from *n*-hexane to afford the desired product 9,10-dimethyl-9,10-dihydro-9,10-ethanoanthracene (17) (6.77 g, 36%, lit<sup>143</sup> 59%) as colourless needle shaped crystals: Mp: 129-130 °C (lit<sup>143</sup> 126-128 °C) ;  $\nu_{\max}$  (CH<sub>2</sub>Cl<sub>2</sub>/cm<sup>-1</sup>): 2924, 2857; <sup>1</sup>H NMR (400 MHz, CDCl<sub>3</sub>):  $\delta_{\text{H}}$  = 7.51 (m, 4H, Ar *H*), 7.36 (m, 4H, Ar *H*), 2.17 (s, 6H, 2 CH<sub>3</sub>), 1.83 (s, 4H, 2 CH<sub>2</sub>); <sup>13</sup>C NMR (101 MHz, CDCl<sub>3</sub>):  $\delta_{\text{C}}$  = 146.56, 125.42, 120.51, 41.93, 36.05, 18.57; TOF-LRMS (EI, m/z): calculated C<sub>18</sub>H<sub>18</sub> 234.14 found: 234.01 [M<sup>+</sup>]. Crystals were prepared by a slow evaporation of a solution of the compound in chloroform. Crystal size: 0.10 × 0.05 × 0.05 mm, orthorhombic, space group *Pccn*, *a* = 14.3872 (2), *b* = 20.7406 (3), *c* = 8.4818 (1) Å, *V* = 2530.96 (6) Å<sup>3</sup>, *Z* = 8;  $\mu$  = 0.07 mm<sup>-1</sup>, 42675 reflections measured, 3822 unique reflections (*R*<sub>int</sub> = 0.055), 3671 reflections with *I* > 2σ(*I*), *R*(%) = 4.42.



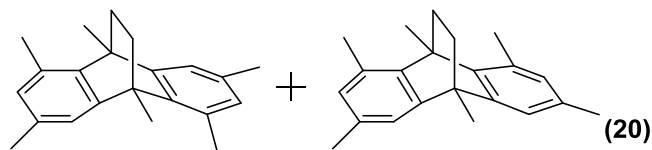
**2,6,9,10-tetramethyl-9,10-dihydro-9,10-ethanoanthracene**

General procedure 14.2b was followed using 2,5-di(3-methylphenyl)hexane-2,5-diol (11) (53.72 g, 180 mmol), toluene (150 ml), aluminium trichloride (24.00 g, 180 mmol) and recrystallisation from *n*-hexane to afford the desired product 2,6,9,10-tetramethyl-9,10-dihydro-9,10-ethanoanthracene (18) (17.45 g, 37%) as colourless needle shaped crystals: Mp: 81-82 °C;  $\nu_{\max}$  ( $\text{cm}^{-1}$ ): 2920, 2858, 1456;  $^1\text{H}$  NMR (500 MHz,  $\text{CDCl}_3$ ):  $\delta_{\text{H}}$  = 7.84 (d,  $J$  = 7.58 Hz, 2H, Ar  $H$ ), 7.81 (s, 2H, Ar  $H$ ), 7.62 (d,  $J$  = 7.58 Hz, 2H, Ar  $H$ ), 3.02 (s, 6H, 2 Ar  $\text{CH}_3$ ), 2.60 (s, 6H, 2  $\text{CH}_3$ ), 2.28 (s, 4H, 2  $\text{CH}_2$ );  $^{13}\text{C}$  NMR (125 MHz,  $\text{CDCl}_3$ ):  $\delta_{\text{C}}$  = 146.65, 143.63, 134.45, 125.68, 121.24, 120.21, 41.41, 36.18, 21.49, 18.49; TOF-HRMS (EI,  $m/z$ ): calculated  $\text{C}_{20}\text{H}_{22}$  262.1722 found: 262.1727 [ $\text{M}^+$ ]. Crystals were prepared by a slow evaporation of a solution of the compound in chloroform. Crystal size: 0.70 × 0.10 × 0.10 mm, orthorhombic, space group *Pccn*,  $a$  = 15.3760 (6),  $b$  = 22.6359 (7),  $c$  = 8.7141 (3) Å,  $V$  = 3032.94 (18) Å<sup>3</sup>,  $Z$  = 8;  $\mu$  = 0.06  $\text{mm}^{-1}$ , 21076 reflections measured, 3612 unique reflections ( $R_{\text{int}}$  = 0.147), 2103 reflections with  $I > 2\sigma(I)$ ,  $R(\%)$  = 7.16.

**2,3,6,7,9,10-hexamethyl-9,10-dihydro-9,10-ethanoanthracene**

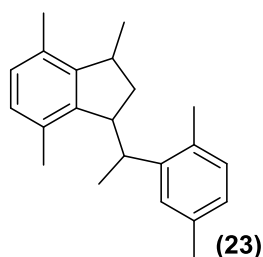
General procedure 14.2b was followed using 2,5-di(3,4-dimethylphenyl)hexane-2,5-diol (13) (41.00 g, 126 mmol), toluene (150 ml), aluminium trichloride (16.75 g, 126 mmol) and recrystallisation from *n*-hexane to afford the desired product 2,3,6,7,9,10-hexamethyl-9,10-dihydro-9,10-ethanoanthracene (19) (6.54 g, 18%) as colourless crystals: Mp: 226-227 °C;  $\nu_{\max}$  ( $\text{cm}^{-1}$ ): 2959, 2938, 2856, 1456;  $^1\text{H}$  NMR (500 MHz,  $\text{CDCl}_3$ ):  $\delta_{\text{H}}$  = 7.40 (s, 4H, Ar  $H$ ), 2.58 (s, 12H, 4 Ar  $\text{CH}_3$ ), 2.28 (s, 6H, 2  $\text{CH}_3$ ), 1.97 (s, 4H, 2  $\text{CH}_2$ );  $^{13}\text{C}$  NMR (125 MHz,  $\text{CDCl}_3$ ):  $\delta_{\text{C}}$  = 144.58, 132.99, 122.11, 41.26, 36.57, 19.94, 18.75; TOF-HRMS (EI,  $m/z$ ): calculated  $\text{C}_{22}\text{H}_{26}$  290.2035 found: 290.2033 [ $\text{M}^+$ ].

**1,3,5,7,9,10-hexamethyl-9,10-dihydro-9,10-ethanoanthracene/1,3,6,8,9,10-hexamethyl-9,10-dihydro-9,10-ethanoanthracene**



General procedure 14.2b was followed using 2,5-di(2,4-dimethylphenyl)hexane-3,5-diol (14) (63.86 g, 196 mmol), toluene (200 ml), aluminium trichloride (26.00 g, 196 mmol) and recrystallisation from acetonitrile to afford the desired product mixture of 1,3,5,7,9,10-hexamethyl-9,10-dihydro-9,10-ethanoanthracene and 1,3,6,8,9,10-hexamethyl-9,10-dihydro-9,10-ethanoanthracene (20) (0.77 g, 1.36%) as colourless crystals: Mp: 167-168 °C;  $\nu_{\max}$  ( $\text{cm}^{-1}$ ): 2958, 2910, 2856, 1467;  $^1\text{H}$  NMR (500 MHz,  $\text{CDCl}_3$ ):  $\delta_{\text{H}}$  = 7.12 (s, 1H, Ar H), 7.11 (s, 1H, Ar H), 6.79 (s, 1H, Ar H), 6.78 (s, 1H, Ar H), 2.65 (s, 3H, Ar  $\text{CH}_3$ ), 2.63 (s, 3H, Ar  $\text{CH}_3$ ), 2.37 (s, 3H, Ar  $\text{CH}_3$ ), 2.35 (s, 3H, Ar  $\text{CH}_3$ ), 2.22 (s, 3H,  $\text{CH}_3$ ), 2.20 (s, 3H,  $\text{CH}_3$ ), 1.94 (s, 2H,  $\text{CH}_2$ ), 1.60 (s, 2H,  $\text{CH}_2$ );  $^{13}\text{C}$  NMR (125 MHz,  $\text{CDCl}_3$ ):  $\delta_{\text{C}}$  = 149.24, 139.94, 134.15, 131.85, 130.92, 120.42, 44.25, 37.57, 24.25, 23.10, 21.12; TOF-HRMS (EI, m/z): calculated  $\text{C}_{22}\text{H}_{26}$  290.2035 found: 290.2044 [ $\text{M}^+$ ].

**1,5,8-trimethyl-3-(ethyl-2-(2,5-dimethylphenyl))indane**



General procedure 14.2b was followed using 2,5-di(2,5-dimethylphenyl)hexane-2,5-diol (15) (10.00 g, 31 mmol), toluene (50 ml), aluminium trichloride (4.08 g, 31 mmol) and recrystallisation from acetonitrile to afford the undesired product 1,5,8-trimethyl-3-(ethyl-2-(2,5-dimethylphenyl))indane (23) (0.9 g, 10%) as colourless crystals: Mp: 127-128 °C;  $\nu_{\max}$  ( $\text{CH}_2\text{Cl}_2/\text{cm}^{-1}$ ): 3040, 2957, 2924;  $^1\text{H}$  NMR (500 MHz,  $\text{CDCl}_3$ ):  $\delta_{\text{H}}$  = 7.21 (s, 1H, Ar H), 7.05 (d,  $J$  = 7.64 Hz, 1H, Ar H), 6.99 (d,  $J$  = 7.64 Hz, 1H, Ar H), 6.95 (d,  $J$  = 7.54 Hz, 1H, Ar H), 6.87 (d,  $J$  = 7.54 Hz, 1H, Ar H), 3.65 (m, 1H, CH), 3.51 (m, 1H, CH), 3.29 (m, 1H, CH), 2.42 (s, 3H, Ar  $\text{CH}_3$ ), 2.35 (s, 3H, Ar  $\text{CH}_3$ ), 2.16 (s, 3H, Ar  $\text{CH}_3$ ), 2.01 (s, 3H, Ar  $\text{CH}_3$ ), 1.51 (2s, 3H,  $\text{CH}_3$ ), 1.27 (2s, 3H,  $\text{CH}_3$ );  $^{13}\text{C}$  NMR (125 MHz,  $\text{CDCl}_3$ ):  $\delta_{\text{C}}$  = 147.19, 144.54, 144.08,

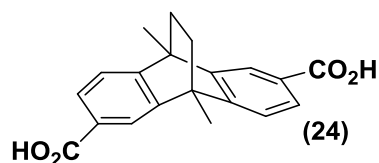
135.07, 133.01, 131.89, 131.20, 130.20, 128.57, 127.91, 126.44; TOF-HRMS (EI, m/z): calculated 292.2191 found: 292.2190 [ $M^+$ ]. Crystals were prepared by a slow evaporation of a solution of the compound in chloroform. Crystal size:  $0.40 \times 0.15 \times 0.15$  mm, Triclinic, space group  $P\bar{1}$ ,  $a = 7.5701$  (6),  $b = 7.6145$  (7),  $c = 15.1260$  (9) Å,  $\alpha = 92.468$  (5)°,  $\beta = 90.324$  (4)°,  $\gamma = 94.855$  (3)°  $V = 867.93$  (12) Å<sup>3</sup>,  $Z = 2$ ;  $\mu = 0.06$  mm<sup>-1</sup>, 6043 reflections measured, 3955 unique reflections ( $R_{\text{int}} = 0.041$ ), 2433 reflections with  $I > 2\sigma(I)$ ,  $R(\%) = 7.81$ .

### **General Procedure (14.2c) for Carboxylic acid Compounds**

(Based on a procedure from literature<sup>144</sup>)

The corresponding dimethyl or tetramethyl compound was suspended in an equal mixture of pyridine and deionised water and the mixture was heated to reflux. Half the specified quantity of potassium permanganate was added in small portions, allowing for foaming between additions and the mixture was refluxed for 12 h. The remaining quantity of potassium permanganate was added in small portions as before and the mixture was refluxed for an additional 24h. The black mixture was filtered hot and the manganese dioxide was washed with hot deionised water. The filtrate was cooled to room temperature and the pyridine/water mixture was removed under vacuum. The solid obtained was dissolved in deionised water and neutralised with concentrated hydrochloric acid to give a white precipitate. The solid was filtered, dried and recrystallised from the appropriate solvent to afford the desired product.

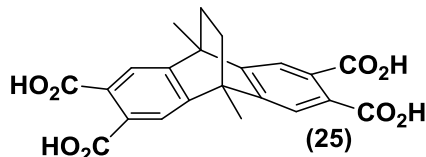
### **9,10-dimethyl-9,10-dihydro-2,6-dicarboxyl-9,10-ethanoanthracene**



General procedure 14.2c was followed using 2,6,9,10-tetramethyl-9,10-dihydro-9,10-ethanoanthracene (18) (5.30 g, 20 mmol), pyridine/deionised water (200 ml) and potassium permanganate (31.92 g, 200 mmol) to afford the desired product 9,10-dimethyl-9,10-dihydro-2,6-dicarboxyl-9,10-ethanoanthracene (24) (5.96 g, 92%) as a colourless powder. Mp: over 300 °C;  $\nu_{\text{max}}$  (cm<sup>-1</sup>): 3100 (br), 2967, 2936, 2868, 1689, 1294, 1269; <sup>1</sup>H NMR (500 MHz, (CD<sub>3</sub>)<sub>2</sub>SO):  $\delta_{\text{H}} = 12.83$  (s, br, 2H, 2 CO<sub>2</sub>H), 7.84 (s, 2H, Ar H), 7.78 (d,  $J = 7.23$  Hz, 2H, Ar H), 7.37 (d,  $J = 7.23$  Hz, 2H, Ar H), 1.93 (s, 6H, 2 CH<sub>3</sub>), 1.52 (s, 4H, 2 CH<sub>2</sub>); <sup>13</sup>C NMR (125

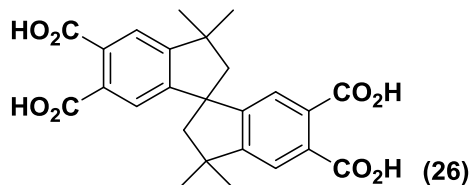
MHz, (CD<sub>3</sub>)<sub>2</sub>SO):  $\delta_{\text{C}}$  = 167.90, 151.05, 145.97, 128.50, 127.57, 121.60, 121.10, 42.32, 35.23, 18.20; TOF-HRMS (EI,  $m/z$ ): calculated C<sub>20</sub>H<sub>18</sub>O<sub>4</sub> 322.1205 found: 322.1200 [M<sup>+</sup>].

### **9,10-dimethyl-9,10-dihydro-2,3,6,7-tetracarboxyl-9,10-ethanoanthracene**



General procedure 14.2c was followed using 2,3,6,7,9,10-hexamethyl-9,10-dihydro-9,10-ethanoanthracene (19) (4.17 g, 14 mmol), pyridine/deionised water (200 ml) and potassium permanganate (22.69 g, 144 mmol) to afford the desired product 9,10-dimethyl-9,10-dihydro-2,3,6,7-tetracarboxyl-9,10-ethanoanthracene (25) (4.88 g, 83%) as an off-white powder. Mp: 287-288 °C;  $\nu_{\text{max}}$  (CH<sub>2</sub>Cl<sub>2</sub>/cm<sup>-1</sup>): 3100 (br), 2965, 1698, 1249; <sup>1</sup>H NMR (500 MHz, (CD<sub>3</sub>)<sub>2</sub>SO):  $\delta_{\text{H}}$  = 13.08 (s, br, 4H, 4 CO<sub>2</sub>H), 7.56 (s, 4H, Ar H), 1.99 (s, 6H, 2 CH<sub>3</sub>), 1.63 (s, 4H, 2 CH<sub>2</sub>); <sup>13</sup>C NMR (125 MHz, (CD<sub>3</sub>)<sub>2</sub>SO):  $\delta_{\text{C}}$  = 169.18, 148.24, 131.01, 121.14, 42.49, 35.00, 17.92; TOF-HRMS (ES,  $m/z$ ): calculated C<sub>22</sub>H<sub>18</sub>O<sub>8</sub> 410.1002 found: 409.0932 [M<sup>+</sup>].

### **3,3,3',3'-octamethyl-6,6',7,7'-tetracarboxyl-1,1'-spirobisindane**

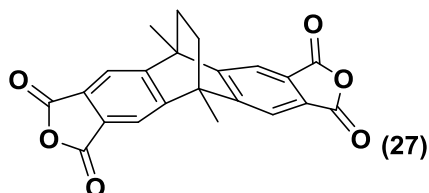


General procedure 14.2c was followed using 3,3,3',3',6,6',7,7'-octamethyl-1,1'-spirobisindane (4) (5.00 g, 15 mmol), pyridine/deionised water (200 ml) and potassium permanganate (23.76 g, 150 mmol) to afford the desired product 3,3,3',3'-octamethyl-6,6',7,7'-tetracarboxyl-1,1'-spirobisindane (26) (6.6 g, 97%) as a colourless powder. Mp: 182-183 °C;  $\nu_{\text{max}}$  (cm<sup>-1</sup>): 3027 (br), 2965, 2866, 1844, 1772, 1349; <sup>1</sup>H NMR (500 MHz, (CD<sub>3</sub>)<sub>2</sub>SO):  $\delta_{\text{H}}$  = 13.02 (s, br, 4H, 4 CO<sub>2</sub>H), 8.11 (s, 2H, Ar H), 7.43 (s, 2H, Ar H), 2.55 (d,  $J$  = 13.29 Hz, 2H, CH<sub>2</sub>), 2.37 (d,  $J$  = 13.29 Hz, 2H, CH<sub>2</sub>), 1.53 (s, 6H, 2 CH<sub>3</sub>), 1.41 (s, 6H, 2 CH<sub>3</sub>); <sup>13</sup>C NMR (125 MHz, (CD<sub>3</sub>)<sub>2</sub>SO):  $\delta_{\text{C}}$  = 163.38, 162.08, 158.54, 131.70, 131.59, 121.79, 120.59, 121.79, 120.59, 58.15, 57.79, 44.52, 44.18, 31.41, 29.70, 29.30; TOF-HRMS (ES,  $m/z$ ): calculated C<sub>25</sub>H<sub>24</sub>O<sub>8</sub> 452.1471 found: 452.1415 [M<sup>+</sup>].

### **General Procedure (14.2d) for Dianhydride Compounds**

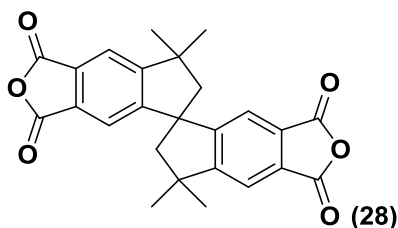
Under a nitrogen atmosphere the corresponding tetra-carboxylic acid was dissolved in acetic anhydride. The mixture was refluxed for 12 h, cooled to room temperature and the acetic anhydride/acetic acid was removed under vacuum to give a black solid. The solid was recrystallised from the appropriate solvent until pure to afford the desired product.

### **9,10-dimethyl-9,10-dihydro-9,10-ethanoanthracene-2,3,6,7-dianhydride**



General procedure 14.2d was followed using 9,10-dimethyl-9,10-dihydro-2,3,6,7-tetracarboxyl-9,10-ethanoanthracene (25) (4.88 g, 12 mmol), acetic anhydride (200 ml) and recrystallisation from tetrahydrofuran to afford the desired product 9,10-dimethyl-9,10-dihydro-9,10-ethanoanthracene-2,3,6,7-dianhydride (27) (2.03 g, 46%) as an off-white powder. Mp: 340-355 °C (dec);  $\nu_{\max}$  ( $\text{CH}_2\text{Cl}_2/\text{cm}^{-1}$ ): 2959, 2863, 1838, 1778, 1286, 1236;  $^1\text{H}$  NMR (500 MHz,  $\text{CDCl}_3$ ):  $\delta_{\text{H}} = 7.98$  (s, 4H, Ar *H*), 2.21 (s, 6H, 2  $\text{CH}_3$ ), 1.83 (s, 4H, 2  $\text{CH}_2$ );  $^{13}\text{C}$  NMR (125 MHz,  $\text{CDCl}_3$ ):  $\delta_{\text{C}} = 162.73, 153.71, 129.96, 118.26, 118.26, 44.34, 34.39, 18.46$ ; TOF-HRMS (EI,  $m/z$ ): calculated  $\text{C}_{22}\text{H}_{14}\text{O}_6$  374.0790 found: 374.0784 [ $\text{M}^+$ ].

### **3,3,3',3'-octamethyl-1,1'-spirobisindane-6,6',7,7'-dianhydride**



General procedure 14.2d was followed using 3,3,3',3'-octamethyl-6,6',7,7'-tetracarboxyl-1,1'-spirobisindane (26) (5 g, 11 mmol), acetic anhydride (200 ml) and recrystallisation from chloroform : *n*-hexane (8:2) to afford the desired product 3,3,3',3'-octamethyl-1,1'-spirobisindane-6,6',7,7'-dianhydride (28) (4.11 g, 89%) as a colourless powder. Mp: 285-286 °C;  $\nu_{\max}$  ( $\text{CH}_2\text{Cl}_2/\text{cm}^{-1}$ ): 2962, 1844, 1777, 1232;  $^1\text{H}$  NMR (500 MHz,  $\text{CDCl}_3$ ):  $\delta_{\text{H}} = 7.79$  (s, 2H, Ar *H*), 7.28 (s, 2H, Ar *H*), 2.52 (d,  $J=13.46$  Hz, 2H,  $\text{CH}_2$ ), 2.32 (d,  $J=13.46$  Hz, 2H,  $\text{CH}_2$ ), 1.47 (s, 6H, 2  $\text{CH}_3$ ), 1.39 (s, 6H, 2  $\text{CH}_3$ );  $^{13}\text{C}$  NMR (125 MHz,  $\text{CDCl}_3$ ):  $\delta_{\text{C}} = 162.48,$

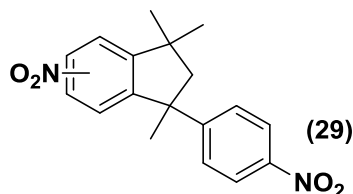
162.06, 158.50, 131.52, 131.39, 121.73, 120.13, 58.70, 57.93, 44.45, 31.52, 29.60; TOF-HRMS (EI,  $m/z$ ): calculated  $C_{25}H_{20}O_6$  416.1260 found: 416.1255 [ $M^+$ ].

### **General Procedure (14.2e) for Dinitro Compounds**

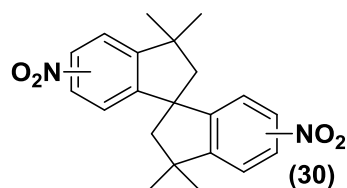
(Based on a procedure from literature<sup>145</sup>)

Trifluoroacetic anhydride was added drop-wise to a mixture of potassium nitrate and the corresponding substrate in acetonitrile. The mixture was stirred for 24 h, after which time a white precipitate had formed. The solvent was removed under vacuum and the residue was stirred in water, then extracted with chloroform to afford a yellow solid. The crude product was subjected to column chromatography (chloroform) to afford the desired product.

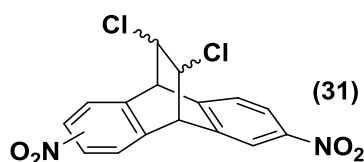
### **6,(7)-nitro-1,3,3-trimethyl-1-(4-nitrophenyl)indane**



General procedure 14.2e was followed using trifluoroacetic anhydride (43.7 ml, 65.07 g, 309 mmol), potassium nitrate (8.94 g, 88 mmol) and 1,3,3-trimethyl-1-phenylindane (1) (10.45 g, 44 mmol) in acetonitrile (150 ml) to afford the desired product 6,(7)-nitro-1,3,3-trimethyl-1-(4-nitrophenyl)indane (29) (10.23 g, 71%) as a colourless powder Mp: 115-127 °C, (lit<sup>211</sup> 110-126 °C);  $\nu_{\max}$  ( $CH_2Cl_2/cm^{-1}$ ): 3064, 2963, 1593, 1520, 1338;  $^1H$  NMR (400 MHz,  $CDCl_3$ ):  $\delta_H$  = 8.09 (m, 4H, Ar *H*), 7.29 (m, 3H, Ar *H*), 2.54 (d,  $J$  = 13.42 Hz, 1H,  $CH_2$ ), 2.38 (d,  $J$  = 13.42 Hz, 1H,  $CH_2$ ), 1.80 + 1.79 (2 s, 3H,  $CH_3$ ), 1.44 + 1.43 (2s, 3H,  $CH_3$ ), 1.13 + 1.11 (2s, 3H,  $CH_3$ );  $^{13}C$  NMR (101 MHz,  $CDCl_3$ ):  $\delta_C$  = 159.69, 157.02, 154.84, 154.08, 149.23, 148.45, 147.87, 146.28, 127.44, 125.61, 123.84, 123.64, 122.94, 120.24, 118.56, 58.93, 58.85, 51.44, 51.14, 43.47, 43.23, 30.48, 30.26, 30.07; TOF-LRMS (EI,  $m/z$ ): calculated  $C_{18}H_{18}N_2O_4$  326.13 found: 326.59 [ $M^+$ ].

**6,(7),6',(7')-dinitro-3,3,3',3'-tetramethyl-1,1'-spirobisindane**

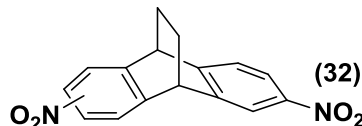
General procedure 14.2e was followed using trifluoroacetic anhydride (79.0 ml, 53.26 g, 253 mmol), potassium nitrate (7.31 g, 72 mmol) and 3,3,3',3'-tetramethyl-1,1'-spirobisindane (3) (10.00 g, 36 mmol) in acetonitrile (400 ml) to afford the desired product 6,(7),6',(7')-dinitro-3,3,3',3'-tetramethyl-1,1'-spirobisindane (30) (12.00 g, 91%) as an off white powder. Mp: 140-141 °C;  $\nu_{\max}$  ( $\text{CH}_2\text{Cl}_2/\text{cm}^{-1}$ ): 3093, 3063, 2958, 2865, 1591, 1522, 1343;  $^1\text{H}$  NMR (500 MHz,  $\text{CDCl}_3$ ):  $\delta_{\text{H}}$  = 8.13 (m, 1H, Ar *H*), 8.05 (m, 2H, Ar *H*), 7.64 (dd,  $J$  = 6.4, 2.1 Hz, 1H, Ar *H*), 7.38 (dd,  $J$  = 8.4, 3.1 Hz, 1H, Ar *H*), 6.92 (dd,  $J$  = 8.4, 3.1 Hz, 1H, Ar *H*), 2.52 (d,  $J$  = 13.3 Hz, 2H,  $\text{CH}_2$ ), 2.35 (m, 2H,  $\text{CH}_2$ ), 1.45 (m, 6H, 2  $\text{CH}_3$ ), 1.42 (m, 6H, 2  $\text{CH}_3$ );  $^{13}\text{C}$  NMR (125 MHz,  $\text{CDCl}_3$ ):  $\delta_{\text{C}}$  = 153.66, 153.47, 152.51, 152.11, 145.69, 145.64, 145.58, 145.46, 142.90, 142.82, 141.54, 141.07, 125.19, 124.95, 122.34, 114.74, 114.49, 114.45, 110.91, 110.72, 108.41, 108.36, 59.96, 59.89, 59.69, 57.62, 56.99, 56.35, 43.39, 43.18, 42.87, 42.64, 31.91, 31.79, 31.70, 31.57, 30.59, 30.23; TOF-HRMS (EI,  $m/z$ ): calculated  $\text{C}_{21}\text{H}_{22}\text{N}_2\text{O}_4$  366.1580 found: 366.1580 [ $\text{M}^+$ ].

**9,10-dihydro-2(3),6(7)-dinitro-11,12-*cis*(*trans*)dichloro-9,10-ethanoanthracene**

General procedure 14.2e was followed using trifluoroacetic anhydride (12.4 ml, 18.73 g, 89 mmol), potassium nitrate (2.57 g, 25 mmol) and 9,10-dihydro-11,12-*cis*(*trans*)dichloro-9,10-ethanoanthracene (5) (3.5 g, 13 mmol) in acetonitrile (50 ml) to afford the desired product 9,10-dihydro-2(3),6(7)-dinitro-11,12-*cis*(*trans*)dichloro-9,10-ethanoanthracene (31) (4.30 g, 93%) as an off-white powder. Mp: 242-243 °C;  $\nu_{\max}$  ( $\text{cm}^{-1}$ ): 3089, 3041, 1517, 1342, 854;  $^1\text{H}$  NMR (500 MHz,  $\text{CDCl}_3$ ):  $\delta_{\text{H}}$  = 8.32 (m, 1H, Ar *H*), 8.29 (m, 1H, Ar *H*), 8.24 (m, 1H, Ar *H*), 8.19 (m, 1H, Ar *H*), 7.60 (m, 2H, Ar *H*), 4.84 (m, 2H, bridge *CH*), 4.55 (m, 2H, bridgehead *CH*);  $^{13}\text{C}$  NMR (125 MHz,  $\text{CDCl}_3$ ):  $\delta_{\text{C}}$  = 147.28, 145.55, 143.51, 140.82, 138.60, 127.64, 125.91, 123.63, 123.10, 121.91, 121.88, 120.24, 120.20, 57.05, 57.03, 57.00, 52.43, 52.35,

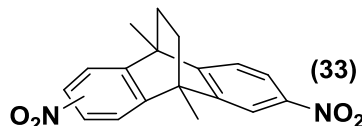
52.27, 52.21; TOF-HRMS (EI,  $m/z$ ): calculated  $C_{16}H_{10}Cl_2N_2O_4$  364.0018 found: 364.0017 [ $M^+$ ].

### 9,10-dihydro-2,6(7)-dinitro-9,10-ethanoanthracene



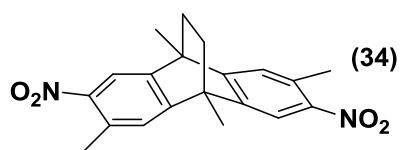
General procedure 14.2e was followed using trifluoroacetic anhydride (40.50 ml, 61.18 g, 290 mmol), potassium nitrate (19.61 g, 194 mmol) and 9,10-dihydro-9,10-ethanoanthracene (7) (20 g, 97 mmol) in acetonitrile (400 ml) to afford the desired product 9,10-dihydro-2,6(7)-dinitro-9,10-ethanoanthracene (32) (28.43 g, 99%) as an off-white powder. Mp: 132-133 °C;  $\nu_{\max}$  ( $cm^{-1}$ ): 2962, 1512, 1336;  $^1H$  NMR (500 MHz,  $CDCl_3$ ):  $\delta_H$  = 8.18 (m, 2H, Ar *H*), 8.08 (m, 1H, Ar *H*), 8.06 (m, 1H, Ar *H*), 7.49 (d,  $J$  = 8.10 Hz, 1H, Ar *H*), 7.47 (d,  $J$  = 8.10 Hz, 1H, Ar *H*), 4.64 (s, 2H, bridgehead *CH*), 1.82 (s, 4H, 2  $CH_2$ );  $^{13}C$  NMR (125 MHz,  $CDCl_3$ ):  $\delta_C$  = 149.83, 149.33, 146.40, 143.94, 143.45, 124.46, 124.38, 122.07, 118.94, 118.83, 44.08, 43.98, 43.90, 25.64, 25.56, 25.49; TOF-HRMS (EI,  $m/z$ ): calculated  $C_{16}H_{12}N_2O_4$  296.0797 found: 296.0800 [ $M^+$ ].

### 9,10-Dimethyl-9,10-dihydro-2,6(7)-dinitro-9,10-ethanoanthracene

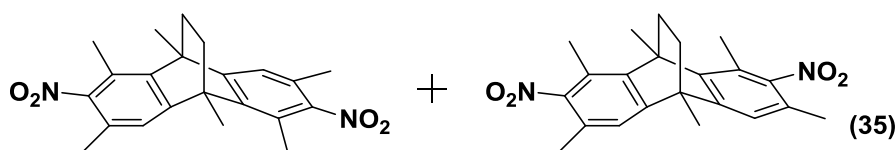


General procedure 14.2e was followed using trifluoroacetic anhydride (37.5 ml, 55.90 g, 270 mmol), potassium nitrate (8.15 g, 81 mmol) and 9,10-dimethyl-9,10-dihydro-9,10-ethanoanthracene (17) (9.00 g, 38.5 mmol) in acetonitrile (350 ml) to afford the desired product 9,10-dimethyl-9,10-dihydro-2,6(7)-dinitro-9,10-ethanoanthracene (33) (11.46 g, 92%) as an off-white powder : Mp: 185-186 °C;  $\nu_{\max}$  ( $CH_2Cl_2/cm^{-1}$ ): 2965, 2922, 2851, 1522, 1343;  $^1H$  NMR (500 MHz,  $CDCl_3$ ):  $\delta_H$  = 8.14 (m, 2H, Ar *H*), 8.06 (d,  $J$  = 8.30 Hz, 1H, Ar *H*), 8.05 (d,  $J$  = 8.30 Hz, 1H, Ar *H*), 7.48 (d,  $J$  = 4.83 Hz, 1H, Ar *H*), 7.46 (d,  $J$  = 4.83 Hz, 1H, Ar *H*), 2.10 (m, 6H, 2  $CH_3$ ) 1.73 (s, 4H, 2  $CH_2$ );  $^{13}C$  NMR (125 MHz,  $CDCl_3$ ):  $\delta_C$  = 152.40, 151.97, 146.96, 146.53, 146.48, 121.67, 121.63, 121.56, 116.15, 116.01, 43.18, 42.90, 42.63, 34.99, 34.91, 34.83, 18.18, 18.05, 17.92; TOF-HRMS (EI,  $m/z$ ): calculated  $C_{18}H_{16}N_2O_4$  324.1110 found: 324.1113 [ $M^+$ ].

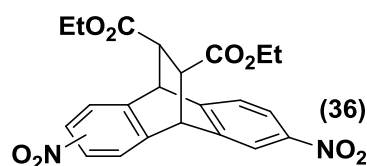


**2,6,9,10-tetramethyl-9,10-dihydro-3,7-dinitro-9,10-ethanoanthracene**

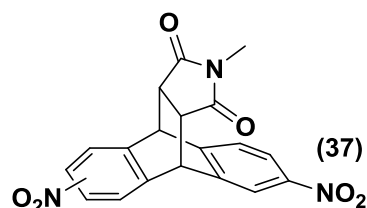
General procedure 14.2e was followed using trifluoroacetic anhydride (18.6 ml, 28.06 g, 133 mmol), potassium nitrate (3.85 g, 38 mmol) and 2,6,9,10-tetramethyl-9,10-dihydro-9,10-ethanoanthracene (18) (5.00 g, 19 mmol) in acetonitrile (150 ml) to afford the desired product 2,6,9,10-tetramethyl-9,10-dihydro-3,7-dinitro-9,10-ethanoanthracene (34) (6.59 g, 98%) as an off-white powder. Mp: 275-276 °C;  $\nu_{\max}$  ( $\text{cm}^{-1}$ ): 2953, 2866, 1508, 1336, 1317;  $^1\text{H}$  NMR (500 MHz,  $\text{CDCl}_3$ ):  $\delta_{\text{H}}$  = 7.90 (s, 2H, Ar *H*), 7.24 (s, 2H, Ar *H*), 2.59 (s, 6H, 2 Ar  $\text{CH}_3$ ), 2.01 (s, 6H, 2  $\text{CH}_3$ ), 1.68 (s, 4H, 2  $\text{CH}_2$ );  $^{13}\text{C}$  NMR (125 MHz,  $\text{CDCl}_3$ ):  $\delta_{\text{C}}$  = 150.77, 147.00, 144.05, 131.83, 125.13, 117.36, 42.04, 35.03, 20.64, 17.95; TOF-HRMS (EI,  $m/z$ ): calculated  $\text{C}_{20}\text{H}_{20}\text{N}_2\text{O}_4$  352.1423 found: 387.1129 [ $\text{M} + \text{Cl}^-$ ].

**1,3,5,7,9,10-hexamethyl-9,10-dihydro-2,6-dinitro-9,10-ethanoanthracene/1,3,6,8,9,10-hexamethyl-9,10-dihydro-2,7-dinitro-9,10-ethanoanthracene**

General procedure 14.2e was followed using trifluoroacetic anhydride (2.6 ml, 3.90 g, 19 mmol), potassium nitrate (0.54 g, 5 mmol) and mixture of 1,3,5,7,9,10-hexamethyl-9,10-dihydro-9,10-ethanoanthracene and 1,3,6,8,9,10-hexamethyl-9,10-dihydro-9,10-ethanoanthracene (20) (0.77 g, 3 mmol) in acetonitrile (100 ml) to afford the desired product, a mixture of 1,3,5,7,9,10-hexamethyl-9,10-dihydro-2,6-dinitro-9,10-ethanoanthracene and 1,3,6,8,9,10-hexamethyl-9,10-dihydro-2,7-dinitro-9,10-ethanoanthracene (35) (0.63 g, 63%) as an off-white powder. Mp: over 300 °C;  $\nu_{\max}$  ( $\text{cm}^{-1}$ ): 2953, 2866, 1517, 1369;  $^1\text{H}$  NMR (500 MHz,  $\text{CDCl}_3$ ):  $\delta_{\text{H}}$  = 7.12 (s, 2H, Ar *H*), 2.44 (s, 6H, 2  $\text{CH}_3$ ), 2.24 (s, 6H, 2 Ar  $\text{CH}_3$ ), 2.16 (s, 6H, 2 Ar  $\text{CH}_3$ ), 2.89 (m, 2H, 2  $\text{CH}_2$ ), 2.52 (m, 2H, 2  $\text{CH}_2$ );  $^{13}\text{C}$  NMR (125 MHz,  $\text{CDCl}_3$ ):  $\delta_{\text{C}}$  = 152.48, 149.45, 140.90, 125.79, 125.69, 123.36, 122.27, 117.19, 44.93, 41.96, 37.26, 36.81, 34.55, 24.34, 20.83, 19.13, 17.31, 17.26, 15.75, 15.65; TOF-HRMS (EI,  $m/z$ ): calculated  $\text{C}_{22}\text{H}_{24}\text{N}_2\text{O}_4$  380.1736 found: 380.1739 [ $\text{M}^+$ ].

**9,10-dihydro-2(3),6(7)-dinitro-9,10-ethanoanthracene-11,12-*trans*-diethyl ester**

General procedure 14.2e was followed using trifluoroacetic anhydride (2.8 ml, 4.17 g, 20 mmol), potassium nitrate (0.58 g, 6 mmol) and 9,10-dihydro-9,10-ethanoanthracene-11,12-*trans*-diethyl ester (8) (1.00 g, 3 mmol) in acetonitrile (30 ml) to afford the desired product 9,10-dihydro-2(3),6(7)-dinitro-9,10-ethanoanthracene-11,12-*trans*-diethyl ester (36) in a quantitative yield as a colourless glass. Mp: 106-130 °C ;  $\nu_{\max}$  (CH<sub>2</sub>Cl<sub>2</sub>/cm<sup>-1</sup>): 2982, 1732, 1616, 1523, 1348; <sup>1</sup>H NMR (400 MHz, CDCl<sub>3</sub>):  $\delta_{\text{H}}$  = 8.13 (s, 1H, Ar *H*), 8.07 (m, 0.5H, Ar *H*), 8.01 (m, 3H, Ar *H*), 7.52 (m, 0.5H, Ar *H*), 7.43 (m, 1H, Ar *H*), 4.91 (s, 2H, bridge *CH*), 4.0 (m, 4H, O-CH<sub>2</sub>), 3.4 (s, 2H, bridgehead *CH*), 1.2 (m, 6H, CH<sub>3</sub>); <sup>13</sup>C NMR (101 MHz, CDCl<sub>3</sub>):  $\delta_{\text{C}}$  = 171.04, 147.89, 147.46, 146.85, 146.61, 146.20, 142.41, 141.98, 141.05, 140.63, 125.99, 125.91, 125.16, 125.10, 122.83, 122.64, 120.24, 120.13, 119.55, 119.47, 61.87, 61.80, 46.94, 46.85, 46.77, 46.69, 46.48, 40.15, 14.26; TOF-HRMS (EI, *m/z*): calculated C<sub>22</sub>H<sub>20</sub>N<sub>2</sub>O<sub>8</sub> 440.1220 found: 440.1220 [M<sup>+</sup>].

**N-methyl-9,10-dihydro-2(3),6(7)-dinitro-9,10-ethanoanthracene-11,12-*cis*-dicarboximide**

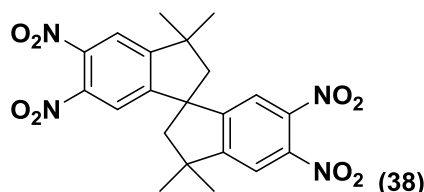
General procedure 14.2e was followed using trifluoroacetic anhydride (3.2 ml, 4.77 g, 23 mmol), potassium nitrate (0.66 g, 7 mmol) and N-methyl-9,10-dihydro-9,10-ethanoanthracene-11,12-*cis*-dicarboximide (9) (0.95 g, 3 mmol) in acetonitrile (30 ml) to afford the desired product N-methyl-9,10-dihydro-2(3),6(7)-dinitro-9,10-ethanoanthracene-11,12-*cis*-dicarboximide (37) in a quantitative yield as a colourless glass. Mp: 125-145 °C;  $\nu_{\max}$  (CH<sub>2</sub>Cl<sub>2</sub>/cm<sup>-1</sup>): 3069, 2950, 1709, 1592, 1520, 1347; <sup>1</sup>H NMR (400 MHz, CDCl<sub>3</sub>):  $\delta_{\text{H}}$  = 8.32 (m, 1H, Ar *H*), 8.17 (m, 3H, Ar *H*), 7.63 (m, 1H, Ar *H*), 7.53 (m, 1H, Ar *H*), 5.10 (m, 2H, bridge *CH*), 3.35 (m, 2H, bridgehead *CH*), 2.62 (s, 3H, N-CH<sub>3</sub>); <sup>13</sup>C NMR (101 MHz, CDCl<sub>3</sub>):  $\delta_{\text{C}}$  = 175.19, 147.30, 147.17, 147.08, 146.84, 144.70, 144.24, 142.00, 141.53, 139.41,

138.94, 127.70, 126.25, 125.52, 125.27, 125.03, 123.23, 123.16, 120.36, 119.95, 119.89, 45.89, 45.75, 45.28, 45.19, 24.78; TOF-LRMS (EI,  $m/z$ ): calculated  $C_{19}H_{13}N_3O_6$  379.08 found: 379.07 [ $M^+$ ].

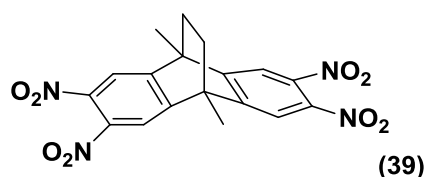
### **General Procedure (14.2f) for Tetranitro Compounds**

Equal quantities of fuming nitric acid (100%) and sulfuric acid (98%) were cooled separately in an ice bath. The cooled nitric acid was slowly added to the sulfuric acid with cooling from an ice bath. The corresponding substrate was added slowly in small portions to the nitration mixture with cooling from an ice bath. The mixture was stirred at room temperature for 1 h and then at 80 °C for 3h. The mixture was cooled to room temperature and slowly added to crushed ice. The precipitate was filtered and the crude product was subjected to column chromatography (chloroform) to afford the desired product as an off white powder.

### **6,6',7,7'-tetranitro-3,3,3',3'-tetramethyl-1,1'-spirobisindane**



General procedure 14.2f was followed using 3,3,3',3'-tetramethyl-1,1'-spirobisindane (3) (5.00 g, 18 mmol), and a 50:50 nitric acid and sulfuric acid mixture (150 ml) to afford the desired product 6,6',7,7'-tetranitro-3,3,3',3'-tetramethyl-1,1'-spirobisindane (38) (7.50 g, 91%) as an off white powder. Mp: 262-263 °C;  $\nu_{max}$  ( $CH_2Cl_2/cm^{-1}$ ): 3093, 3025, 2965, 2925, 1538, 1367, 1342;  $^1H$  NMR (500 MHz,  $(CD_3)_2CO$ ):  $\delta_H$  = 8.07 (s, 2H, Ar *H*), 7.85 (s, 2H, Ar *H*), 2.74 (d,  $J$  = 13.45 Hz, 2H,  $CH_2$ ), 2.60 (d,  $J$  = 13.45 Hz, 2H,  $CH_2$ ), 1.60 (s, 6H, 2  $CH_3$ ), 1.53 (s, 6H, 2  $CH_3$ );  $^{13}C$  NMR (125 MHz,  $(CD_3)_2CO$ ):  $\delta_C$  = 159.16, 154.36, 143.60, 143.05, 121.90, 119.81, 58.25, 57.87, 44.71, 30.32, 28.26; TOF-HRMS (EI,  $m/z$ ): calculated  $C_{21}H_{20}N_4O_8$  456.1281 found: 456.1278 [ $M^+$ ].

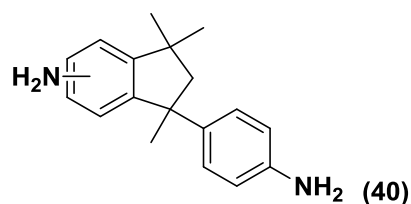
**9,10-dimethyl-9,10-dihydro-2,3,6,7-tetranitro-9,10-ethanoanthracene**

General procedure 14.2f was followed using 9,10-dimethyl-9,10-dihydro-9,10-ethanoanthracene (17) (6.00 g, 25 mmol) and a 50:50 nitric acid and sulfuric acid mixture (150 ml) to afford the desired product 9,10-dimethyl-9,10-dihydro-2,3,6,7-tetranitro-9,10-ethanoanthracene (39) (8.42 g, 79%) as an off white powder. Mp: above 300 °C;  $\nu_{\max}$  ( $\text{CH}_2\text{Cl}_2/\text{cm}^{-1}$ ): 2956, 2867, 1570, 1509, 1321;  $^1\text{H}$  NMR (500 MHz,  $(\text{CD}_3)_2\text{SO}$ ):  $\delta_{\text{H}} = 8.14$  (s, 4H, Ar H), 2.08 (s, 6H, 2  $\text{CH}_3$ ), 1.74 (s, 4H, 2  $\text{CH}_2$ );  $^{13}\text{C}$  NMR (125 MHz,  $(\text{CD}_3)_2\text{SO}$ ):  $\delta_{\text{C}} = 150.88, 140.98, 119.16, 44.18, 34.00, 17.54$ ; TOF-HRMS (EI,  $m/z$ ): calculated  $\text{C}_{18}\text{H}_{14}\text{N}_4\text{O}_8$  414.0812 found: 449.0488 [ $\text{M} + \text{Cl}$ ]. Crystals were prepared by a slow evaporation of a solution of the compound in chloroform. Crystal size:  $0.5 \times 0.35 \times 0.3$  mm, Triclinic, space group  $\text{P}\bar{1}$ ,  $a = 8.3273$  (3),  $b = 9.8882$  (2),  $c = 10.7493$  (3) Å,  $\alpha = 90.344$  (2)°,  $\beta = 98.347$  (1)°,  $\gamma = 91.939$  (2)°,  $V = 875.19$  (4) Å<sup>3</sup>,  $Z = 2$ ;  $\mu = 0.13$  mm<sup>-1</sup>, 5890 reflections measured, 3975 unique reflections ( $R_{\text{int}} = 0.019$ ), 3507 reflections with  $I > 2\sigma(I)$ ,  $R(\%) = 3.9$ .

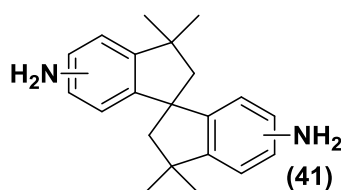
**General Procedure (14.2g) for Diamino Compounds**

(A modified procedure from literature<sup>147</sup>)

Under a nitrogen atmosphere, the corresponding dinitro compound was dissolved in a suitable solvent (de-oxygenated). Raney nickel and hydrazine monohydrate was added and the mixture was refluxed for 24 h. The colourless mixture was cooled in ice and filtered under nitrogen. The organic phase was extracted and the solvent was removed under vacuum at 25 °C to afford the desired product.

**6,(7)-amino-1,3,3-trimethyl-1-(4-aminophenyl)indane**

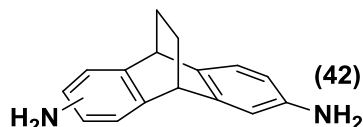
General procedure 14.2 g was followed using 6,(7)-nitro-1,3,3-trimethyl-1-(4-nitrophenyl)indane (29) (3.00 g, 9 mmol) in ethanol (150 ml), Raney nickel (~40 mg) and hydrazine monohydrate (7.36 g, 7.1 ml, 147 mmol). The organic phase was extracted with diethyl ether and the solvent was removed under vacuum at 25 °C to afford the desired product 6,(7)-amino-1,3,3-trimethyl-1-(4-aminophenyl)indane (40) as a colourless glass in a quantitative yield. Mp: 41-46 °C (lit<sup>211</sup> 47-54 °C);  $\nu_{\max}$  (CH<sub>2</sub>Cl<sub>2</sub>/cm<sup>-1</sup>): 3434, 3349, 3215, 3006, 2955, 2861, 1618, 1511; <sup>1</sup>H NMR (400 MHz, CDCl<sub>3</sub>):  $\delta_{\text{H}}$  = 6.84 (m, 3H, Ar H), 6.40 (m, 4H, Ar H), 3.43 (s, br, 4H, 2 NH<sub>2</sub>), 2.27 (m, 1H, 0.5 CH<sub>2</sub>), 2.02 (m, 1H, 0.5 CH<sub>2</sub>), 1.51 (m, 3H, CH<sub>3</sub>), 1.19 (m, 3H, CH<sub>3</sub>), 0.92 (m, 3H, CH<sub>3</sub>); <sup>13</sup>C NMR (101 MHz, CDCl<sub>3</sub>):  $\delta_{\text{C}}$  = 153.62, 151.00, 146.06, 145.64, 144.27, 144.15, 142.66, 141.77, 141.32, 139.57, 127.84, 127.74, 125.72, 123.23, 115.04, 114.88, 114.40, 111.61, 109.29, 68.12, 60.07, 59.86, 50.20, 49.60, 42.86, 42.35, 31.61, 31.47, 31.01, 30.89, 30.61, 25.90; TOF-LRMS (EI, m/z): calculated C<sub>18</sub>H<sub>22</sub>N<sub>2</sub> 266.18 found 266.18 [M<sup>+</sup>]

**6,(7),6',(7')-diamino-3,3,3',3'-tetramethyl-1,1'-spirobisindane**

General procedure 14.2g was followed using 6,(7),6',(7')-dinitro-3,3,3',3'-tetramethyl-1,1'-spirobisindane (30) (4.00 g, 12 mmol) in diethyl ether (200 ml), Raney nickel (~40 mg) and hydrazine monohydrate (11.5 ml, 11.90 g, 238 mmol). The organic phase was extracted with diethyl ether and the solvent was removed under vacuum at 25 °C to afford the desired product 6,(7),6',(7')-diamino-3,3,3',3'-tetramethyl-1,1'-spirobisindane (41) as a colourless glass in a quantitative yield. Mp: 164-168 °C;  $\nu_{\max}$  (CH<sub>2</sub>Cl<sub>2</sub>/cm<sup>-1</sup>): 3446, 3366, 3213, 2951, 2860, 1619, 1495, 1319; <sup>1</sup>H NMR (500 MHz, CDCl<sub>3</sub>):  $\delta_{\text{H}}$  = 7.00 (m, 1H, Ar H), 6.64 (m, 4H, Ar H), 6.20 (s, 1H, Ar H), 3.56 (s, br, 4H, 2 NH<sub>2</sub>), 2.34 (m, 2H, CH<sub>2</sub>), 2.24 (m, 2H, CH<sub>2</sub>),

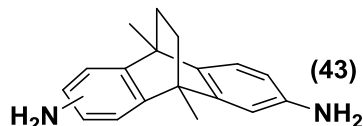
1.38 (m, 12H,  $CH_3$ );  $^{13}C$  NMR (125 MHz,  $CDCl_3$ ):  $\delta_C = 159.74, 156.71, 154.06, 154.03, 151.09, 150.98, 148.18, 124.97, 124.90, 123.52, 123.47, 123.37, 123.32, 123.12, 123.10, 119.64, 119.59, 117.81, 117.80, 58.99, 58.98, 58.85, 58.80, 57.87, 57.56, 57.25, 44.14, 44.03, 43.93, 43.82, 31.46, 31.42, 31.36, 31.34, 29.81, 29.72, 29.70, 29.59$ ; TOF-HRMS (ES,  $m/z$ ): calculated  $C_{21}H_{26}N_2$  306.2096 found: 348.2430 [ $M + CH_3CNH^+$ ] (solvent).

### **9,10-dihydro-2,6(7)-diamino-9,10-ethanoanthracene**



General procedure 14.2g was followed using 9,10-dihydro-2,6(7)-dinitro-9,10-ethanoanthracene (32) (5.00 g, 17 mmol) in tetrahydrofuran (200 ml), Raney nickel (~40 mg) and hydrazine monohydrate (16.4 ml, 18.90 g, 34 mmol). The organic phase was extracted with dichloromethane and the solvent was removed under vacuum at 25 °C to afford the desired product 9,10-dihydro-2,6(7)-diamino-9,10-ethanoanthracene (42) as a colourless powder in a quantitative yield. Mp: 181-185 °C (dec);  $\nu_{max}$  ( $cm^{-1}$ ): 3402, 3354, 3003, 2949, 2864, 1620, 1481;  $^1H$  NMR (500 MHz,  $CDCl_3$ ):  $\delta_H = 7.01$  (d,  $J = 7.74$  Hz, 1H, Ar  $H$ ), 7.00 (d,  $J = 7.74$  Hz, 1H, Ar  $H$ ), 6.64 (m, 2H Ar  $H$ ), 6.41 (m, 2H, Ar  $H$ ), 4.10 (m, 2H, bridgehead  $CH$ ), 3.48 (s, br, 4H, 2  $NH_2$ ), 1.68 (s, 4H, 2  $CH_2$ );  $^{13}C$  NMR (125 MHz,  $CDCl_3$ ):  $\delta_C = 145.85, 144.91, 144.13, 143.97, 135.25, 134.24, 123.78, 123.53, 111.77, 111.56, 111.21, 110.95, 44.44, 43.38, 42.33, 27.69, 27.20, 26.73$ ; TOF-HRMS (EI,  $m/z$ ): calculated  $C_{16}H_{16}N_2$  236.1313 found: 236.1311 [ $M^+$ ].

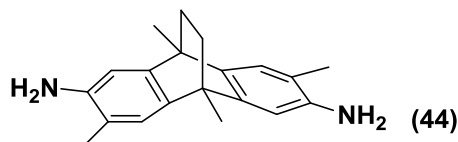
### **9,10-dimethyl-9,10-dihydro-2,6(7)-diamino-9,10-ethanoanthracene**



General procedure 14.2g was followed using 9,10-dimethyl-9,10-dihydro-2,6(7)-dinitro-9,10-ethanoanthracene (33) (4.10 g, 13 mmol) in diethyl ether (200 ml), Raney nickel (~40 mg) and hydrazine monohydrate (12.3 ml, 12.66 g, 253 mmol) to afford the desired product 9,10-dimethyl-9,10-dihydro-2,6(7)-diamino-9,10-ethanoanthracene (43) as a colourless powder in a quantitative yield.. Mp: 62-64 °C;  $\nu_{max}$  ( $CH_2Cl_2/cm^{-1}$ ): 3456, 3342, 3261, 2958, 2933, 2857, 1619, 1476;  $^1H$  NMR (500 MHz,  $CDCl_3$ ):  $\delta_H = 7.03$  (d,  $J = 7.9$  Hz, 2H, Ar  $H$ ), 6.66 (d,  $J =$

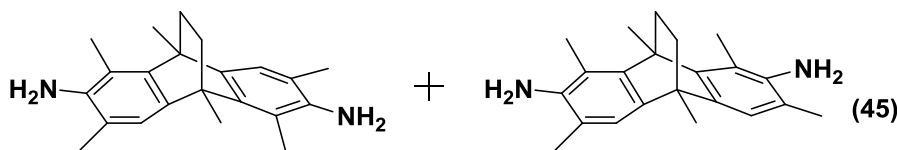
3.30 Hz, 1H, Ar *H*), 6.65 (d,  $J = 3.30$  Hz, 1H, Ar *H*), 6.45 (m, 2H, Ar *H*), 3.39 (s, br, 4H, 2  $NH_2$ ), 1.88 (m, 6H, 2  $CH_3$ ), 1.61 (s, 4H, 2  $CH_2$ );  $^{13}C$  NMR (125 MHz,  $CDCl_3$ ):  $\delta_C = 148.33$ , 147.53, 143.83, 143.66, 137.80, 136.93, 120.99, 120.67, 111.40, 111.19, 108.77, 108.45, 65.85, 41.72, 41.04, 40.37, 36.43, 36.20, 36.00, 18.42, 15.29; TOFHRMS (EI,  $m/z$ ): calculated  $C_{18}H_{20}N_2$  264.1626 found: 264.1635 [ $M^+$ ].

### **2,6,9,10-tetramethyl-9,10-dihydro-3,7-diamino-9,10-ethanoanthracene**



General procedure 14.2g was followed using 2,6,9,10-tetramethyl-9,10-dihydro-3,7-dinitro-9,10-ethanoanthracene (34) (4.00 g, 11 mmol) in tetrahydrofuran (200 ml), Raney nickel (~40 mg) and hydrazine monohydrate (11.0 ml, 11.36 g, 227 mmol) to afford the desired product 2,6,9,10-tetramethyl-9,10-dihydro-3,7-diamino-9,10-ethanoanthracene (44) as a colourless powder in a quantitative yield. Mp: 219-220 °C;  $\nu_{max}$  ( $CH_2Cl_2/cm^{-1}$ ): 3420, 3332, 3235, 2935, 2857, 1624, 1476, 1327;  $^1H$  NMR (500 MHz,  $CDCl_3$ ):  $\delta_H = 7.04$  (s, 2H, Ar *H*), 6.72 (s, 2H, Ar *H*), 3.50 (s, br, 4H, 2  $NH_2$ ), 2.23 (s, 6H, 2 Ar  $CH_3$ ), 1.99 (s, 6H, 2 bridgehead  $CH_3$ ), 1.71 (s, 4H, 2  $CH_2$ );  $^{13}C$  NMR (125 MHz,  $CDCl_3$ ):  $\delta_C = 146.21$ , 141.83, 137.14, 122.61, 118.17, 108.35, 40.74, 36.56, 18.72, 17.42; TOF-HRMS (ES,  $m/z$ ): calculated  $C_{20}H_{24}N_2$  292.1939 found: 293.2013 [ $M + H^+$ ].

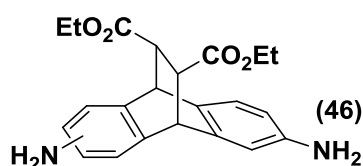
### **1,3,5,7,9,10-hexamethyl-9,10-dihydro-2,6-diamino-9,10-ethanoanthracene/1,3,6,8,9,10-hexamethyl-9,10-dihydro-2,7-diamino-9,10-ethanoanthracene**



General procedure 14.2g was followed using a mixture of 1,3,5,7,9,10-hexamethyl-9,10-dihydro-2,6-dinitro-9,10-ethanoanthracene/1,3,6,8,9,10-hexamethyl-9,10-dihydro-2,7-dinitro-9,10-ethanoanthracene (35) (0.63 g, 2 mmol) in tetrahydrofuran (50 ml), Raney nickel (~40 mg) and hydrazine monohydrate (1.6 ml, 1.66 g, 33 mmol) to afford the desired product, a mixture of 1,3,5,7,9,10-hexamethyl-9,10-dihydro-2,6-diamino-9,10-ethanoanthracene/1,3,6,8,9,10-hexamethyl-9,10-dihydro-2,7-diamino-9,10-ethanoanthracene

(45) as a colourless glass in a quantitative yield. Mp: 98-105 °C;  $\nu_{\max}$  ( $\text{cm}^{-1}$ ): 3441, 3350, 2924, 2852, 1618, 1460;  $^1\text{H}$  NMR (500 MHz,  $\text{CDCl}_3$ ):  $\delta_{\text{H}}$  = 7.22 (s, 2H, Ar *H*), 3.67 (s, br, 4H, 2  $\text{NH}_2$ ), 2.65 (s, 6H, 2  $\text{CH}_3$ ), 2.44 (s, 6H, 2 Ar  $\text{CH}_3$ ), 2.41 (s, 6H, 2 Ar  $\text{CH}_3$ ), 2.14 (m, 2H,  $\text{CH}_2$ ), 1.78 (m, 2H,  $\text{CH}_2$ );  $^{13}\text{C}$  NMR (125 MHz,  $\text{CDCl}_3$ ):  $\delta_{\text{C}}$  = 146.17, 142.07, 141.36, 139.36, 123.28, 121.40, 120.68, 118.10, 117.32, 44.10, 43.81, 38.94, 38.50, 30.59, 25.80, 18.31, 14.31; TOF-HRMS (EI,  $m/z$ ): calculated  $\text{C}_{22}\text{H}_{28}\text{N}_2$  320.2252 found: 320.2246 [ $\text{M}^+$ ].

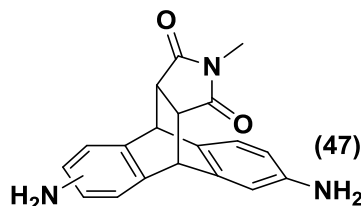
### **9,10-dihydro-2(3),6(7)-diamino-9,10-ethanoanthracene-11,12-*trans*-diethyl ester**



General procedure 14.2g was followed using 9,10-dihydro-2(3),6(7)-dinitro-9,10-ethanoanthracene-11,12-*trans*-diethyl ester (36) (1.00 g, 2 mmol) in tetrahydrofuran (20 ml) and hydrazine monohydrate (1.14 g, 1.1 ml, 23 mmol) to afford the desired product 9,10-dihydro-2(3),6(7)-diamino-9,10-ethanoanthracene-11,12-*trans*-diethyl ester (46) as a colourless glass in a quantitative yield. Mp: 91-98 °C;  $\nu_{\max}$  ( $\text{CH}_2\text{Cl}_2/\text{cm}^{-1}$ ): 3445, 3369, 3225, 2978, 1722, 1625;  $^1\text{H}$  NMR (400 MHz,  $\text{CDCl}_3$ ):  $\delta_{\text{H}}$  = 6.98 (m, 1H, Ar *H*), 6.88 (m, 1.5H, Ar *H*), 6.62 (m, 1H, Ar *H*), 6.51 (m, 0.5H, Ar *H*), 6.32 (m, 2H, Ar *H*), 4.4 (m, 2H, 2 bridge *CH*), 3.98 (m, 4H, 2 O- $\text{CH}_2$ ), 3.37 (s, br, 4H, 2  $\text{NH}_2$ ), 3.28 (m, 2H, 2 bridgehead *CH*), 1.14 (t,  $J$  = 7.13 Hz, 6H, 2  $\text{CH}_3$ ),  $^{13}\text{C}$  NMR (101 MHz,  $\text{CDCl}_3$ ):  $\delta_{\text{C}}$  = 172.64, 144.45, 144.27, 144.19, 144.03, 143.23, 141.45, 131.60, 130.69, 125.11, 124.84, 124.03, 112.67, 112.49, 112.37, 111.65, 111.37, 60.92, 48.57, 48.05, 47.59, 47.06, 46.12, 45.31, 40.15, 30.34, 14.35; TOF-HRMS (EI,  $m/z$ ): calculated  $\text{C}_{22}\text{H}_{24}\text{N}_2\text{O}_4$  380.1736 found: 380.1736 [ $\text{M}^+$ ].



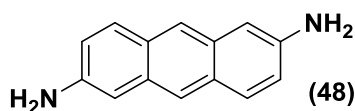
**N-methyl-9,10-dihydro-2(3),6(7)-diamino-9,10-ethanoanthracene-11,12-cis-dicarboximide**



General procedure 14.2g was followed using N-methyl-9,10-dihydro-2(3),6(7)-dinitro-9,10-ethanoanthracene-11,12-*cis*-dicarboximide (37) (1.0 g, 3 mmol) in tetrahydrofuran (20 ml), hydrazine monohydrate (1.32 g, 1.3 ml, 26 mmol) to afford the desired product N-methyl-9,10-dihydro-2(3),6(7)-diamino-9,10-ethanoanthracene-11,12-*cis*-dicarboximide (47) as a colourless glass in a quantitative yield. Mp: 156-163 °C;  $\nu_{\max}$  (CH<sub>2</sub>Cl<sub>2</sub>/cm<sup>-1</sup>): 3444, 3361, 3228, 2955, 1770, 1694, 1622, 1485; <sup>1</sup>H NMR (400 MHz, (CD<sub>3</sub>)<sub>2</sub>SO):  $\delta_{\text{H}}$  = 7.00 (m, 1H, Ar *H*), 6.78 (m, 1H, Ar *H*), 6.65 (m, 1H, Ar *H*), 6.42 (m, 1H, Ar *H*), 6.28 (m., 2H, Ar *H*), 4.94 (s, br, 4H, 2 NH), 4.30 (m, 2H, 2 bridge CH), 3.38 (s, 2H, 2 bridgehead CH), 2.42 (s, 3H, N-CH<sub>3</sub>); <sup>13</sup>C NMR (101 MHz, (CD<sub>3</sub>)<sub>2</sub>SO):  $\delta_{\text{C}}$  = 177.08, 177.19, 147.51, 146.79, 143.02, 140.36, 129.52, 126.29, 124.60, 124.23, 110.74, 110.47, 110.33, 110.19, 47.45, 47.00, 44.21, 44.20, 23.88; TOF-LRMS (EI, *m/z*): calculated C<sub>19</sub>H<sub>17</sub>N<sub>3</sub>O<sub>2</sub> 319.1321 found: 319.1321 [M<sup>+</sup>].

**2,6-diaminoanthracene**

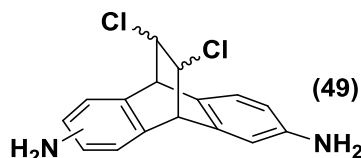
(A modified procedure from literature<sup>148</sup>)



Under a nitrogen atmosphere, zinc mesh (30.00 g, 450 mmol) was slowly added to a suspension of 2,6-diaminoanthraquinone (13.10 g, 55 mmol) in sodium hydroxide solution (125 ml, 2M). Ethanol (20 ml) was added to inhibit foaming and the mixture was refluxed for 48 h. The brown solid was filtered from the mixture and washed with hot water until washings were clear. The crude product was subjected to soxhlet extraction over one week (acetone) under a nitrogen atmosphere. Recrystallisation of the extract afforded the desired product 2,6-diaminoanthracene (48) (3.16 g, 28%, lit<sup>148</sup> 40%) as bright yellow crystals: Mp: 231-232 °C (dec), (lit<sup>148</sup> 230 °C);  $\nu_{\max}$  (CH<sub>2</sub>Cl<sub>2</sub>/cm<sup>-1</sup>): 3403, 3326, 3204, 3009 2957, 1635, 1572, 1475; <sup>1</sup>H NMR (400 MHz, (CD<sub>3</sub>)<sub>2</sub>SO):  $\delta_{\text{H}}$  = 7.88 (s, 2H, Ar *H*), 7.64 (d, *J* = 8.9 Hz, 2H,

Ar *H*), 6.93 (d,  $J = 8.9$  Hz, 2H, Ar *H*), 6.8 (s, 2H, Ar *H*), 5.24 (s, br, 4H, 2  $\text{NH}_2$ );  $^{13}\text{C}$  NMR (101 MHz,  $(\text{CD}_3)_2\text{SO}$ ):  $\delta_{\text{C}} = 144.02, 130.62, 127.91, 127.24, 121.33, 120.45, 103.72$ ; TOF-LRMS (EI,  $m/z$ ): calculated  $\text{C}_{14}\text{H}_{12}\text{N}_2$  208.1 found: 208.1 [ $\text{M}^+$ ].

**9,10-dihydro-2(3),6(7)-diamino-11,12-*cis(trans)*dichloro-9,10-ethanoanthracene**

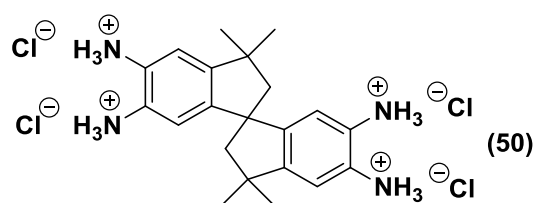


Under a nitrogen atmosphere, 9,10-dihydro-2(3),6(7)-dinitro-11,12-*cis(trans)*dichloro-9,10-ethanoanthracene (31) (4.30 g, 12 mmol) was dissolved in a refluxing mixture of concentrated hydrochloric acid (100 ml) and ethanol (100 ml). Tin powder (13.98 g, 118 mmol) was added in small portions and the mixture was refluxed for 16 h. The mixture was cooled to room temperature and the ethanol was removed under vacuum. The mixture was neutralised with sodium hydroxide solution (1M) and the precipitate was filtered and dried under nitrogen. The precipitate was washed with tetrahydrofuran and the filtrate was collected. The solvent was removed under vacuum to afford the desired product 9,10-dihydro-2(3),6(7)-diamino-11,12-*cis(trans)*dichloro-9,10-ethanoanthracene (49) as a colourless powder in a quantitative yield. Mp: 117-120 °C;  $\nu_{\text{max}}$  ( $\text{cm}^{-1}$ ): 3363, 3286, 3014, 2958, 1622, 1489, 904, 730;  $^1\text{H}$  NMR (500 MHz,  $\text{CDCl}_3$ ):  $\delta_{\text{H}} = 7.00$  (m, 2H, Ar *H*), 6.62 (m, 1H, Ar *H*), 6.52 (m, 1H, Ar *H*), 6.42 (m, 1H, Ar *H*), 6.33 (m, 1H, Ar *H*), 4.35 (m, 2H, bridge *CH*), 4.16 (m, 2H, bridgehead *CH*), 3.51 (s, br, 4H, 2  $\text{NH}_2$ );  $^{13}\text{C}$  NMR (125 MHz,  $\text{CDCl}_3$ ):  $\delta_{\text{C}} = 145.78, 145.61, 145.34, 145.28, 145.12, 142.31, 141.47, 141.10, 140.28, 139.81, 139.02, 138.82, 130.88, 129.96, 128.75, 127.82, 127.32, 127.05, 126.71, 126.71, 125.60, 125.33, 124.54, 124.32, 113.96, 113.75, 113.14, 113.10, 112.93, 112.90, 111.66, 111.43, 59.59, 59.42, 59.26, 59.21, 59.10, 58.88, 52.91, 52.72, 51.99, 51.82, 51.80, 50.90$ ; TOF-HRMS (EI,  $m/z$ ): calculated  $\text{C}_{16}\text{H}_{14}\text{Cl}_2\text{N}_2$  304.0534 found: 304.0536 [ $\text{M}^+$ ].

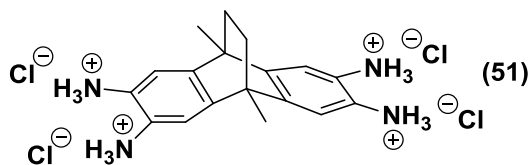
**General Procedure (14.2h) for Tetraamine Hydrochloride Salts**

(A modified procedure from literature<sup>149</sup>)

Under a nitrogen atmosphere, the corresponding tetranitro compound was dissolved in a refluxing mixture of ethanol and concentrated hydrochloric acid. Tin powder was added in small portions and the mixture was refluxed for 16 h and the mixture was cooled to room temperature. The white precipitate was filtered, washed with concentrated hydrochloric acid, then ethanol and dried under nitrogen to afford the desired product.

**6,6',7,7'-tetraamino-3,3,3',3'-tetramethyl-1,1'-spirobisindane hydrochloride**

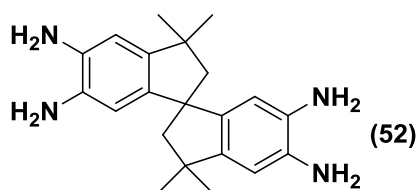
General procedure 14.2h was followed using 6,6',7,7'-tetranitro-3,3,3',3'-tetramethyl-1,1'-spirobisindane (38) (5.00 g, 11 mmol), ethanol (100 ml), concentrated hydrochloric acid (100 ml) and tin powder (13.00 g, 110 mmol) to afford the desired product 6,6',7,7'-tetraamino-3,3,3',3'-tetramethyl-1,1'-spirobisindane hydrochloride (50) (5.15 g, 97%) as colourless crystals. Mp: 239-241 °C;  $\nu_{\max}$  (cm<sup>-1</sup>): 3398, 2818, 2542, 1489, 1109; <sup>1</sup>H NMR (500 MHz, (CD<sub>3</sub>)<sub>2</sub>SO):  $\delta_{\text{H}}$  = 9.10 (s, br, 12H, 4 NH<sub>3</sub><sup>+</sup>), 7.17 (s, 2H, Ar H), 6.70 (s, 2H, Ar H), 2.32 (d,  $J$  = 13.14 Hz, 2H, CH<sub>2</sub>), 2.13 (d,  $J$  = 13.14 Hz, 2H, CH<sub>2</sub>), 1.33 (s, 6H, 2 CH<sub>3</sub>), 1.26 (s, 6H, 2 CH<sub>3</sub>); <sup>13</sup>C NMR (125 MHz, (CD<sub>3</sub>)<sub>2</sub>SO):  $\delta_{\text{C}}$  = 147.47, 128.44, 118.07, 116.33, 56.99, 43.38, 31.64, 30.49, 25.60; TOF-HRMS (ES, m/z): calculated C<sub>21</sub>H<sub>32</sub>C<sub>14</sub>N<sub>4</sub> 482.13198 found: 338.2408 [M-2HCl-2Cl<sup>+</sup>].

**9,10-dimethyl-9,10-dihydro-2,3,6,7-tetraamino-9,10-ethanoanthracene hydrochloride**

General procedure 14.2h was followed using 9,10-dimethyl-9,10-dihydro-2,3,6,7-tetraamino-9,10-ethanoanthracene (39) (5.00 g, 12 mmol), ethanol (100 ml), concentrated hydrochloric acid (100 ml) and tin powder (14.32 g, 120 mmol) to afford the desired product 9,10-dimethyl-9,10-dihydro-2,3,6,7-tetraamino-9,10-ethanoanthracene hydrochloride (51) (5.28, 99%) as colourless crystals. Mp: 256-258 °C;  $\nu_{\max}$  (cm<sup>-1</sup>): 3655, 2852, 2548, 1627, 1475; <sup>1</sup>H NMR (500 MHz, CDCl<sub>3</sub>):  $\delta_{\text{H}}$  = 8.97 (s, br, 12H, 4 NH<sub>3</sub><sup>+</sup>), 7.04 (s, 4H, Ar H), 1.76 (s, 6H, 2 CH<sub>3</sub>), 1.50 (s, 4H, 2 CH<sub>2</sub>); <sup>13</sup>C NMR (125 MHz, CDCl<sub>3</sub>):  $\delta_{\text{C}}$  = 142.29, 126.42, 114.26, 41.01, 35.72, 18.40; TOF-HRMS (ES, m/z): calculated C<sub>18</sub>H<sub>24</sub>Cl<sub>4</sub>N<sub>4</sub> 440.0928 found: 296.1709 [M-2HCl-2Cl<sup>+</sup>].

**General Procedure (14.2i) for Tetraamino Compounds**

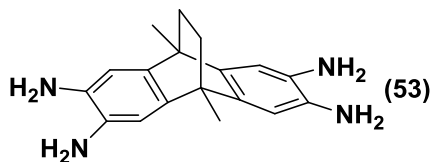
The corresponding Tetraamine Salt was dissolved in deionised (deoxygenated) water and cooled in an ice bath. The salt was neutralised with the slow addition of sodium hydroxide (1M) to form a white precipitate. The precipitate was filtered and dried under nitrogen to afford the desired product.

**6,6',7,7'-tetraamino-3,3,3',3'-tetramethyl-1,1'-spirobisindane**

General procedure 14.2i was followed using 6,6',7,7'-tetraamino-3,3,3',3'-tetramethyl-1,1'-spirobisindane hydrochloride (50) (5.15 g, 11 mmol) to afford the desired product 6,6',7,7'-tetraamino-3,3,3',3'-tetramethyl-1,1'-spirobisindane (52) as a colourless powder in a quantitative yield. Mp: 105-106 °C;  $\nu_{\max}$  (cm<sup>-1</sup>): 3323, 3211, 2947, 2858, 1498, 1319; <sup>1</sup>H NMR (500 MHz, CDCl<sub>3</sub>):  $\delta_{\text{H}}$  = 6.51 (s, 2H, Ar H), 6.19 (s, 2H, Ar H), 3.36 (s, br, 4H, 2 NH<sub>2</sub>), 3.21 (s, br, 4H, 2 NH<sub>2</sub>), 2.25 (d, *J* = 12.9 Hz, 2H, CH<sub>2</sub>), 2.13 (d, *J* = 12.9 Hz, 2H, CH<sub>2</sub>), 1.32 (s, 6H, 2 CH<sub>3</sub>), 1.28 (s, 6H, 2 CH<sub>3</sub>); <sup>13</sup>C NMR (125 MHz, CDCl<sub>3</sub>):  $\delta_{\text{C}}$  = 144.47, 142.92,

134.12, 112.45, 109.79, 59.91, 56.98, 42.91, 31.77, 30.55; TOF-HRMS (EI,  $m/z$ ): calculated  $C_{21}H_{28}N_4$  336.2314 found: 336.2312 [ $M^+$ ].

### **9,10-dimethyl-9,10-dihydro-2,3,6,7-tetraamino-9,10-ethanoanthracene**

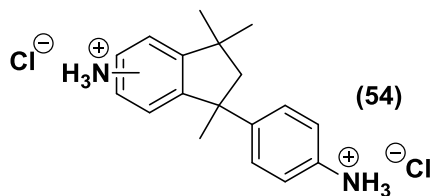


General procedure 14.2i was followed using 9,10-dimethyl-9,10-dihydro-2,3,6,7-tetraamino-9,10-ethanoanthracene hydrochloride (51) (5.28 g, 12 mmol) to afford the desired product 9,10-dimethyl-9,10-dihydro-2,3,6,7-tetraamino-9,10-ethanoanthracene (53) as a colourless powder in a quantitative yield. Mp: 310-311 °C (dec);  $\nu_{\max}$  ( $\text{cm}^{-1}$ ): 3369, 3318, 3191, 2959, 2929, 2855, 1662, 1483, 1321;  $^1\text{H}$  NMR (500 MHz,  $\text{CDCl}_3$ ):  $\delta_{\text{H}}$  = 6.62 (s, 4H, Ar *H*), 3.25 (s, br, 8H, 4  $\text{NH}_2$ ), 1.78 (s, 4H, 2  $\text{CH}_2$ ), 1.55 (s, 6H, 2  $\text{CH}_3$ );  $^{13}\text{C}$  NMR (125 MHz,  $\text{CDCl}_3$ ):  $\delta_{\text{C}}$  = 139.31, 131.35, 110.14, 40.46, 36.59, 18.59; TOF-HRMS (ES,  $m/z$ ): calculated  $C_{18}H_{22}N_4$  294.1844 found: 295.1921 [ $M+\text{H}^+$ ].

### **General Procedure (14.2j) for Diamine Hydrochloride Salts**

The corresponding diamine compound was dissolved in diethyl ether (deoxygenated) and cooled in an ice bath. A stream of dry hydrogen chloride gas (generated from calcium chloride and concentrated hydrochloric acid) was bubbled through the solution to form a white precipitate. The precipitate was filtered and dried under nitrogen to afford the desired product.

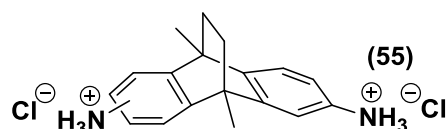
### **6,(7)-amino-1,3,3-trimethyl-1-(4-aminophenyl)indane hydrochloride**



General procedure 14.2j was followed using 6,(7)-amino-1,3,3-trimethyl-1-(4-aminophenyl)indane (40) (5.00 g, 19 mmol) to afford the desired product 6,(7)-amino-1,3,3-trimethyl-1-(4-aminophenyl)indane hydrochloride (54) as a colourless powder in a

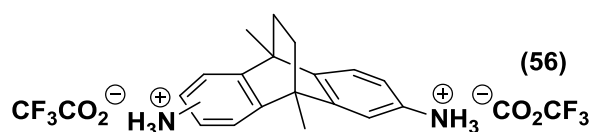
quantitative yield. Mp: 166-167 °C (dec);  $\nu_{\max}$  ( $\text{cm}^{-1}$ ): 2825, 2559, 1506, 1489;  $^1\text{H}$  NMR (500 MHz,  $\text{D}_2\text{O}$ ):  $\delta_{\text{H}} = 7.22$  (m, 7H, Ar *H*), 2.83 (m, 1H,  $\text{CH}_2$ ), 2.09 (d,  $J = 13.14$  Hz, 1H,  $\text{CH}_2$ ), 1.52 (s, 1.5H,  $\text{CH}_3$ ), 1.49 (s, 1.5H,  $\text{CH}_3$ ), 1.17 (s, 1.5H,  $\text{CH}_3$ ), 1.14 (s, 1.5H,  $\text{CH}_3$ ), 0.86 (s, 1.5H,  $\text{CH}_3$ ), 0.83 (s, 1.5H,  $\text{CH}_3$ );  $^{13}\text{C}$  NMR (125 MHz,  $\text{D}_2\text{O}$ ):  $\delta_{\text{C}} = 154.92, 153.74, 151.70, 151.58, 150.54, 149.45, 129.25, 128.56, 128.39, 128.35, 127.52, 126.58, 124.60, 122.83, 122.77, 122.44, 121.67, 119.58, 58.30, 50.49, 50.31, 42.66, 42.45, 30.00, 29.34$ ; TOF-HRMS (ES,  $m/z$ ): calculated  $\text{C}_{18}\text{H}_{24}\text{Cl}_2\text{N}_2$  338.1317 found: 267.1852 [ $\text{M}-2\text{Cl}^{2+}$ ].

### **9,10-dimethyl-9,10-dihydro-2,6(7)-diamino-9,10-ethanoanthracene hydrochloride**



General procedure 14.2j was followed using 9,10-dimethyl-9,10-dihydro-2,6(7)-diamino-9,10-ethanoanthracene (43) (5.00 g, 19 mmol) to afford the desired product 9,10-dimethyl-9,10-dihydro-2,6(7)-diamino-9,10-ethanoanthracene hydrochloride (55) as a colourless powder in a quantitative yield. Mp: 201-202 °C (dec);  $\nu_{\max}$  ( $\text{cm}^{-1}$ ): 2854, 2575, 1614, 1475;  $^1\text{H}$  NMR (500 MHz,  $\text{D}_2\text{O}$ ):  $\delta_{\text{H}} = 7.44$  (m, 2H, Ar *H*), 7.32 (m, 2H, Ar *H*), 7.18 (m, 2H, Ar *H*), 2.12 (s, 4H, 2  $\text{CH}_2$ ), 1.92 (s, 6H, 2  $\text{CH}_3$ );  $^{13}\text{C}$  NMR (125 MHz,  $\text{D}_2\text{O}$ ):  $\delta_{\text{C}} = 148.44, 146.98, 127.59, 127.52, 122.31, 120.22, 115.68, 42.14, 41.99, 34.75, 30.32, 17.36, 17.24, 17.11$ ; TOF-HRMS (ES,  $m/z$ ): calculated  $\text{C}_{18}\text{H}_{22}\text{Cl}_2\text{N}_2$  336.1160 found: 265.1700 [ $\text{M} - \text{HCl} - \text{Cl}^+$ ].

### **9,10-dimethyl-9,10-dihydro-2,6(7)-diamino-9,10-ethanoanthracene trifluoroacetate**



Under a nitrogen atmosphere, 9,10-dimethyl-9,10-dihydro-2,6(7)-diamino-9,10-ethanoanthracene (43) (5.00 g, 19 mmol) was dissolved in diethyl ether (deoxygenated) (200 ml) and cooled in an ice bath. Trifluoroacetic acid (2.9 ml, 4.31 g, 38 mmol) in diethyl ether (deoxygenated) (10 ml) was added drop-wise to form a yellow precipitate. The precipitate was filtered and dried under nitrogen to afford the desired product 9,10-dimethyl-9,10-dihydro-2,6(7)-diamino-9,10-ethanoanthracene trifluoroacetate (56) as a yellow powder in a quantitative yield. Mp: 62-63 °C (dec);  $\nu_{\max}$  ( $\text{cm}^{-1}$ ): ;  $^1\text{H}$  NMR (500 MHz,  $\text{CD}_3\text{OD}$ ):  $\delta_{\text{H}} = 7.45$

(d,  $J = 8.06$  Hz, 1H, Ar  $H$ ), 7.44 (d,  $J = 8.06$  Hz, 1H, Ar  $H$ ), 7.33 (m, 2H, Ar  $H$ ), 7.19 (d,  $J = 8.06$  Hz, 1H, Ar  $H$ ), 7.17 (d,  $J = 8.06$  Hz, 1H, Ar  $H$ ), 2.00 (s, 4H, 2  $CH_2$ ), 1.66 (s, 6H, 2  $CH_3$ );  $^{13}C$  NMR (125 MHz,  $CD_3OD$ ):  $\delta_C = 163.38, 163.24, 162.97, 148.20, 147.92, 145.99, 145.72, 129.66, 121.67, 117.1, 114.82, 41.95, 41.75, 41.54, 35.16, 35.09, 35.04, 17.18, 17.06, 16.59$ ;  $^{19}F$  NMR (300 MHz,  $CD_3OD$ ):  $\delta_F = -76.61$  (s, 6F, 2  $CF_3$ ); TOF-HRMS (ES,  $m/z$ ): calculated  $C_{22}H_{22}F_6N_2O_4$  492.1484 found: 265.1725 [ $M - 2CF_3CO_2 - H^+$ ].

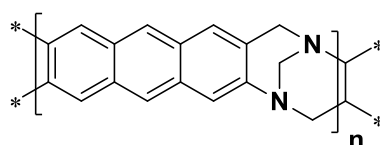
## **14.3: Polymers Synthesis**

### **14.3.1a: Tröger's Base Polymers**

#### **General Procedure (14.3.1a) for Tröger's Base Polymerisations**

Under a nitrogen atmosphere, the corresponding diamino monomer was dissolved or suspended in dimethoxymethane and the solution was cooled in an ice bath. Trifluoroacetic acid was added drop-wise over 30 min and the mixture was stirred for an appropriate time at room temperature. The viscous orange to dark red mixture was slowly poured into aqueous ammonium hydroxide solution and stirred vigorously for 2 h during which a white to yellow solid was formed. The solid was collected by filtration, washed with water and then acetone until the washings were clear. The resulting white powder was dissolved in chloroform and methanol was added drop-wise until the solution became turbid. The solution was stirred for a further 30 min to precipitate a gel. The re-precipitation from chloroform was repeated twice. The polymer was dissolved in chloroform and added drop-wise to *n*-hexane with vigorous stirring and the precipitated fine powder was filtered. The white powder was refluxed in methanol for 24 h, filtered and then dried in a vacuum oven at 120 °C for 9 h to afford the desired polymer.

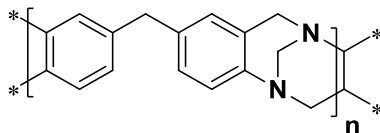
#### **Anth.TB**



General procedure 14.3.1a was followed using 2,6-diaminoanthracene (1g, 4.8 mmol), dimethoxymethane (2.27 ml, 1.1 g 14.4 mmol), trifluoroacetic acid (10 ml) and 3 days stirring time. The resulting brown powder (1.12 g, 95%) was insoluble in all common

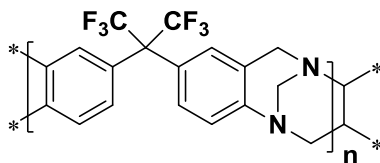
solvents and acids.  $v_{\max}$  ( $\text{cm}^{-1}$ ): 2910, 1655, 1570, 1296; BET surface area =  $1 \text{ m}^2/\text{g}$ ; total pore volume =  $0.0131 \text{ cm}^3/\text{g}$  at ( $P/P_0 = 0.9814$ ); TGA analysis: Initial weight loss due to thermal degradation commences at  $\sim 377 \text{ }^\circ\text{C}$  with a 30% loss of mass below  $1000 \text{ }^\circ\text{C}$ .

### **DPM.TB**



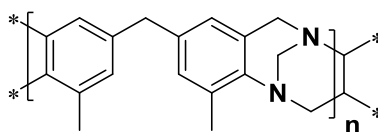
General procedure 14.3.1a was followed using 4,4'-diaminophenylmethane (3.0 g, 15.1 mmol), dimethoxymethane (4.0 ml, 3.46 g, 45.4 mmol), trifluoroacetic acid (25.0 ml) and 1h stirring time. The resulting dark orange jelly was slowly poured into aqueous ammonium hydroxide solution and stirred vigorously for 24 h to form an orange powder. The solid was filtered, washed with water and then acetone until washings were clear. The resulting orange solid (3.50 g, 99%) was insoluble in all common solvents and acids:  $v_{\max}$  ( $\text{cm}^{-1}$ ): 2891, 2841, 1487, 1203; BET surface area =  $0.82 \text{ m}^2/\text{g}$ ; total pore volume =  $0.007 \text{ cm}^3/\text{g}$  at ( $P/P_0 = 0.9814$ ); TGA analysis: Initial weight loss due to thermal degradation commences at  $\sim 362 \text{ }^\circ\text{C}$  with a 39% loss of mass below  $1000 \text{ }^\circ\text{C}$ .

### **HFIP.TB**

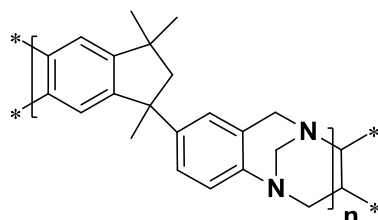


General procedure 14.3.1a was followed using 4,4'-(hexafluoroisopropylidene)dianiline (1.50 g, 5 mmol), dimethoxymethane (2.0 ml, 1.70 g, 22 mmol), trifluoroacetic acid (12.5 ml) and 6 h stirring time. The resulting dark red mixture was slowly poured into aqueous ammonium hydroxide solution and stirred vigorously for 24 h to form a colourless powder. The solid was filtered, washed with water and then acetone. The resulting colourless powder (1.61 g, 97%) was insoluble in all common solvents and acids:  $v_{\max}$  ( $\text{cm}^{-1}$ ): 2980, 1614, 1516, 1244, 1165; BET surface area =  $20 \text{ m}^2/\text{g}$ ; total pore volume =  $0.1372 \text{ cm}^3/\text{g}$  at ( $P/P_0 = 0.9814$ ); TGA analysis: Initial weight loss due to thermal degradation commences at  $\sim 280 \text{ }^\circ\text{C}$  with a 65% loss of mass below  $1000 \text{ }^\circ\text{C}$ .



**DMDPM.TB**

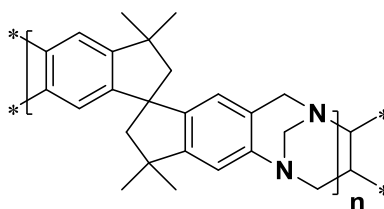
General procedure 14.3.1a was followed using 4,4'-diamino-3,3'-dimethylphenylmethane (3.0 g, 13 mmol), dimethoxymethane (5.9 ml, 5.04 g, 66 mmol), trifluoroacetic acid (25.0 ml) and 3 days stirring time to afford the desired polymer DMDPM.TB (3.07 g, 88%) as an off white powder.  $\nu_{\max}$  ( $\text{cm}^{-1}$ ): 3002, 2946, 2842, 1671, 1476, 1438, 1329, 1213.  $^1\text{H}$  NMR (500 MHz,  $\text{CDCl}_3$ ):  $\delta_{\text{H}}$  = 6.81 (br, s, 2H, Ar *H*), 6.58 (br, s, 2H, Ar *H*), 4.54 (br, m, 2H, N- $\text{CH}_2$ -Ar), 4.29 (br, s, 2H, N- $\text{CH}_2$ -N), 3.95 (br, m, 2H, N- $\text{CH}_2$ -Ar), 3.67 (br, s, 2H,  $\text{CH}_2$ ), 2.37 (br, s, 6H, 2  $\text{CH}_3$ ).  $^{13}\text{C}$  NMR (125 MHz,  $\text{CDCl}_3$ ):  $\delta_{\text{C}}$  = 144.21, 136.40, 132.91, 129.37, 128.06, 124.52, 67.53, 54.97, 41.07, 17.13; GPC (Chloroform):  $M_{\text{n}}$  = 49,600,  $M_{\text{w}}$  = 94,600; BET surface area = 38  $\text{m}^2/\text{g}$ ; total pore volume = 0.1378  $\text{cm}^3/\text{g}$  at  $(P/P_0) = 0.9814$ ; TGA analysis: Initial weight loss due to thermal degradation commences at  $\sim 357$   $^{\circ}\text{C}$  with a 45% loss of mass below 1000  $^{\circ}\text{C}$ . LRMS (acetone washings) (MALDI,  $m/z$ ): calculated repeating unit  $\text{C}_{18}\text{H}_{18}\text{N}_2$ : 262.36 found: 787.07 (cyclic trimer), 1049.23 (cyclic tetramer), 1311 (cyclic pentamer), 1574.16 (cyclic hexamer), 1836.40 (cyclic heptamer), 2098.48 (cyclic octamer).

**TMPI.TB**

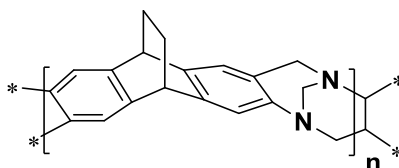
General procedure 14.3.1a was followed using 6,(7)-amino-1,3,3-trimethyl-1-(4-aminophenyl)indane (3.0 g, 11 mmol), dimethoxymethane (2.9 ml, 2.57 g, 34 mmol), trifluoroacetic acid (30.0 ml) and 16 h stirring time to afford the desired polymer TMPI.TB (2.12 g, 62%) as a white powder.  $\nu_{\max}$  ( $\text{cm}^{-1}$ ): 2953, 2860, 1612, 1570, 1489, 1325, 1203;  $^1\text{H}$  NMR (500 MHz,  $\text{CDCl}_3$ ):  $\delta_{\text{H}}$  = 6.60 (br, m, 5H, Ar *H*), 4.44 (br, m, 2H, N- $\text{CH}_2$ -N), 4.10 (br, m, 4H, 2 N- $\text{CH}_2$ -Ar), 2.10 (br, s, 1H, 0.5  $\text{CH}_2$ ), 1.86 (br, s, 1H, 0.5  $\text{CH}_2$ ), 1.34 (br, s, 3H,  $\text{CH}_3$ ), 1.05 (br, s, 3H,  $\text{CH}_3$ ), 0.81 (br, s, 3H,  $\text{CH}_3$ );  $^{13}\text{C}$  NMR (125 MHz,  $\text{CDCl}_3$ ):  $\delta_{\text{C}}$  = 145.61, 126.91, 125.85, 124.48, 122.73, 121.42, 66.67, 59.10, 58.55, 50.22, 42.45, 30.77; GPC

(Chloroform):  $M_n = 700$ ,  $M_w = 4,200$ ; BET surface area =  $535 \text{ m}^2/\text{g}$ ; total pore volume =  $0.16 \text{ cm}^3/\text{g}$  at  $(P/P_0) = 0.9814$ ; TGA analysis: Initial weight loss due to thermal degradation commences at  $\sim 349 \text{ }^\circ\text{C}$  with a 43% loss of mass below  $1000 \text{ }^\circ\text{C}$ . LRMS (acetone washings) (MALDI,  $m/z$ ): calculated repeating unit  $\text{C}_{21}\text{H}_{22}\text{N}_2$ : 302.42 found: 606 (cyclic dimer), 909 (cyclic trimer), 1211 (cyclic tetramer), 1514 (cyclic pentamer), 1818 (cyclic hexamer), 2120 (cyclic heptamer), 2424 (cyclic octamer) 2726 (cyclic nonamer), 3029 (cyclic decamer), 3333 (cyclic undecamer), 3636 (cyclic dodecamer), 3939 (cyclic tridecamer), 4242 (cyclic pentadecamer), 4545 (cyclic hexadecamer), 4848 (cyclic heptadecamer).

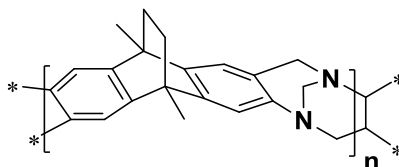
### **SBI.TB**



General procedure 14.3.1a was followed using 6,(7),6',(7')-diamino-3,3,3',3'-tetramethyl-1,1'-spirobisindane (3.00 g, 10 mmol), dimethoxymethane (4.42 ml, 50 mmol), trifluoroacetic acid (25 ml) and 48h stirring time to afford the desired polymer SBI.TB (2.45 g, 73%) as a white powder.  $\nu_{\text{max}}$  ( $\text{cm}^{-1}$ ): 2949, 2891, 1614, 1479, 1409, 1372;  $^1\text{H}$  NMR (500 MHz,  $\text{CDCl}_3$ ):  $\delta_{\text{H}} = 6.72$  (br, m, 4H, Ar *H*), 4.66 (br, s, 2H, N- $\text{CH}_2$ -N), 4.22 (br, s, 4H, 2 N- $\text{CH}_2$ -Ar), 2.24 (br, s, 4H, 2  $\text{CH}_2$ ), 1.32 (br, s, 12H, 4  $\text{CH}_3$ );  $^{13}\text{C}$  NMR (125 MHz,  $\text{CDCl}_3$ ):  $\delta_{\text{C}} = 148.3$ -146.8, 125.9, 123.4-117.1, 67.8-64.7, 61.6-59.2, 58.9-57.9, 57.5-56.0, 43.5-41.8, 32.5-30.9, 30.8-29.3; GPC (Chloroform):  $M_n = 96,000$ ,  $M_w = 360,000$ ; BET surface area =  $745 \text{ m}^2/\text{g}$ ; total pore volume =  $0.542 \text{ cm}^3/\text{g}$  at  $(P/P_0) = 0.9814$ ; TGA analysis: Initial weight loss due to thermal degradation commences at  $\sim 435 \text{ }^\circ\text{C}$  with a 32% loss of mass below  $1000 \text{ }^\circ\text{C}$ .

**DHEA.TB**

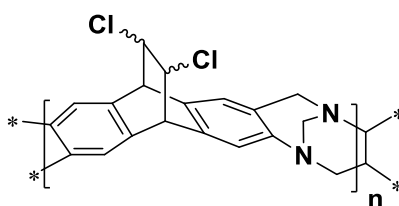
General procedure 14.3.1a was followed using 9,10-dihydro-2,6(7)-diamino-9,10-ethanoanthracene (3.00 g, 13 mmol), dimethoxymethane (5.6 ml, 4.83 g, 63 mmol), trifluoroacetic acid (25 ml) and 2 h stirring time to afford the desired polymer DHEA.TB (3.15 g, 91%) as a white powder.  $\nu_{\max}$  ( $\text{cm}^{-1}$ ): 2933, 2846, 1507, 1469, 1421;  $^1\text{H}$  NMR (500 MHz,  $\text{CDCl}_3$ ):  $\delta_{\text{H}}$  = 6.84 (br, m, 4H, Ar *H*), 4.60 (br, s, 2H, N- $\text{CH}_2$ -N), 4.05 (br, s, 4H, 2 N- $\text{CH}_2$ -Ar), 1.56 (s, br, 6H, 2 bridgehead  $\text{CH}$  + 2 bridge  $\text{CH}_2$ ).  $^{13}\text{C}$  NMR (100 MHz, solid state):  $\delta_{\text{C}}$  = 146.45 (br), 143.32 (br), 140.18 (br), 125.15 (br), 120.60 (br), 68.07 (br), 59.65 (br), 44.87 (br), 27.54 (br); GPC (Chloroform):  $M_{\text{n}}$  = 9,200,  $M_{\text{w}}$  = 49,300. BET surface area = 843  $\text{m}^2/\text{g}$ ; total pore volume = 0.6178  $\text{cm}^3/\text{g}$  at ( $P/P_0$  = 0.9814); TGA analysis: Initial weight loss due to thermal degradation commences at  $\sim 260$   $^{\circ}\text{C}$  with a 10% loss of mass below 400  $^{\circ}\text{C}$  consistent with the loss of an ethylene fragment from the ethanoanthracene unit via a retro Diels-Alder reaction<sup>172</sup> and a further 24% mass loss below 1000  $^{\circ}\text{C}$ .

**DMEA.TB**

General procedure 14.3.1a was followed using 9,10-dimethyl-9,10-dihydro-2,6(7)-diamino-9,10-ethanoanthracene (3.00 g, 11 mmol), dimethoxymethane (5.0 ml, 4.32 g, 56 mmol), trifluoroacetic acid (25 ml) and 48 h stirring time to afford DMEA.TB (2.60 g, 76%) as a white powder.  $\nu_{\max}$  ( $\text{cm}^{-1}$ ): 2935, 2858, 1452, 1411, 1328;  $^1\text{H}$  NMR (500 MHz,  $\text{CDCl}_3$ ):  $\delta_{\text{H}}$  = 7.28 (br, m, 4H, Ar *H*), 4.57 (br, s, 2H, N- $\text{CH}_2$ -N), 4.05 (br, s, 4H, 2 N- $\text{CH}_2$ -Ar), 1.81 (br, m, 6H, 2  $\text{CH}_3$ ), 1.65 (br, m, 4H, 2  $\text{CH}_2$ ).  $^{13}\text{C}$  NMR (125 MHz,  $\text{CDCl}_3$ ):  $\delta_{\text{C}}$  = 146.22-143.67, 142.54-140.01, 120.53-114.08, 66.55, 58.59, 41.02, 36.01, 18.41; GPC (Chloroform):  $M_{\text{n}}$  = 40,700,  $M_{\text{w}}$  = 155,800. BET surface area = 1028  $\text{m}^2/\text{g}$ ; total pore volume = 0.75  $\text{cm}^3/\text{g}$  at ( $P/P_0$  = 0.9814); TGA analysis: A 4% loss of weight occurred at between 20-50  $^{\circ}\text{C}$ . Initial weight loss due to thermal degradation commences at  $\sim 260$   $^{\circ}\text{C}$  with a 10% loss of mass

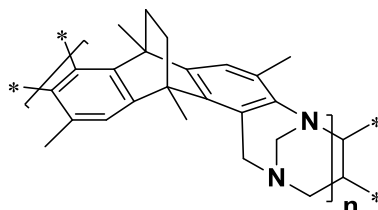
below 400 °C consistent with the loss of an ethylene fragment from the ethanoanthracene unit via a retro Diels-Alder reaction<sup>172</sup> and a further 15% mass loss below 1000 °C. LRMS (acetone washings) (MALDI,  $m/z$ ): calculated repeating unit  $C_{21}H_{20}N_2$ : 300.41 found: 603.68 (cyclic dimer), 901.95 (cyclic trimer), 1201.95 (cyclic tetramer), 1503.19 (cyclic pentamer), 1802.66 (cyclic hexamer), 2103.71 (cyclic heptamer), 2403.97 (cyclic octamer), 2703.69 (cyclic nonamer), 3006.24 (cyclic decamer), 3306.23 (cyclic undecamer), 3608.45 (cyclic dodecamer), 3909.23 (cyclic tridecamer), 4208.66 (cyclic pentadecamer).

### DCEA.TB



General procedure 14.3.1a was followed using 9,10-dihydro-2(3),6(7)-diamino-11,12-*cis(trans)*dichloro-9,10-ethanoanthracene (3.0 g, 10 mmol), dimethoxymethane (4.4 ml, 3.74 g, 49 mmol), trifluoroacetic acid (25 ml), 3 d stirring time and no purification to afford the desired polymer DCEA.TB (2.91 g, 88%) as a light brown powder.  $\nu_{\max}$  ( $\text{cm}^{-1}$ ): 2941, 2858, 1644, 1612, 1469, 1344;  $^1\text{H NMR}$  (500 MHz,  $(\text{CD}_3)_2\text{SO}$ ):  $\delta_{\text{H}} = 7.40$  (br, s, 4H, Ar *H*), 4.58 (br, m, 6H, N- $\text{CH}_2$ -N + 2 N- $\text{CH}_2$ -Ar), 4.04 (br, m, 4H, 4 *CH*); BET surface area = 360  $\text{m}^2/\text{g}$ ; total pore volume = 0.4246  $\text{cm}^3/\text{g}$  at ( $P/P_0 = 0.9814$ ), A 3% loss of weight occurred at between 20-50 °C. Initial weight loss due to thermal degradation commences at ~ 250 °C with a 20% loss of mass below 400 °C consistent with the loss  $\text{Cl}_2$  from the bridge unit to form dibenzobarrelene and a further 24% mass loss below 1000 °C.

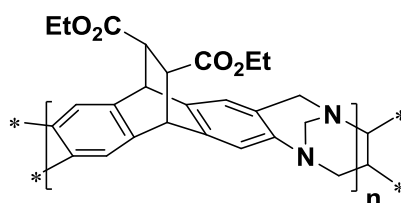
### TMEA.TB



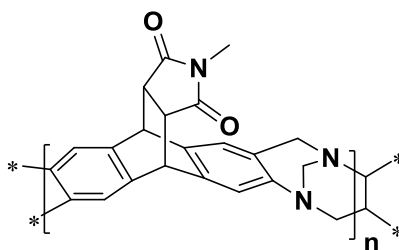
General procedure 14.3.1a was followed using 2,6,9,10-tetramethyl-9,10-dihydro-3,7-diamino-9,10-ethanoanthracene (3.0 g, 10 mmol), dimethoxymethane (4.5 ml, 3.0 g, 51

mmol), trifluoroacetic acid (15 ml) and 7 d stirring time to afford oligomers of the polymer TMEA.TB (1.43 g, 43%) as a white powder.  $\nu_{\max}$  ( $\text{cm}^{-1}$ ): 2935, 2889, 1614, 1568, 1454, 1433;  $^1\text{H}$  NMR (500 MHz,  $\text{CDCl}_3$ ):  $\delta_{\text{H}}$  = 7.19 (br, m, 2H, Ar *H*), 4.85 (br, m, 4H, 2 N- $\text{CH}_2$ -Ar), 3.77 (br, m, 2H, N- $\text{CH}_2$ -N), 2.40 (br, m, 4H, 2  $\text{CH}_2$ ), 2.02 (br, m, 6H, 2 Ar  $\text{CH}_3$ ), 1.57 (br, m, 6H, 2  $\text{CH}_3$ ).  $^{13}\text{C}$  NMR (125 MHz,  $\text{CDCl}_3$ ):  $\delta_{\text{C}}$  = 146.94, 138.16, 128.01, 122.93, 117.81, 113.25, 63.50, 53.77, 44.39, 41.40, 38.34, 36.19, 18.51; BET surface area = 70  $\text{m}^2/\text{g}$ ; total pore volume = 0.3069  $\text{cm}^3/\text{g}$  at ( $\text{P}/\text{P}_0 = 0.9814$ ); TGA analysis: Initial weight loss due to thermal degradation commences at  $\sim 260$   $^\circ\text{C}$  with a 60% loss of mass below 1000  $^\circ\text{C}$ . LRMS (acetone washings) (MALDI,  $m/z$ ): calculated repeating unit  $\text{C}_{23}\text{H}_{24}\text{N}_2$ : 328.46 found: 949.42 (linear trimer), 1279.52 (linear tetramer), 1606.63 (linear pentamer), 1935.77 (linear hexamer).

### DEEEA.TB



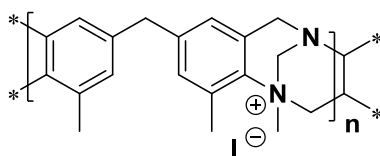
General procedure 14.3.1a was followed using 9,10-dihydro-2(3),6(7)-diamino-9,10-ethanoanthracene-11,12-*trans*-diethyl ester (1g, 2.6 mmol), dimethoxymethane (0.69ml, 0.6 g, 7.8 mmol), trifluoroacetic acid (10 ml) and 3 days stirring time to afford oligomers of the polymer DEEEA TB (0.60 g, 55%) as a light brown powder.  $\nu_{\max}$  ( $\text{cm}^{-1}$ ): 2974, 1712, 1469, 1182, 1020;  $^1\text{H}$  NMR (500 MHz,  $\text{CDCl}_3$ ):  $\delta_{\text{H}}$  = 6.72 (br, m, 4H, Ar *H*), 4.45 (br, m, 4H, 2  $\text{CH}_2$ ), 3.97 (br, m, 6H, N- $\text{CH}_2$ -N + 2 N- $\text{CH}_2$ -Ar), 3.24 (br, m, 4H, 4 CH), 1.11 (br, m, 6H, 2  $\text{CH}_3$ );  $^{13}\text{C}$  NMR (125 MHz,  $\text{CDCl}_3$ ):  $\delta_{\text{C}}$  = 172.24, 146.10, 139.21, 128.86, 127.04, 119.25, 61.19, 47.75, 41.30, 14.33; BET surface area = 0  $\text{m}^2/\text{g}$ ; total pore volume = 0.009  $\text{cm}^3/\text{g}$  at ( $\text{P}/\text{P}_0 = 0.9814$ ); TGA analysis: Initial weight loss due to thermal degradation commences at  $\sim 360$   $^\circ\text{C}$  with a 40% loss of mass below 600  $^\circ\text{C}$  consistent with the loss of a diethyl fumarate fragment from the ethanoanthracene units via a retro Diels-Alder reaction and a further 20% mass loss below 1000  $^\circ\text{C}$ .

**NMDCEA.TB**

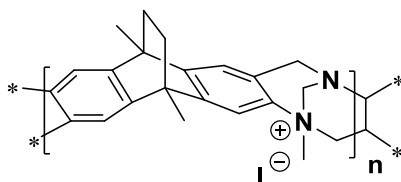
General procedure 14.3.1a was followed using N-methyl-9,10-dihydro-2(3),6(7)-diamino-9,10-ethanoanthracene-11,12-*cis*-dicarboximide (1.0 g, 3.1 mmol), dimethoxymethane (0.83 ml, 0.72 g, 9.4 mmol), trifluoroacetic acid (10 ml) and 3 days stirring to afford oligomers of the polymer NMDCEA TB (0.82 g, 73%) as a light brown powder.  $\nu_{\max}$  ( $\text{cm}^{-1}$ ): 2922, 1693, 1427, 1278;  $^1\text{H}$  NMR (500 MHz,  $\text{CDCl}_3$ ):  $\delta_{\text{H}} = 7.03$  (m, 4H, Ar *H*), 4.64 (m, 4H, 2 N- $\text{CH}_2$ -Ar), 4.03 (m, 2H, N- $\text{CH}_2$ -N), 3.02 (m, 3H,  $\text{CH}_3$ ), 2.36 (m, 4H, 4 CH).  $^{13}\text{C}$  NMR (125 MHz,  $\text{CDCl}_3$ ):  $\delta_{\text{C}} = 176.95, 176.63, 146.22, 140.51, 138.17, 136.91, 127.20, 124.65, 122.55, 122.53, 120.84, 58.53, 47.03, 47.00, 45.32, 24.28$ ; BET surface area = 2  $\text{m}^2/\text{g}$ ; total pore volume = 0.009  $\text{cm}^3/\text{g}$  at ( $P/P_0 = 0.9814$ ); TGA analysis: Initial weight loss due to thermal degradation commences at  $\sim 300$   $^\circ\text{C}$  with a 32% loss of mass below 1000  $^\circ\text{C}$ .

**14.3.2: Quaternerised Tröger's Base PIMs****General Procedure (14.3.2a) for Methyl Iodide TB Polymers**

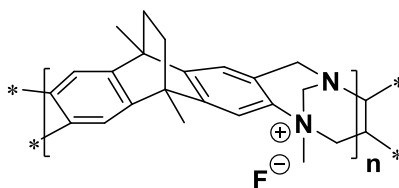
The Tröger's base polymer was suspended in dimethyl sulfoxide and methyl iodide was added. The mixture was stirred for 16 h by which time the mixture had become a dark brown solution. The mixture was poured into a large quantity of deionised water and the brown precipitate was filtered. The polymer was washed with hot deionised water and dried under a stream of nitrogen. The polymer was refluxed in methanol for 24 h, filtered and then dried in a vacuum oven at 60  $^\circ\text{C}$  for 9 h to afford the desired polymer.

**DMDPM.TB Me.I**

General procedure 14.3.2a was followed using DMDPM.TB (2.00 g, 8 mmol), methyl iodide (2.4 ml, 5.41 g, 38 mmol) in dimethyl sulfoxide (50 ml) to afford the desired polymer DMDPM.TB Me.I in a quantitative yield as a dark brown powder.  $\nu_{\max}$  ( $\text{cm}^{-1}$ ): 2924, 1674, 1475, 1437, 1211;  $^1\text{H}$  NMR (500 MHz,  $(\text{CD}_3)_2\text{SO}$ ):  $\delta_{\text{H}} = 6.82$  (br, m, 2H, Ar *H*), 6.57 (br, m, 2H, Ar *H*), 4.21 (br, m, 2H, N- $\text{CH}_2$ -N), 4.16 (br, m, 2H, N- $\text{CH}_2$ -Ar), 3.86 (br, m, 2H, N- $\text{CH}_2$ -Ar), 3.65 (br, m, 3H,  $\text{N}^+\text{CH}_3$ ), 2.69 (br, m, 2H,  $\text{CH}_2$ ), 2.27 (br, m, 6H, 2 Ar  $\text{CH}_3$ );  $^{13}\text{C}$  NMR (125 MHz,  $(\text{CD}_3)_2\text{SO}$ ):  $\delta_{\text{C}} = 136.94, 132.53, 129.48, 128.12, 79.68, 54.79, 22.78, 17.27$ ; BET surface area (degassed at 60 °C) = 74  $\text{m}^2/\text{g}$ ; total pore volume = 0.3400  $\text{cm}^3/\text{g}$  at ( $P/P_0 = 0.9814$ ); TGA analysis: Initial weight loss due to thermal degradation commences at ~ 100 °C with a 35% loss of mass below 400 °C, consistent with the loss of one equivalent of methyl iodide. A further 30% mass was lost below 1000 °C.

**DMEA.TB Me.I**

General procedure 14.3.2a was followed using DMEA.TB (2.00 g, 7 mmol), methyl iodide (2.1 ml, 4.73 g, 33 mmol) in dimethyl sulfoxide (ml) to afford the desired polymer DMEA.TB Me.I in a quantitative yield as a dark brown powder.  $\nu_{\max}$  ( $\text{cm}^{-1}$ ): 2904, 1610, 1405;  $^1\text{H}$  NMR (500 MHz,  $(\text{CD}_3)_2\text{SO}$ ):  $\delta_{\text{H}} = 7.47$  (br, m, 4 H, Ar *H*), 4.26 (br, m, 6H, 2 N- $\text{CH}_2$ -Ar + N- $\text{CH}_2$ -N), 2.93 (br, s, 3H,  $\text{N}^+\text{CH}_3$ ), 2.77 (br, s, 4H,  $\text{CH}_2$ ), 1.94 (br, s, 6H, 2  $\text{CH}_3$ ); BET surface area (degassed at 60 °C) = 116  $\text{m}^2/\text{g}$ ; total pore volume = 0.1013  $\text{cm}^3/\text{g}$  at ( $P/P_0 = 0.9814$ ); TGA analysis: Initial weight loss due to thermal degradation commences at ~ 100 °C with a 38% loss of mass below 400 °C, consistent with the loss of one equivalent of methyl iodide and an ethylene fragment from the ethanoanthracene unit via a retro Diels-Alder reaction<sup>172</sup>. A further 15% mass was lost below 1000 °C.

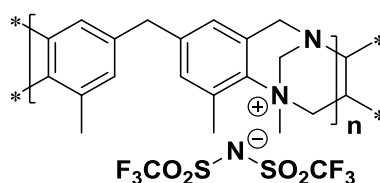
**DMEA.TB Me.F**

DMEA.TB Me.I (1.00 g, 2 mmol) was suspended in sodium fluoride solution (50 ml, 1.0 M) and the mixture was stirred for 24 h by which time the mixture had become a light brown colour. The polymer was filtered, washed with hot deionised water and dried under a stream of nitrogen. The polymer was then dried in a vacuum oven at 120 °C for 9 h to afford the desired polymer DMEA.TB Me.F in a quantitative yield.  $\nu_{\max}$  (cm<sup>-1</sup>): 2930, 2862, 1614, 1450; <sup>1</sup>H NMR (500 MHz, (CD<sub>3</sub>)<sub>2</sub>SO):  $\delta_{\text{H}}$  = 6.64 (br, m, 4 H, Ar *H*), 4.27 (br, m, 6H, 2 N-CH<sub>2</sub>-Ar + N-CH<sub>2</sub>-N), 2.43 (br, m, 3H, N<sup>+</sup>CH<sub>3</sub>), 1.52 (br, m, 10H, 2 CH<sub>2</sub> + 2 CH<sub>3</sub>); BET surface area = 454 m<sup>2</sup>/g; total pore volume = 0.3096 cm<sup>3</sup>/g at (P/P<sub>o</sub> = 0.9814); TGA analysis: Initial weight loss due to thermal degradation commences at ~ 165 °C with a 19% loss of mass below 300 °C consistent with the loss of one equivalent of methyl fluoride and an ethylene fragment from the ethanoanthracene unit via a retro Diels-Alder reaction<sup>172</sup>. A further 35% mass was lost below 1000 °C.

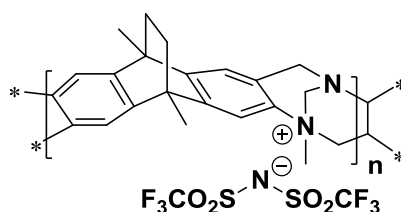
**General Procedure (14.3.2b) for Trifluoromethanesulfonimide TB Polymers**

The methyl iodide quaternerised Tröger's base polymer was suspended in a solution of lithium bistriflimide in methanol. The mixture was stirred under reflux for 16 h by which time the mixture had changed from a dark brown to a light orange suspension. The mixture was filtered, washed with hot methanol and dried under a stream of nitrogen. The polymer was refluxed in methanol for 24 h, filtered and then dried in a vacuum oven at 120 °C for 9 h to afford the desired polymer.



**DMDPM.TB Me.BTFSI**

General procedure 14.3.2b was followed using DMDPM.TB Me.I (1.00 g, 3 mmol), lithium bistriflimide (3.55 g, 12 mmol) and methanol (50 ml) to afford the desired polymer DMDPM.TB Me.BTFSI in a quantitative yield as an orange powder.  $\nu_{\max}$  ( $\text{cm}^{-1}$ ): 2939, 1739, 1477, 1442, 1350, 1192, 1057;  $^1\text{H}$  NMR (500 MHz,  $(\text{CD}_3)_2\text{CO}$ ):  $\delta_{\text{H}}$  = 6.88 (br, m, 4H, Ar *H*), 5.18 (br, m, 4H, N- $\text{CH}_2$ -Ar + N- $\text{CH}_2$ -N), 4.26 (br, m, 2H, N- $\text{CH}_2$ -Ar), 3.87 (br, s, 3H,  $\text{N}^+\text{CH}_3$ ), 2.74 (br, m, 2H,  $\text{CH}_2$ ), 2.26 (br, m, 6H, 2 Ar  $\text{CH}_3$ );  $^{13}\text{C}$  NMR (125 MHz,  $(\text{CD}_3)_2\text{CO}$ ):  $\delta_{\text{C}}$  = 131.56, 129.17, 124.49, 121.45, 118.89, 81.88, 64.52, 54.80, 54.26, 51.93, 21.97, 16.34, 16.08;  $^{19}\text{F}$  NMR (300 MHz,  $(\text{CD}_3)_2\text{CO}$ ):  $\delta_{\text{F}}$  = -79.60 (s, 6F, 2  $\text{CF}_3$ ); BET surface area = 0  $\text{m}^2/\text{g}$ ; total pore volume = 0.0089  $\text{cm}^3/\text{g}$  at ( $\text{P}/\text{P}_0 = 0.9814$ ); TGA analysis: Initial weight loss due to thermal degradation commences at  $\sim 300$   $^\circ\text{C}$  with a 57% loss of mass below 1000  $^\circ\text{C}$ .

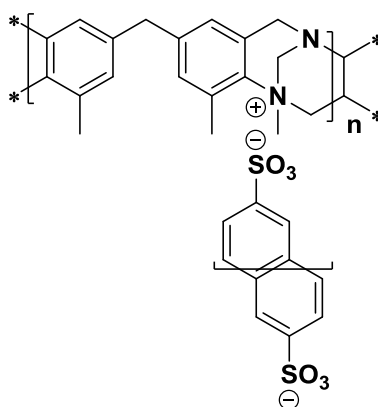
**DMEA.TB Me.BTFSI**

General procedure 14.3.2b was followed using DMEA.TB Me.I (1.00 g, 2 mmol), lithium bistriflimide (3.25 g, 11 mmol) and methanol (50 ml) to afford the desired polymer DMEA.TB Me.BTFSI in a quantitative yield as an orange powder.  $\nu_{\max}$  ( $\text{cm}^{-1}$ ): 2933, 1446, 1344, 1321, 1176, 1130, 1051;  $^1\text{H}$  NMR (500 MHz,  $(\text{CD}_3)_2\text{CO}$ ):  $\delta_{\text{H}}$  = 7.25 (br, m, 4H, Ar *H*), 5.24 (br, m, 6H, 2 N- $\text{CH}_2$ -Ar + N- $\text{CH}_2$ -N), 3.89 (br, s, 3H,  $\text{N}^+\text{CH}_3$ ), 3.23 (br, m, 10H, 2  $\text{CH}_2$  + 2  $\text{CH}_3$ );  $^{19}\text{F}$  NMR (300 MHz,  $(\text{CD}_3)_2\text{CO}$ ):  $\delta_{\text{F}}$  = -79.21 (s, 6F, 2  $\text{CF}_3$ ); BET surface area = 24  $\text{m}^2/\text{g}$ ; total pore volume = 0.0842  $\text{cm}^3/\text{g}$  at ( $\text{P}/\text{P}_0 = 0.9814$ ); TGA analysis: Initial weight loss due to thermal degradation commences at  $\sim 260$   $^\circ\text{C}$  with a 50% loss of mass below 1000  $^\circ\text{C}$ .

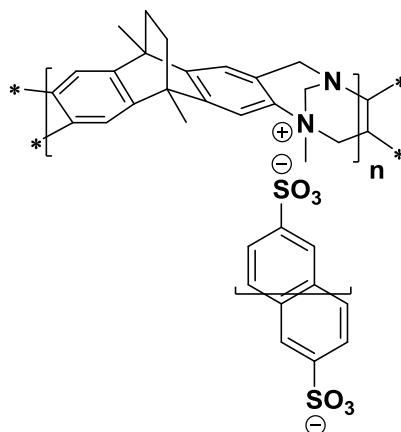
### **General Procedure (14.3.2c) for Naphthalene Disulfonic acid TB Polymers**

The methyl iodide quaternerised Tröger's base polymer was suspended in a solution of 2,6-naphthalenedisulfonic acid disodium salt in deionised water. The mixture was stirred under reflux for 16 h by which time the mixture had changed from a dark brown to an off white suspension. The mixture filtered, washed with hot deionised water and dried under a stream of nitrogen. The polymer was refluxed in methanol for 24 h, filtered and then dried in a vacuum oven at 120 °C for 9 h to afford the desired polymer.

### **DMDPM.TB Me.NDSA**



General procedure 14.3.2c was followed using DMDPM.TB Me.I (1.00 g, 3 mmol), 2,6-naphthalenedisulfonic acid disodium salt (4.10 g, 12 mmol) and deionised water (50 ml) to afford the desired polymer DMDPM.TB Me.NDSA in a quantitative yield as an off-white powder.  $\nu_{\max}$  ( $\text{cm}^{-1}$ ): 3001, 1737, 1716, 1477, 1357, 1215;  $^1\text{H}$  NMR (500 MHz,  $(\text{CD}_3)_2\text{SO}$ ):  $\delta_{\text{H}}$  = 8.05 (br, s, 1H, Naph Ar *H*), 7.73 (br, s, 1H, Naph Ar *H*), 7.66 (br, s, 1H, Naph Ar *H*), 6.93 (br, m, 4H, Ar *H*), 5.16 (br, m, 2H, N- $\text{CH}_2$ -N), 4.52 (br, m, 2H, N- $\text{CH}_2$ -Ar), 3.99 (br, m, 2H, N- $\text{CH}_2$ -Ar), 3.43 (br, s, 3H,  $\text{N}^+\text{CH}_3$ ), 2.61 (br, s, 2H,  $\text{CH}_2$ ), 2.23 (br, s, 6H, 2  $\text{CH}_3$ ); BET surface area = 0  $\text{m}^2/\text{g}$ ; total pore volume = 0.0336  $\text{cm}^3/\text{g}$  at ( $P/P_0 = 0.9814$ ); TGA analysis: Initial weight loss due to thermal degradation commences at  $\sim 300$  °C with a 55% loss of mass below 1000 °C.

**DMEA.TB Me.NDSA**

General procedure 14.3.2c was followed using DMEA.TB Me.I (1.00 g, 2 mmol), 2,6-naphthalenedisulfonic acid disodium salt (3.76 g, 11 mmol) and deionised water (50 ml) to afford the desired polymer DMEA.TB Me.NDSA in a quantitative yield as an off-white powder. The resulting powder was insoluble in all common solvents.  $\nu_{\max}$  ( $\text{cm}^{-1}$ ): 2864, 1626, 1450, 1178, 1028; BET surface area = 3  $\text{m}^2/\text{g}$ ; total pore volume = 0.3542  $\text{cm}^3/\text{g}$  at (P/P<sub>0</sub> = 0.9814); TGA analysis: Initial weight loss due to thermal degradation commences at ~ 260 °C with a 52% loss of mass below 1000 °C.

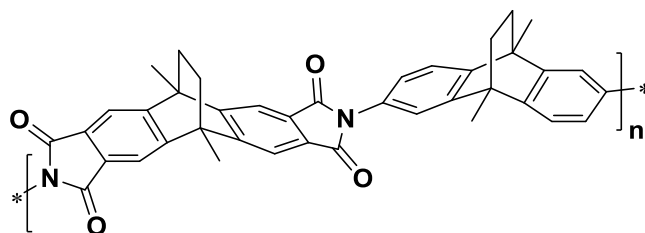
**14.3.3: Polyimides****General Procedure (14.3.3a) for Polyimide Synthesis (via ester-acid)**

(A modified procedure from literature<sup>181</sup>)

Under a nitrogen atmosphere, the bis-anhydride was dissolved in ethanol in a two-necked flask equipped with a reflux condenser. Triethylamine was injected and the mixture was refluxed for 1h. The side arm was opened to remove the solvent under a stream of nitrogen to give a light brown semi-solid. A solution of the diamine in NMP was added and the mixture was heated to 80 °C for 1 h. The side arm was opened occasionally to remove ethanol formed in the reaction. The mixture was gradually heated to 200 °C over 3 h and any water formed was removed by opening the side arm. The temperature was maintained until the desired viscosity was achieved. The mixture was cooled to room temperature and diluted with chloroform. The mixture was poured into ethanol to precipitate a light brown solid. The solid was collected by filtration, washed with ethanol and then acetone until the washings were clear. The resulting powder was dissolved in chloroform and methanol was added drop-wise until the solution became turbid. The solution was stirred for a further 30 min to precipitate a

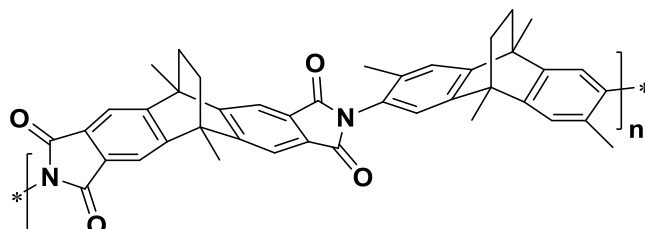
gel. The re-precipitation from chloroform was repeated twice. The polymer was dissolved in chloroform and added drop-wise to *n*-hexane with vigorous stirring and the precipitated fine powder was filtered. The light brown powder was refluxed in methanol for 24 h, filtered and then dried in a vacuum oven at 120 °C for 9 h to afford the desired polymer.

### DMEA.DMEA.PI



General procedure 14.3.3a was followed using 9,10-dimethyl-9,10-dihydro-2,6(7)-diamino-9,10-ethanoanthracene (0.8560 g, 3.24 mmol), 9,10-dimethyl-9,10-dihydro-9,10-ethanoanthracene-2,3,6,7-dianhydride (1.2121 g, 3.24 mmol), ethanol (15 ml), triethylamine (1.6383 g, 2.26 ml, 16.19 mmol) and NMP (5 ml) to afford DMEA.DMEA.PI (1.76 g, 90%) as a brown powder.  $\nu_{\max}$  (cm<sup>-1</sup>): 2962, 2900, 1774, 1712, 1363, 743; <sup>1</sup>H NMR (500 MHz, CDCl<sub>3</sub>):  $\delta_{\text{H}}$  = 7.46 (br, s, 4H, Ar *H*), 7.43 (br, s, 6H, Ar *H*), 2.01 (br, s, 8H, 4 *CH*<sub>2</sub>), 1.70 (br, s, 12H, 4 *CH*<sub>3</sub>); GPC (Chloroform):  $M_{\text{n}}$  = 21,700,  $M_{\text{w}}$  = 67,000. BET surface area = 373 m<sup>2</sup>/g; total pore volume = 0.2839 cm<sup>3</sup>/g at (P/P<sub>0</sub> = 0.9814); TGA analysis: Initial weight loss due to thermal degradation commences at ~ 260 °C with a 9% loss of mass below 400 °C consistent with the loss of an ethylene fragment from the ethanoanthracene units via a retro Diels-Alder reaction<sup>172</sup> and a further 31% mass loss below 1000 °C.

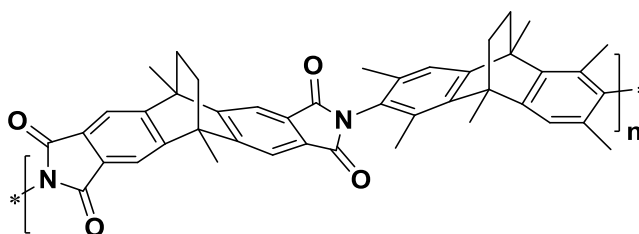
### DMEA.TMEA.PI



General procedure 14.3.3a was followed using 2,6,9,10-tetramethyl-9,10-dihydro-3,7-diamino-9,10-ethanoanthracene (0.5420 g, 1.85 mmol), 9,10-dimethyl-9,10-dihydro-9,10-ethanoanthracene-2,3,6,7-dianhydride (0.6938 g, 1.85 mmol), ethanol (15 ml), triethylamine (0.9385 g, 1.29 ml, 9.27 mmol) and NMP (5 ml) to afford DMEA.TMEA.PI (0.85 g, 73%) as

a brown powder.  $\nu_{\max}$  ( $\text{cm}^{-1}$ ): 2970, 1778, 1716, 1359, 746;  $^1\text{H}$  NMR (500 MHz,  $\text{CDCl}_3$ ):  $\delta_{\text{H}}$  = 7.88 (br, s, 4H, Ar *H*), 7.18 (br, s, 2H, Ar *H*), 6.98 (br, s, 2H, Ar *H*), 2.06 (br, s, 8H, 4  $\text{CH}_2$ ), 1.85 (br, m, 18H, 6  $\text{CH}_3$ ).  $^{13}\text{C}$  NMR (125 MHz,  $\text{CDCl}_3$ ):  $\delta_{\text{C}}$  = 167.85, 167.41, 152.18, 147.04, 144.63, 132.93, 130.38, 127.51, 123.32, 120.16, 116.35, 44.03, 41.50, 35.11, 18.65, 18.12; GPC (Chloroform):  $M_n$  = 49,400,  $M_w$  = 63,900. BET surface area = 622  $\text{m}^2/\text{g}$ ; total pore volume = 0.4606  $\text{cm}^3/\text{g}$  at ( $P/P_0$  = 0.9814); TGA analysis: Initial weight loss due to thermal degradation commences at  $\sim 260$   $^\circ\text{C}$  with a 9% loss of mass below 400  $^\circ\text{C}$  consistent with the loss of an ethylene fragment from the ethanoanthracene units via a retro Diels-Alder reaction<sup>172</sup> and a further 46% mass loss below 1000  $^\circ\text{C}$ .

### **DMEA.HMEA.PI**



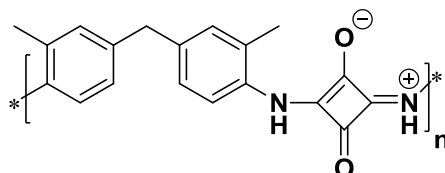
General procedure 14.3.3a was followed using a mixture of 1,3,5,7,9,10-hexamethyl-9,10-dihydro-2,6-diamino-9,10-ethanoanthracene/1,3,6,8,9,10-hexamethyl-9,10-dihydro-2,7-diamino-9,10-ethanoanthracene (0.9126 g, 2.85 mmol), 9,10-dimethyl-9,10-dihydro-9,10-ethanoanthracene-2,3,6,7-dianhydride (1.066 g, 2.85 mmol), ethanol (15 ml), triethylamine (1.4409 g, 1.98 ml, 14.24 mmol) and NMP (5 ml) to afford DMEA.HMEA.PI (1.62 g, 86%) as a brown powder.  $\nu_{\max}$  ( $\text{cm}^{-1}$ ): 2970, 1737, 1726, 1365, 748;  $^1\text{H}$  NMR (500 MHz,  $\text{CDCl}_3$ ):  $\delta_{\text{H}}$  = 7.97 (br, s, 4H, Ar *H*), 7.21 (br, m, 2H, Ar *H*), 2.18 (br, m, 32H, 4  $\text{CH}_2$  + 8  $\text{CH}_3$ ).  $^{13}\text{C}$  NMR (125 MHz,  $\text{CDCl}_3$ ):  $\delta_{\text{C}}$  = 168.03, 152.28, 130.36, 128.26, 116.47, 44.80, 44.19, 18.65, 15.81; GPC (Chloroform):  $M_n$  = 19,300,  $M_w$  = 28,100. BET surface area = 694  $\text{m}^2/\text{g}$ ; total pore volume = 0.6418  $\text{cm}^3/\text{g}$  at ( $P/P_0$  = 0.9814); TGA analysis: Initial weight loss due to thermal degradation commences at  $\sim 260$   $^\circ\text{C}$  with a 9% loss of mass below 400  $^\circ\text{C}$  consistent with the loss of an ethylene fragment from the ethanoanthracene units via a retro Diels-Alder reaction<sup>172</sup> and a further 30% mass loss below 1000  $^\circ\text{C}$ .

### 14.3.4 Polysquaraines

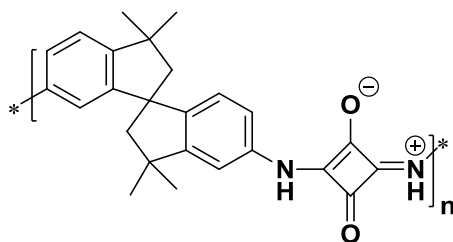
#### General Procedure (14.3.4a) for Polysquaraine Polymers

Under a nitrogen atmosphere, the corresponding diamino monomer and 3,4-dihydroxy-3-cyclobutene-1,2-dione (squaric acid) were suspended in anhydrous dimethyl sulfoxide. The mixture was heated to 120 °C for 12 h to give a viscous bright yellow solution. The mixture was poured into ethanol, filtered and washed with hot ethanol until washings were clear. The resulting yellow powder was dissolved in dimethyl sulfoxide and ethanol was added dropwise until the solution became turbid. The solution was stirred for a further 30 min and the precipitated powder was filtered. The yellow powder was refluxed in methanol for 24 h, filtered and then dried in a vacuum oven at 120 °C for 9 h to afford the desired polymer.

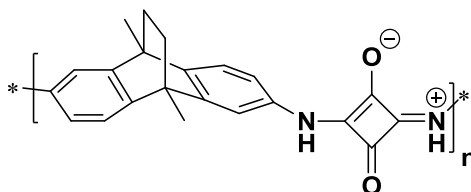
#### DMDPM.PSQU



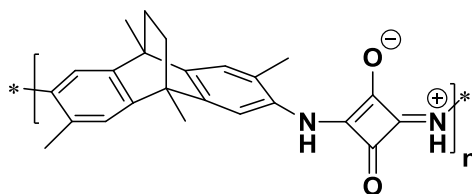
General procedure 14.3.4a was followed using 4,4'-diamino-3,3'-dimethylphenylmethane (1.00 g, 4.42 mmol), 3,4-dihydroxy-3-cyclobutene-1,2-dione (0.5039 g, 4.42 mmol) and anhydrous dimethyl sulfoxide (20 ml) to afford DMDPM.PSQU (1.2932 g, 96%) as a bright yellow powder.  $\nu_{\max}$  (cm<sup>-1</sup>): 2943, 1604, 1531, 1394; <sup>1</sup>H NMR (500 MHz, (CD<sub>3</sub>)<sub>2</sub>SO):  $\delta_{\text{H}}$  = 10.74 (br, s, 1H, N<sup>+</sup>H), 9.35 (br, s, 1H, NH), 7.06 (br, m, 6H, Ar H), 3.19 (br, s, 2H, CH<sub>2</sub>), 2.26 (br, s, 6H, 2 CH<sub>3</sub>); BET surface area 45 m<sup>2</sup>/g; total pore volume = 0.3366 cm<sup>3</sup>/g at (P/P<sub>0</sub> = 0.9814); TGA analysis: Initial weight loss due to thermal degradation commences at ~ 300 °C with a 19% loss of mass below 400 °C and a further 37% mass loss below 1000 °C.

**SBI.PSQU**

General procedure 14.3.4a was followed using 6,(7),6',(7')-diamino-3,3,3',3'-tetramethyl-1,1'-spirobisindane (1.00 g, 3.27 mmol), 3,4-dihydroxy-3-cyclobutene-1,2-dione (0.3734 g, 3.27 mmol) and anhydrous dimethyl sulfoxide (20 ml) to afford SBI.PSQU (1.2493 g, 99%) as a bright yellow powder.  $\nu_{\max}$  ( $\text{cm}^{-1}$ ): 2995, 1599, 1532, 1408;  $^1\text{H}$  NMR (500 MHz,  $(\text{CD}_3)_2\text{SO}$ ):  $\delta_{\text{H}}$  = 11.07 (br, s, 1H,  $\text{N}^+\text{H}$ ), 9.58 (br, s, 1H,  $\text{NH}$ ), 7.04 (br, m, 6H, Ar  $H$ ), 2.06 (br, m, 4H, 2  $\text{CH}_2$ ), 1.06 (br, s, 12H, 4  $\text{CH}_3$ ); BET surface area 62  $\text{m}^2/\text{g}$ ; total pore volume = 0.4036  $\text{cm}^3/\text{g}$  at ( $\text{P}/\text{P}_0 = 0.9814$ ); TGA analysis: Initial weight loss due to thermal degradation commences at  $\sim 300$   $^\circ\text{C}$  with a 53% loss of mass below 1000  $^\circ\text{C}$ .

**DMEA.PSQU**

General procedure 14.3.4a was followed using 9,10-dimethyl-9,10-dihydro-2,6(7)-diamino-9,10-ethanoanthracene (1.2024g, 4.57 mmol), 3,4-dihydroxy-3-cyclobutene-1,2-dione (0.5207 g, 4.57 mmol) and anhydrous dimethyl sulfoxide (20 ml) to afford DMEA.PSQU (1.538 g, 99%) as a bright yellow powder.  $\nu_{\max}$  ( $\text{cm}^{-1}$ ): 2958, 1597, 1529, 1406;  $^1\text{H}$  NMR (500 MHz,  $(\text{CD}_3)_2\text{SO}$ ):  $\delta_{\text{H}}$  = 9.84 (br, s, 1H,  $\text{N}^+\text{H}$ ), 7.92 (br, s, 1H,  $\text{NH}$ ), 7.47 (br, s, 2H, Ar  $H$ ), 7.17 (br, s, 4H, Ar  $H$ ), 1.87 (br, s, 6H, 2  $\text{CH}_3$ ), 1.52 (br, s, 4H, 2  $\text{CH}_2$ ); BET surface area 67  $\text{m}^2/\text{g}$ ; total pore volume = 0.3264  $\text{cm}^3/\text{g}$  at ( $\text{P}/\text{P}_0 = 0.9814$ ); TGA analysis: Initial weight loss due to thermal degradation commences at  $\sim 260$   $^\circ\text{C}$  with a 43% loss of mass below 1000  $^\circ\text{C}$ .

**TMEA.PSQU**

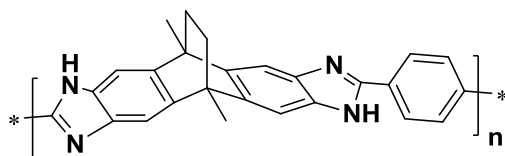
General procedure 14.3.4a was followed using 2,6,9,10-tetramethyl-9,10-dihydro-3,7-diamino-9,10-ethanoanthracene (0.9162 g, 3.14 mmol), 3,4-dihydroxy-3-cyclobutene-1,2-dione (0.3586 g, 3.14 mmol) and anhydrous dimethyl sulfoxide (20 ml) to afford TMEA.PSQU (1.1048 g, 95%) as a bright yellow powder.  $\nu_{\max}$  ( $\text{cm}^{-1}$ ): 2910, 1585, 1516, 1400;  $^1\text{H}$  NMR (500 MHz,  $(\text{CD}_3)_2\text{SO}$ ):  $\delta_{\text{H}}$  = 10.55 (br, s, 1H,  $\text{N}^+\text{H}$ ), 9.18 (br, s, 1H,  $\text{NH}$ ), 7.07 (br, m, 2H, Ar  $H$ ), 6.85 (br, m, 2H, Ar  $H$ ), 2.06 (br, s, 6H, 2 Ar  $\text{CH}_3$ ), 1.61 (br, s, 6H, 2  $\text{CH}_3$ ), 1.27 (br, s, 4H, 2  $\text{CH}_2$ ); BET surface area 68  $\text{m}^2/\text{g}$ ; total pore volume = 0.4792  $\text{cm}^3/\text{g}$  at ( $P/P_0 = 0.9814$ ); TGA analysis: Initial weight loss due to thermal degradation commences at  $\sim 260$   $^\circ\text{C}$  with a 52% loss of mass below 1000  $^\circ\text{C}$

**14.3.5: Polybenzimidazoles****General Procedure (14.3.5a) for Polybenzimidazoles**

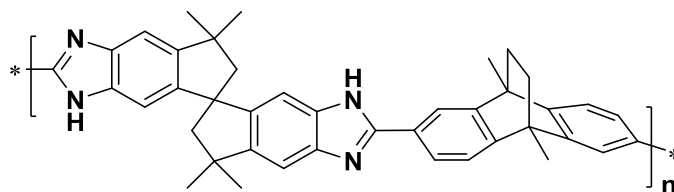
(A modified procedure from literature<sup>196</sup>)

Under a nitrogen atmosphere, the corresponding tetraamino monomer and dicarboxylic acid were suspended in polyphosphoric acid. The mixture was slowly heated to 190  $^\circ\text{C}$  over 1h and then stirred for a further 16h. The dark brown viscous mixture was cooled to room temperature, slowly poured into crushed ice and neutralised with saturated sodium bicarbonate solution. The light brown precipitate was filtered, washed with hot water and then acetone until washings were clear. The powder was refluxed in methanol for 24 h, filtered and then dried in a vacuum oven at 120  $^\circ\text{C}$  for 9 h to afford the desired polymer.

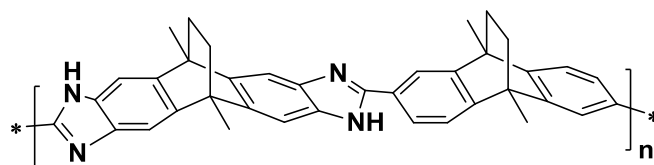


**DMEA.Benz.PBI**

General procedure 14.3.5a was followed using 9,10-dimethyl-9,10-dihydro-2,3,6,7-tetraamino-9,10-ethanoanthracene (2.0145 g, 6.8 mmol), benzene-1,4-dicarboxylic acid (1.1368 g, 6.8 mmol) and polyphosphoric acid (50 ml) to afford DMEA.Benz.PBI (2.58 g, 97%) as a dark brown powder.  $\nu_{\max}$  ( $\text{cm}^{-1}$ ): 3026, 2962, 1587, 1377;  $^1\text{H}$  NMR (500 MHz,  $\text{CF}_3\text{CO}_2\text{D}$ ):  $\delta_{\text{H}} = 9.43$  (br, m, 4H, Ar *H*), 8.90 (br, s, 4H, Ar *H*), 3.30 (br, m, 10H, 2  $\text{CH}_3$  + 2  $\text{CH}_2$ );  $^{13}\text{C}$  NMR (125 MHz,  $\text{CF}_3\text{CO}_2\text{D}$ ):  $\delta_{\text{C}} = 147.15, 145.84, 131.32, 129.28, 128.63, 127.19, 126.00, 117.56, 115.30, 113.04, 110.79, 105.99, 42.49, 34.08, 17.13$ ; BET surface area 1  $\text{m}^2/\text{g}$ ; total pore volume = 0.0140  $\text{cm}^3/\text{g}$  at ( $\text{P}/\text{P}_0 = 0.9814$ ); TGA analysis: Initial weight loss due to thermal degradation commences at  $\sim 200$   $^\circ\text{C}$  with a 28% mass loss below 1000  $^\circ\text{C}$ .

**SBI.DMEA.PBI**

General procedure 14.3.5a was followed using 6,6',7,7'-tetraamino-3,3,3',3'-tetramethyl-1,1'-spirobisindane (2.0045 g, 6.0 mmol), 9,10-dimethyl-9,10-dihydro-2,6-dicarboxyl-9,10-ethanoanthracene (1.9204 g, 6.0 mmol) and polyphosphoric acid (50 ml) to afford SBI.DMEA.PBI (3.29 g, 94%) as a dark brown powder.  $\nu_{\max}$  ( $\text{cm}^{-1}$ ): 2941, 2814, 1440, 1381;  $^1\text{H}$  NMR (500 MHz,  $\text{CF}_3\text{CO}_2\text{D}$ ):  $\delta_{\text{H}} = 9.15$  (br, m, 7H, Ar *H*), 8.86 (br, m, 3H, Ar *H*), 3.78 (br, m, 2H,  $\text{CH}_2$ ), 3.29 (br, m, 6H, 3  $\text{CH}_2$ ), 2.72 (br, m, 18H, 6  $\text{CH}_3$ ); BET surface area = 10  $\text{m}^2/\text{g}$ ; total pore volume = 0.0289  $\text{cm}^3/\text{g}$  at ( $\text{P}/\text{P}_0 = 0.9814$ ); TGA analysis: Initial weight loss due to thermal degradation commences at  $\sim 200$   $^\circ\text{C}$  with a 17% loss of mass below 400  $^\circ\text{C}$  and a further 48% mass loss below 1000  $^\circ\text{C}$ .

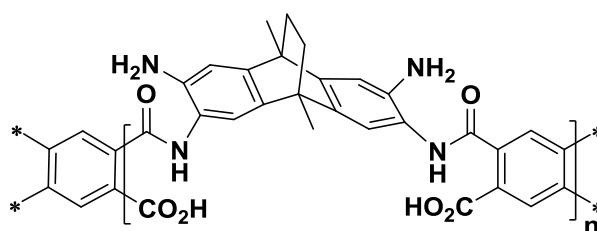
**DMEA.DMEA.PBI**

General procedure 14.3.5a was followed using 9,10-dimethyl-9,10-dihydro-2,3,6,7-tetraamino-9,10-ethanoanthracene (2.0030 g, 6.8 mmol), 9,10-dimethyl-9,10-dihydro-2,6-dicarboxyl-9,10-ethanoanthracene (2.1932 g, 6.8 mmol) and polyphosphoric acid (50 ml) to afford DMEA.DMEA.PBI (3.56 g, 96%) as a dark brown powder.  $\nu_{\max}$  ( $\text{cm}^{-1}$ ): 3051, 1608, 1444, 1045;  $^1\text{H NMR}$  (500 MHz,  $\text{CF}_3\text{CO}_2\text{D}$ ):  $\delta_{\text{H}}$  = 7.14 (br, m, 10H, Ar *H*), 1.55 (br, s, 6H, 2  $\text{CH}_3$ ), 1.50 (br, s, 6H, 2  $\text{CH}_3$ ), 1.89 (br, m, 8H, 4  $\text{CH}_2$ ); BET surface area = 29  $\text{m}^2/\text{g}$ ; total pore volume = 0.0990  $\text{cm}^3/\text{g}$  at ( $P/P_0 = 0.9814$ ); TGA analysis: Initial weight loss due to thermal degradation commences at  $\sim 200$   $^{\circ}\text{C}$  with a 21% loss of mass below 600  $^{\circ}\text{C}$  and a further 29% mass loss below 1000  $^{\circ}\text{C}$ .

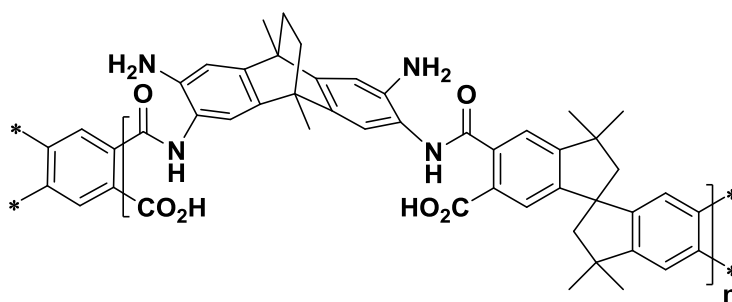
**14.3.6: Polyamide Amino Acids****General Procedure (14.3.6a) for Polyamide amino acids**

(A modified procedure from literature<sup>206</sup>)

Under a nitrogen atmosphere, the corresponding tetraamine hydrochloride salt was dissolved in anhydrous dimethyl sulfoxide and the solution was cooled in an ice bath. A solution of the corresponding dianhydride monomer in anhydrous pyridine and dimethyl sulfoxide was added drop-wise over 2 h. The yellow mixture was stirred for 1 h at which point the mixture had become viscous. The mixture was quenched in water, filtered and the precipitate was washed with hot deionised water followed by ethanol. The powder was refluxed in methanol for 24 h, filtered and then dried in a vacuum oven at 70  $^{\circ}\text{C}$  for 9 h to afford the desired polymer.

**DMEA.Benz.PAAA**

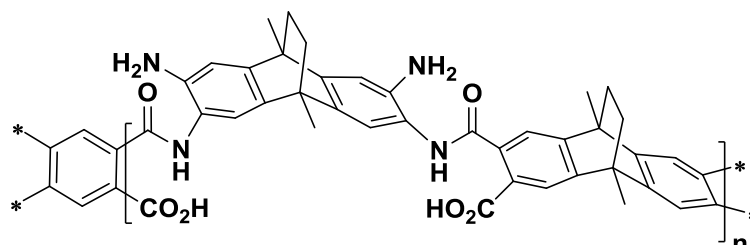
General procedure 14.3.6a was followed 9,10-dimethyl-9,10-dihydro-2,3,6,7-tetraamino-9,10-ethanoanthracene hydrochloride (1.0000 g, 2.27 mmol) in anhydrous dimethyl sulfoxide (10 ml), benzene-1,2,4,5-dianhydride (0.4955 g, 2.27 mmol) in anhydrous pyridine (0.7 ml, 0.7187 g, 9.09 mmol) and dimethyl sulfoxide (10 ml) to afford DMEA.Benz.PAAA (1.1401 g, 98%) as a yellow powder.  $\nu_{\max}$  ( $\text{cm}^{-1}$ ): 2956, 1734, 1628, 1345;  $^1\text{H}$  NMR (500 MHz,  $\text{CF}_3\text{CO}_2\text{D}$ ):  $\delta_{\text{H}}$  = 9.74 (br, m, 4H, Ar *H*), 8.88 (br, m, 2H, Ar *H*), 3.29 (br, s, 4H, 2  $\text{CH}_2$ ), 3.05 (br, s, 3H,  $\text{CH}_3$ ), 2.63 (br, s, 3H,  $\text{CH}_3$ ); BET surface area = 0  $\text{m}^2/\text{g}$ ; TGA analysis: Initial weight loss due to thermal degradation commences at  $\sim 150$   $^{\circ}\text{C}$  with a mass loss of 20% below 400  $^{\circ}\text{C}$  consistent with combined water loss from imide and pyrrolone formation and the loss of an ethylene fragment from the ethanoanthracene unit via a retro Diels-Alder reaction<sup>172</sup>. A further 36% mass was lost below 1000 $^{\circ}\text{C}$ .

**DMEA.SBI.PAAA**

General procedure 14.3.6a was followed using 9,10-dimethyl-9,10-dihydro-2,3,6,7-tetraamino-9,10-ethanoanthracene hydrochloride (1.0000 g, 2.27 mmol) in anhydrous dimethyl sulfoxide (10 ml), 3,3,3',3'-octamethyl-1,1'-spirobisindane-6,6',7,7'-dianhydride (0.9459 g, 2.27 mmol) in anhydrous pyridine (0.7 ml, 0.7187 g, 9.09 mmol) and dimethyl sulfoxide (10 ml) to afford DMEA.SBI.PAAA (1.5901 g, 98%) as a yellow powder.  $\nu_{\max}$  ( $\text{cm}^{-1}$ ): 2954, 1720, 1583, 1344;  $^1\text{H}$  NMR (500 MHz,  $\text{CF}_3\text{CO}_2\text{D}$ ):  $\delta_{\text{H}}$  = 8.29 (br, m, 8H, Ar *H*), 3.29 (br, s, 4H,  $\text{CH}_2$ ), 2.86 (br, m, 4H,  $\text{CH}_2$ ), 2.00 (br, m, 18H, 6  $\text{CH}_3$ ); BET surface area = 0  $\text{m}^2/\text{g}$ ; TGA analysis: Initial weight loss due to thermal degradation commences at  $\sim 150$   $^{\circ}\text{C}$

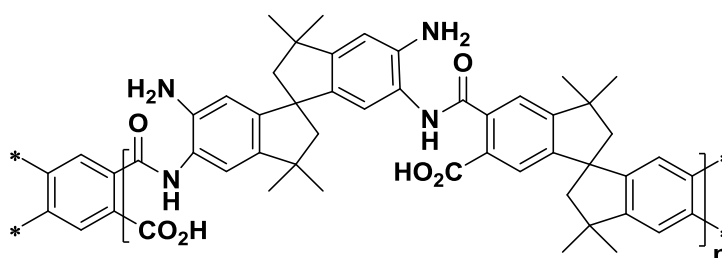
with a mass loss of 18% below 400 °C consistent with combined water loss from imide and pyrrolone formation and the loss of an ethylene fragment from the ethanoanthracene unit via a retro Diels-Alder reaction<sup>172</sup>. A further 39% mass was lost below 1000°C.

### DMEA.DMEA.PAAA



General procedure 14.3.6a was followed using 9,10-dimethyl-9,10-dihydro-2,3,6,7-tetraamino-9,10-ethanoanthracene hydrochloride (1.1760 g, 2.67 mmol) in anhydrous dimethyl sulfoxide (10 ml), 9,10-dimethyl-9,10-dihydro-9,10-ethanoanthracene-2,3,6,7-dianhydride (1.0000 g, 2.67 mmol) in anhydrous pyridine (0.9 ml, 0.8452 g, 10.69 mmol) and dimethyl sulfoxide (10 ml) to afford DMEA.DMEA.PAAA (2.6300 g, 98%) as a yellow powder.  $\nu_{\max}$  (cm<sup>-1</sup>): 2962, 1776, 1722, 1591, 1379; <sup>1</sup>H NMR (500 MHz, CF<sub>3</sub>CO<sub>2</sub>D):  $\delta_{\text{H}}$  = 8.97 (br, m, 8H, Ar H), 3.38 (br, m, 12H, 4 CH<sub>3</sub>), 2.96 (br, s, 8H, 4 CH<sub>2</sub>); BET surface area = 0 m<sup>2</sup>/g; TGA analysis: Initial weight loss due to thermal degradation commences at ~ 150 °C with a mass loss of 19% below 400 °C consistent with combined water loss from imide and pyrrolone formation and the loss of an ethylene fragment from the ethanoanthracene unit via a retro Diels-Alder reaction<sup>172</sup>. A further 23% mass was lost below 1000°C.

### SBL.SBL.PAAA



General procedure 14.3.6a was followed using 6,6',7,7'-tetraamino-3,3,3',3'-tetramethyl-1,1'-spirobisindane hydrochloride (1.0000 g, 2.07 mmol) in anhydrous dimethyl sulfoxide (10 ml), 3,3,3',3'-octamethyl-1,1'-spirobisindane-6,6',7,7'-dianhydride (0.8634 g, 2.07 mmol) in anhydrous pyridine (0.7 ml, 0.6559 g, 8.29 mmol) and dimethyl sulfoxide (10 ml)

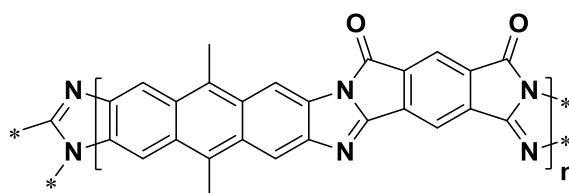
to afford SBI.SBI.PAAA (1.5436 g, 99%) as a yellow powder.  $\nu_{\max}$  ( $\text{cm}^{-1}$ ): 2955, 2864, 1778, 1716, 1363;  $^1\text{H}$  NMR (500 MHz,  $\text{CF}_3\text{CO}_2\text{D}$ ):  $\delta_{\text{H}}$  = 8.62 (br, m, 8H, Ar H), 3.48 (br, m, 8H, 4  $\text{CH}_2$ ), 2.44 (br, s, 24H, 8  $\text{CH}_3$ ); BET surface area = 0  $\text{m}^2/\text{g}$ ; TGA analysis: Initial weight loss due to thermal degradation commences at  $\sim 150$   $^{\circ}\text{C}$  with a mass loss of 9% below 400  $^{\circ}\text{C}$  consistent with combined water loss from imide and pyrrolone formation. A further 32% mass was lost below 1000 $^{\circ}\text{C}$ .

### 14.3.7: Polypyrrolones

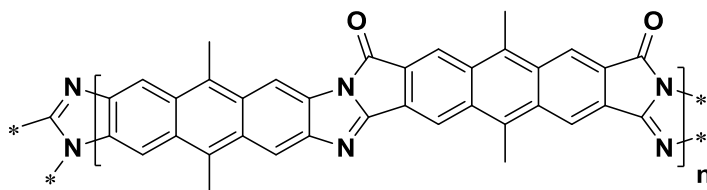
#### General Procedure (14.3.7a) for Polypyrrolones

Under a nitrogen atmosphere the polyamide amino acid precursor polymer was placed in a ceramic boat crucible and positioned inside a wire wound single zone tube furnace. The furnace was ramped 10 $^{\circ}\text{C}$  /min to 200  $^{\circ}\text{C}$  for 1 h, then 10 $^{\circ}\text{C}$  /min to 300  $^{\circ}\text{C}$  for 4 h and cooled to room temperature. The dark brown powder was refluxed in methanol for 24 h, filtered and then dried in a vacuum oven at 120  $^{\circ}\text{C}$  for 9 h to afford the desired polymer.

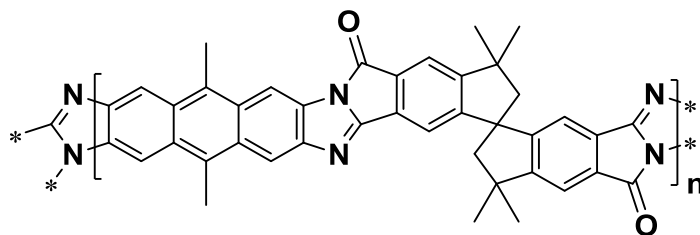
#### DMAnth.Benz.PPy



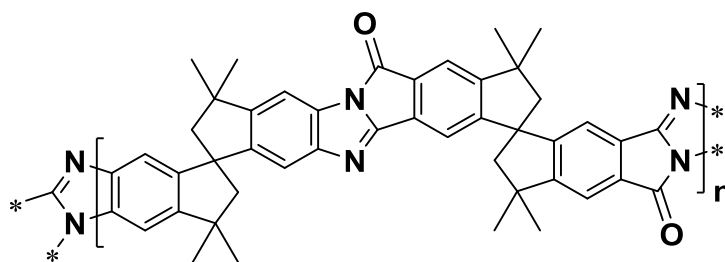
General procedure 14.3.7a was followed using DMEA.Benz.PAAA (1.00 g, 1.95 mmol) to afford the desired polymer DMAnth.Benz.PPy (0.7865 g, 98%) as a dark brown powder.  $\nu_{\max}$  ( $\text{cm}^{-1}$ ): 2047, 1782, 1732, 1620, 1338, 715;  $^{13}\text{C}$  NMR (100 MHz, solid state):  $\delta_{\text{C}}$  = 196.92 (br), 168.23 (br), 142.63 (br), 14.47 (br); BET surface area = 68  $\text{m}^2/\text{g}$ ; total pore volume = 0.2621  $\text{cm}^3/\text{g}$  at ( $P/P_0 = 0.9814$ ); TGA analysis: Initial weight loss due to thermal degradation commences at  $\sim 382$   $^{\circ}\text{C}$  with a 46% loss of mass below 1000  $^{\circ}\text{C}$ .

**DMAnth.DMAntH.PPy**

General procedure 14.3.7a was followed using DMEA.DMEA.PAAA (1.00 g, 1.50 mmol) to afford the desired polymer DManth.DMAntH.PPy (0.7984 g, 99%) as a dark brown powder.  $\nu_{\max}$  ( $\text{cm}^{-1}$ ): 2918, 1770, 1716, 1616, 1357, 743;  $^{13}\text{C}$  NMR (100 MHz, solid state):  $\delta_{\text{C}}$  = 196.43 (br), 165.63 (br), 146.30 (br), 129.17 (br), 13.35 (br); BET surface area = 45  $\text{m}^2/\text{g}$ ; total pore volume = 0.3108  $\text{cm}^3/\text{g}$  at ( $P/P_0 = 0.9814$ ); TGA analysis: Initial weight loss due to thermal degradation commences at  $\sim 477$   $^{\circ}\text{C}$  with a 29% loss of mass below 1000  $^{\circ}\text{C}$ .

**DMAnth.SBI.PPy**

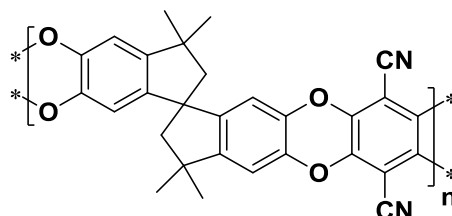
General procedure 14.3.7a was followed using DMEA.SBI.PAAA (1.00 g, 1.41 mmol) to afford the desired polymer DManth.SBI.PPy (0.8402 g, 98%) as a dark brown powder.  $\nu_{\max}$  ( $\text{cm}^{-1}$ ): 2951, 1778, 1728, 1610, 1361, 752;  $^{13}\text{C}$  NMR (100 MHz, solid state):  $\delta_{\text{C}}$  = 195.40 (br), 166.37 (br), 152.03 (br), 127.60 (br), 57.94 (br), 43.35 (br), 30.23 (br), 14.08 (br); BET surface area (powder) = 149  $\text{m}^2/\text{g}$ ; total pore volume = 0.1456  $\text{cm}^3/\text{g}$  at ( $P/P_0 = 0.9814$ ); TGA analysis: Initial weight loss due to thermal degradation commences at  $\sim 400$   $^{\circ}\text{C}$  with a 33% loss of mass below 1000  $^{\circ}\text{C}$ .

**SBI.SBI.PPy**

General procedure 14.3.7a was followed using SBI.SBI.PAAA (1.00 g, 1 mmol) to afford the desired polymer SBI.SBI.PPy (0.8926 g, 99%) as a dark brown powder.  $\nu_{\max}$  ( $\text{cm}^{-1}$ ): 2953, 1755, 1699, 1622, 1359, 785;  $^{13}\text{C}$  NMR (100 MHz, solid state):  $\delta_{\text{C}}$  = 198.28 (br), 165.78 (br), 149.97 (br), 132.25 (br), 57.75 (br), 43.40 (br), 30.67 (br); BET surface area = 284  $\text{m}^2/\text{g}$ ; total pore volume = 0.2166  $\text{cm}^3/\text{g}$  at ( $P/P_0 = 0.9814$ ); TGA analysis: Initial weight loss due to thermal degradation commences at  $\sim 480$   $^{\circ}\text{C}$  with a 26% loss of mass below 1000  $^{\circ}\text{C}$ .

**14.4: Membrane Cross-linking****PIM-1**

(Based on a procedure from literature<sup>73</sup>)

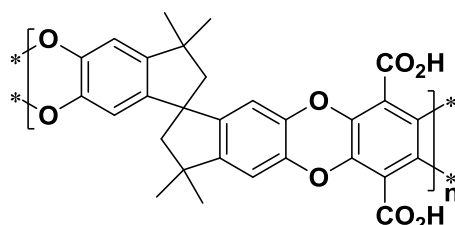


A mixture of 3,3,3',3'-tetramethyl-1,1'-spirobisindane-5,5',6,6'-tetrol (5.0000 g, 14.69 mmol), 2,3,5,6 tetrafluorophthalonitrile (2.9389 g, 14.69 mmol, recrystallised from ethanol) and anhydrous potassium carbonate (16.2390 g, 117.50 mmol) in anhydrous dimethylformamide (100 ml) was stirred at 65-70  $^{\circ}\text{C}$  for 72 h. The bright yellow mixture was cooled to room temperature, poured into water (500 ml) and stirred for 1 hr. The solid was collected by filtration, washed with water and then acetone until the washings were clear. The resulting powder was dried, dissolved in tetrahydrofuran and methanol was added drop-wise until the solution became turbid. The solution was stirred for a further 30 min to precipitate a gel. The polymer was then dissolved in tetrahydrofuran and added drop-wise to a mixture of methanol and acetone (500 ml, 1:1) with vigorous stirring and the precipitated fine powder was filtered. The powder was refluxed in methanol for 24 h, filtered and then dried in a vacuum oven at

120 °C for 9 h to afford the desired polymer (6.65 g, 92%, lit<sup>73</sup> 95%) as a bright yellow powder.  $\nu_{\max}$  (polymer film) ( $\text{cm}^{-1}$ ): 2953, 2864, 2241, 1445, 1262, 1009;  $^1\text{H NMR}$  (250 MHz,  $\text{CDCl}_3$ ):  $\delta_{\text{H}}$  = 6.81 (br, s, 2H, Ar *H*), 6.42 (br, s, 2H, Ar *H*), 1.56 (br, m, 4H, 2  $\text{CH}_2$ ), 1.31 (br, m, 12H, 4  $\text{CH}_3$ ); GPC (Chloroform):  $M_{\text{n}}$  = 60,400,  $M_{\text{w}}$  = 194,700. BET surface area = 812  $\text{m}^2/\text{g}$ ; total pore volume = 0.7648  $\text{cm}^3/\text{g}$  at ( $P/P_0 = 0.9814$ ); TGA analysis (polymer film): Initial weight loss due to thermal degradation commences at ~ 500 °C with a 87% loss of mass below 1000 °C.

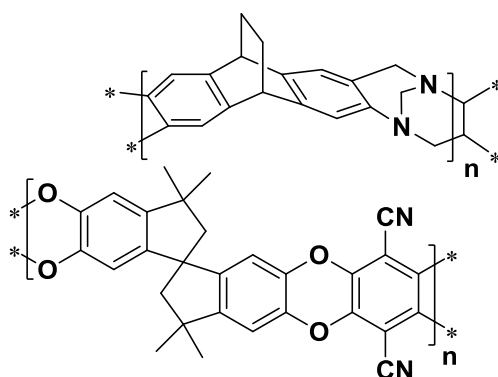
### PIM-1.CO<sub>2</sub>H

(Based on a procedure from literature<sup>93</sup>)

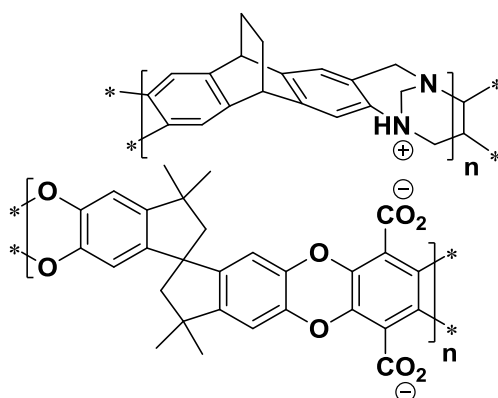


PIM-1 (1.00 g, 2 mmol) was suspended in a solution of ethanol (50 ml) and saturated sodium hydroxide solution (50 ml) and refluxed for 24 h. The dark grey mixture was filtered and refluxed in deionised water containing a few drops of hydrochloric acid (pH 4) for 1h. The light grey mixture was filtered, washed with deionised water and then acetone until washings were clear. The powder was refluxed in methanol for 24 h, and dried in a vacuum oven at 120 °C for 9 h to afford the desired polymer PIM-1.CO<sub>2</sub>H (1.02g, 94%) as a dark grey powder.  $\nu_{\max}$  ( $\text{cm}^{-1}$ ): 2949, 2855, 1672, 1601, 1487, 1437, 1314, 1003; BET surface area = 399  $\text{m}^2/\text{g}$ ; total pore volume = 0.2833  $\text{cm}^3/\text{g}$  at ( $P/P_0 = 0.9814$ ); TGA analysis: A 15% loss of weight occurred between 200-400 °C. Initial weight loss due to thermal degradation commences at ~ 400 °C with a 35% loss of mass below 1000 °C.



**PIM-1 10%.DHEA.TB 90%**

PIM-1 (0.075 g) and DHEA.TB (0.675 g) were dissolved in HPLC chloroform (10 ml) and stirred thoroughly overnight. A film was cast in a 10 cm PTFE dish in the normal manor to give a flexible light yellow film. The film was refluxed in methanol for 24 h, and dried in a vacuum oven at 120 °C for 9 h. A second sample containing PIM-1 (0.100 g) and DHEA.TB (0.900 g) in HPLC chloroform (20 ml) was precipitated into methanol and filtered. The powder was refluxed in methanol for 24 h, filtered and then dried in a vacuum oven at 120 °C for 9 h to afford a light yellow powder.  $\nu_{\max}$  (polymer film) ( $\text{cm}^{-1}$ ): 3329 (br) , 2937, 2868, 1624, 1560, 1467, 1419; BET surface area = 655  $\text{m}^2/\text{g}$ ; total pore volume = 0.4918  $\text{cm}^3/\text{g}$  at ( $P/P_0 = 0.9814$ ); TGA analysis (polymer film): Initial weight loss due to thermal degradation commences at ~ 260 °C with a 27% loss of mass below 1000 °C.

**PIM-1.CO<sub>2</sub>H 10%.DHEA.TB 90%**

One half of a film containing PIM-1 10% and DHEA.TB 90% was placed into a solution of ethanol (100 ml) and saturated sodium hydroxide solution (100 ml) and refluxed for 24 h. The film was boiled in deionised water containing a few drops of hydrochloric acid (pH 4) for 1h and then washed with deionised water. The film was refluxed in methanol for 24 h,

and dried in a vacuum oven at 120 °C for 9 h to give a flexible light orange film. A powdered sample was treated with the same procedure to afford a light orange powder.  $v_{\max}$  (polymer film) ( $\text{cm}^{-1}$ ): 3329 (br), 2939, 2868, 1618, 1475, 1433; BET surface area = 253  $\text{m}^2/\text{g}$ ; total pore volume = 0.3182  $\text{cm}^3/\text{g}$  at ( $P/P_o = 0.9814$ ); TGA analysis (polymer film): A 6% loss of weight occurred between 100-300 °C. Initial weight loss due to thermal degradation commences at ~ 300 °C with a 26% loss of mass below 1000 °C.

## **Bibliography**

1. D. A. Rouquerol, C. W. Fairbridge, D. H. Everett, J. M. Haynes, N. Pernicone, J. D. F. Ramsay, K. S. W. Sing and K. K. Unger, *Pure and Applied Chemistry*, 1994, 66, 1739-1758.
2. H. Furukawa and O. M. Yaghi, *Journal of the American Chemical Society*, 2009, 131, 8875-8883.
3. D. Zhao, D. Yuan and H.-C. Zhou, *Energy & Environmental Science*, 2008, 1, 222-235.
4. S. Sircar, W. E. Waldron, M. B. Rao and M. An, *Separation and Purification Technology*, 1999, 17, 11-20.
5. N. B. McKeown, P. M. Budd and D. Book, *Macromolecular Rapid Communications*, 2007, 28, 995-1002.
6. P. M. Budd, N. B. McKeown, B. S. Ghanem, K. J. Msayib, D. Fritsch, L. Starannikova, N. Belov, O. Sanfirova, Y. Yampolskii and V. Shantarovich, *Journal of Membrane Science*, 2008, 325, 851-860.
7. T. Masuda, E. Isobe, T. Higashimura and K. Takada, *Journal of the American Chemical Society*, 1983, 105, 7473-7474.
8. S. V. Y. s. Adymkanov, Y. P. ; Polyakov, A. M. ; Budd, P. M. ; Reynolds, K. J. ; McKeown, N. B. ; Msayib, K. J., *POLYMER SCIENCE SERIES A*, 2008, 50, 444-450
9. J. Shailaja, P. H. Lakshminarasimhan, A. R. Pradhan, R. B. Sunoj, S. Jockusch, S. Karthikeyan, S. Uppili, J. Chandrasekhar, N. J. Turro and V. Ramamurthy, *The Journal of Physical Chemistry A*, 2002, 107, 3187-3198.
10. C. C. Freyhardt, M. Tsapatsis, R. F. Lobo, K. J. Balkus and M. E. Davis, *Nature*, 1996, 381, 295-298.
11. S. M. Csicsery, *Zeolites*, 1984, 4, 202-213.
12. Y. Wang, N. B. McKeown, K. J. Msayib, G. A. Turnbull and I. D. W. Samuel, *Sensors*, 2011, 11, 2478-2487.
13. A. Dyer, T. Las and M. Zubair, *Journal of Radioanalytical and Nuclear Chemistry*, 2000, 243, 839-841.
14. J. Parmentier, F. O. M. Gaslain, O. Ersen, T. A. Centeno and L. A. Solovyov, *Langmuir*, 2013, 30, 297-307.
15. B. H. Davis and K. S. W. Sing, in *Handbook of Porous Solids*, Wiley, Hoboken, New Jersey, 2008, DOI: 10.1002/9783527618286.ch1, pp. 1-23.
16. A. Corma, M. J. Diaz-Cabanas, J. Martinez-Triguero, F. Rey and J. Rius, *Nature*, 2002, 418, 514-517.
17. Y. Zheng, X. Li and P. K. Dutta, *Sensors*, 2012, 12, 5170-5194.
18. D. J. C. Yates, *Canadian Journal of Chemistry*, 1968, 46, 1695-1701.
19. C. Quintelas, Z. Rocha, B. Silva, B. Fonseca, H. Figueiredo and T. Tavares, *Chemical Engineering Journal*, 2009, 152, 110-115.
20. H. v. B. Jansen J. C., E. M. Flanigen, P. A. Jacobs, in *Studies in Surface Science and Catalysis*, Elsevier, 2001, vol. Volume 137, pp. 175-227.
21. M. Boronat, P. M. Viruela and A. Corma, *Journal of the American Chemical Society*, 2004, 126, 3300-3309.
22. H. K. Chae, D. Y. Siberio-Perez, J. Kim, Y. Go, M. Eddaoudi, A. J. Matzger, M. O'Keeffe and O. M. Yaghi, *Nature*, 2004, 427, 523-527.
23. O. K. Farha, I. Eryazici, N. C. Jeong, B. G. Hauser, C. E. Wilmer, A. A. Sarjeant, R. Q. Snurr, S. T. Nguyen, A. Ö. Yazaydin and J. T. Hupp, *Journal of the American Chemical Society*, 2012, 134, 15016-15021.
24. Q. Yan, Y. Lin, C. Kong and L. Chen, *Chemical Communications*, 2013, 49, 6873-6875.
25. K. K. Tanabe and S. M. Cohen, *Chemical Society Reviews*, 2011, 40, 498-519.

26. P. Horcajada, T. Chalati, C. Serre, B. Gillet, C. Sebrie, T. Baati, J. F. Eubank, D. Heurtaux, P. Clayette, C. Kreuz, J.-S. Chang, Y. K. Hwang, V. Marsaud, P.-N. Bories, L. Cynober, S. Gil, G. Ferey, P. Couvreur and R. Gref, *Nature Materials*, 2010, 9, 172-178.
27. J. G. Nguyen and S. M. Cohen, *Journal of the American Chemical Society*, 2010, 132, 4560-4561.
28. M. Shah, M. C. McCarthy, S. Sachdeva, A. K. Lee and H.-K. Jeong, *Industrial & Engineering Chemistry Research*, 2011, 51, 2179-2199.
29. M. Mastalerz, *Angewandte Chemie International Edition*, 2008, 47, 445-447.
30. P. Kuhn, M. Antonietti and A. Thomas, *Angewandte Chemie International Edition*, 2008, 47, 3450-3453.
31. F. J. Uribe-Romo, J. R. Hunt, H. Furukawa, C. Klöck, M. O'Keeffe and O. M. Yaghi, *Journal of the American Chemical Society*, 2009, 131, 4570-4571.
32. A. P. Côté, A. I. Benin, N. W. Ockwig, M. O'Keeffe, A. J. Matzger and O. M. Yaghi, *Science*, 2005, 310, 1166-1170.
33. O. M. Yaghi, M. O'Keeffe, N. W. Ockwig, H. K. Chae, M. Eddaoudi and J. Kim, *Nature*, 2003, 423, 705-714.
34. H. M. El-Kaderi, J. R. Hunt, J. L. Mendoza-Cortés, A. P. Côté, R. E. Taylor, M. O'Keeffe and O. M. Yaghi, *Science*, 2007, 316, 268-272.
35. J. L. Mendoza-Cortes, T. A. Pascal and W. A. Goddard, *The Journal of Physical Chemistry A*, 2011, 115, 13852-13857.
36. S.-Y. Ding, J. Gao, Q. Wang, Y. Zhang, W.-G. Song, C.-Y. Su and W. Wang, *Journal of the American Chemical Society*, 2011, 133, 19816-19822.
37. S. S. Han, H. Furukawa, O. M. Yaghi and W. A. Goddard, *Journal of the American Chemical Society*, 2008, 130, 11580-11581.
38. R. W. Tilford, S. J. Mugavero, P. J. Pellechia and J. J. Lavigne, *Advanced Materials*, 2008, 20, 2741-2746.
39. Y. Zhou, Z. Wang, P. Yang, X. Zu and F. Gao, *Journal of Materials Chemistry*, 2012, 22, 16964-16970.
40. S. Wan, J. Guo, J. Kim, H. Ihee and D. Jiang, *Angewandte Chemie International Edition*, 2009, 48, 3207-3207.
41. H. Jüntgen, *Fuel*, 1986, 65, 1436-1446.
42. J. L. Lu, *Toxicology Letters*, 2006, 164, Supplement, S186.
43. J. R. M. Rattier, W. Gernjak, A. Joss and J. Keller, *Journal of Water Reuse and Desalination*, 2012, 2 No, 127-139
44. S. Manocha, *Sadhana*, 2003, 28, 335-348.
45. P. Ehrenfreund and B. H. Foing, *Science*, 2010, 329, 1159-1160.
46. L. Li, P. A. Quinlivan and D. R. U. Knappe, *Carbon*, 2002, 40, 2085-2100.
47. D. Hulicova-Jurcakova, M. Seredych, G. Q. Lu and T. J. Bandoz, *Advanced Functional Materials*, 2009, 19, 438-447.
48. M. E. Ramos, P. R. Bonelli, A. L. Cukierman, M. M. L. Ribeiro Carrott and P. J. M. Carrott, *Journal of Hazardous Materials*, 2010, 177, 175-182.
49. G. I. Rosenberg, A. S. Shabaeva, V. S. Moryakov, T. G. Musin, M. P. Tsyurupa and V. A. Davankov, *Reactive Polymers, Ion Exchangers, Sorbents*, 1983, 1, 175-182.
50. B. Li, R. Gong, Y. Luo and B. Tan, *Soft Matter*, 2011, 7, 10910-10916.
51. J.-H. Ahn, J.-E. Jang, C.-G. Oh, S.-K. Ihm, J. Cortez and D. C. Sherrington, *Macromolecules*, 2005, 39, 627-632.
52. C. D. Wood, B. Tan, A. Trewin, H. Niu, D. Bradshaw, M. J. Rosseinsky, Y. Z. Khimyak, N. L. Campbell, R. Kirk, E. Stöckel and A. I. Cooper, *Chemistry of Materials*, 2007, 19, 2034-2048.
53. B. C. Pan, Y. Xiong, A. M. Li, J. L. Chen, Q. X. Zhang and X. Y. Jin, *Reactive and Functional Polymers*, 2002, 53, 63-72.

54. M.-L. Chen, Y.-L. Liu, X.-W. Xing, X. Zhou, Y.-Q. Feng and B.-F. Yuan, *Chemistry – A European Journal*, 2013, 19, 1035-1041.
55. Q. Zhou, M. Wang, A. Li, C. Shuang, M. Zhang, X. Liu and L. Wu, *Frontiers of Environmental Science & Engineering*, 2013, 7, 412-419.
56. B. Li, X. Huang, L. Liang and B. Tan, *Journal of Materials Chemistry*, 2010, 20, 7444-7450.
57. Y. Jiao, F. H. Stillinger and S. Torquato, *Physical Review Letters*, 2008, 100, 245504.
58. Y. Jiao, F. H. Stillinger and S. Torquato, *Physical Review E*, 2009, 79, 041309.
59. N. T. Tsui, A. J. Paraskos, L. Torun, T. M. Swager and E. L. Thomas, *Macromolecules*, 2006, 39, 3350-3358.
60. T. M. Long and T. M. Swager, *Advanced Materials*, 2001, 13, 601-604.
61. A. Del Regno and F. R. Siperstein, *Microporous and Mesoporous Materials*, 2013, 176, 55-63.
62. J. K. E. Walker, PhD, Cardiff University, , 2011.
63. M. Heuchel, D. Fritsch, P. M. Budd, N. B. McKeown and D. Hofmann, *Journal of Membrane Science*, 2008, 318, 84-99.
64. P. M. Budd, N. B. McKeown and D. Fritsch, *Journal of Materials Chemistry*, 2005, 15, 1977-1986.
65. K. Nagai, A. Higuchi and T. Nakagawa, *Journal of Polymer Science Part B: Polymer Physics*, 1995, 33, 289-298.
66. K. D. Dorkenoo and P. H. Pfromm, *Macromolecules*, 2000, 33, 3747-3751.
67. Y. Hu, M. Shiotsuki, F. Sanda, B. D. Freeman and T. Masuda, *Macromolecules*, 2008, 41, 8525-8532.
68. H. Zhang, S. Wang and S. G. Weber, *Journal of Membrane Science*, 2013, 443, 115-123.
69. J. C. Jansen, F. Tasselli, E. Tocci and E. Drioli, *Desalination*, 2006, 192, 207-213.
70. E. S. Finkelshtein, K. L. Makovetskii, M. L. Gringolts, Y. V. Rogan, T. G. Golenko, L. E. Starannikova, Y. P. Yampolskii, V. P. Shantarovich and T. Suzuki, *Macromolecules*, 2006, 39, 7022-7029.
71. B. S. Ghanem, N. B. McKeown, P. M. Budd, J. D. Selbie and D. Fritsch, *Advanced Materials*, 2008, 20, 2766-2771.
72. B. S. Ghanem, K. J. Msayib, N. B. McKeown, K. D. M. Harris, Z. Pan, P. M. Budd, A. Butler, J. Selbie, D. Book and A. Walton, *Chemical Communications*, 2007, 67-69.
73. P. M. Budd, E. S. Elabas, B. S. Ghanem, S. Makhseed, N. B. McKeown, K. J. Msayib, C. E. Tattershall and D. Wang, *Advanced Materials*, 2004, 16, 456-459.
74. P. M. Budd, B. Ghanem, K. Msayib, N. B. McKeown and C. Tattershall, *Journal of Materials Chemistry*, 2003, 13, 2721-2726.
75. N. B. McKeown, P. M. Budd, K. J. Msayib, B. S. Ghanem, H. J. Kingston, C. E. Tattershall, S. Makhseed, K. J. Reynolds and D. Fritsch, *Chemistry – A European Journal*, 2005, 11, 2610-2620.
76. B. S. Ghanem, M. Hashem, K. D. M. Harris, K. J. Msayib, M. Xu, P. M. Budd, N. Chaukura, D. Book, S. Tedds, A. Walton and N. B. McKeown, *Macromolecules*, 2010, 43, 5287-5294.
77. N. B. McKeown, S. Makhseed and P. M. Budd, *Chemical Communications*, 2002, DOI: 10.1039/B207642J, 2780-2781.
78. H. Izumikawa, T. Masuda and T. Higashimura, *Polymer Bulletin*, 1991, 27, 193-199.
79. J. Jia and G. L. Baker, *Journal of Polymer Science Part B: Polymer Physics*, 1998, 36, 959-968.
80. R. W. Baker, *Membrane Technology and Applications*, Wiley, Hoboken, New Jersey, 2012.
81. 8056732 2011.
82. N. N. Li, A. G. Fane, W. S. W. Ho and T. Matsuura, *Advanced Membrane Technology and Applications*, Wiley, Hoboken, New Jersey, 2011.
83. N. Morlière, C. Vallières, L. Perrin and D. Roizard, *Journal of Membrane Science*, 2006, 270, 123-131.

84. M. L. Cecopieri-Gómez, J. Palacios-Alquisira and J. M. Domínguez, *Journal of Membrane Science*, 2007, 293, 53-65.
85. S. Sridhar, R. S. Veerapur, M. B. Patil, K. B. Gudasi and T. M. Aminabhavi, *Journal of Applied Polymer Science*, 2007, 106, 1585-1594.
86. W. F. Yong, F. Y. Li, T.-S. Chung and Y. W. Tong, *Journal of Materials Chemistry A*, 2013, 1, 13914-13925.
87. Y. Liu, C. Pan, M. Ding and J. Xu, *Polymer International*, 1999, 48, 832-836.
88. M. Al-Masri, H. R. Kricheldorf and D. Fritsch, *Macromolecules*, 1999, 32, 7853-7858.
89. B. S. Ghanem, N. B. McKeown, P. M. Budd, N. M. Al-Harbi, D. Fritsch, K. Heinrich, L. Starannikova, A. Tokarev and Y. Yampolskii, *Macromolecules*, 2009, 42, 7881-7888.
90. N. B. McKeown and P. M. Budd, *Chemical Society Reviews*, 2006, 35, 675-683.
91. P. M. Budd, K. J. Msayib, C. E. Tattershall, B. S. Ghanem, K. J. Reynolds, N. B. McKeown and D. Fritsch, *Journal of Membrane Science*, 2005, 251, 263-269.
92. D. Fritsch, P. Merten, K. Heinrich, M. Lazar and M. Priske, *Journal of Membrane Science*, 2012, 401-402, 222-231.
93. N. Du, G. P. Robertson, J. Song, I. Pinnau and M. D. Guiver, *Macromolecules*, 2009, 42, 6038-6043.
94. F. Y. Li, Y. Xiao, T.-S. Chung and S. Kawi, *Macromolecules*, 2012, 45, 1427-1437.
95. B. S. Ghanem, N. B. McKeown, P. M. Budd and D. Fritsch, *Macromolecules*, 2008, 41, 1640-1646.
96. Z. Sun, L. Jin, S. He, Y. Zhao, M. Wei, D. G. Evans and X. Duan, *Green Chemistry*, 2012, 14, 1909-1916.
97. E. Paez-Mozo, N. Gabriunas, R. Maggi, D. Acosta, P. Ruiz and B. Delmon, *Journal of molecular catalysis*, 1994, 91, 251-258.
98. H. Shirai, A. Maruyama, K. Kobayashi, N. Hojo and K. Urushido, *Journal of Polymer Science: Polymer Letters Edition*, 1979, 17, 661-666.
99. N. B. McKeown, *Journal of Materials Chemistry*, 2000, 10, 1979-1995.
100. H. J. Mackintosh, P. M. Budd and N. B. McKeown, *Journal of Materials Chemistry*, 2008, 18, 573-578.
101. K. K. Mohanty, *AIChE Journal*, 1992, 38, 1303-1304.
102. R. W. Smithwick, *Powder Technology*, 1982, 33, 201-209.
103. I. Langmuir, *Journal of the American Chemical Society*, 1917, 39, 1848-1906.
104. J. Szekeley, J. W. Evans and H. Y. Sohn, *Gas-solid reactions*, New York : Academic Press, 1976.
105. S. Brunauer, P. H. Emmett and E. Teller, *Journal of the American Chemical Society*, 1938, 60, 309-319.
106. I. M. K. Ismail, *Carbon*, 1990, 28, 423-434.
107. W. G. McMillan and E. Teller, *The Journal of Physical Chemistry*, 1951, 55, 17-20.
108. R. Pierotti and J. Rouquerol, *Pure and Applied Chemistry*, 1985, 57, 603-619.
109. O. Carmody, R. Frost, Y. Xi and S. Kokot, *Surface Science*, 2007, 601, 2066-2076.
110. R. W. Baker, *Membrane Separation Systems: Recent Developments and Future Directions*, Park Ridge: Noyes Data Corporation, 1991.
111. B. Freeman, Y. Yampolskii and I. Pinnau, *Materials Science of Membranes for Gas and Vapor Separation*, Wiley, Hoboken, New Jersey, 2006.
112. Y.-L. Li and K.-L. Tung, *Journal of Membrane Science*, 2008, 319, 286-297.
113. W. Echt, in *UOP Separex™ Membrane Systems*, Press Release, UOP Honeywell.
114. D. R. Paul and Y. P. Yampol'skii, *Polymeric Gas Separation Membranes*, CRC press, Boca Raton, Florida, 1993.
115. T. Matsuura, *Synthetic Membranes and Membrane Separation Processes*, CRC press, Boca Raton, Florida, 1993.
116. R. W. Baker, *Membrane Technology and Applications*, Wiley, Hoboken, New Jersey, 2004.

117. K. Kamide, S.-i. Manabe, H. Makino, T. Nohmi, H. Narita and T. Kawai, *Polymer Journal*, 1983, 15, 179-193.
118. T. Graham, *Philosophical Magazine and Journal of Science*, 1866, 401-420.
119. B. Freeman and Y. Yampolskii, *Membrane Gas Separation*, Wiley, Hoboken, New Jersey, 2011.
120. H. L. Frisch, *Journal of Applied Polymer Science*, 1970, 14, 1657-1657.
121. W. R. Vieth, J. M. Howell and J. H. Hsieh, *Journal of Membrane Science*, 1976, 1, 177-220.
122. D. W. Breck, *Zeolite molecular sieves: structure, chemistry, and use*, Wiley, Hoboken, New Jersey, 1973.
123. B. I. Baker. R.W, *Chemtech*, 1986, 16, 232.
124. M. Mulder, *Basic Principles of Membrane Technology*, Springer, New York, 1996.
125. K. Mohanty and M. K. Purkait, *Membrane Technologies and Applications*, CRC press, Boca Raton, Florida, 2011.
126. L. M. Robeson, *Journal of Membrane Science*, 1991, 62, 165-185.
127. L. M. Robeson, *Journal of Membrane Science*, 2008, 320, 390-400.
128. M. Macchione, J. C. Jansen, G. De Luca, E. Tocci, M. Longeri and E. Drioli, *Polymer*, 2007, 48, 2619-2635.
129. J. C. Jansen, K. Friess and E. Drioli, *Journal of Membrane Science*, 2011, 367, 141-151.
130. L. Liu, A. Chakma, X. Feng and D. Lawless, *The Canadian Journal of Chemical Engineering*, 2009, 87, 456-465.
131. D. G. Pye, H. H. Hoehn and M. Panar, *Journal of Applied Polymer Science*, 1976, 20, 287-301.
132. C. R. Mason, L. Maynard-Atem, K. W. J. Heard, B. Satilmis, P. M. Budd, K. Friess, M. Lanč, P. Bernardo, G. Clarizia and J. C. Jansen, *Macromolecules*, 2014, 47, 1021-1029.
133. C. R. Mason, L. Maynard-Atem, N. M. Al-Harbi, P. M. Budd, P. Bernardo, F. Bazzarelli, G. Clarizia and J. C. Jansen, *Macromolecules*, 2011, 44, 6471-6479.
134. H. B. Park, S. H. Han, C. H. Jung, Y. M. Lee and A. J. Hill, *Journal of Membrane Science*, 2010, 359, 11-24.
135. M. Calle and Y. M. Lee, *Macromolecules*, 2011, 44, 1156-1165.
136. M. Hojo, T. Ichi and K. Shibato, *Journal of Organic Chemistry*, 1985, 50, 1478-1482.
137. K. S. Khuong, W. H. Jones, W. A. Pryor and K. N. Houk, *Journal of the American Chemical Society*, 2005, 127, 1265-1277.
138. A. Hoffman, *Journal of the American Chemical Society*, 1929, 51, 2542-2547.
139. L. R. C. Barclay and R. A. Chapman, *Canadian Journal of Chemistry*, 1964, 42, 25-35.
140. R. M. Roberts and M. B. Abdel-Baset, *The Journal of Organic Chemistry*, 1976, 41, 1698-1701.
141. S. J. Cristol and N. L. Hause, *Journal of the American Chemical Society*, 1952, 74, 2193-2197.
142. P. Yates and P. Eaton, *Journal of the American Chemical Society*, 1960, 82, 4436-4437.
143. L. R. C. Barclay and R. A. Chapman, *Canadian Journal of Chemistry*, 1965, 43, 1754-1760.
144. F. K. Fujikawa F, Tadayuki *Journal of the Pharmaceutical Society of Japan*, 1944, 64, 7.
145. J. V. Crivello, *The Journal of Organic Chemistry*, 1981, 46, 3056-3060.
146. M. Mastalerz, S. Sieste, M. Cenić and I. M. Oppel, *The Journal of Organic Chemistry*, 2011, 76, 6389-6393.
147. A. Furst and R. E. Moore, *Journal of the American Chemical Society*, 1957, 79, 5492-5493.
148. M. A. Rabjohns, P. Hodge and P. A. Lovell, *Polymer*, 1997, 38, 3395-3407.
149. M. M. Faul and O. R. Thiel, in *Encyclopedia of Reagents for Organic Synthesis*, Wiley, Hoboken, New Jersey, 2001.
150. Tröger.J, *Journal für Praktische Chemie*, 1887, 36, 225-245.
151. M. A. Spielman, *Journal of the American Chemical Society*, 1935, 57, 583-585.
152. S. B. Larson and C. S. Wilcox, *Acta Crystallographica Section C*, 1986, 42, 224-227.
153. S. Sergeev, *Helvetica Chimica Acta*, 2009, 92, 415-444.

154. P. S. Kalsi, *Stereochemistry Conformation and Mechanism*, New Age International, New Delhi, 2005.
155. B. M. Wepster, *Recueil des Travaux Chimiques des Pays-Bas*, 1953, 72, 661-672.
156. E. Marquis, J. Graton, M. Berthelot, A. Planchat and C. Laurence, *Canadian Journal of Chemistry*, 2004, 82, 1413-1422.
157. Ö. V. Rúnarsson, J. Artacho and K. Wärnmark, *European Journal of Organic Chemistry*, 2012, 2012, 7015-7041.
158. E. Poli, E. b. Merino, U. Díaz, D. Brunel and A. Corma, *The Journal of Physical Chemistry C*, 2011, 115, 7573-7585.
159. X. Du, Y. Sun, B. Tan, Q. Teng, X. Yao, C. Su and W. Wang, *Chemical Communications*, 2010, 46, 970-972.
160. L. Peters, A. Hussain, M. Follmann, T. Melin and M. B. Hägg, *Chemical Engineering Journal*, 2011, 172, 952-960.
161. M. Fukae and T. Inazu, *Journal of inclusion phenomena*, 1984, 2, 223-229.
162. R. A. Johnson, R. R. Gorman, R. J. Wnuk, N. J. Crittenden and J. W. Aiken, *Journal of Medicinal Chemistry*, 1993, 36, 3202-3206.
163. U. Maitra, B. G. Bag, P. Rao and D. Powell, *Journal of the Chemical Society, Perkin Transactions 1*, 1995, 2049-2056.
164. B. G. Bag and U. Maitra, *Synthetic Communications*, 1995, 25, 1849-1856.
165. E. C. Wagner, *Journal of the American Chemical Society*, 1935, 57, 1296-1298.
166. E. C. Wagner, *The Journal of Organic Chemistry*, 1954, 19, 1862-1881.
167. W. V. Farrar, *Journal of Applied Chemistry*, 1964, 14, 389-399.
168. C. A. M. Abella, M. Benassi, L. S. Santos, M. N. Eberlin and F. Coelho, *The Journal of Organic Chemistry*, 2007, 72, 4048-4054.
169. WO2012035328 A1 M. Carta, M. Croad and N. B. McKeown, 2010.
170. A. Abdolmaleki, S. Heshmat-Azad and M. Kheradmand-fard, *Journal of Applied Polymer Science*, 2011, 122, 282-288.
171. B. Dolensky, M. Havlik and V. Kral, *Chemical Society Reviews*, 2012, 41, 3839-3858.
172. Y. Chung, B. F. Duerr, T. A. McKelvey, P. Nanjappan and A. W. Czarnik, *The Journal of Organic Chemistry*, 1989, 54, 1018-1032.
173. M. Carta, R. Malpass-Evans, M. Croad, Y. Rogan, J. C. Jansen, P. Bernardo, F. Bazzarelli and N. B. McKeown, *Science*, 2013, 339, 303-307.
174. M. S. McCaig and D. R. Paul, *Polymer*, 2000, 41, 629-637.
175. R. Uddin, P. Hodge, M. S. Chisholm and P. Eustace, *Journal of Materials Chemistry*, 1996, 6, 527-532.
176. A. H. Frazer, B. C. Anderson, L. C. Garver and T. Fukunaga, *Journal of Polymer Science: Polymer Chemistry Edition*, 1985, 23, 2779-2790.
177. Y. Leng, J. Liu, P. Jiang and J. Wang, *Catalysis Communications*, 2013, 40, 84-87.
178. J. Zaidi and T. Matsuura, *Polymer Membranes for Fuel Cells*, Springer, New York, 2010.
179. D. A. Lenev, D. G. Golovanov, K. A. Lyssenko and R. G. Kostyanovsky, *Tetrahedron: Asymmetry*, 2006, 17, 2191-2194.
180. J. C. Jansen, K. Friess, G. Clarizia, J. Schauer and P. Izák, *Macromolecules*, 2010, 44, 39-45.
181. T. M. Moy, C. D. DePorter and J. E. McGrath, *Polymer*, 1993, 34, 819-824.
182. Y.-C. Kung and S.-H. Hsiao, *Journal of Materials Chemistry*, 2011, 21, 1746-1754.
183. L. B. Nohara, M. L. Costa, M. A. Alves, M. F. K. Takahashi, E. L. Nohara and M. C. Rezende, *Materials Research*, 2010, 13, 245-252.
184. H. E. Sprenger and W. Ziegenbein, *Angewandte Chemie International Edition in English*, 1966, 5, 894-894.
185. A. Nagai, X. Chen, X. Feng, X. Ding, Z. Guo and D. Jiang, *Angewandte Chemie International Edition*, 2013, 52, 3770-3774.



186. A. Treibs and K. Jacob, *Angewandte Chemie International Edition in English*, 1965, 4, 694-694.
187. E. Terpetschnig and J. R. Lakowicz, *Dyes and Pigments*, 1993, 21, 227-234.
188. E. Terpetschnig, H. Szmecinski and J. Lakowicz, *Journal of Fluorescence*, 1993, 3, 153-155.
189. V. E. de Oliveira, G. S. de Carvalho, M. I. Yoshida, C. L. Donnici, N. L. Speziali, R. Diniz and L. F. C. de Oliveira, *Journal of Molecular Structure*, 2009, 936, 239-249.
190. E. E. Havinga, W. ten Hoeve and H. Wynberg, *Synthetic Metals*, 1993, 55, 299-306.
191. D. E. Lynch, U. Geissler and K. A. Byriel, *Synthetic Metals*, 2001, 124, 385-391.
192. C. Prabhakar, K. Bhanuprakash, V. J. Rao, M. Balamuralikrishna and D. N. Rao, *The Journal of Physical Chemistry C*, 2010, 114, 6077-6089.
193. W.-J. Lee, D.-S. Kim and J.-H. Kim, *Korean Journal of Chemical Engineering*, 2000, 17, 143-148.
194. H. Vogel and C. S. Marvel, *Journal of Polymer Science*, 1961, 50, 511-539.
195. W. Wrasidlo and H. H. Levine, *Journal of Polymer Science Part A: General Papers*, 1964, 2, 4795-4808.
196. L. Xiao, H. Zhang, E. Scanlon, L. S. Ramanathan, E.-W. Choe, D. Rogers, T. Apple and B. C. Benicewicz, *Chemistry of Materials*, 2005, 17, 5328-5333.
197. N. Fahl and M. Faile, in *High-Tech Fibrous Materials*, American Chemical Society, Michigan, 1991, vol. 457, ch. 14, pp. 238-247.
198. M. Tan, H. J. Davis, U. S. O. o. W. Research, Technology and C. R. Company, *High Flux PBI Reverse Osmosis Membranes for Desalination and Water Reuse: Final Report*, Celanese Research Company, New York, 1978.
199. D. R. Pesiri, B. Jorgensen and R. C. Dye, *Journal of Membrane Science*, 2003, 218, 11-18.
200. F. Dawans and C. S. Marvel, *Journal of Polymer Science Part A: General Papers*, 1965, 3, 3549-3571.
201. V. L. Bell and G. F. Pezdirtz, *Journal of Polymer Science Part B: Polymer Letters*, 1965, 3, 977-984.
202. J. G. Colson, R. H. Michel and R. M. Paufler, *Journal of Polymer Science Part A-1: Polymer Chemistry*, 1966, 4, 2349-2349.
203. L. E. Karre, Keller, L.B., Miller, L.J., *Development and processing of pyrrolic polymers*, National Aeronautics and Space Administration, Langley research center, 1969.
204. C. M. Zimmerman and W. J. Koros, *Journal of Polymer Science Part B: Polymer Physics*, 1999, 37, 1235-1249.
205. R. L. Burns and W. J. Koros, *Macromolecules*, 2003, 36, 2374-2381.
206. N. V. L. Bell G. F. Pezdirtz, *ACS Presentation*, 1965.
207. L. M. Costello, D. R. B. Walker and W. J. Koros, *Journal of Membrane Science*, 1994, 90, 117-130.
208. B. Garrigues, C. Laporte, R. Laurent, A. Laporterie and J. Dubac, *Liebigs Annalen*, 1996, 1996, 739-741.
209. S. Alibert, C. Santelli-Rouvier, M. Castaing, M. Berthelot, G. Spengler, J. Molnar and J. Barbe, *European Journal of Medicinal Chemistry*, 2003, 38, 253-263.
210. S. A. Rao and M. Periasamy, *Tetrahedron Letters*, 1988, 29, 1583-1586.
211. I. V. Farr, D. Kratzner, T. E. Glass, D. Dunson, Q. Ji and J. E. McGrath, *Journal of Polymer Science Part A: Polymer Chemistry*, 2000, 38, 2840-2854.

## Publications

- **An Efficient Polymer Molecular Sieve for Membrane Gas Separations.** Mariolino Carta, Richard Malpass-Evans, Matthew Croad, Yulia Rogan, Johannes C. Jansen, Paola Bernardo, Fabio Bazzarelli and Neil B. McKeown: *Science*, 2013, 339, 6117, 303-307.
- **Polymers of intrinsic microporosity in electrocatalysis: Novel pore rigidity effects and lamella palladium growth.** Fengjie Xiaa, Mu Pana, Shichun Mua, Richard Malpass-Evans, Mariolino Carta, Neil B. McKeown, Gary A. Attard, Ashley Brew, David J. Morgan and Frank Marken: *Electrochimica Acta*, 2014, 128, 3-9.
- **Polymers of Intrinsic Microporosity Containing Tröger Base for CO<sub>2</sub> Capture.** Annalaura Del Regno, Aleksandra Gonciaruk, Laura Leay, Mariolino Carta, Matthew Croad, Richard Malpass-Evans, Neil B. McKeown, and Flor R. Siperstein: *Industrial & Engineering Chemistry Research*, 2013, 52 (47), 16939–16950.
- **A highly permeable polyimide with enhanced selectivity for membrane gas separations.** Yulia Rogan, Richard Malpass-Evans, Mariolino Carta, Michael Lee, Johannes C. Jansen, Paola Bernardo, Gabriele Clarizia, Elena Tocci, Karel Friess, Marek Lanč and Neil B. McKeown: *Journal of Materials Chemistry A*, 2014, 2, 4874-4877.
- **Triptycene Induced Enhancement of Membrane Gas Selectivity for Microporous Tröger's Base Polymers.** Mariolino Carta, Matthew Croad, Richard Malpass-Evans, Johannes C. Jansen, Paola Bernardo, Gabriele Clarizia, Karel Friess, Marek Lanč and Neil B. McKeown: *Advanced Materials*, 2014, 1521-4095.
- **Intrinsically Porous Polymer Protects Catalytic Gold Particles for Enzymeless Glucose Oxidation.** Yuanyang Rong, Richard Malpass-Evans, Mariolino Carta, Neil B. McKeown, Gary A. Attard and Frank Marken: *Electroanalysis*, 2014, 1521-4109.
- **High Density Heterogenisation of Molecular Electrocatalysts in a Rigid Intrinsically Microporous Polymer Host.** Yuanyang Rong, Richard Malpass-Evans, Mariolino Carta, Neil B. McKeown, Gary A. Attard and Frank Marken: *Electrochemistry Communications*, 2014, 46, 26-29.
- **The Synthesis of Microporous Polymers using Tröger's Base Formation.** Mariolino Carta, Richard Malpass-Evans, Matthew Croad, Yulia Rogan, Michael Lee, Ian Rose and Neil B. McKeown: *Journal of Polymer Science Part A: Polymer Chemistry*, 2014, 5, 5267-5272.
- **Metastable Ionic Diodes Derived from an Amine-Based Polymer of Intrinsic Microporosity.** Elena Madrid, Yuanyang Rong, Mariolino Carta, Neil B. McKeown, Richard Malpass-Evans, Gary A. Attard, Tomos J. Clarke, Stuart H. Taylor, Yi-Tao Long, Frank Marken: *Angewandte Chemie*, 2014, in press.
- **Design and Synthesis of Polymers of Intrinsic Microporosity for Membrane-Based Gas Separations.** Neil B. McKeown, Mariolino Carta, Grazia Bezzu, Richard Malpass-Evans, Michael Lee, Ian Rose, Johannes C. Jansen, Paola Bernardo, Gabriele Clarizia: *248th ACS National Meeting & Exposition, San Francisco*, 2014.
- **Molecular Modelling and Gas Permeation Properties of a Polymer of Intrinsic Microporosity composed of Ethanoanthracene and Tröger's base units.** Elena Tocci, Luana De Lorenzo, Paola Bernardo, Gabriele Clarizia, Fabio Bazzarelli, Neil B. McKeown, Mariolino Carta, Richard Malpass-Evans, Karel Friess, Kryštof Pilnáček, Marek Lanč, Yuri P. Yampolskii, Ludmila Strarannikova, Viktor Shantarovich, Michele Mauri, Johannes C. Jansen: *Macromolecules*, 2014, in press.